Dissertation

Biological characterization of farnesyl-mediated protein-protein interactions

Zur Erlangung des akademischen Grades eines

Doktors der Naturwissenschaften

(Dr. rer. nat.)

von der Fakultät für Chemie und Chemische Biologie

an der Technischen Universität Dortmund

vorgelegt von

M. Sc. Michael Andre Winzker

aus Viersen, Nordrhein-Westfalen

Dortmund 2019

Die vorliegende Arbeit entstand im Zeitraum von August 2015 bis August 2019 unter der Anleitung von Prof. Dr. Dr. h.c. Herbert Waldmann an der Fakultät für Chemie und Chemische Biologie der Technischen Universität Dortmund und dem Max-Planck-Institut für molekulare Physiologie in Dortmund.

Dekan: Prof. Dr. Stefan M. Kast

1. Gutachter: Prof. Dr. Dr. h.c. Herbert Waldmann
2. Gutachter: Prof. Dr. Martin Engelhard

Teile dieser Arbeit wurden bereits in folgendem Beitrag veröffentlicht:

1. S. Mosalaganti*, J. Keller*, A. Altenfeld*, M. Winzker, P. Rombaut, M. Saur, A. Petrovic, A. Wehenkel, S. Wohlgemuth, F. Müller et al., *J. Cell Biol.* **2017**, *216*, 961. *these authors contributed equally

Table of Content

1 Zusammenfassung

Das prenyl-bindende Protein PDEδ spielt eine wichtige Rolle in der zellulären Verteilung von diversen prenylierten Proteinen. Ein prominenter Bindungspartner ist die kleine GTPase KRas. Eine Punktmutation in diesem Proto-Onkogen ist in ca. 30% aller Tumoren zu finden und führt zu einem unkontrollierten Wachstums- und Differenzierungsprozess der Zellen. Die Behandlung von KRas-abhängigen Tumoren durch gezielte KRas-Inhibierung erweist sich als äußert schwierig, weshalb andere Behandlungsmöglichkeiten benötigt werden. Eine vielversprechende Methode ist die Unterbindung der korrekten, zelluläre Lokalisierung von KRas durch die Inhibition der Interaktion von KRas und PDEδ. Durch die Fehllokalisierung von KRas kommt es zu reduziertem Zellwachstum und Zelltod in KRas-abhängigen Krebszelllinien. Vorangegangene Studien konnten zeigen, dass pikomolare PDEδ–Inhibitoren jedoch nur mikromolare zelluläre Aktivität aufweisen. Diese Aktivitätslücke lässt sich durch einen weiteren, allosterisch-bindenden Interaktionspartner von PDEδ namens Arl2 erklären. Dieser stabilisiert eine inaktive Konformation von PDEδ und erzwingt die Freigabe von Bindungspartnern und Inhibitoren. Um dem entgegenzuwirken und den inhibitorischen Effekt auf PDEδ zu erhöhen, könnte das Konzept des gezielten Proteinabbaus auf die pikomolaren Inhibitoren angewandt werden. Dabei soll durch die Rekrutierung einer E3-Ubiquitin-Ligase eine Ubiquitinierung von PDEδ stattfinden, durch die der Abbau von PDEδ induziert wird.

Im Rahmen dieser Arbeit wurden Inhibitoren basierend auf dem Prinzip des gezielten Proteinabbaus synthetisiert und mittels biophysikalischen und zellbasierten Testsystemen validiert. Zunächst wurden proteindegradierende Substanzen entworfen, um die zelluläre PDEδ–Konzentration zu reduzieren. Dazu wurden ausgehend vom pikomolaren PDEδ-Inhibitor Deltasonamide 1 und dem E3-Ligase-bindenden Pomalidomide PROTACs (engl. *proteolysis targeting chimeras*) synthetisiert. Pomalidomide rekrutiert Cereblon, eine E3-Ubiquitin-Ligase, die in artifizielle Nähe zu PDEδ gebracht wird und für den Abbau von PDEδ sorgt. Nachdem gezeigt werden konnte, dass die Affinität zu PDEδ nur leicht beeinträchtig ist, wurde der Effekt der Verbindungen auf Zellen untersucht. Es konnte gezeigt werden, dass die PDEδ-PROTACs zu reduzierten PDEδ–Mengen von bis zu 84% Reduktion nach 24-stündiger Behandlung führen. Durch simultane Inhibition des Proteasoms während der Behandlung mit dem PDEδ-PROTAC konnte gezeigt werden, dass der Abbau über das Proteasom stattfindet.

Nach Behandlung mit den PROTAC-Substanzen konnten auch nanoLuc-PDEδ und mCherry-PDEδ-Fusionskonstrukte erfolgreich abgebaut werden. Die unterschiedlichen Konstrukte ermöglichen einen detaillierteren Einblick in die Dynamiken des PDEδ-Abbaus.

Die Selektivität der Substanzen wurde mittels massenspektrometrischer Proteom-Analyse untersucht. Von 4800 quantifizierten Proteinen wurde nur die zelluläre PDEδ-Menge vermindert. Dieses Ergebnis lässt darauf schließen, dass der erhaltene PDEδ-PROTAC sehr selektiv für den Abbau von PDEδ ist. Zusätzlich wurde festgestellt, dass der aktive und inaktive PROTAC, sowie Deltasonamide 1 die zelluläre Menge von Proteinen des Mevalonat-(Cholesterol)-Biosynthesewegs erhöhen. Eine Reactom-Analyse zeigte, dass die Expression von vielen der hochregulierten Proteine von einem SRE-abhängigen (engl. *sterol regulatory element*) Promotor gesteuert wird. Alle Substanzen stimulierten die SRE-abhängige Expression und erhöhten nicht nur die Proteinmengen der Enzyme, sondern bewirkten auch eine Anhäufung von Metaboliten des Cholesterol-Biosyntheseweges. Vermutlich stören die Substanzen die korrekte Lokalisierung eines prenylierten Bindungspartners von PDEδ und induzieren so diesen Phänotyp.

Diese Arbeit zeigt, dass gezielter Proteinabbau ein vielversprechendes Konzept zur Regulierung von Proteinmengen und deren Aktivität ist. Die erhaltenen PDEδ-PROTACs können als molekulare Werkzeuge eingesetzt werden, um zelluläre PDEδ-Mengen zu reduzieren und dessen Dynamik und Funktion weiter aufzuklären.

Im zweiten Teil dieser Arbeit wurde die Bindesstelle und -partner von Spindly, einem Protein, das an der Kinetochor-Organisation beteiligt ist, innerhalb des Rod-ZW10-Zwilch-Komplexes identifiziert. Dazu wurden photoaktivierbare Farnesylanaloga synthetisiert und Spindly artifiziell mit diesen modifiziert. Durch Bestrahlung mit Licht wird eine kovalente Bindung zwischen farnesyliertem Spindly und dem unbekannten Bindungspartner erzeugt, wodurch dieser massenspektrometrisch identifiziert werden kann. Diese Erkenntniss hilft den komplexen Prozess der Chromosomensegregation weiter aufzuklären und zeigt eine neue Klasse von Farnesyl-bindenden Proteinen.

2 Summary

The prenyl-binding protein PDEδ plays a crucial role in the translocation of the small GTPase KRas, whose constitutively active mutants are found in ca. 30% of all tumors. Since the treatment of KRas-dependent tumors by targeting KRas has proven to be extremely challenging, interfering with its localization may be a more attractive approach. Previous studies have shown that inhibition of PDEδ by picomolar ligands lead only to micromolar cellular activity. This activity gap results from the activity of the releasing-factor Arl2, which binds to PDEδ in a farnesyl-independent manner and stabilizes an inactive conformation that results in the release of the ligands from the farnesyl binding pocket. To overcome this problem, Proteolysis-targeting chimeras (PROTACs) based on the picomolar PDEδ-inhibitor Deltasonamide 1 and Pomalidomide-mediated recruitment of an E3 ubiquitin ligase were synthesized, which are supposed to induce degradation of PDEδ.

By proper selection of an attachment site for a linker, low nanomolar affinity against PDEδ could be retained for the heterobifunctional molecule. Since efficient protein degradation relies on productive ternary complex formation, three PROTACs with different linker lengths were synthesized. All three PDEδ PROTACs were able to reduce cellular PDEδ levels with a maximal degradation efficiency (D_{max}) between 65 and 85% after 24 h, whereas an inactive PROTAC, which could not recruit the E3 ligase, did not induce degradation. The most effective PROTAC showed a D_{max} of 83.6% and a half-maximal degradation concentration (DC_{50}) of 48 nM in Panc Tu-I cells after 24 h. Furthermore, PDEδ degradation by the PROTACs was prevented by inhibition of proteasome function. In addition, PDEδ PROTACs proved to induce degradation of nanoLuc-PDEδ and mCherry-PDEδ fusion proteins. The luminescence and fluorescence read-outs offer the opportunity to gain deeper insight into the degradation dynamics of PDEδ PROTACs by increasing the throughput and live cell imaging. Proteome profiling by mass spectrometry revealed that the PROTACs are highly selective for PDEδ, as out of 4800 identified proteins, only PDEδ showed reduced cellular levels upon PROTAC treatment. The level of many proteins of the mevalonate pathway were elevated after PROTACs and Deltasonamide 1 treatment. As a reactome analysis revealed, most upregulated proteins were under the transcriptional control of the sterol regulatory element (SRE)-promotor and the

active PROTAC and Deltasonamide 1 proved to activate an SRE-responsive reporter gene assay.

PDEδ interacts with different prenylated proteins and is involved in their localization in the cell. By interfering with PDEδs activity through chemical inhibition or knockdown, these binding partners are mislocalized. The function of those proteins was impaired, which leads to the upregulation of enzymes of the lipid metabolism.

The results show that targeted protein degradation is a valuable strategy for modulating protein levels. This new PDEδ PROTACs can be used to remove PDEδ and fusion proteins from the cell to elucidate there dynamics and cellular functions.

In the second part of this thesis the binding site and partner of Spindly a protein involved in kinetochore organization was identified within the Rod-ZW10-Zwilch complex. This finding partially resolves the complex organization of chromosome segregation and demonstrates a new class of farnesyl binding proteins.

Part A

The Design, Synthesis and Biological Characterization of PDEδ-targeting PROTACs

3 Part A

3.1 Introduction

3.1.1 The molecular chaperone PDEδ

The Retinal rod rhodopsin-sensitive cGMP 3',5'-cyclic phosphodiesterase subunit delta (PDEδ) is a 150 amino acid large protein, which was first identified as a subunit of the cGMP phosphodiesterase (PDE) from retinal cells. Most PDEs are multimeric proteins with different catalytic subunits in which the catalytic center is build-up by the α- and β-subunit, whereas the smaller γ-subunit is responsible for inhibitory function within the complex.[2] The interaction of PDEδ with the α– and β–subunit of PDE6 solubilizes the PDE6 complex from the membrane and desensitizes the photo transduction.[3] PDEδ binds the prenylated C-termini of the α- and β-subunits and therefore solubilizes the whole complex. PDEδ is ubiquitously expressed and present in nearly all species. Furthermore, the amino acid sequence is highly conserved throughout vertebrates and invertebrates with approximately 50 to 70% homology.

The structure of PDEδ is dominated by an immunoglobulin β-barrel, which forms a hydrophobic pocket highly complementary to Rho GDP-dissociation inhibitor (RhoGDI) and Protein unc-119 homolog A (UNC119).[4,1,5] While RhoGDI and PDEδ preferably bind prenylated proteins, UNC119 specifically binds to myristoylated proteins.[4]

Table 1: The interaction partners of PDEδ identified in a yeast two-hybrid screen.[1] f = farnesyl moiety, gg = geranylgeranyl moiety.

Protein name	Prenylation	Protein name	Prenylation
PDEα	f	Rab13	f
PDEβ	gg	Rab28	f
GRK1	f	Rheb	f
GRK7	gg	Rho6	f
cTγ	f	Rap1a	gg
Tγ	f	Rap1b	gg
DmPDE5/6	gg	Rap2a	gg
HRas	f	Rap2b	gg
NRas	f	RhoA	gg
KRas	f	RhoB	gg
RPGR	gg	Prostacyclin-R	f
Lamin-B1	f	INPP5E	f
Lamin-B2	f	Arl2-GTP	-
Prelamin-A/C; Lamin-A/C	f	Arl3-GTP	-
Rab8	gg		

Since PDEδ is ubiquitously expressed throughout all cell types, it presumably has more functions than only solubilizing PDE6. Initially, yeast two-hybrid screens revealed that PDEδ binds to different small GTPases of the Ras and Rho families (Table 1).

Co-crystallographic studies of PDEδ and Ras homolog enriched in brain (Rheb) have shown that the interaction is limited to a farnesyl moiety and the last five to ten amino acids of Rheb´s C-terminus. Despite structural similarities between RhoGDI and PDEδ, their binding mode is different. RhoGDI additionally binds the switch region of GTPases, which makes its binding mode depending on the activity state. In contrast, Rheb binds deeper into PDEδ´s pocket than CDC42 into RhoGDI´s prenyl binding site (Figure 1A).[1] Through this additional binding surface, PDEδ compensates the missing interaction with Rheb´s switch region and therefore binding is independent of the GTP-bound state of Rheb.[6] This is in line with observations that binding affinities for PDEδ do not substantially change between synthetic KRas peptides and semisynthetic full length KRas, explaining the low specificity of PDEδ binding partners.[7]

Apart from farnesyl-dependent interactions, PDEδ has an allosteric binding site to interact with proteins of the ADP-ribosylation factor-like (Arl) family. Binding of Arl2 and Arl3 occurs through the β-sheets of PDEδ and stabilizes one out of an ensemble of interconverting conformations of PDEδ (Figure 1B). When Arl2/3 are bound to PDEδ, it is in a closed conformation and the farnesyl binding pocket is not accessible for prenylated moieties. In the unbound form, PDEδ is open and accessible for prenylated cargos.

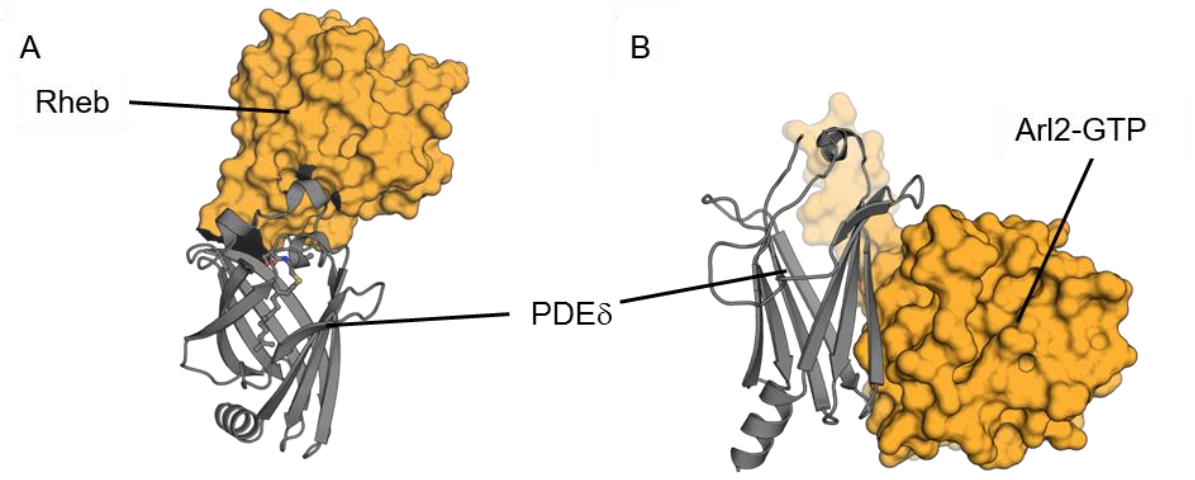

Figure 1: The crystal structure of PDEδ in complex with Rheb and Arl2-GTP. (A) The crystal structure of PDEδ in grey and the farnesylated Rheb in orange (PDB: 3T5G). (B) The crystal structure of PDEδ in grey and the allosteric binder Arl2-GTP in orange (PDB: 1KSH).

Thus, the system consisting of PDEδ, Arl2/3 and prenylated proteins can act as a transport system that loads and unloads proteins, i.e. can translocate proteins through binding of Arl2/3 within the cell.[6]

Recent studies revealed a role of PDEδ in the transport of proteins to the primary cilium. Inositol polyphosphate 5-phosphatase (INPP5E) and X-linked retinitis pigmentosa GTPase regulator (RPGR) showed mechanisms depending on PDEδ.[8,9] INPP5E binds with high affinity to PDEδ and cannot be released by Arl2 in contrast to KRas or Rheb. This high-affinity binders can only be released by Arl3-GTP, which suggests that PDEδ has a sorting function for different cargos.[10,9]

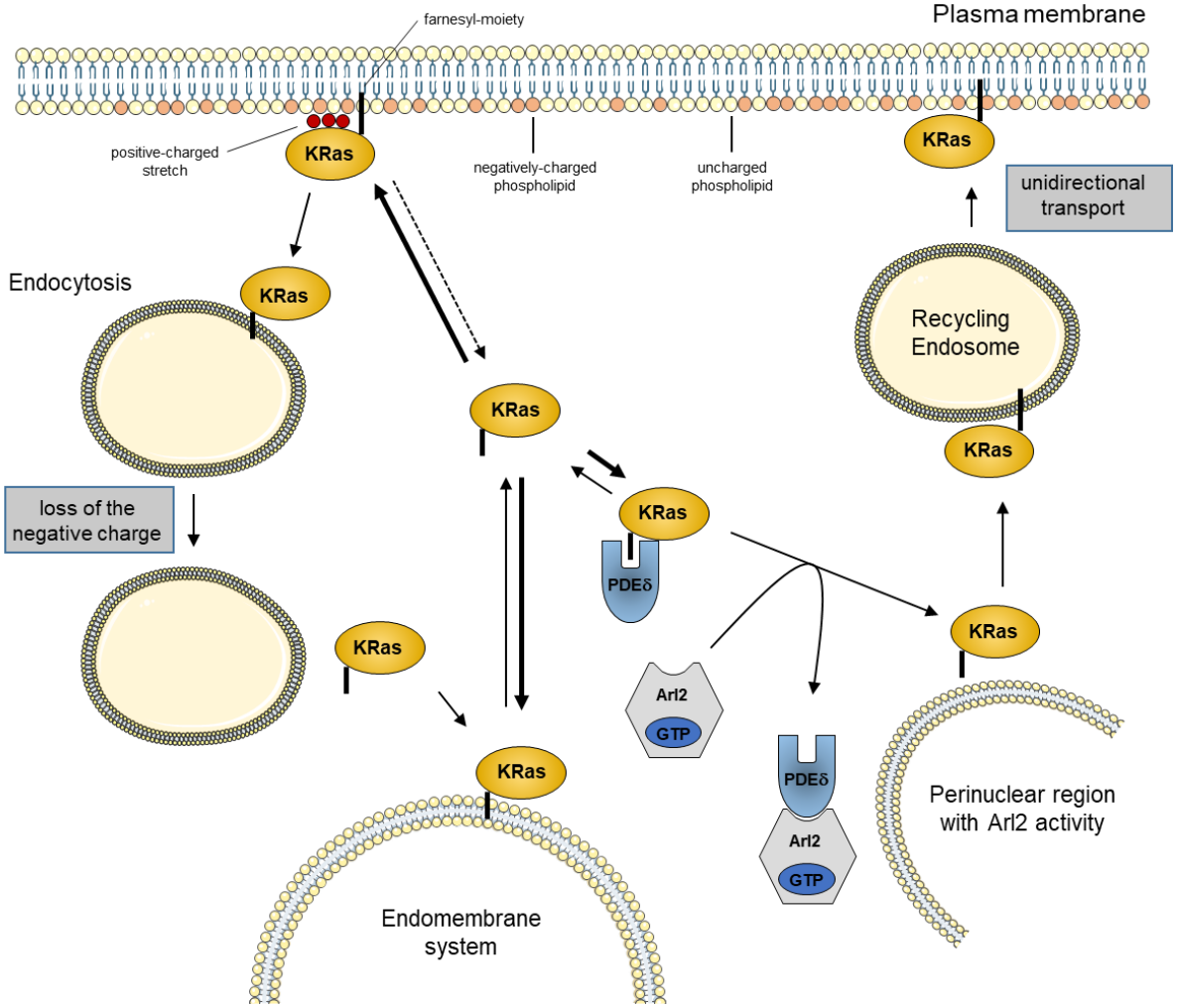

Figure 2: The KRas cycle mediated by PDEδ and Arl2. KRas delocalizes from the plasma membrane by endocytosis and spontaneously dissociates from the membrane into the cytosol. After the loss of negative charge from the membrane of the endocytic vesicles, KRas dissociates into the cytosol and binds to the endomembrane system. There it is solubilized by PDEδ and, as a complex, is transported through the cytosol. At the perinuclear region, Arl2 activity pushes KRas out of PDEδ, so that KRas binds to the negatively charged recycling endosomes. Through vesicular transport, KRas is translocated back to the plasma membrane.[11]

Another prominent cargo of PDEδ is the proto-oncogene KRas. As a member of the Ras family, KRas is responsible for the signal transduction in the mitogen-activated protein kinase / extracellular signal-related kinase (MAPK/ERK) signaling pathway and is therefore involved in differentiation, cell proliferation, metabolism and motility.[11]

Following epidermal growth factor (EGF) binding to the receptor tyrosine kinases and subsequent activation, KRas becomes activated by the exchange of GDP to GTP. Active KRas transduces the extracellular signal via the RAF, MEK 1/2, ERK 1/2 cascade to the nucleus. The translocation of KRas to the plasma membrane is critical for successful signal transduction and is regulated by PDEδ. Besides the farnesyl moiety, KRas bears a positively charged polylysine stretch. This mediates higher affinity towards the negatively charged plasma membrane than to uncharged endomembrane. KRas at the plasma membrane is endocytosed and then distributed to the endomembrane system. KRas has less affinity towards these membranes, because of the loss of their negative charge causing PDEδ to dissociate into the cytoplasm. Because of the Arl2-GTP localization at perinuclear membranes, PDEδ´s cargo is released at this region, which leads to locally increased KRas concentrations. From there, KRas associates with the recycling endosome, and is then transported to the plasma membrane (Figure 2).[12]

KRas mutations, which lead to constitutively active mutants, are found in ca. 30% of all tumors. Since the treatment of KRas-dependent tumors by targeting KRas has proven to be extremely challenging, interfering with its localization has been recently considered as an alternative and more attractive approach.[13] Therefore, several inhibitors that bind into the PDEδ pocket were successfully developed. Inhibition of the interaction of PDEδ and KRas showed the mislocalization of KRas throughout the cell and reduced oncogenic signaling.[13–15] Although PDEδ inhibitors have shown picomolar affinities for PDEδ in *in vitro* experiments, cellular effects such as reduced MAPK/ERK-signaling and cell growth of KRas-dependent cell lines occur only in a micromolar range. This activity gap results from the activity of the releasing-factor Arl2-GTP, which binds to PDEδ and releases the ligands from the binding pocket. Different PDEδ inhibiting agents were developed by Waldmann *et al.* to overcome this issue. The first inhibitor was identified through a high-throughput Alpha screen with a farnesylated KRas peptide and His-tagged PDEδ.[13] Several benzimidazole hits were identified and yielded Deltarasin as nanomolar binder through structure-guided design (Figure 3A).

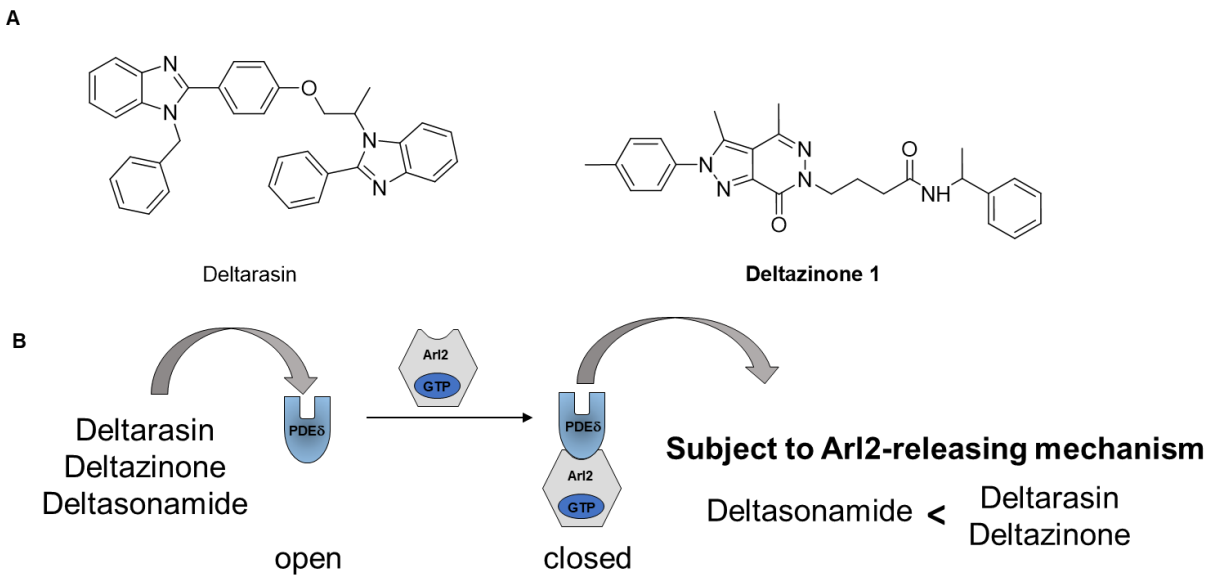

Figure 3: The inhibition of PDEδ. (A) First PDEδ inhibitor identified by Waldmann *et al.*. (B) Schematic figure of the release of PDEδ-inhibiting agents.

As a next generation, pyrazolopyridazinones were identified as PDEδ binding agents with a K_D of 8 nM (Figure 3A). These inhibitors are subject to the Arl-dependent releasing mechanism and are therefore impractical agents to impair with PDEδs function in cellular assays. Deltasonamide was the first inhibitor, which showed picomolar affinity for PDEδ and resisted being fast released by Arl2 (Figure 4B).

However, all three generations lack the ability to efficiently target PDEδ in cells and therefore to interrupt KRas signaling.

Furthermore, as PDEδ is responsible for the translocation of prenylated proteins, blocking the prenyl binding pocket might lead to general problems for the cell. Computational analysis revealed that approximately 2% of the proteome is prenylated (see paragraph 4.1.1).[16] Assuming that PDEδ is a chaperone for a portion of these proteins due to its non-specific binding mode, its inhibition could cause severe problems within the cell by generally affecting the localization of prenylated proteins. As the role of PDEδ within the cell still remains poorly understood, new tool compounds that interrogate its activity need to be developed. The design of tool compounds that induce degradation of PDEδ by the proteasome could be an efficient and unique approach to further interrogate the function of PDEδ. The theoretical framework for carrying this out is discussed in the following sections.

3.1.2 The ubiquitin system

The proteome of a cell is dynamic and steadily adjusting to extracellular influences, even when a cell is not undergoing growth or division. Intracellular protein levels are controlled by synthesis and degradation.[17] Different proteins have distinct turnover rates, which range from seconds to months.[18,17]

A common mechanism to recycle most short-lived proteins is carried out by the ubiquitin system. Ubiquitin is a highly conserved 76-amino acid protein, which is covalently attached to proteins and generally directs them for proteasome degradation. The ubiquitin-mediated degradation regulates the levels of proteins involved in cell-cycle progression, signal transduction, transcriptional regulation, receptor down-regulation and endocytosis.[19] For the ubiquitin protein ligation, three sequentially activated proteins are needed (Figure 4). In the first step, the C-terminal glycine of ubiquitin is activated in an ATP-dependent step by an ubiquitin activating enzyme, E1 (Activation). In an intermediate step, ubiquitin adenylate is formed, followed by the release of pyrophosphate PP_i and subsequent formation of an active thioester between ubiquitin and E1. In the second step, ubiquitin is transferred to an E2 enzyme, an ubiquitin-carrier protein (Conjugation).

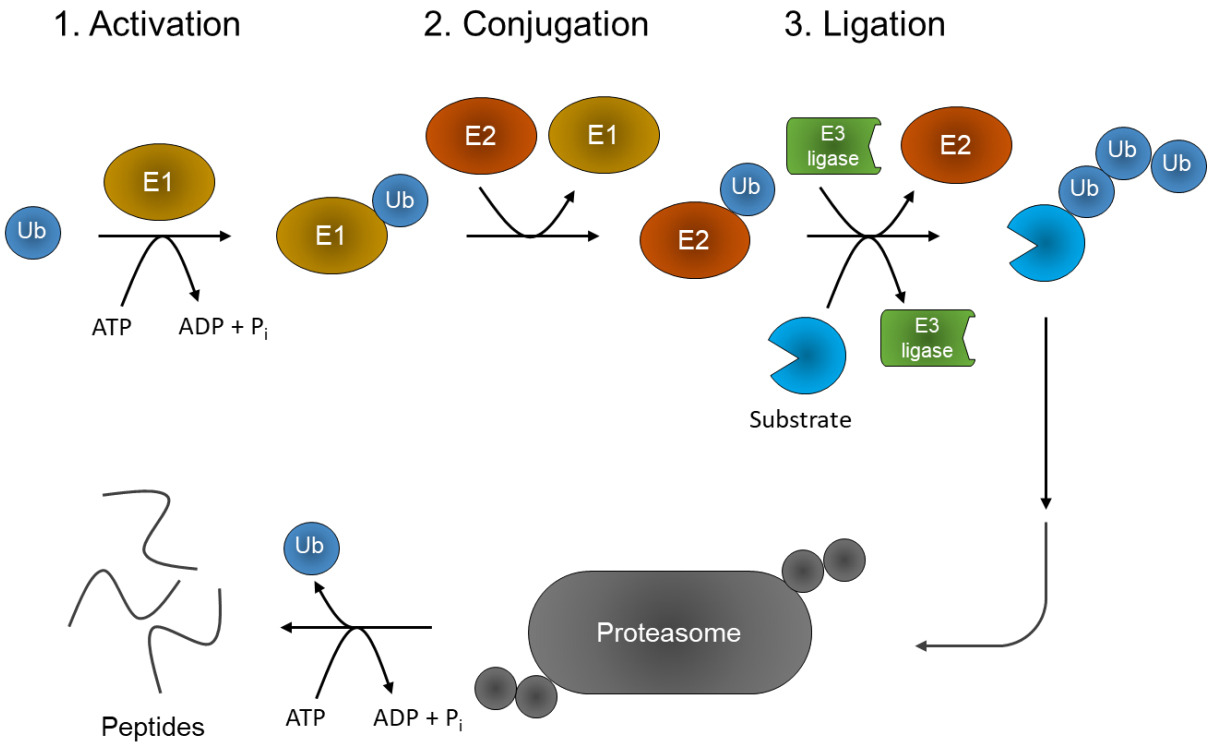

Figure 4: The ubiquitin system. The ubiquitin activating enzyme E1 is loaded with ubiquitin, which is then transferred to the E2 enzyme. The E3 ligase translocates to the substrate, which leads to the proximity-induced ubiquitination of the substrate. Polyubiquitinated substrates are recognized by the proteasome, which proteolytically cleaves the protein into peptides.

In the last step, ubiquitin is covalently linked to the target protein, which is catalyzed by an E3 ubiquitin ligase (Ligation). There is only one E1, 20-40 E2 enzymes and hundreds of E3 ligases or multimeric complexes present in cells.[20] E3 ligases are mainly responsible for substrate specificity. They simultaneously bind proteins bearing a specific recognition signal and the ubiquitin-carrier protein E2. Two different mechanisms are known to transfer ubiquitin from E2 to the protein. In the case of the Hect-domain family, ubiquitin is first transferred from appropriate E2 enzymes to cysteine residues of E3. This loaded E3-ubiquitin acts then as a donor for amide bond formation with the substrate. In a different mechanism, E2 directly transfers the ubiquitin to the acceptor protein without an intermediate step. After a substrate is labelled with the first ubiquitin, a polyubiquitin chain is formed by the linkage of a specific lysine (commonly Lys^{48}) to the previous ubiquitin.[19]

Proteins labelled with polyubiquitin are recognized by the 26S proteasome. It is formed by an ATP-dependent assembly of a 20S proteasome containing 19S "cap" or regulatory complexes. The 19S includes several ATPase subunits which are involved in the specific action of 26S on ubiquitinated proteins. The 26S proteasome generates different types of products: free peptides, short peptides linked to ubiquitin, and polyubiquitinylated peptides. Ubiquitin is cleaved off from peptides by hydrolases and can be reused by the ubiquitin system. Short and free peptides are further degraded by cytosolic peptidases yielding to free amino acids. Abnormalities in the ubiquitin system can cause pathological conditions, including malignant transformation.[19]

3.1.3 Targeted protein degradation

Current biomedical research is mainly focused on chemical inhibition, genetic knockdowns, knockout animal models, biologics and mutagenesis screens to elucidate complex signaling networks in biology. Protein inhibition by small molecules remains a mainstay in drug development and applied therapeutics.

Chemical inhibition is carried out with small molecules that bind to the enzyme or receptor to modulate its function. This has two main limitations: First, inhibitors need to bind into the active site or allosterically to inhibit protein function. This classifies the main part of the proteome as undruggable since many drug targets lack a binding site to interfere with their function.[21] Second, these inhibitors need to be bound to the protein to stay active. Low off-rates are necessary to occupy the main cellular portion of the targeted protein. To reach high binding occupancy, high dosing is often needed, leading to undesired off-target effects.[22]

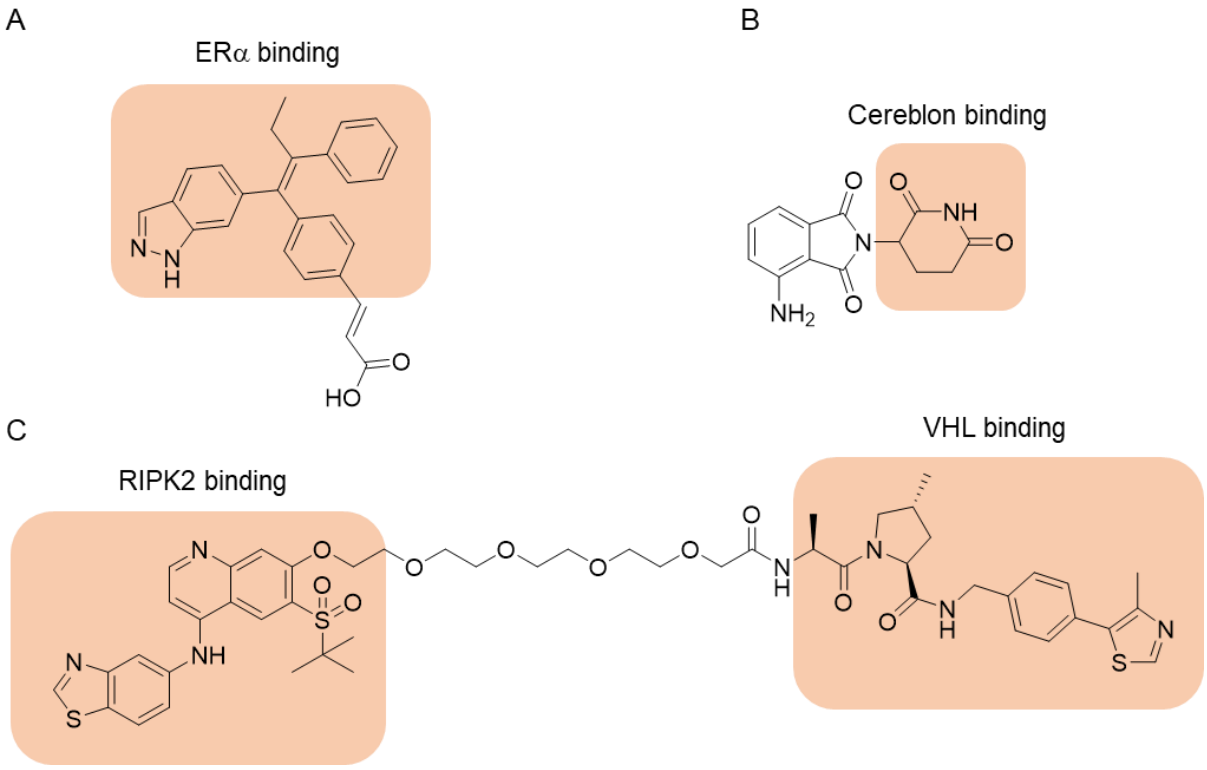

Figure 5: Compounds that are used in targeted degradation approaches. (A) Selective estrogen receptor downregulators (SERDs) that leads to the degradation of the estrogen receptor α (ERα). (B) ImiDs, which bind to the E3 ligase cereblon. This motive can be used for hijacking cereblon to induce protein degradation. (C) PROTAC, which binds RIPK2 and the E3 ligase VHL and induces protein degradation of RIPK2

In contrast, a chemical knockdown could overcome these limitations. By inducing protein degradation, their cellular level is reduced, preventing them from performing their function. A commonly used method to reduce cellular protein levels is by siRNA knockdown. Small RNA sequences are administered to the cell and induce RNA cleavage of the respective complementary sequences. This technique has applicability in cell biology but has important limitations, which prevents it from being broadly used as a therapeutic approach. The bioavailability of siRNA is limited, since RNA is highly negatively charged and therefore not passing the membrane without using special delivering systems like liposomes. In addition, it only interrupts protein synthesis on the RNA level, which is problematic for long-lived proteins. Promoting protein degradation with small molecules should overcome these limitations.

One class of degradation-inducing compounds are selective estrogen receptor down-regulators (SERDs) (Figure 5A). This class of compounds was identified as inhibitors of the estrogen receptor α (ERα) that decrease cellular receptor levels.[23] Although these compounds might be the oldest of this class, their mechanism of action is not well understood.

The current understanding is that upon compound binding, certain hydrophobic motifs of ERα are presented to chaperones, which triggers ERα degradation by recruiting the proteasome.[24] Therefore, rational design strategies cannot be applied to this approach and more complex screening techniques are required. Recent high-throughput assays concentrate on exposing relevant hydrophobic surfaces and monitoring intracellular ERα levels.[25] Although these small molecules lead to target degradation and have shown clinical success, their applicability in other systems is limited. It is hard to predict which structural properties a small molecule needs to have to induce protein degradation upon binding. To overcome this restricted applicability, more general techniques were established.[26]

Proteolysis-targeting chimeras (PROTACs) have been developed in the past 15 years as a general strategy to affect protein degradation using small molecules. They showed high usability through rational design strategies on a broad spectrum of proteins. PROTACs are heterobifunctional molecules consisting of a ligand that binds to a protein of interest and a second ligand that targets an E3 ubiquitin ligase, connected via a chemical linker (Figure 7). During the design of PROTACs, three features must be optimized, which have a significant influence on the activity. First, the binding mode of the parent molecule should be known and groups of the ligand which facing the solvent have to be synthetically available for linker attachment. Second, recruiting the correct E3 ligase is crucial for successful degradation. Third, a proper linker length and type needs to be selected.

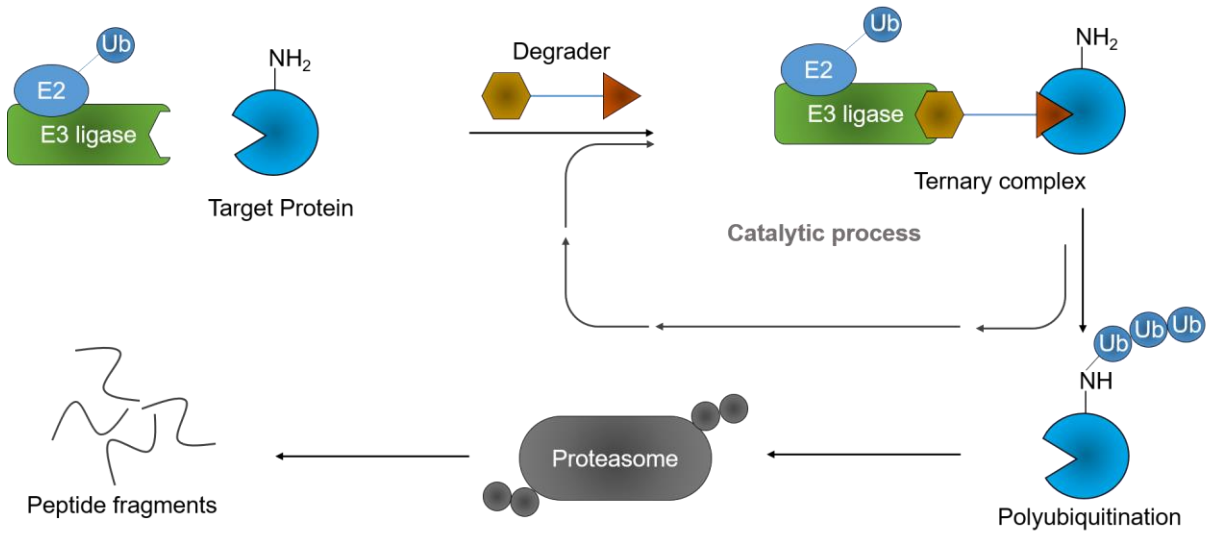

Figure 6: Targeted protein degradation by PROTACs. A heterobifunctional molecule (Degrader) binds to the target protein and an E3 ubiquitin ligase, thus, bringing both in artificial proximity. Through this proximity amino-groups of the target protein are polyubiquitinated and therefore labeled for proteasomal degradation. Ub: ubiquitin.

All features need to lead to an active ternary complex which achieves polyubiquitination of a lysine, which can be recognized by the proteasome (further details in paragraph 1, Figure 6).[27,28]

The first reported PROTAC was built-up from the natural product ovalicin and a peptidic ligand for the E3 ligase CRL1 F-box protein β-TRCP.[29] Some key features of active PROTACs were demonstrated using this initial PROTAC (e.g. ternary complex formation, ubiquitination activity and limited degradation of its target protein).[30] Based on these early studies, several key lessons have been learned. Firstly, PROTACs are able to hijack different E3 ligases for selective protein degradation (e.g. β-TRCP, MDM2, CIAP and von Hippel-Lindau).[31] Secondly, small molecules have been employed to recruit E3 ligases for protein degradation. Thirdly, these PROTACs are very limited in their potency. This early generation of PROTACs only partially degraded the protein of interest despite applying micromolar concentrations. Due to their size and charge, cell permeability is a key contributor to this lack of potency. To overcome these limitations, high-affinity small-molecule E3 ligase ligands had to be established. Therefore, a small molecule-based von Hippel-Lindau (VHL)-binder was developed and employed to degrade bromodomain-containing protein 4 (BRD4), the receptor interacting serine/threonine protein kinase 2 (RIPK2) and the nuclear hormone receptor estrogen-related receptor α (ERRα) (Figure 5B). Recently, a new E3 ligase binder was discovered as useful in this context. Immunomodulatory drugs (ImiDs) bind to the E3 ligase cereblon (CRBN) and were successfully employed to degrade BRD4 (Figure 5C).[32] In each case, these PROTACs achieved nearly complete removal of the protein of interest at low nanomolar concentrations.[33]

The PROTAC strategy has shown its advantages compared to chemical inhibition in terms of modularity and potency and might be the system of choice for targeting the undruggable proteome. In the future, even more E3 ligases could be hijacked and used for targeted protein degradation and this may open the opportunity to develop better molecular tools to be used in drug discovery.[34]

3.1.4 The design and properties of PROTACs

PROTAC-induced protein degradation offers a new approach to target intracellular proteins. In contrast to chemical inhibition, protein levels are reduced by hijacking and making use of the cellular recycling machinery. PROTACs are heterobifunctional molecules consisting of a small molecule ligand of a given protein target connected via a linker to a warhead targeting an E3 ligase. To establish a productive PROTAC for a selected target many features of the different parts need to be considered (Figure 7A).

To successfully design a functional PROTAC, a target needs to be selected with a known small-molecule ligand. The ligand can be obtained from any *in vitro* binding assay and does not need to show an inhibitory effect of the protein's function. Since this approach is uninfluenced by where the ligand binds, diverse small molecules binding at different protein sites can be considered as affinity tags for a selected target. Hence, PROTACs offer the opportunity to develop small-molecule binders of undruggable targets, which do not impair protein function but show binding affinities, expanding the drug-target space. In addition to their synthetic availability, structure-activity relationships of the compound class should be available, since a site for linker attachment needs to be identified (Figure 7B). Once a suitable protein target with a small-molecule ligand is selected and a linker attachment site is found the E3 ligase ligand can be chosen.

Currently, only four of more than 600 E3 ligases have been validated and exploited for PROTAC development: von Hippel-Lindau (VHL), Cereblon (CRBN), E3 ubiquitin-protein ligase Mdm2 (MDM2) and cellular Inhibitor of Apoptosis Protein 1 (cIAP1) (Figure 8).[35]

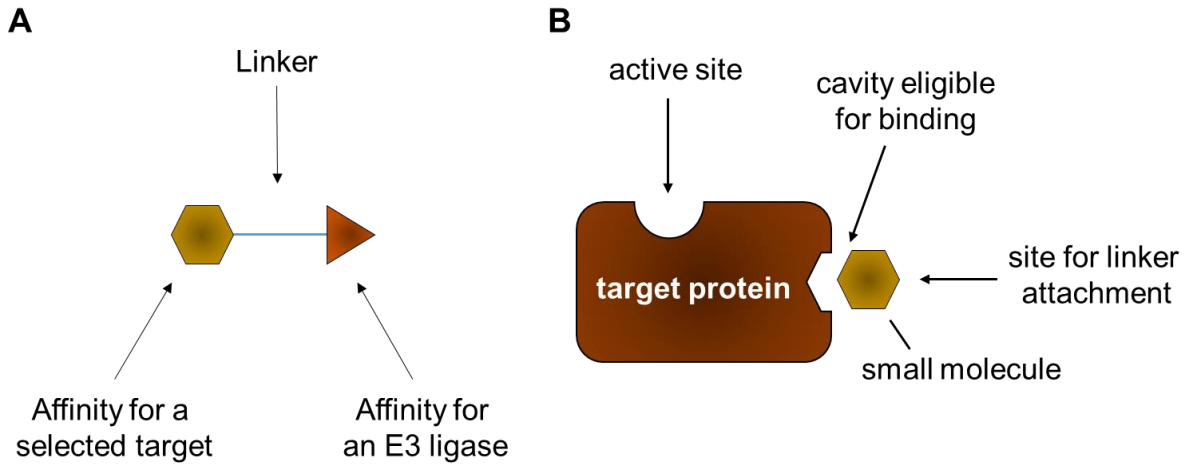

Figure 7: The structure and design of a PROTAC. (A) The heterobifunctional molecule consists of small molecule ligand and a second molecule for an E3 ligase connected via a linker. (B) Different binding site to target a protein with small molecules.

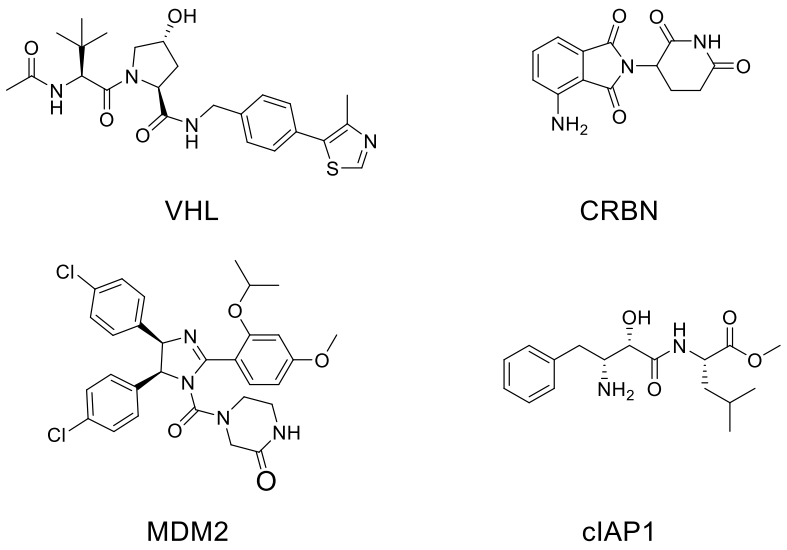

Figure 8: The structure of E3 ligase ligands. VHL: von Hippel-Lindau; cLAP1: cellular inhibitor of apoptosis protein-1; MDM2: E3 ubiquitin-protein ligase Mdm2; CRBN: cereblon.

All four ligases have known small-molecule ligands and can successfully degrade their respective targets when used in a PROTAC. Although these ligases showed applicability, some of them have limitations, which need to be considered. The small-molecule ligand of cIAP1 suffered from issues of self-degradation, thus limiting its utility.[36]

Also PROTACs bearing the ImiDs showed effects on protein levels of neo-substrates such as MEIS2, Ikaros, Aiolos and casein kinase 1 alpha, therefore impeding ternary complex formation and causing off-target effects.[37] The recruitment of E3 ligases may have different unwanted effects that need to be elucidated in control experiments.

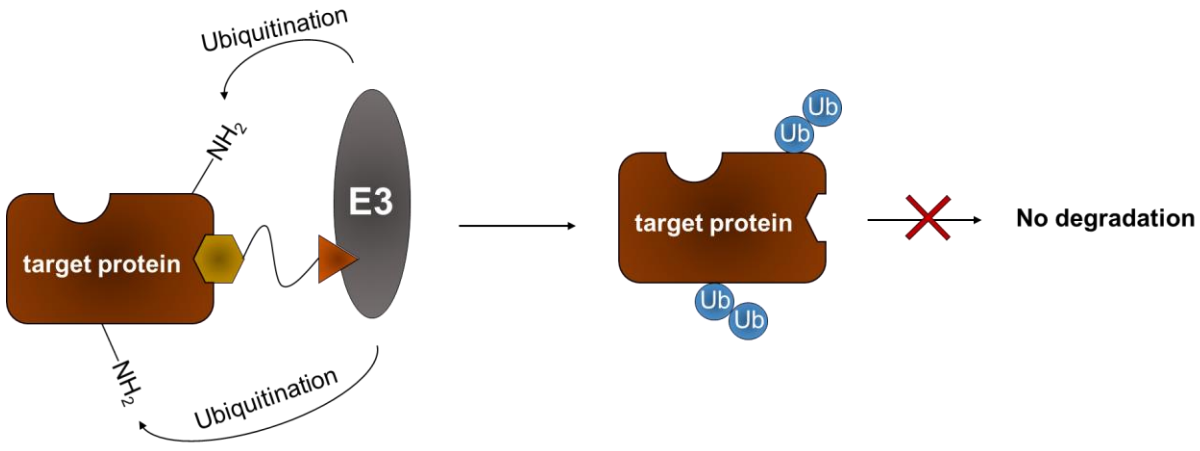

Figure 9: The formation of an unproductive ternary complex. The linker connecting the small-molecule ligand and the E3 ligase ligand is too ling, which leads to an unproductive complex formation. The ligase ubiquitinates many amino functionalities on the surface and is not restricted to one. Therefore, polyubiquitination does not occur and the target protein is not recognized by the proteasome. Ub: Ubiquitin.

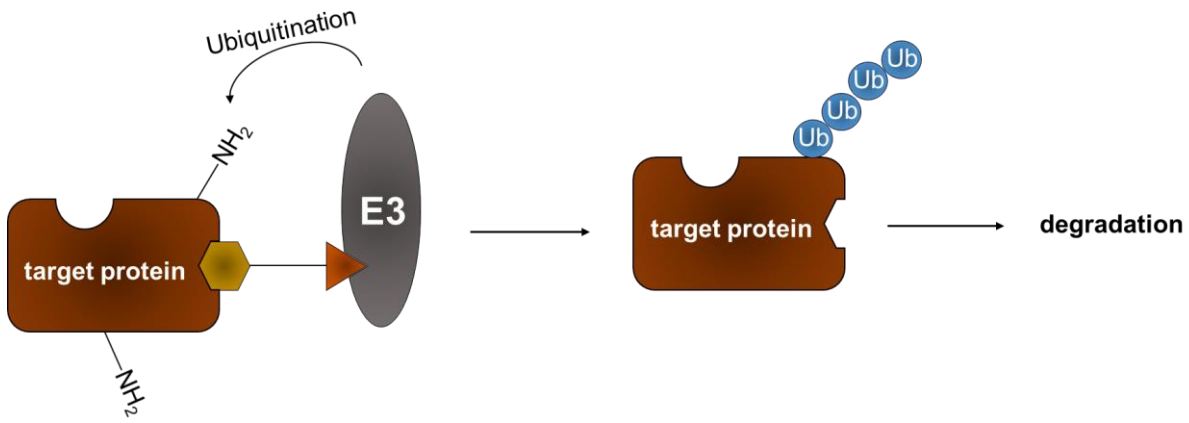

Figure 10: The formation of a productive ternary complex. The PROTAC consists of a linker, which restricts the E3 ligase to site. The target protein is polyubiquitinated and recognized by the proteasome, which leads to its degradation. Ub: Ubiquitin.

An efficient way to monitor off-target effects is to examine proteome-wide changes by proteomics when working with different E3 ligases. Comparison in changes of protein levels after the recruitment of different E3 ligases can be compared to elucidate the different impact of these E3 ligase ligands for a selected target.[38] In the future, additional E3 ligase ligands will be available and their cellular effects would be explored, making the selection for a certain E3 ligase ligand more rational.

In PROTACs, both ligands are connected via a linker, which induces proximity between the target protein and the E3 ligase. In order to ubiquitinate the target protein, a productive ternary complex rather than a complex with high affinity needs to be formed. An appropriate linker nature and length must lead to a correct distance and orientation between E3 ligase and target protein, allowing it to be ubiquitinated. Only if polyubiquitination occurs, will the target protein be recognized and degraded by the proteasome (Figure 9 and Figure 10). Not only the correct linker length and rigidity are crucial for the efficacy of a PROTAC. A linker can also promote membrane permeability and cooperative effects. For example, by choosing an alkyl linker over an ethylene glycol linker, hydrophobicity increases and can therefore enhance cell permeability. On the other hand, solubility decreases and non-specific binding of the PROTAC can occur. Many features need to be considered before choosing a linker. In addition, different linker types can interact with the target protein through hydrophobic interactions, thus sustaining ternary complex formation. Selecting the right linker type and length for the chosen set-up can support the properties of a PROTAC and its cellular efficacy.

Once the PROTAC is designed, several variants with different E3 ligase ligands and linker lengths and types are typically synthesized.

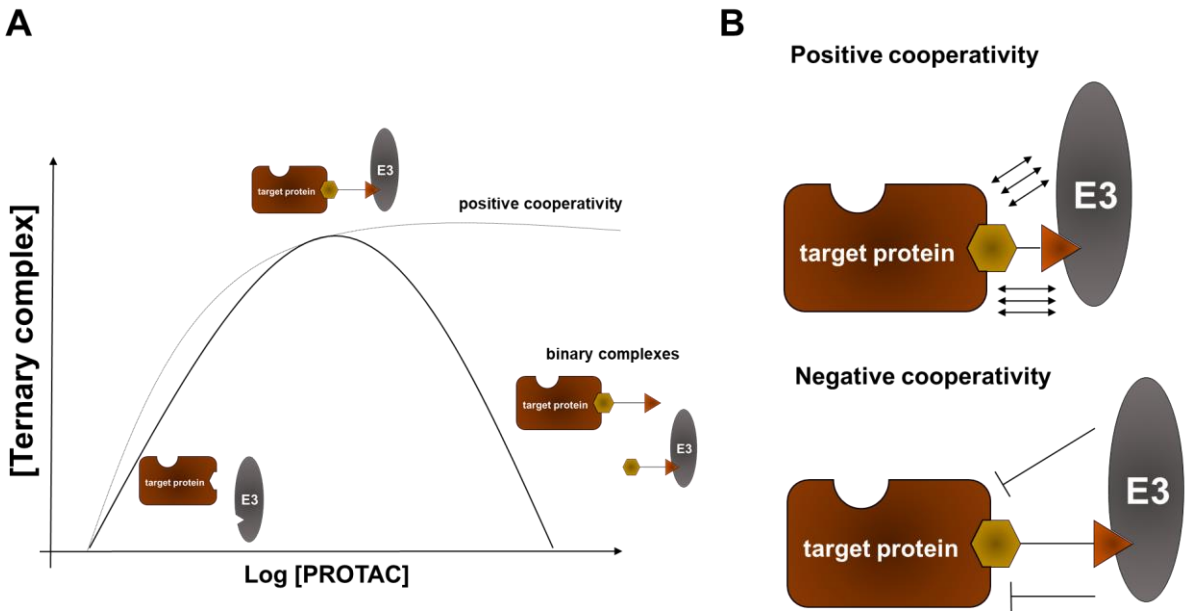

Figure 11: A mechanistic insights into PROTAC-mediated ternary complex formation. (A) The dependency of ternary complex formation on PROTAC concentration. The bell-shaped behavior is also known as the hook effect. (B) Interactions between the E3 ligase and a target protein can lead to positive and negative cooperativity. Ub: Ubiquitin.

Binding to the target protein and E3 ligase has to be verified using biophysical experiments such as fluorescence polarization, isothermal titration calorimetry or surface plasmon resonance prior to investigating cellular efficacy. The main difference between a chemical inhibition and a PROTAC-mediated protein degradation is the formation of a ternary complex. While in chemical inhibition higher concentrations lead to higher target occupancy and stronger inhibitory effect, higher PROTAC concentrations can lead to the opposite effect. Mathematical models describe this behavior and predict a bell-shaped dependency on PROTAC concentrations.[39] At high PROTAC concentrations, the formation of binary unproductive complexes is observed. This effect is known as the hook effect (Figure 11A).[40–42] However, cooperative effects triggered by protein-protein interactions between the E3 ligase and the target protein can support or prevent proper complex formation (Figure 11B).

It could be shown that positive cooperativity can minimize the negative result of the hook effect on the complex's productivity.[41] In general, cooperative effects can lead to increased selectivity. This was observed for MZ1, a PROTAC designed to degrade bromodomain-containing protein 4 (BRD4). The crystal structure revealed many interactions between BRD4 and the linker and it was shown that this leads to higher potency and selectivity between individual BRD family members.[42]

In order to streamline and accelerate PROTAC development, additional techniques and design strategies need to be implemented leading to a robust PROTAC discovery pipeline.[43,44] Therefore, new targets and E3 ligases are investigated, which will increase the toolbox for PROTAC design and eventually expand the knowledge in the field.

3.2 Motivation and Aim

The focus in the first part of this thesis was the design, synthesis and application of degradation-inducing compounds to influence the cellular function of PDEδ. It was shown that inhibiting the PDEδ-KRas interaction decreases oncogenic signaling and reduces cell growth. Several PDEδ-targeting agents were developed to target KRas signaling. Although these PDEδ inhibitors have picomolar affinities, cellular activity could only be seen at micromolar concentrations. This gap proved to result from the activity of the releasing-factor Arl2, which releases the PDEδ cargo. This circumstance raises the need for new potent PDEδ inhibiting agents, which do not rely on high target occupancy.

To overcome this problem, impairment of PDEδ function by chemical knockdown rather than chemical inhibition was envisioned. Chemical knockdown by targeted protein degradation relies on event-driven pharmacology and the negative influence of the releasing mechanism of Arl2 might decrease. PROTACs do not permanently need to occupy PDEδs binding pocket to execute its inhibitory effect. Therefore, new PROTACs should be designed and synthesized based on the last generation picomolar PDEδ inhibitor Deltasonamide 1. Subsequent biological evaluation of PDEδ degradation and proteome analysis should give new insights into PDEδs cellular function.

Furthermore, the concept of targeted protein degradation should be applied to transmembrane proteins. To test the applicability of the PROTAC methodology new compounds starting from recently reported glucose uptake inhibitors should be developed.

3.3 Results and Discussion

3.3.1 The design and synthesis of PDEδ-targeting PROTACs

Deltasonamide 1 was selected as suitable starting point as it is the most potent PDEδ binder developed so far.[14] It has a picomolar affinity for PDEδ and a known binding mode, facilitating the selection of the site for attachment of different linkers coupled to pomalidomide derivatives, which are known to bind the E3 ligase CRBN.

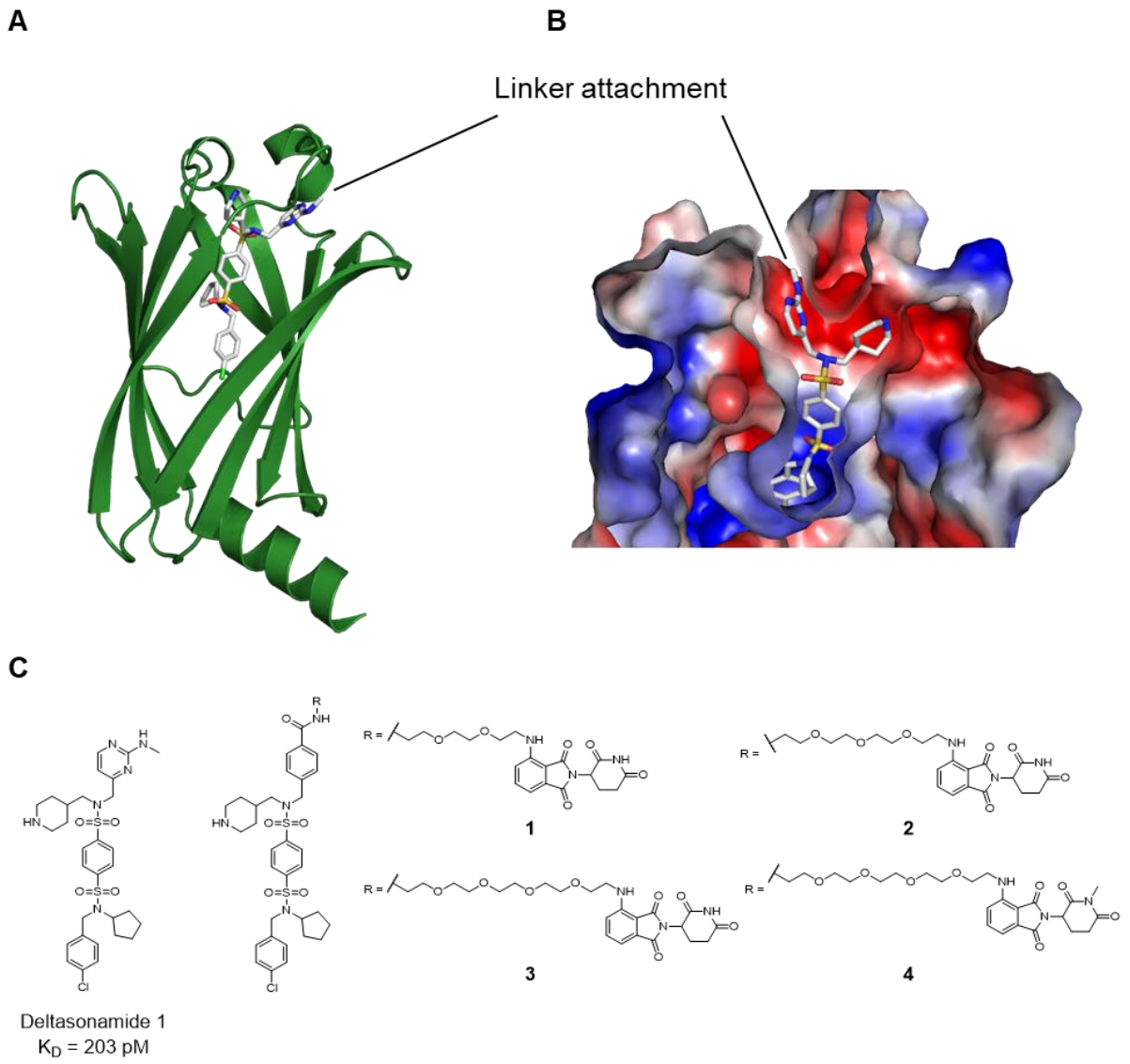

Figure 12: The design of PDEδ-targeting PROTACs. (A) Deltasonamide 1 in complex with PDEδ. PDB: 5ML3 (B) Opening of PDEδ binding pocket illustrated by the electrostatic surface. PDB: 5ML3. (A) and (B) Suitable site for linker attachment is shown. (C) Chemical structure of Deltasonamide 1. (D) Three different proposed PROTACs to target PDEδ bearing different linker lengths and an inactive probe unable to bind cereblon to obtain a negative control.

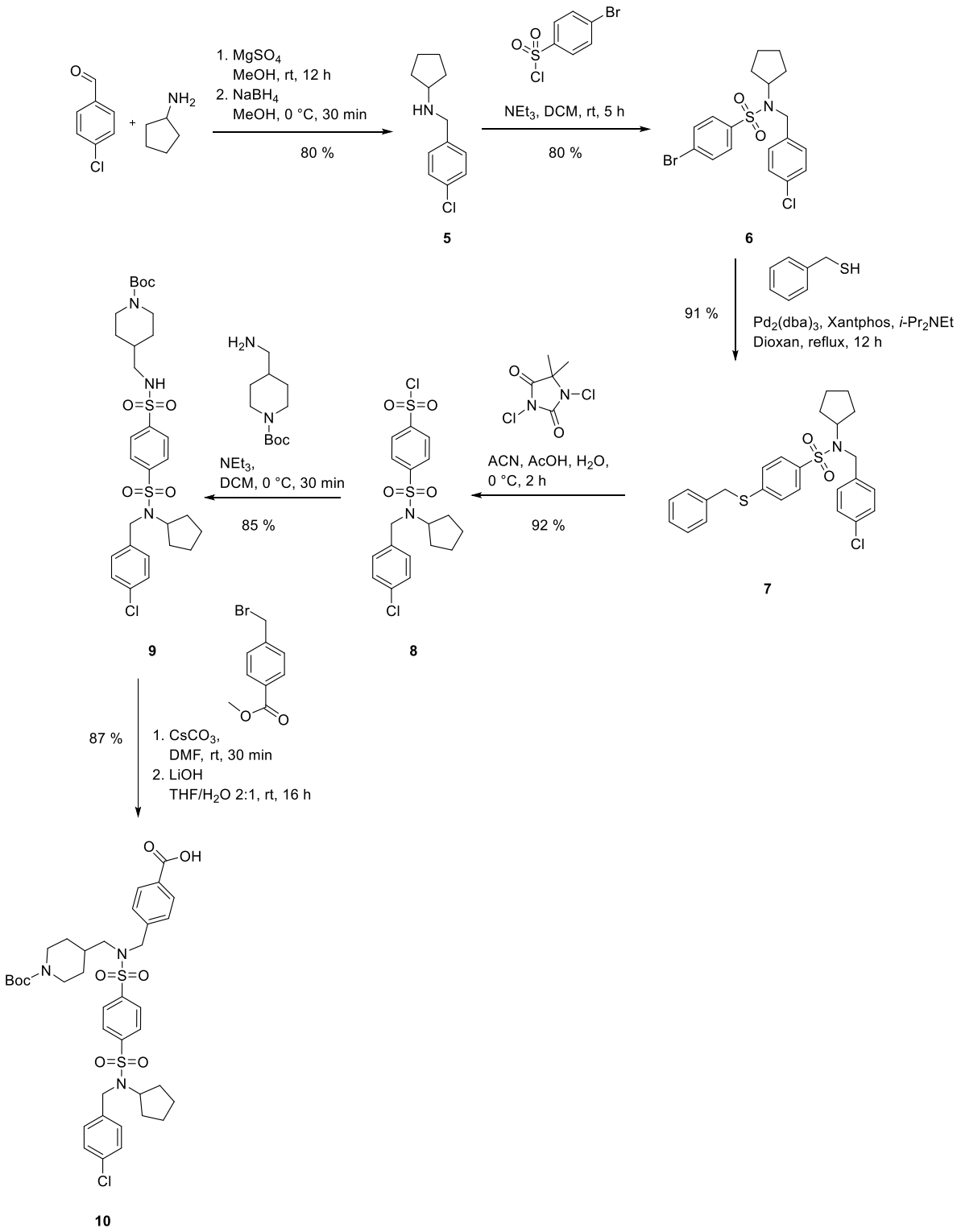

Figure 13: The synthesis of the PDEδ-binding part of the PDEδ-targeting PROTACs.

Previous studies showed that modifications of the aminopyrimidine part of Deltasonamide 1 were tolerated with regard to PDEδ affinity since this region points out of the opening of the prenyl binding pocket (Figure 12C). By replacing the aminopyrimidine heterocycle with a phenyl ring the affinity for PDEδ drops from 203 pM to 8 nM but leads to a more accessible point for the PROTAC synthesis (Figure 12).[14]

The PDEδ-binding part of the PROTAC was synthesized by starting with a reductive amination between cyclopentamine and 4-chlorobenzaldehyde (Figure 13). The corresponding secondary amine **5** was used to obtain the sulfonamide **6** by substitution of 4-bromobenzenesulfonyl chloride by the amine. The aromatic bromide was substituted with benzyl mercaptan in a palladium catalyzed manner. The resulting thiol **7** was transformed into the sulfonyl chloride **8** through treatment with 1,3-dichloro-5,5-dimethylhydantoin.[45]

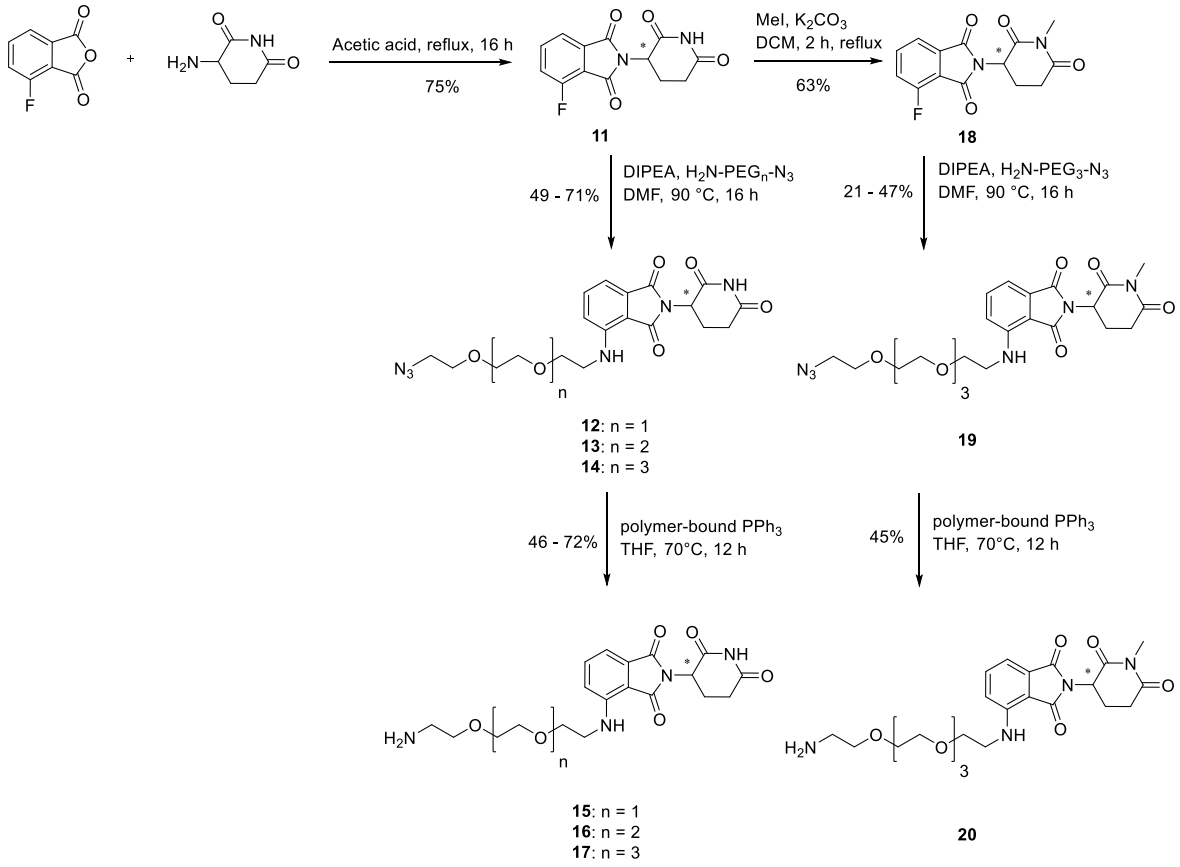

Figure 14: The synthesis of pomalidomide-based E3-ligase binders.

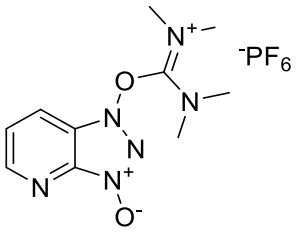

Hexafluorophosphate **A**zabenzotriazole **T**etramethyl **U**ronium

HATU

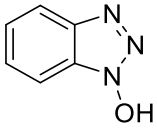

N-**H**ydr**o**xy**b**enzo**t**riazole

HOBt

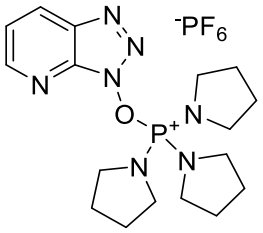

PyBOP

Figure 15: The different coupling reagents used to obtain the heterobifunctional PROTAC molecules.

The second sulfonamide **9** was generated through substitution of the electrophile **8** with a Boc-protected 4-aminopiperidine. The resulting product **9** was used in a nucleophilic substitution to obtain the carboxylic ester, which was hydrolyzed using lithium hydroxide to obtain the hydrolyzed product **10**. The carboxylic acid can undergo an amide coupling after activation with PyBOP with the E3 ligase recruiting part of the final molecule.

As the second functionality of the PROTAC it was planned to use a pomalidomide-based scaffold. The pomalidomide-based warhead was synthesized by condensation of fluorophthalic acid and aminopiperidinedione (Figure 14). The resulting fluorinated thalidomide analogue **11** was the starting point for the synthesis of active and inactive PROTACs. An inactive pomalidomide-based warhead was obtained by N-methylation of **11** to the fluoroaryl compound **18**. The methyl group abolishes the affinity of the ligand towards CRBN and therefore prevents ligase recruitment.[32] In the next step, the precursors **11** and **18** needed to be connected to a linker. This is a crucial part of the molecule, since PROTAC activity strongly depends on the linker length. Many properties rely on the correct linker length to maintain proper polyubiquitination (see paragraph 3.1.4).[44] Therefore, a set of compounds with different linker length was synthesized to analyze the effect of the spacer. To maximize the chances of PDEδs association to CRBN, the highly conformationally flexible oligoethylene glycol linker was chosen. The linker was attached to **11** or **18** through nucleophilic aromatic substitution. In the next step the azide moiety on the linker was reduced by a Staudinger reaction using a polymer-supported triphenylphosphine.

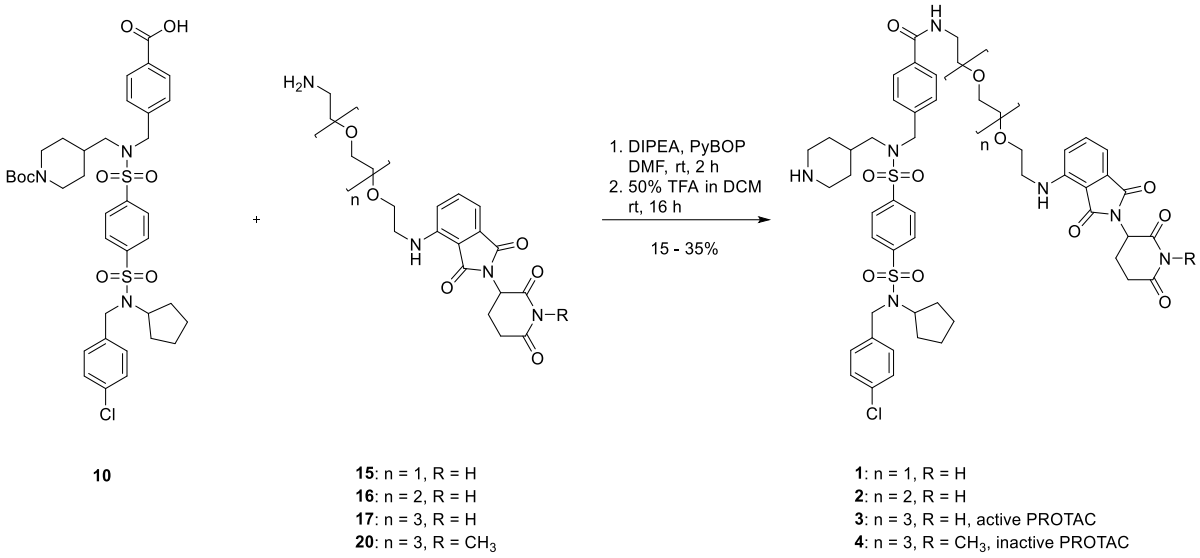

Figure 16: The coupling of the PDEδ binding part and an E3 ligase ligand to obtain heterobifunctional molecules.

In the last step of the synthesis, both parts of the heterobifunctional molecule were connected via an amide bond formation to obtain active and inactive PROTAC molecules. Different coupling reagents needed to be tested since the first attempts using HATU or HOBt failed to form the final product. Product formation was only observed using the more reactive coupling reagent PyBOP (Figure 15), probably due to the moderate nucleophilicity of the corresponding benzoic acid. Different activation reagents such as dicyclohexylcarbodiimide led to complex mixtures and were therefore unsuitable. In the final step, a Boc deprotection using 50% TFA in dichloromethane led to the desired products (Figure 16).

Three active PROTACs were successfully synthesized with different linker lengths (**1**, **2** and **3**) in addition to the respective inactive PROTAC **4** corresponding to the most active PROTAC **3** (see paragraph 3.3.3).

3.3.2 The characterization of PDEδ-PROTACs

Potential PDEδ-targeting PROTACs were designed and synthesized based on the picomolar PDEδ inhibitor Deltasonamide 1, which binds into the prenyl-binding pocket of PDEδ (paragraph 3.3.1). To investigate whether attachment of the linker to the inhibitor affects its affinity for PDEδ, a competitive fluorescence anisotropy assay was performed. The nanomolar PDEδ-binder atorvastatin coupled to FITC served as a tracer to determine the apparent binding constants of the PROTACs (Figure 17).[14]

Deltasonamide 1 forms up to 10 non-covalent interactions to PDEδ, which results in high *in vitro* affinities (K_D = 203 pM).[14] In comparison to that, the PROTACs form less non-covalent interactions, which leads to higher affinities. To investigate the binding affinities, PROTAC probes **3** and **4** were used to displace atorvastatin-FITC (K_D = 7.6 nM). Both probes show high apparent binding constants of 46.5 nM and 20.7 nM, respectively (Figure 17B), which is less potent than the parent compound Deltasonamide 1. It is assumed that the synthesized PROTACs bind less efficiently to PDEδ, in part because the aminopyrimidine ring that ensures strong binding via 3 H-bond interactions was replaced by a benzoic acid.

Previous studies showed that PDEδ is subject to the Arl2/3-mediated releasing mechanism, which releases low affinity cargos of PDEδ.[46,6] This needs to be considered when inhibiting PDEδ, because only picomolar inhibitors (Deltasonamide 1) have a higher resistance to be displaced by Arl2.[14]

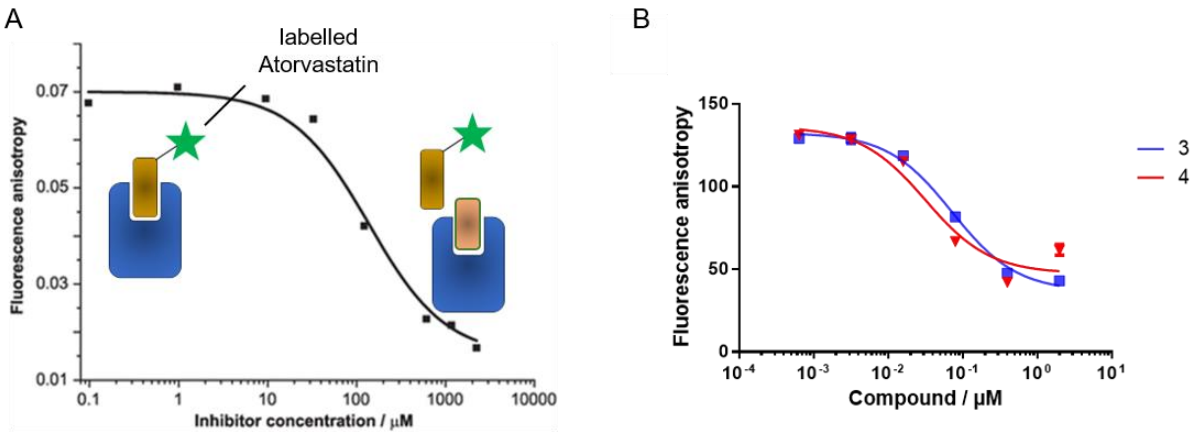

Figure 17: The competitive fluorescent polarization assay to determine the affinity of the probes to PDEδ. A) FITC-labelled atorvastatin was incubated with His_6-PDEδ and excited with polarized light. The polarization of emitted light changes upon displacement with competitors. This change is used to calculate an apparent binding constant. B) PROTAC probes **3** and **4** were titrated to compete FITC-labelled atorvastatin out of PDEδ pocket to determine apparent K_D values. Data are mean values ± SD (n=3). Non-linear regression was employed to obtain the binding constants: 46.5 nM for probe **3** and 20.7 nM for probe **4**.

Both PROTAC probes **3** and **4** bind to PDEδ with nanomolar affinities, i.e. lower affinities than Deltasonamide 1 and are therefore expected to be released from the PDEδ prenyl binding pocket by Arl2/3.

However, PROTAC efficacy is based on event-driven pharmacology, which does not rely on high target occupancy to impair protein function. PROTACs need to stay bound to the target as long as ubiquitination occurs. If the ternary complex between PDEδ, PROTAC and E3 ligase forms and induces ubiquitination, PDEδ will be degraded regardless of whether the PROTACs are released by Arl2/3. *In cell* degradation studies of PDEδ will indicate whether PDEδ-targeting PROTACs residence time is sufficient for PDEδ degradation.

Additionally, PROTACs show a catalytic mode-of-action. Once PDEδ is degraded, the inhibitor is released and can therefore induce the formation of a new ternary complex and ubiquitination. In theory, less amount of inhibitor is needed to impair PDEδ function. Therefore, lower binding affinities might be tolerated and degradation efficiency should be determined in cell-based experiments.

3.3.3 The characterization of the induced degradation of PDEδ by PROTACs

PROTACs cause the depletion of target proteins in cellular environment by hijacking the ubiquitination machinery. To investigate whether the synthesized PROTAC probes reduce cellular levels of PDEδ, Jurkat cells were treated with 1 µM of PROTAC **1**, **2**, **3** or DMSO for 24 h and 48 h and protein levels of PDEδ and the reference β-tubulin were determined by immunoblotting.

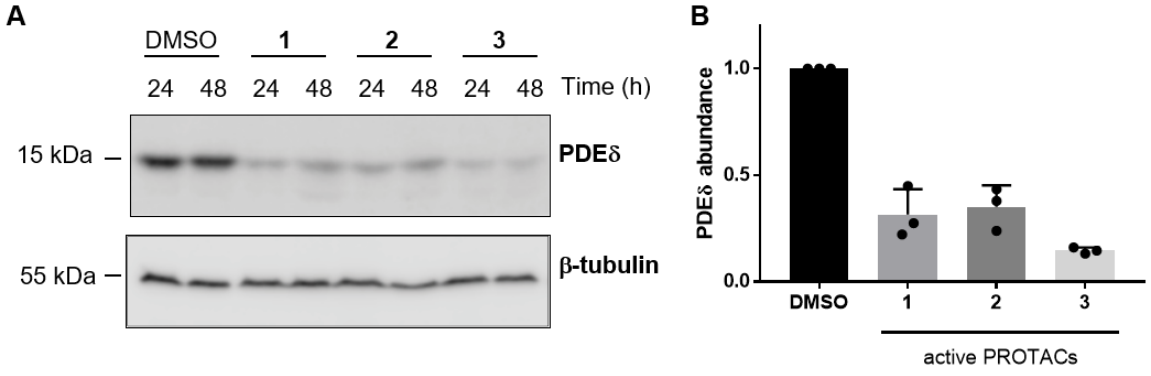

Figure 18: PDEδ degradation depends on the linker length in the PROTAC. (A) Jurkat cells were treated with 1 µM of PROTAC **1**, **2** or **3** or DMSO as a control. Then, cells were lysed and whole protein lysates were subjected to SDS-PAGE and subsequent immunoblotting. PDEδ and β-tubulin as a reference were visualized with specific antibodies. (B) Band intensities from A were quantified and normalized to the respective reference. Data are mean values ± SD (n=3) related to DMSO sample values.

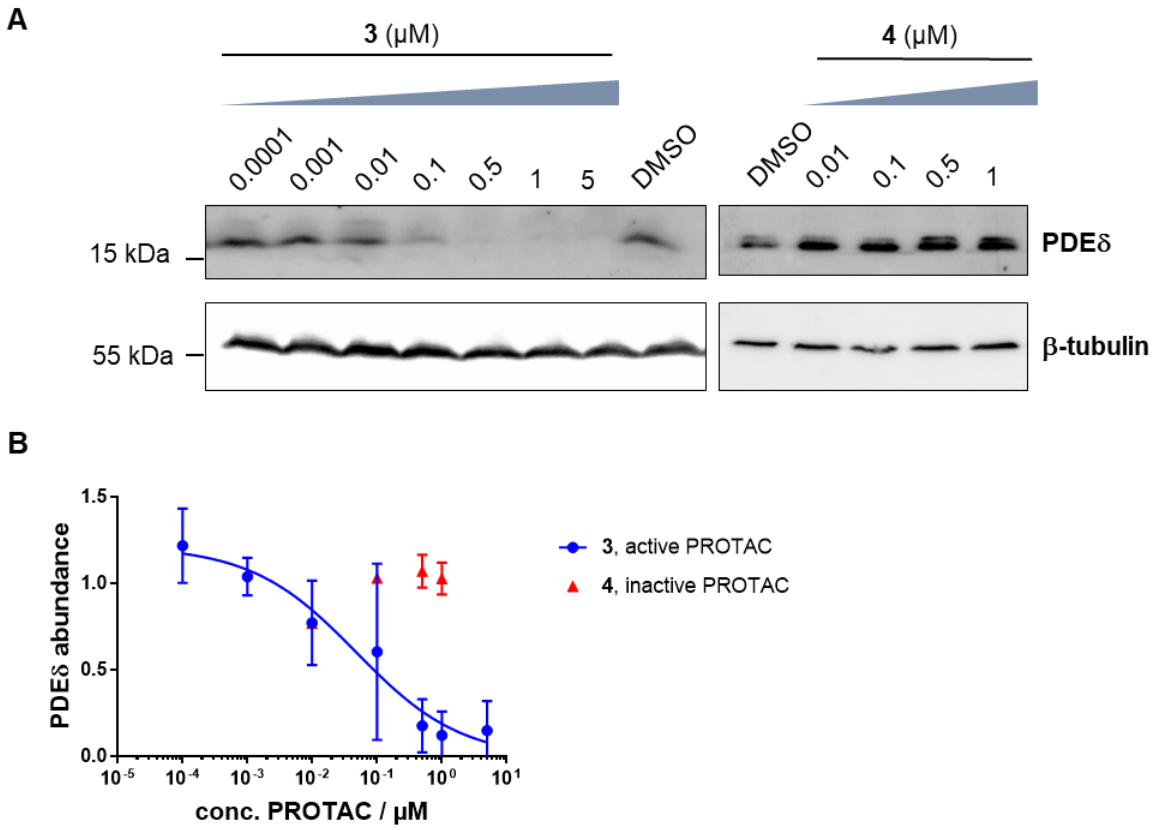

Figure 19: The concentration-dependent degradation of PDEδ by PROTACs. (A) Upon treatment of Panc Tu-I cells with PROTAC **3**, **4** or DMSO cellular protein levels of PDEδ and the reference β-tubulin were determined by immunoblotting. (B) Band intensities from A were quantified, normalized to the intensities of the bands of β-tubulin and then related to the values of DMSO, which was set to 1. Mean values ± SD of the band intensities (n=3) are shown. A non-linear regression line was calculated for PROTAC **3**-treated cells using Prism 7.

Protein depletion was induced with all three probes bearing different linker lengths with a maximal degradation efficacy (D_{max}) between 65% and 85%, and tetraethylene glycol was shown to be the most efficient linker. Additionally, lowered PDEδ levels could be sustained for 48 h with no significant difference in the D_{max} (Figure 18). The PROTAC with the longest linker **3** was the most efficient and, therefore, used for further characterization.

In order to determine the concentration dependence of PDEδ depletion by PROTACs was determined in the pancreatic cell line Panc Tu-I. These cells rely on oncogenic KRas signaling for proliferation, which can be reduced by inhibition of the interaction of PDEδ with KRas.[13,15] This makes Panc Tu-I a relevant cell line for testing PROTAC efficiency. Cells were treated with different concentrations of the most active PROTAC, i.e., PROTAC **3,** and the inactive PROTAC **4** for 24 h. A concentration-dependent degradation of PDEδ was induced, when cells were treated with PROTAC **3** with a D_{max} of 83.4%.

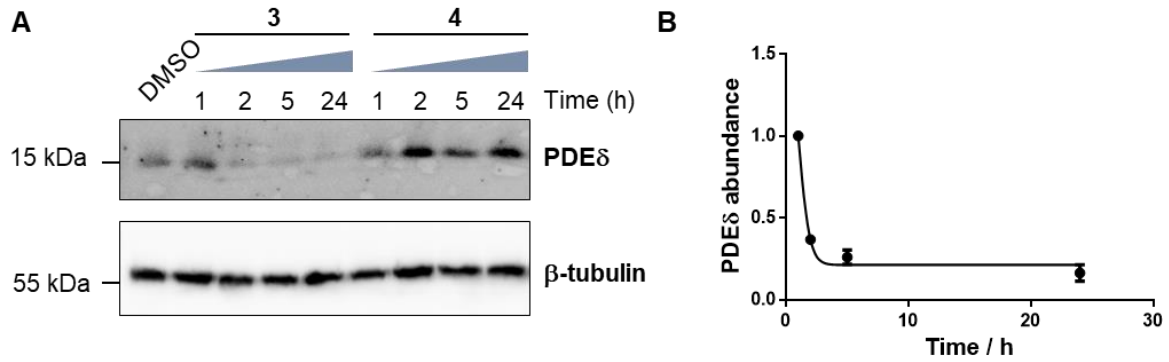

Figure 20: The rime-dependent degradation of PDEδ by PROTACs. (A) Panc Tu-I cells were treated with PROTAC **3**, **4** or DMSO and cellular PDEδ levels were determined by immunoblotting. (B) Band intensities for the treatment with PROTAC **3** from A were quantified, normalized to the intensities of the bands of β-tubulin and then related to the values of DMSO, which were set to 1. Data are mean values ± SD (n=3).

In contrast, when cells were treated with the inactive PROTAC **4**, which is unable to recruit an E3 ligase, PDEδ levels were not reduced (Figure 19A). PROTAC **3** reduced PDEδ levels with a half-maximal degradation concentration (DC_{50}) of 48 nM (Figure 19B).

To investigate the time course of the induced degradation Panc Tu-I cells were treated with 1 µM of the compounds for different time periods. Upon treatment with PROTAC **3** cellular PDEδ concentration reached a minimum after 5 h with 16.4% of residual PDEδ levels, which lasted for 24 h. In contrast, treatment with the inactive PROTAC **4** did not lead to degradation of PDEδ (Figure 20A and B).

PROTACs recruit an E3 ligase, which leads to a proximity-induced ubiquitination of the target protein. Ubiquitinated proteins are subject to proteasomal degradation, hence, blocking the proteasome should restore cellular protein levels upon treatment with a PROTAC. To investigate whether PDEδ degradation was sustained by the proteasome, the small molecule MG132 was used to block proteasome activity during treatment with PROTAC **3** (Figure 21A). PDEδ levels were restored upon co-treatment of Panc Tu-I cells with MG132 and PROTAC **3**, thus, decreased PDEδ levels result from proteasomal activity.

PROTACs derived from the PDEδ-binder Deltasonamide 1, which recruit the E3 ligase are able to degrade PDEδ in cellular environment. The most efficient PROTAC degrades PDEδ with a D_{max} of 85.4% and a DC_{50} of 48 nM and maintains reduced PDEδ levels for 24 h. The inactive PROTAC **4** does not reduce cellular PDEδ concentrations, thus, degradation relies on the recruitment of an E3 ligase and proximity-induced ubiquitination. Although the maximal degradation was already reached by treating the cells with 500 nM of PROTAC **3** for 24 h,

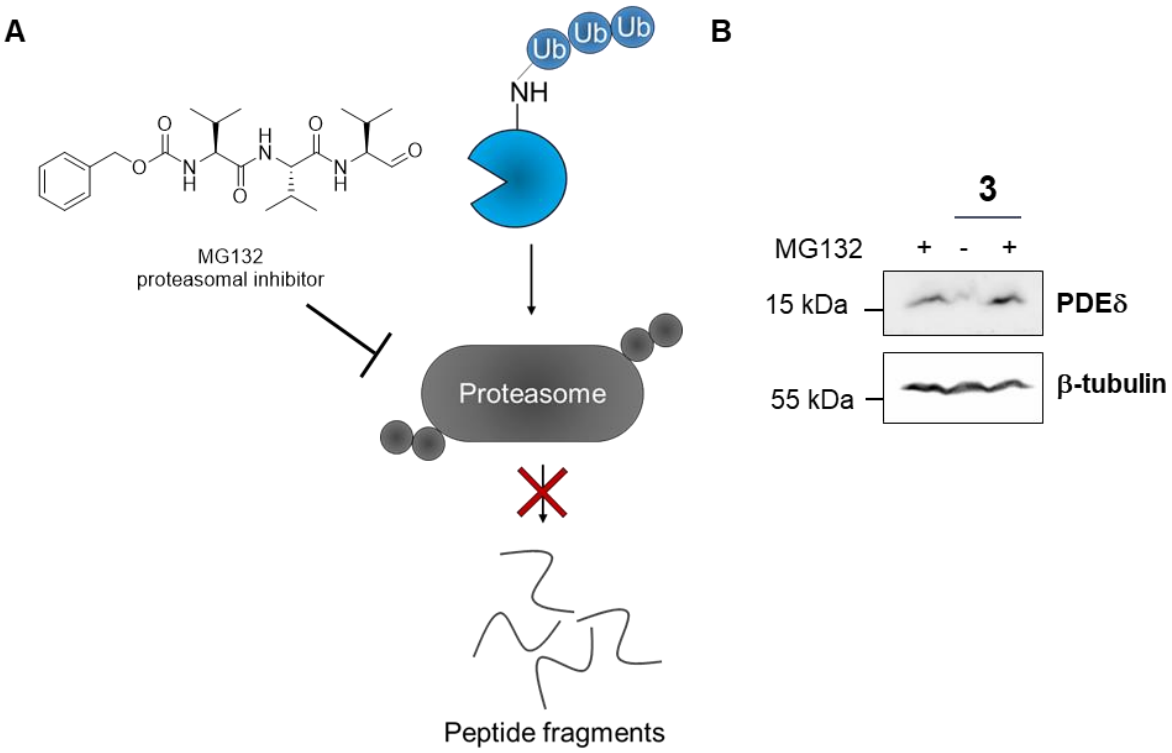

Figure 21: The PDEδ-degradation depends on the proteasomal activity. (A) Ubiquitinated proteins are subject to proteasomal degradation. MG132 is a proteasome inhibitor, which blocks proteasomal degradation. (B) Panc Tu-I cells were treated with 1 µM PROTAC **3** while blocking proteasomal activity with 10 µM MG132 a proteasome inhibitor. Cellular PDEδ levels were visualized by immunoblotting.

increasing the PROTAC concentration did not reduce PDEδ levels further. A reason for this could be the effect of the releasing-factor Arl2, which stabilizes the inactive conformation of PDEδ, thus, abolishing binding of the inhibitor. Although PROTACs lead to a chemical knockdown of proteins based on an event-driven pharmacology, they need to bind for a certain time frame to induce ubiquitination. If Arl2 was releasing the bound PROTACs off PDEδ before they could induce proximity-driven ubiquitination, PDEδ levels would be retained. This effect is even stronger when less PDEδ is present in the cell, since the ratio of Arl2 to PDEδ increases, which leads to higher fractions of PDEδ bound to Arl2. However, PDEδ could successfully be degraded by PROTAC **3**, and its function within the cell can be investigated upon chemical knockdown using these tool compounds.

3.3.4 The degradation of PDEδ fusion proteins

PROTACs cause the degradation of their respective targets and should also lead to degradation of proteins fused to the PROTAC target. This approach can be applied to fused reporter proteins such as luciferases or fluorescent proteins to characterize the degradation dynamics.

I generated a HeLa cell line stably expressing a NanoLuc luciferase-PDEδ fusion protein. NanoLuc activity was determined by treating the cells with the substrate furimazine, which was converted to furimamide with emission of light (luminescence). This luminescence signal was used as a direct read-out of the NanoLuc luciferase and thus, PDEδ levels (Figure 22A). HeLa-nanoLuc-PDEδ cells were treated with different concentrations of PROTAC **3** or **4** for 24 h prior to determination of the luciferase activity. While treatment with PROTAC **3** lowered luciferase activity in a concentration-dependent manner, inactive PROTAC **4** did not affect the activity of NanoLuc (Figure 22B). In the presence of active PROTAC **3** NanoLuc activity decreased until it reached a plateau at 30% residual activity. It is assumed that cellular NanoLuc levels are maintained by synthesis and degradation, which reaches a homeostasis when the induced degradation was as fast as the synthesis of the construct. This approach allows the analysis of PDEδ degradation in an easy and scalable approach (96-well plate or even 384-well format) since the NanoLuc detection system is highly sensitive and well established.

Furthermore, changes in the fluorescence of HEK293T cells transiently expressing a mCherry-PDEδ fusion protein upon treatment with the PDEδ PROTACs were monitored (Figure 23A).

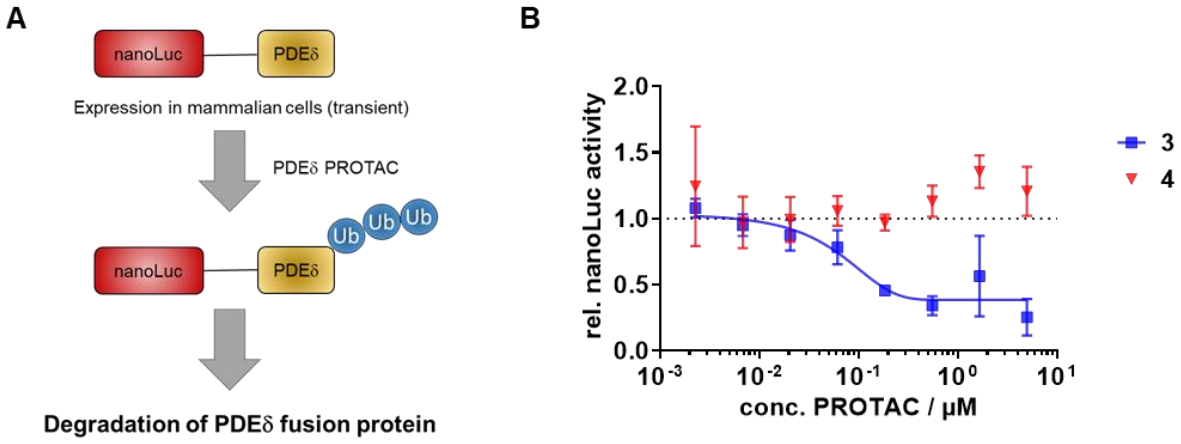

Figure 22: The degradation of NanoLuc-PDEδ fusion protein. (A) Schematic representation of PROTAC-induced NanoLuc-fusion protein degradation. HeLa cells stably expressing NanoLuc-PDEδ were treated with PDEδ PROTAC. This treatment leads to ubiquitination of PDEδ followed by degradation of the fusion protein. (B) HeLa cells expressing the NanoLuc-PDEδ fusion protein were treated with different concentrations of PROTAC **3**, **4** or DMSO and luciferase activity was measured after 24 h. Luminescence signals were normalized to the signal of DMSO-treated cells and set to 1. Data are mean values ± SD (n=3). Ub: Ubiquitin.

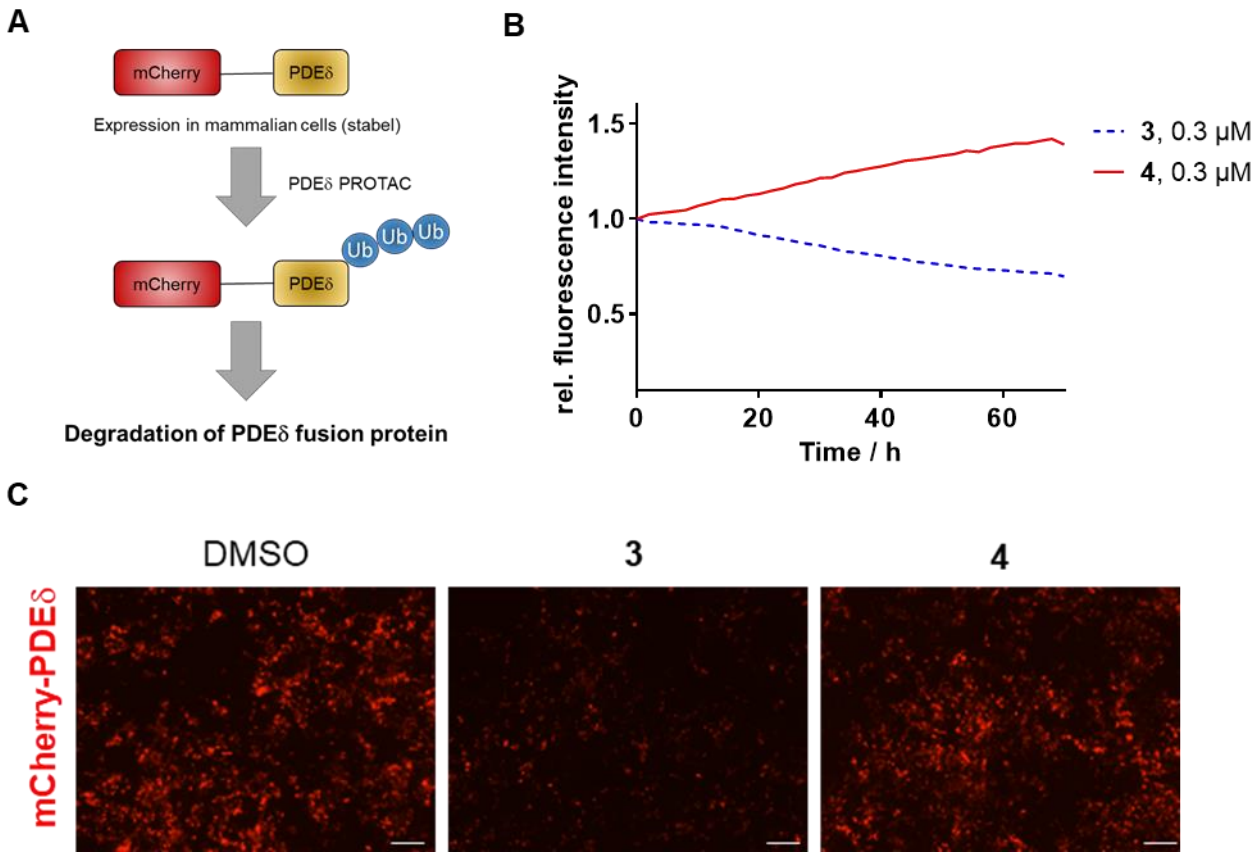

Figure 23: The degradation of mCherry-PDEδ PROTACs. (A) Schematic representation of PROTAC-induced mCherry-fusion protein degradation. Cells transiently expressing mCherry-PDEδ were treated with PDEδ PROTACs which lead to the ubiquitination of the fusion protein followed by its degradation. (B) HEK293T cells transiently expressing mCherry-PDEδ were treated with 0.3 µM PROTAC **3**, **4** or DMSO. Fluorescence was monitored over time using live-cell imaging and normalized to the fluorescence signal of DMSO-treated cells to the respective time, which was set to 1 at the beginning of the treatment. (C) Images of cells treated with PROTAC **3**, **4** or DMSO after 24 h. Scale bar: 100 µm, Ub: Ubiquitin.

Live-cell imaging offers the opportunity for real-time analysis of PDEδ degradation during the treatment with PDEδ PROTACs. Treatment of HEK293T cells, which were transfected with mCherry-PDEδ, with active PROTAC **3** led to a steady decrease of mCherry fluorescence, whereas treatment with inactive PROTAC **4** even increased the fluorescence signal over time (Figure 23B). After 65 h of treatment, the mCherry fluorescence decreased by 30 % compared to time point 0. Compared to the D_{max} of PDEδ PROTACs (D_{max} = 16.4%) for endogenous PDEδ, the D_{max} of the fusion protein is increased. This indicates that the strong overexpression of mCherry-PDEδ overloads the cellular recycling machinery and thus PROTACs efficiency was reduced.

PDEδ PROTACs successfully degrade fusion proteins of PDEδ such as luciferase-PDEδ and mCherry-PDEδ. Since the detection was in an artificial system due to overexpression of fusion proteins, the D_{max} differs compared to endogenous levels.

To overcome this problem, a weaker or inducible promoter can be used to find more appropriate conditions, which mimic endogenous PDEδ levels.

3.3.5 Proteome profiling of PDEδ PROTACs

Bioactive substances can impair cellular proteome following treatment. Degradation-inducing compounds cause downregulation of their respective targets. Therefore, proteome profiling was performed to determine the changes in the proteome upon treatment with PDEδ PROTACs.

Panc Tu-1 cells were treated for 24 h with PDEδ PROTACs **3** and **4** and Deltasonamide 1. Then, cells were lysed, and proteins digested into their respective peptides. These peptides were modified with isobaric tandem mass tags, which allow the proper quantification of protein levels by mass spectrometry. Unfortunately, MS analysis did not identify any PDEδ peptides, which are needed for identification and quantification. Reasons for this could be superpositions with more abundant peptides of other proteins. However, when HeLa cells were used for MS analysis, PDEδ showed strong signals. Following, HeLa cells were used for MS analysis of PDEδ PROTAC selectivity. Therefore, HeLa cells were treated for 24 h with PROTAC **3**, **4** or Deltasonamide 1 or DMSO as a control (Figure 24A and B).

From 4800 identified proteins in each data set, only PDEδ was significantly downregulated by PROTAC **3** (31.7%) compared to the DMSO control. Treatment with the inactive PROTAC **4** or Deltasonamide 1 caused slight upregulation of cellular PDEδ protein levels, i.e. +11% and +10%, respectively (Figure 24C). These results indicate that PROTAC **3** is highly selective for PDEδ degradation. Interestingly, several proteins were upregulated in PROTAC **3**-treated cells (appendix Table 7). The 30 most upregulated proteins were subjected to a reactome analysis tool to determine overrepresented pathways.[47] The analysis revealed highly significant overrepresentation (p-value < $1.1*10^{-16}$) of proteins regulated by the sterol regulatory element binding protein (SREBP) and related pathways such as cholesterol and lipid metabolism (Table 2). From the analyzed proteins, 18 entries had been clustered to be involved in SREBP-dependent regulation of cholesterol biosynthesis and 25 entries had been clustered to be involved in lipid metabolism in general.

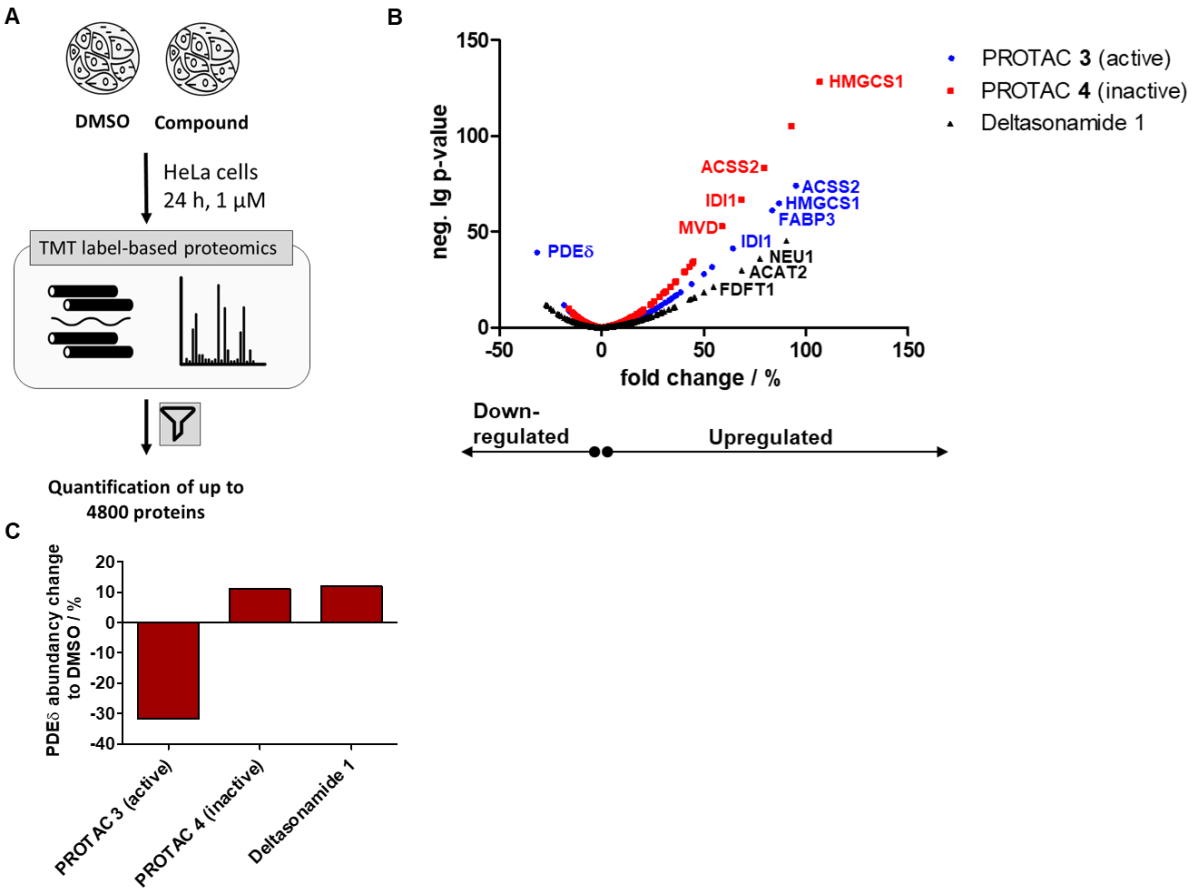

Figure 24: Proteomic changes upon treatment with PDEδ PROTACs and Deltasonamide 1. (A) Experimental procedure for proteome profiling. HeLa cells were treated with 1 µM of PROTAC **3**, **4** or Deltasonamide 1 or DMSO as a control for 24 h and subjected to TMT-labelling followed by mass spectrometry. (B) Up to 4800 protein were identified and quantified. Each dot represents the mean p-value vs. the change in abundance (n=3). (C) HeLa cells were treated with 1 µM of PROTAC **3**, **4** or Deltasonamide 1 for 24 h, followed by protein level determination by mass spectrometry. Quantified protein levels of PDEδ are shown for cells that were treated with the respective compound.

More precisely, most of these proteins are enzymes and are involved in the cholesterol biosynthesis, in particular hydroxymethylglutaryl-CoA synthase (HMGCS1, +87%), acetyl-coenzyme A synthetase (ACSS2, +95%), diphosphomevalonate decarboxylase (MVD, +36%), isopentenyl-diphosphate delta-isomerase 1 (IDI1, 64%), which are responsible for isoprenoid synthesis from acetyl-CoA (appendix Figure 49). Apart from enzymes involved in lipid metabolism, additional proteins were identified as upregulated in all three experiments, e.g. amyloid beta A4 protein (APP, +54%), ethanolamine-phosphate cytidylyltransferase (PCYT2, +24%), WW domain-binding protein 2 (WBP2, +28%) and cob(I)yrinic acid a,c-diamide adenosyltransferase (MMAB, +22%). An interactome analysis using the STRING tool did not reveal a connection between these proteins and PDEδ (appendix Figure 48).[48]

Table 2: The overrepresented pathway determined by the reactome analysis tool. The reactome analysis of the 30 most upregulated proteins in HeLa cells upon treatment with 1 µM of PROTAC **3**, **4** or Deltasonamide 1 for 24 h. Values are p-values which indicates how significant the result is.

	p-value		
Pathway name	PROTAC **3**	PROTAC **4**	Deltasonamide 1
Activation of gene expression by SREBF (SREBP)	$1.1*10^{-16}$	$1.1*10^{-16}$	$1.2*10^{-3}$
Regulation of cholesterol biosynthesis by SREBP (SREBF)	$1.1*10^{-16}$	$1.1*10^{-16}$	$1.2*10^{-3}$
Metabolism of steroids	$1.1*10^{-16}$	$1.1*10^{-16}$	$1.2*10^{-3}$
Cholesterol biosynthesis	$2.0*10^{-14}$	$3.9*10^{-11}$	-
Metabolism of lipids	$1.5*10^{-14}$	$4.7*10^{-10}$	$2.2*10^{-2}$
Metabolism	$2.8*10^{-7}$	$6.5*10^{-8}$	$2.2*10^{-2}$

When treated with PROTAC **3**, **4** or Deltasonamide 1, protein levels of enzymes of the lipid metabolism are impaired in HeLa cells as revealed by MS analysis. The effect is not pronounced for PROTAC **3** and was also seen in cells treated with PROTAC **4** and Deltasonamide 1. This implies that a standard chemical inhibition of PDEδ mediates this influence. The effect on lipid metabolism seems to depend either on the chemical inhibition of PDEδ or on unknown additional targets of the chemotype (for more details see paragraph 3.3.7).

3.3.6 The upregulation of enzymes of the lipid metabolism

The proteome profiling experiments revealed that after treatment with bisulfonamide-based PDEδ-targeting modalities, protein levels of enzymes of the lipid metabolism were elevated. To confirm the mass spectrometry-based results, immunoblotting experiments were performed. Therefore, HeLa cells were treated with 1 µM of PROTAC **3**, **4**, Deltasonamide 1 or DMSO and cell lysates were subjected to SDS-PAGE, followed by immunoblotting. HMGCS1 was chosen as reference since it was identified as strongly upregulated (+87%) in the proteome profiling experiments and is regulated by SREBP (Figure 24 and appendix Figure 49). Treatment with PROTAC **3**, **4** and Deltasonamide 1 led to elevated HMGCS1 levels with the strongest increase detected for Deltasonamide 1 and PROTAC **4** (Figure 25A). The compounds increased HMGCS1 protein levels to a different extent, which could result from different binding affinities to PDEδ, i.e. Deltasonamide 1 (K_D=203 pM), PROTAC **4** (K_D=20.8 nM) and PROTAC **3** (K_D=46.5 nM).

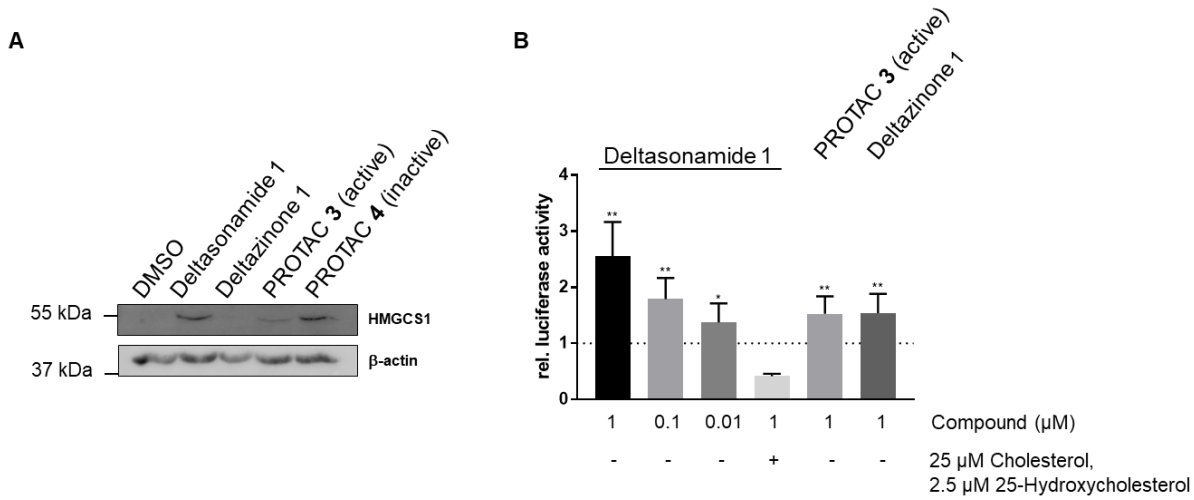

Figure 25: The influence of PDEδ-targeting modalities on lipid metabolism. (A) HeLa cells were treated with 1 μM of the compounds for 24 h and lysates were subjected to immunoblotting to detect protein levels of HMGCS1 and β-actin a reference protein. (B) HeLa cells were transfected with a firefly luciferase under the transcriptional control of SRE. Additionally, a *Renilla* luciferase under the control of a housekeeping gene was co-transfected and used for normalization. After treatment with the compounds and oxysterols luciferase activity was measured. Values were normalized to the value for the *Renilla* luciferase and DMSO-treated cells, which was set to 1. Data are mean values ± SD (n=3). *: $p \leq 0.05$, **: $p \leq 0.01$, ***: $p \leq 0.001$.

The influence on SRE-dependent transcriptional activation was investigated. As revealed by the reactome analysis, many of the upregulated enzymes are under the transcriptional control of the sterol regulatory element (SRE), which is bound by sterol regulatory element-binding protein (SREBP). In its inactive form, SREBP is located at the endoplasmic reticulum in a ternary complex with sterol regulatory element-binding protein cleavage-activating protein (SCAP) and insulin-induced gene 1 protein (INSIG-1). At low cellular cholesterol levels, SCAP undergoes a conformational change, which leads to the dissociation of INSIG-1. Then, SREBP and SCAP are transported via COP-II vesicles to the Golgi. In the membrane of the Golgi, SREBP is cleaved twice resulting in a cytosolic form, which is translocated by importin β to the nucleus. In the nucleus, SREBP binds with other transcription factors to SRE and induces transcription of genes involved in cholesterol biosynthesis, e.g. *ACSS2* and *HMGCS1* (Figure 26).[49]

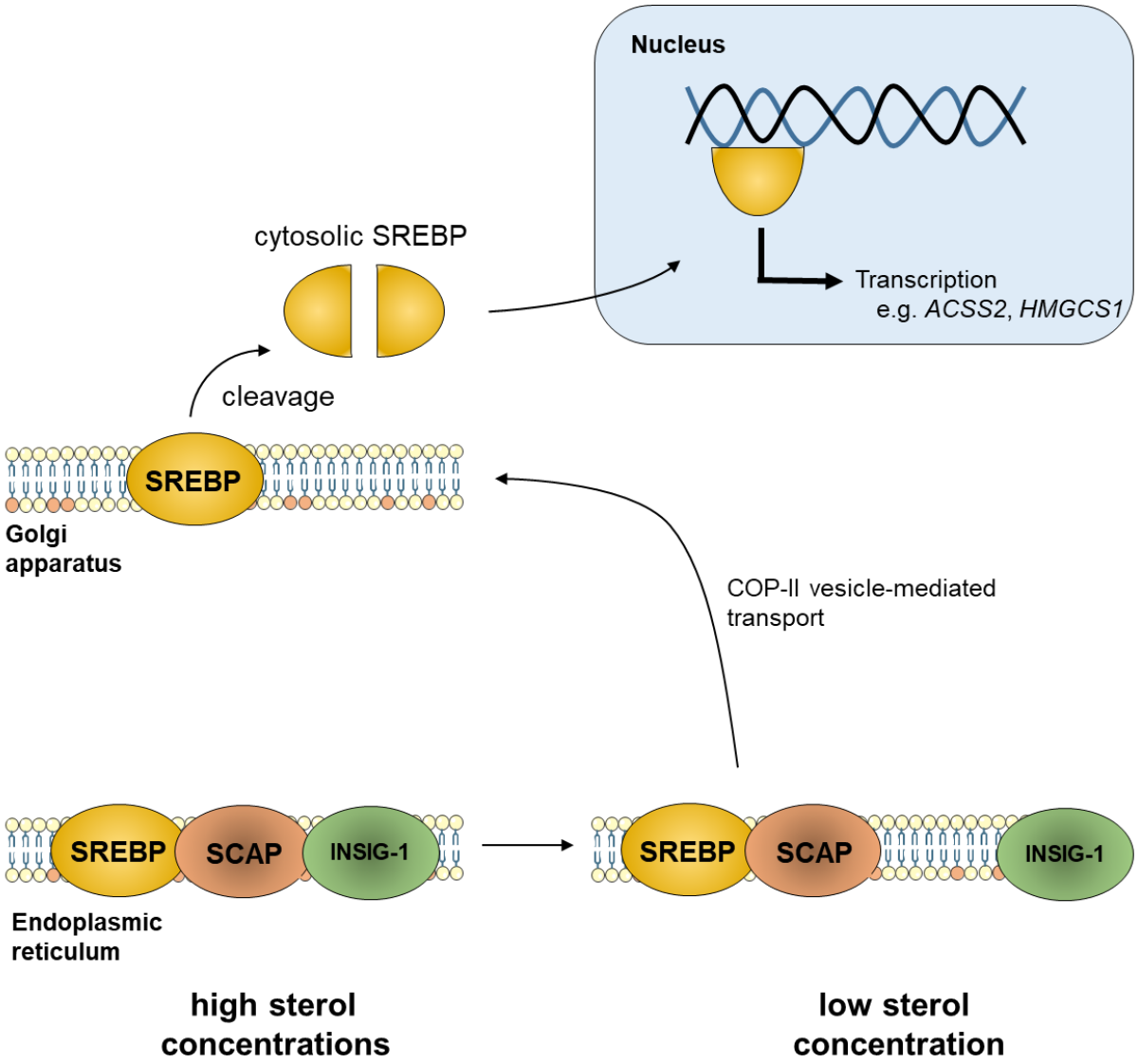

Figure 26: The activation of SREBP-dependent transcription. At high cellular sterol concentrations SREBP, SCAP and INSIG-1 are located at the endoplasmic reticulum. When sterol levels drop, INSIG-1 dissociates from the ternary complex and SREBP is transported to the Golgi apparatus via COP-II vesicle-mediated transport. At the Golgi SREBP is cleaved into its cytosolic form. This form is translocated into the nucleus where it activates the transcription of *ACSS2*, *HMGCS1* and other genes involved in lipid metabolism. SREBP: sterol regulatory element-binding protein; SCAP: Sterol regulatory element-binding protein cleavage-activating protein; INSIG-1: Insulin-induced gene 1 protein; ACSS2: Acetyl-coenzyme A synthetase *HMGCS1*: Hydroxymethylglutaryl-CoA synthase.

To address the question whether the upregulation on the mevalonate pathway enzymes by Deltasonamide 1 and PDEδ PROTACs **3**, **4** was caused by activation of SRE, a SRE-dependent reporter gene assay was established. Therefore, HeLa cells were transfected with a firefly luciferase under the transcriptional control of SRE and a constitutively expressed *Renilla* luciferase as reference. HeLa cells were treated 24 h after transfection with PROTAC **3**, **4**, Deltasonamide 1 or DMSO for 24 h followed by luciferase activity determination.

A

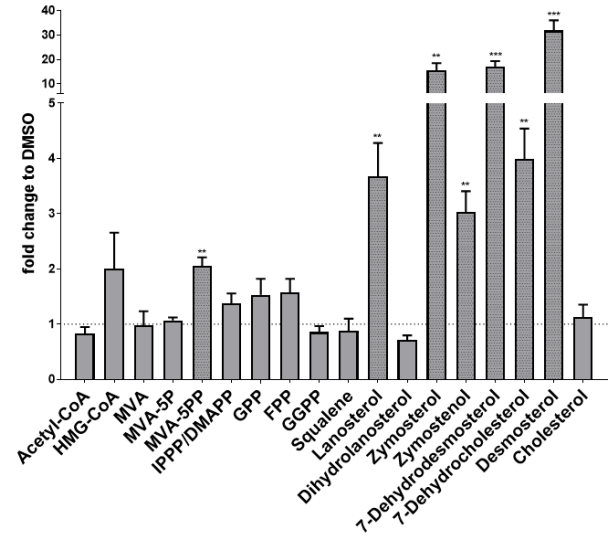

B

	DMSO	Deltasonamide 1	
	c (nmol/mg)	c (nmol/mg)	fold change
MVA-5PP	1.60	3.30	2.1
Lanosterol	0.73	2.67	3.7
Zymosterol	0.32	4.99	15.5
Zymostenol	2.73	8.27	3.0
7-Dehydrodesmosterol	1.41	23.96	17.0
7-Dehydrocholesterol	0.57	2.26	4.0
Desmosterol	1.72	54.86	31.9
Cholesterol	4752.40	5356.16	1.1

Figure 27: The influence of PDEδ-targeting modalities on lipid metabolite levels. (A) HeLa cells were treated with 1 µM Deltasonamide 1 for 24 h. Extracted metabolites were quantified by mass spectrometry. Values were normalized to the value of DMSO-treated cells to obtain fold changes. (B) Absolute values of metabolite quantification. MVA: Mevalonic acid, IPPP: Isopropyl pyrophosphate, HMG-CoA: 3-Hydroxy-3-methylglutaryl-CoA, DMAP: Dimethylallyl pyrophosphate, GPP: Geranyl pyrophosphate, FPP: Farnesyl pyrophosphate.

A concentration dependent activation of the SRE-promoter upon treatment with Deltasonamide 1 of 2.5-fold at a concentration of 1 µM and a weaker activation upon treatment with 1 µM PROTAC **3** of 1.5-fold were observed. To investigate whether the PDEδ-inhibitors act upstream or downstream of SREBP, cells were simultaneously treated with 25 µM cholesterol, 2.5 µM 25-hydroxycholesterol and 1 µM of the compounds (Figure 25B). No activation of the promotor under these conditions was observed, suggesting a mode-of-action upstream of SREBP. Since increased levels of enzymes of the lipid metabolism should also have an influence on lipid metabolites, HeLa cells were treated with 1 µM Deltasonamide 1. Metabolites were extracted with organic solvents and quantified by using reference standards and mass spectrometry. The analysis revealed elevated levels for mevalonic acid-5-pyrophosphate (MVA-5PP, 2.1-fold), lanosterol (4-fold), zymosterol (16-fold), zymostenol (3-fold), 7-dehydrodesmosterol (17-fold), 7-dehydrocholesterol (4-fold) and desmosterol (32-fold) upon compound treatment (Figure 27A and B). Thus, treatment of cells with Deltasonamide 1 leads to accumulation of cholesterol biosynthesis intermediates but not cholesterol. In DMSO-treated cells, cholesterol precursors are present at low concentrations, i.e. 4752.4 nmol/mg.

In contrast, the cholesterol concentration in Deltasonamide 1-treated cells was 1.1-fold higher, i.e., 5356.16 nmol/mg. The cholesterol concentration may not be further increased upon treatment with Deltasonamide 1, and therefore does not increase significantly.

In summary, bis-sulfonamide-based PDEδ-inhibitors elevated the levels of proteins involved in the lipid metabolism and of intermediates of cholesterol biosynthesis. Although these inhibitors bind PDEδ with low nanomolar or picomolar affinities, different binding partners than PDEδ can not be excluded. The used concentration in MS analysis experiments was 1 µM and is three to four orders of magnitude higher than the *in vitro* affinities for PDEδ, thus if this is a PDEδ- or chemotype-mediated phenotype remains to be answered (detailed discussion in paragraph 3.3.7).

3.3.7 The PDEδ- vs. chemotype-mediated phenotype

Cells treated with bis-sulfonamide-based PDEδ inhibitors showed increased levels of enzymes involved in lipid metabolism and accumulation of cholesterol precursors. An analysis by the online tool STRING, which covers known and predicted protein-protein-interactions, indicates that no connection is known between PDEδ and the regulation of lipid enzymes or metabolites. To address the question of whether this effect is based on PDEδ inhibition or the bis-sulfonamide chemotype, PDEδ-targeting agents of a different chemotype were used. Therefore Deltazinone 1 was chosen, which is based on a pyrazolopyridazinone scaffold and binds into PDEδs prenyl-binding pocket with a K_D of 8 nM (Figure 28).[15]

To investigate whether Deltazinone 1 has an influence on lipid metabolism, analogous experiments to those carried out with Deltasonamide 1 and PROTACs **3** and **4** were performed. HeLa cells were treated with 1 µM Deltazinone 1 followed by immunoblotting to indicate changes in cellular HMGCS1 levels as seen after treatment with Deltasonamide 1 and PROTAC **3** and **4**. No increased cellular protein levels could be detected after Deltazinone 1 treatment (Figure 25A). The reason for this could either be the low sensitivity of the immunoblotting or the missing effect on lipid metabolism. When HeLa cells were treated with DMSO, no HMGCS1 protein could be detected although it was identified in the proteome profiling. HMGCS1 was only identified, when cells were treated with Deltasonamide 1, PROTAC **3** or **4**. If Deltazinone 1 had an influence on enzymes involved in lipid metabolism, it could be so low that it did not cross the detection limit of the assay. To investigate whether the compound has an influence on transcription, a more sensitive assay needed to be performed. Since the SRE-dependent reporter gene assay showed increased transcription after treatment with Deltasonamide 1 even at 100 nM, this assay might be sensitive enough to detect an influence of Deltazinone 1 on lipid metabolism (see paragraph 3.3.6).

HeLa cells transfected with a SRE-dependent firefly luciferase were treated with 1 µM of Deltazinone 1. After 24 h, a significant increase in luciferase activity was detected (Figure 25B).

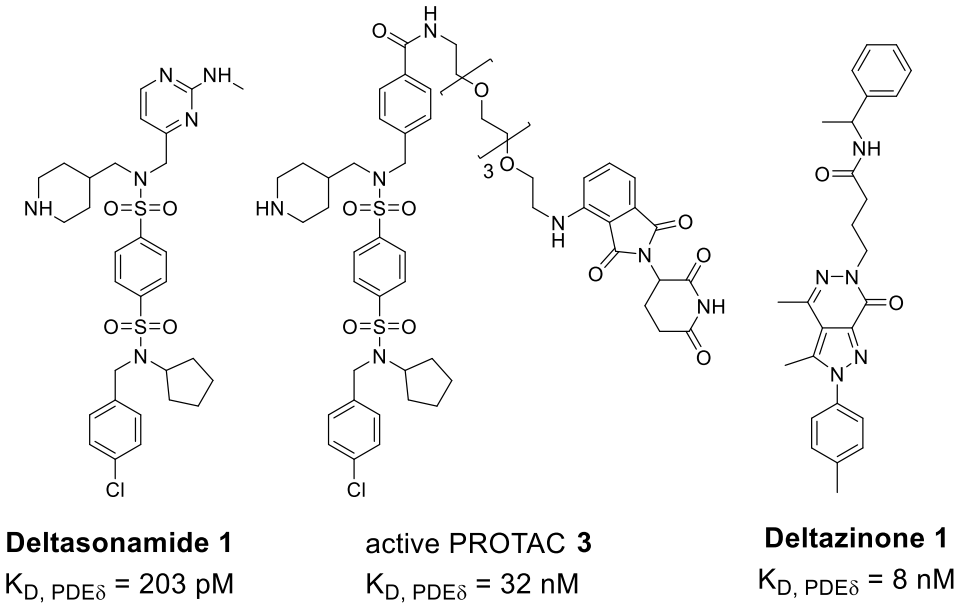

Figure 28: The structures of PDEδ-inhibiting molecules.

While Deltazinone 1 treatment did not show increased HMGCS1 levels, SRE-dependent transcription was stimulated. The different binding constants of both chemotypes could be the reason for different outcomes in the assays. Bis-sulfonamide-based compounds are less pronounced subjects of Arl2-releasing mechanism compared to Deltazinone 1. This leads to a lowered residence time of Deltazinone 1 and less inhibition at PDEδ.[14] Thus, Deltazinone 1 is less efficient than Deltasonamide 1, PROTAC **3** and **4** and has a lower influence on lipid metabolism.

Nevertheless, these results support the hypothesis that PDEδ inhibition and not reduction in PDEδ levels cause the influence on lipid metabolism. Lowered cellular PDEδ concentrations did not have a stronger influence on the level of proteins of the lipid metabolism, although a combinatorial effect of chemical knockdown and chemical inhibition occurs. A PROTAC is still a chemical inhibitor of PDEδ. The remaining 14.6% of cellular PDEδ could be sufficient to sustain PDEδ-dependent cellular function, thus, the remaining PDEδ cannot be targeted by PROTACs because of the low cytoplasmic bioavailability of 0.6% as seen for Deltasonamide 1 (Table 3).[14] However, whether PROTACs efficiency also suffers from low cytoplasmic bioavailability needs to be shown in further experiments.

Table 3: The summary of biological effects of PDEδ-targeting agents.

	Deltasonamide 1	Active PROTAC, 3	Inactive PROTAC, 4	Deltazinone 1
Chemotype	Bis-sulfonamide	Bis-sulfonamide	Bis-sulfonamide	Pyrazolopyridazinones
$K_{D,\ PDE\delta}$	203 pM	46.5 nM	20.7 nM	8 nM
PDEδ, D_{max}	unknown	85.4%	no	unknown
Upregulation of HMGCS	strong	weak	strong	no
SRE-activation	strong	weak	unknown	weak
Arl2-releasing *in vitro*	no	unknown	unknown	yes

As only one out of several experiments indicates a PDEδ-mediated phenotype, a different interpretation of the results needs to be considered. A chemotype-mediated phenotype could be based on off-target effects of the bis-sulfonamide scaffold of Deltasonamide 1, PROTAC **3** and **4**. To address the selectivity of Deltasonamide 1, previous studies used thermal proteome profiling.[14] Even though thermal proteome profiling (TPP) showed high selectivity of Deltasonamide 1 towards PDEδ, stabilization of proteins by chemical entities upon thermal treatment is different to chemical inhibition.[14,50] TPP relies on the concept that ligand binding interferes with protein stability during thermal unfolding. Inhibitors can bind to targets without having any effect on protein thermal stability and vice versa, thus, cannot be identified in TPP experiments. When Deltasonamide 1 was used in TPP, only 60S ribosomal protein L31 (RPL31) was stabilized by the compound. Since no link was found between lipid metabolism and RPL31, and ribosomal proteins often occur as false positive hits, RPL31 was excluded as hit. However, to confirm the selectivity profile of Deltasonamide 1, small-molecule pulldown experiments could be performed, thus, elucidating new targets connected to the regulation of enzymes in the lipid metabolism.

In parallel, RNA-mediated knockdown of PDEδ can be performed to investigate the influence of PDEδ depletion on lipid metabolism. However, knockdown efficiency needs to be higher than 84.6% to exclude remaining PDEδ activity as seen in previous studies.[15,14] If these experiments reveal a PDEδ-mediated influence on lipid metabolism, new interaction partners or functions of those need to be considered and investigated.

3.3.8 The influence of PDEδ inhibition on SREBP activation

The ROS accumulation assay was performed by Julian Wilke.

After treatment with PDEδ-targeting agents cells showed increased cellular levels of enzymes involved in lipid metabolism and cholesterol precursors. Most agents could activate SRE-dependent gene transcription (Paragraph 3.3.6). To elucidate the link between PDEδ inhibition and SREBP activation, the cholesterol-independent regulation of SREBP was investigated.

Lipid biosynthesis is crucial for cell growth and therefore SREBP regulation is part of a more complex mechanism than only cholesterol sensing. Numerous studies have linked SREBP regulation with the Akt pathway via insulin signaling, in which mTOR activation is required for signal transduction.[51] MTOR is a kinase regulated by many factors such as Rheb to govern cellular metabolism, cell growth and proliferation.[52] Rheb is a farnesylated GTP-binding protein known to be subject to PDEδ-mediated translocation.[53,52,46] Cells treated with PDEδ inhibitors showed mislocation of Rheb, thus, interfering with its activity. If PDEδ inhibition has an influence on mTOR activity, phosphorylation of mTOR should change, which could be monitored with phospho-immunoblotting. Therefore, HeLa cells were treated with Deltasonamide 1 followed by determination of cellular mTOR levels and the respective phosphorylation levels by immunoblotting. Deltasonamide 1 treatment did not have an influence on the activation level of mTOR as seen in the band intensities (Figure 29).

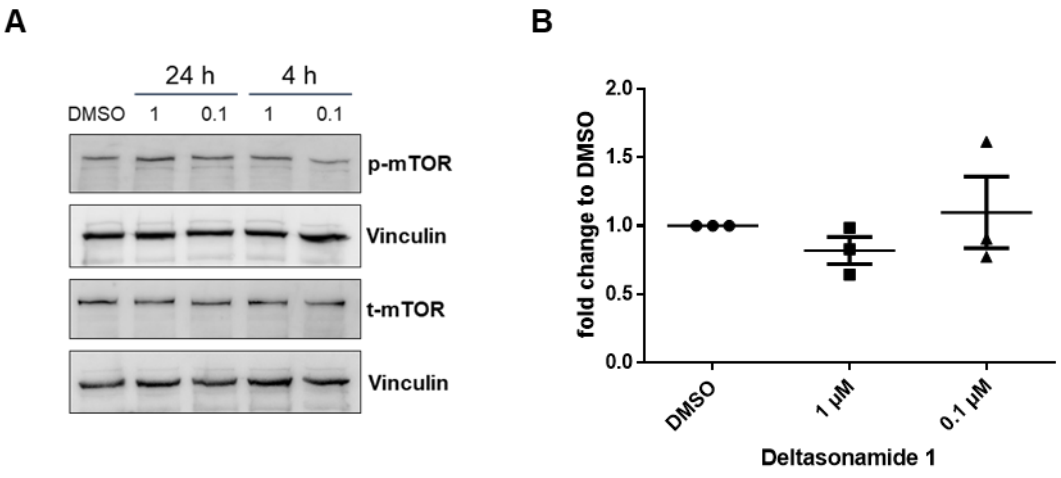

Figure 29: The influence on mTOR phosphorylation upon treatment with Deltasonamide 1. (A) HeLa cells were treated with 1 µM Deltasonamide 1 and lysates were subjected to immunoblotting to detect cellular mTOR phosphorylation levels and vinculin as a reference. (B) Band intensities for the treatment with Deltasonamide 1 from A were quantified, normalized to the intensities of the bands of vinculin and t-mTOR and then related to the values of DMSO, which were set to 1. Data are mean values ± SD (n=3). p-mTOR: phosphorylated mTOR; t-mTOR: total cellular mTOR.

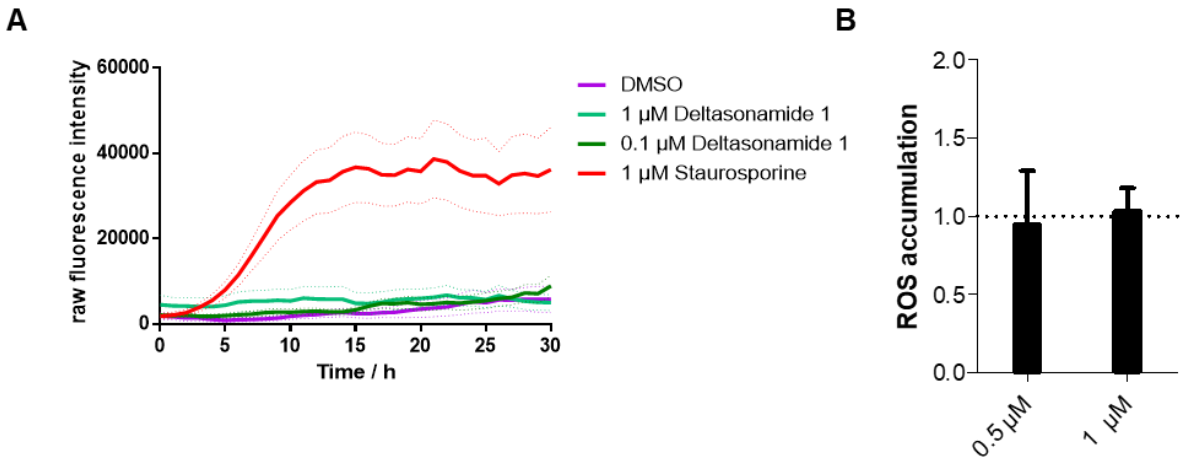

Figure 30: The determination of Caspase 3/7 activity and ROS accumulation after Deltasonamide 1 treatment. (A) HeLa cells were treated with Deltasonamide 1, Staurosporine or DMSO in presence of a substrate of caspase 3/7, which becomes fluorescent after cleavage by active caspase 3/7. Data are mean values ± SD (n=4). Dotted lines represent the SD. (B) HeLa cells were treated with Deltasonamide 1 for 24 h. After 23 h GM-H_2DCFDA, CDNB and Hoechst were added to the cells to detect cellular ROS levels and nuclei. Fluorescent values were normalized to the nuclei and the value for cells treated for 1 h with 10 µM CDNB, which was set to 1. Data are mean values ± SD (n=3). CDNB: 1-chloro-2,4-dinitrobenzene.

Previous studies suggested that PDEδ inhibition may have an inactivating effect rather than an activating effect on mTOR.[54] Rheb needs to co-localize with mTOR in order to regulate it. Interference with the localization mechanism of Rheb by PDEδ leads to less co-localization of both proteins and therefore less activation of mTOR.

In addition, the influence of PDEδ-targeting agents on apoptosis was investigated. It is known that SREBP is cleaved by caspase 3/7 during apoptosis leading to the cytosolic form of SREBP. Higher cytosolic concentrations of SREBP increase the transcription of related genes of the lipid metabolism.[55] To elucidate whether the upregulation of enzymes of the lipid metabolism was an effect of cells entering apoptosis, two different assays were performed. In the first assay, fluorescent-based live-cell imaging was carried out to monitor caspase 3/7 activity. Therefore, a substrate, which is cleaved by caspase 3/7, was applied to the cells during compound treatment. The substrate becomes fluorescent after cleavage and is thus a marker for caspase 3/7 activity. HeLa cells were treated with Deltasonamide 1 and Staurosporine as a reference compound causing apoptosis. Cells became apoptotic after treatment with Staurosporine, thus fluorescence intensity increases, whereas no elevated fluorescence intensities were monitored after treatment with Deltasonamide 1. Hence, Deltasonamide 1 treatment does not lead to apoptosis in HeLa cells at 1 µM.

In the second assay, reactive oxygen species (ROS) levels were determined by a ROS-sensitive sensor. ROS accumulation often occurs in early stages of apoptosis and therefore indicates active Caspase 3/7.[56] HeLa cells were treated with 1 µM Deltasonamide 1 and ROS species were detected after 24 h. No increased fluorescence per cell had been monitored, thus, no accumulation of ROS occurred. Cells treated with Deltasonamide 1 at 1 µM for 24 h did not become apoptotic as indicated by low caspase 3/7 activity and intracellular ROS levels. Therefore, SREBP activation by Deltasonamide 1 was not an outcome of cells entering apoptosis.

The link between PDEδ and SREBP-dependent metabolism remains unclear. Unknown binding partners of PDEδ could have an influence on SREBP activation and need to be discovered. In a recent study, Del Sal *et al.* described the Ras homolog gene family member A (RhoA) as a negative regulator of SREBP activation and lipid metabolism.[57] RhoA is a small GTPase, which is geranylgeranylated and known to be involved in acto-myosin dynamics. Upon prenylation, RhoA localizes to the plasma membrane and causes actin polymerization and actomyosin contraction via downstream effector activation. Inhibition of RhoA prenylation leads to increased activation of SREBP-1 and subsequent transcription of related genes of the lipid metabolism. This study established a new role of SREBP-1 as transducer between extracellular forces and lipid metabolism. As PDEδ is a chaperone for prenylated proteins and causes their localization, proper RhoA localization could also rely on the interaction with PDEδ. By now RhoA was only identified in yeast-2-hybrid screens and a functional connection is unknown since it is known that RhoA is bound and distributed by RhoGDI.[58] However, interfering with RhoA translocation mechanism by blocking PDEδs prenyl binding pocket could cause similar effects than inhibiting its prenylation, since RhoA needs to locate to the plasma membrane to fulfill its function, but an interaction between these two proteins was only found in yeast-2-hybrid screens and needs to be validated first.[4,1]

Furthermore, PDEδ binds different types of farnesylated proteins, which are involved in many cellular pathways.[57] Perhaps, inhibition of PDEδ affects the translocation of many proteins and may lead to a pleiotropic phenotype.

3.3.9 The effects of PDEδ inhibition on downstream signaling in cells

PDEδ binds farnesylated proteins such as KRas and Rheb and is responsible for their translocation within the cell. To ensure signal transduction, these proteins need to be enriched at their respective membranes. By blocking the prenyl-binding pocket of PDEδ with inhibitors, correct translocation of these proteins is disrupted and related downstream effects on MAPK pathway or mTOR activation are impaired (Figure 31A and B). As a read-out for pathway activity, the phosphorylation levels of ERK1/2 and ribosomal protein S6 (S6P) were determined.

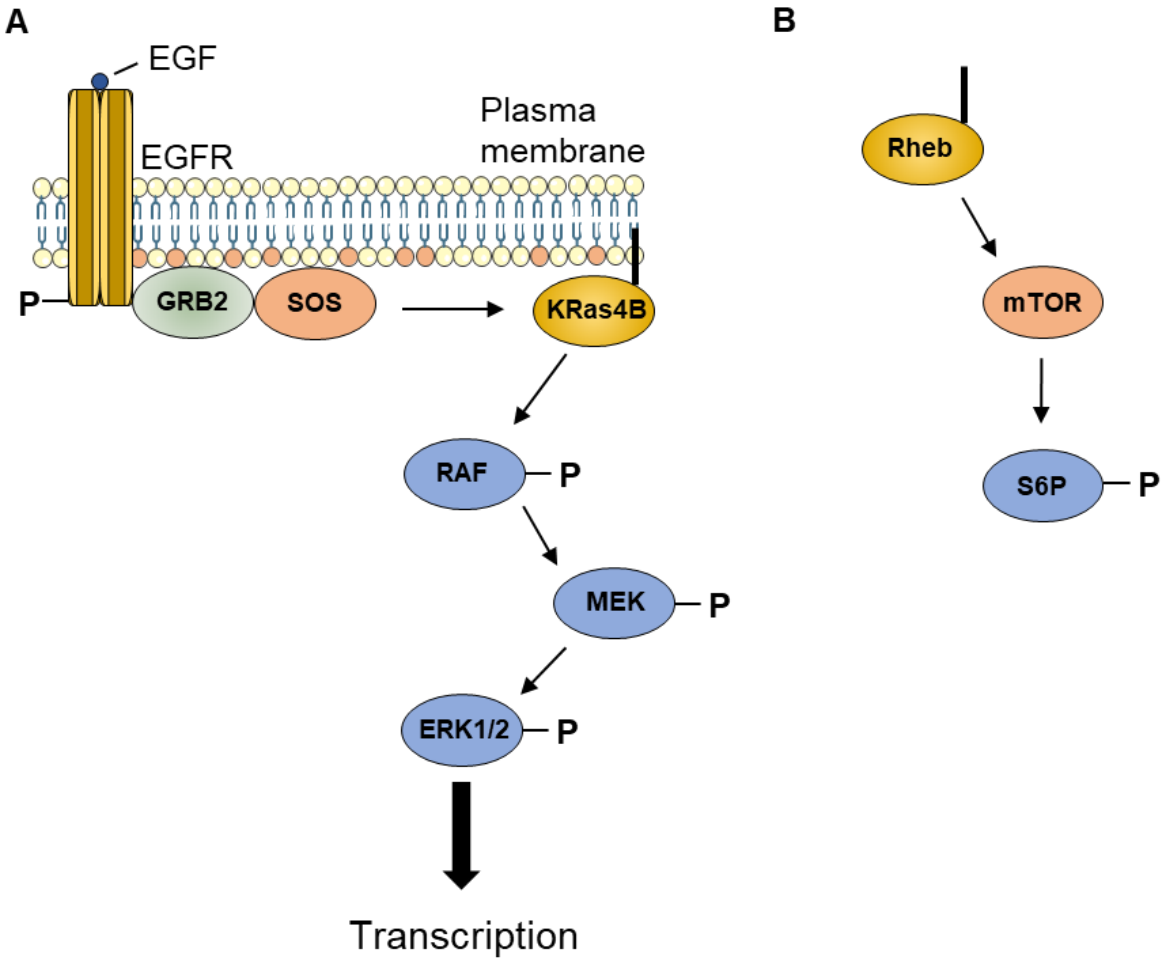

Figure 31: The representation of the MAP-Kinase pathway and the relation of Rheb and mTOR. (A) If the extracellular stimulus EGF binds to EGFR, the receptor gets autophosphorylated and GRB2 followed by SOS are recruited to the plasma membrane. SOS is a GEF for KRas4B and activated KRas through GTP exchange, which binds to RAF. RAF phosphorylates MEK and MEK phosphorylates ERK1/2. ERK 1/2 translocate to the nucleus and induce transcription. (B) Rheb binds and activates mTOR. Activated mTOR phosphorylates S6P. EGF: epidermal growth factor; EGFR: EGF receptor; GRB2: Growth factor receptor-bound protein 2; SOS: Son Of Sevenless; GEF: Guanine nucleotide exchange factor; RAF: RAF proto-oncogene serine/threonine-protein kinase; MEK: Mitogen-activated protein kinase kinase; ERK1/2: Extracellular signal-regulated kinases; Rheb: Ras homolog enriched in brain; mTOR: mammalian target of rapamycin; S6P: ribosomal protein S6.

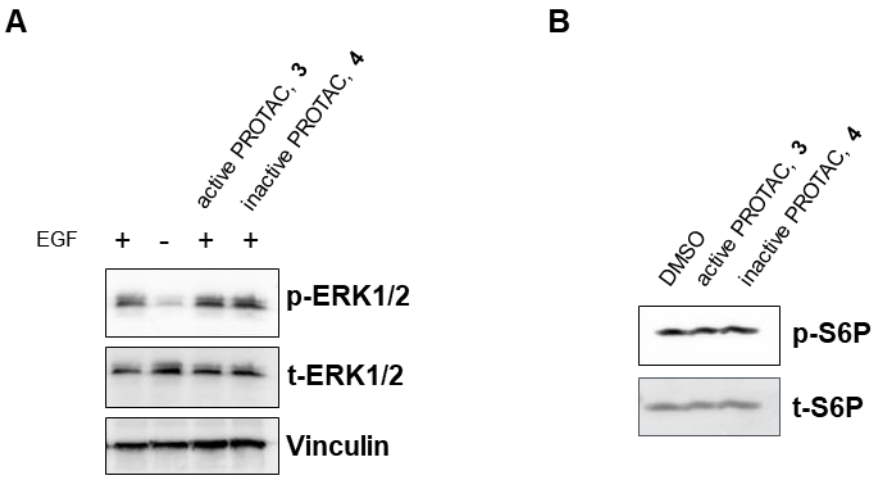

Figure 32: The downstream effects of PDEδ PROTACs. (A) HeLa cells were cultivated in EGF-reduced medium and treated with PROTAC **3**, **4** or DMSO for 24 h. MAPK pathway was activated 5 min prior to cell lysis by adding EGF. Cell lysates were subjected to SDS-PAGE followed by immunoblotting. (B) Cells and lysate were treated as described in A and cellular S6P and activation levels were determined by immunoblotting. p-ERK1/2: phosphorylation levels of ERK, t-ERK 1/2: total cellular ERK concentration; p-S6P: phosphorylation levels of S6P; t-S6P: total cellular S6P concentrations.

Therefore, HeLa cells were treated with 1 µM PROTAC **3**, **4** or DMSO in epidermal growth factor-(EGF)-reduced medium (0.5% fetal bovine serum) to reduce pathway activity to its minimum. Then, EGF was added to the cells to activate the pathway and observe the effect of PDEδ degradation on ERK1/2 phosphorylation. Prior to lysis, cells were incubated for 5 min with EGF to fully activate the pathways and monitor the highest influence of mislocated KRas on the phosphorylation levels of ERK1/2 by immunoblotting using specific antibodies. When the MAPK pathway was not activated with EGF, phosphorylation levels (Figure 32A). If degradation of PDEδ impairs the activity of the MAPK pathway, band intensities for phosphorylated ERK1/2 are expected to decrease. However, no changes in the phosphorylation levels of ERK1/2 could be detected after treatment with PROTACs **3** and **4**.

To investigate Rheb-dependent activation of S6P, HeLa cells were treated with the PROTACs **3**, **4** and DMSO and cellular phosphorylation levels of S6P were determined by immunoblotting. If PDEδ degradation impairs Rheb localization, mTOR activation was expected to decrease along with S6P phosphorylation levels. However, no change in band intensities were detected, thus, phosphorylation levels of S6P were not impaired by PDEδ degradation (Figure 32B).

After treatment with highly potent PDEδ inhibitors Deltazinone 1 or Deltasonamide 1 (K_D of 8 nM and 203 pM, respectively), ERK1/2 and S6P phosphorylation levels dropped.[14,15] The affinity of PDEδ PROTACs is between 32 nM and 72 nM and, therefore, too high to occupy most prenyl binding pockets of cellular PDEδ to inhibit PDEδ-related pathways.

Although PDEδ is degraded by the active PROTAC **3**, the remaining PDEδ in the cell appears to be sufficient to sustain cellular translocation of interaction partners.

3.3.10 Design, synthesis and proteomic profiling of glucose uptake inhibitors and related PROTACs

The synthesis and 2-DG uptake assay was performed by Dr. George Karageorgis.

The fusion of an E3 ligase-targeting warhead to inhibitors can lead to more active compounds, since protein degradation along with chemical inhibition can be induced. Chromopynone-1 is known to inhibit glucose uptake by binding to glucose transporters GLUT-1 and GLUT-3.[59] These membrane proteins are responsible for the transport of glucose through the membrane, thus maintaining cellular energy levels. GLUTs are promising targets in drug discovery since tumor cells sustain their cellular energy levels mainly from glucose rather than other energy sources. By inhibiting the glucose uptake, cancer cells lose their energy source and become apoptotic.[60] The pseudo-natural product Chromopynone-1 was recently discovered as a glucose uptake inhibitor with a half-maximal inhibitory concentration (IC_{50}) for 2-DG glucose uptake inhibition of 0.9 µM in HCT116 cells.[59]

To explore whether the concept of targeted protein degradation can be applied to glucose transporters, PROTACs based on Chromopynone-1 were designed and synthesized (Figure 33A). To develop an efficient PROTAC, the selection of a linker attachment site is crucial to retain affinity to the glucose transporter. Since no crystal structure of Chromopynone-1 in complex with any GLUT is known, a prediction of the correct linker attachment point is only based on the known structure-activity relationships. For potent inhibition of 2-deoxy-D-glucose (2-DG) glucose uptake, only minor changes around the central scaffold such as methylation at the 5-position or the exchange of oxygen to sulfur are tolerated.[59] The most changes can be applied to the benzyl moiety, which can be replaced by biphenyl, alkyl or dimethoxyphenyl substituents. The IC_{50} drops one order of magnitude and remains between 1.7 to 11.7 µM when the aforementioned substitutions are applied (Figure 33B). However, this position was chosen as site for the linker attachment. The compound was synthesized and provided by Dr. George Karageorgis (for synthesis see paragraph 5.1.3). To elucidate whether the attachment site at the compound interfered with its activity, it was tested in a 2-DG uptake assay.

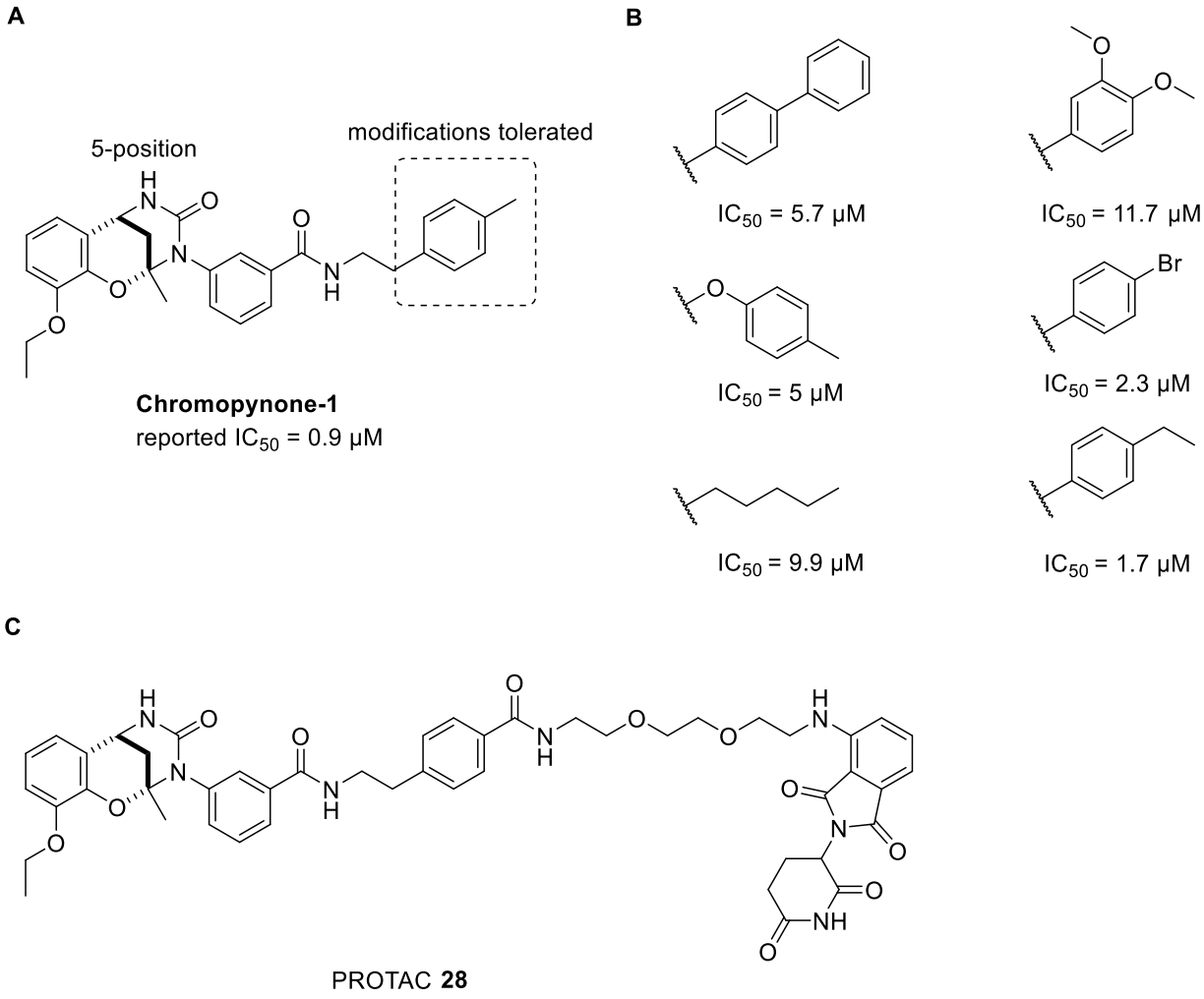

Figure 33: The design of Chromopynone-1-based PROTACs. (A) Structure of Chromopynone-1, a glucose uptake inhibitor. (B) Different substituents for the labelled position from A (dotted square). IC_{50} referring to a 2-DG uptake assay. (C) The obtained heterobifunctional molecule to degrade GLUT-1 and -3 after the design principles from A and B.

Therefore, HCT-116 cells were treated with 2-DG in the presence of PROTAC **28**. After 30 min, cellular 2-DG concentration was measured by a coupled enzymatic assay (see appendix Figure 50). PROTAC **28** had an IC_{50} of 1.0 µM in HCT-116 cells (Figure 34). Compared to the parent compound, which had an IC_{50} of 0.9 µM, this was only a minor drop in activity, which matched the claims of the designed strategy.

To investigate whether glucose transporters were degraded by PROTAC **28** and which effect this had on cellular pathways, proteome profiling was performed. Therefore, HeLa cells were treated with 1 µM of PROTAC **28** or Chromopynone-1 for 24 h followed by the quantification of cellular protein levels by TMT-labelled mass spectrometry.

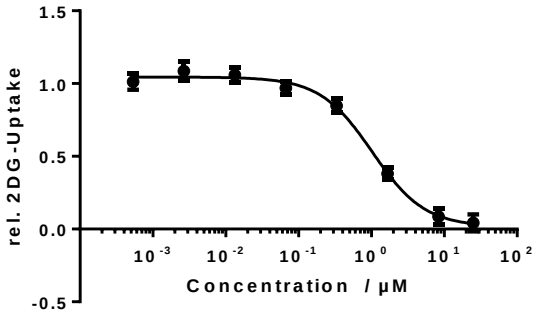

Figure 34: The 2-DG uptake assay of PROTAC 28. HeLa cells were treated with 2-DG and PROTAC **28** or DMSO. After cell lysis cellular 2-DG concentrations were determined with a coupled enzymatic assay. The obtained fluorescent values were normalized to the values for DMSO-treated cells, which were set to 1. Data are mean values ± SD (n=3).

Since both compounds bear the same chemotype, similar effects on some proteins and pathways were expected. In addition, the PROTAC **28** should recruit CRBN, an E3 ligase, which was supposed to ubiquitinate the glucose transporter and label it for degradation.

The 30 most up- and downregulated proteins were analyzed by an online reactome analysis tool to identify overrepresented pathways influenced by compound treatment.[47] First, upregulated proteins were analyzed. PROTAC **28** treated cells showed overrepresented pathways associated with mothers against decapentaplegic homolog 4 (SMAD4) and defective SLC34A3 hereditary hypophosphatemic rickets with hypercalciuria (appendix Table 8). Chromopynone-1 upregulated proteins related to striated muscle contraction, G1/S-specific transcription and smooth muscle contraction (appendix Table 10). From the 30 proteins used for the analysis, only two were associated with each of the respective pathways, which resulted in high p-values between $3.6*10^{-3}$ and $7.4*10^{-3}$ (Table 2). No similarities either between the upregulated proteins or the overrepresented pathways for PROTAC **28** and Chromopynone-1 were observed. In addition, the obtained high p-values resulted in no statistical significance, and no link to a specific pathway can be identified. Proteins that were downregulated when cells were treated with a protein degradation-inducing compound could be new target proteins of the compound.

If PROTAC **28** induced degradation of GLUT-1 or -3, a decrease in cellular protein levels should be detectable by mass spectrometry. However, from 4900 proteins identified in the proteome profiling, only GLUT-1 but not GLUT-3 was identified by mass spectrometry. GLUT-1 levels were slightly increased after PROTAC **28** treatment and slightly decreased after Chromopynone-1, i.e. 5.5% and -1.7% respectively (Figure 35A and B). These inconclusive data suggest that cellular GLUT-1 levels were not impaired after treatment with PROTAC **28** and therefore no active PROTAC was developed.

Subsequently, the 30 most downregulated proteins after treatment with PROTAC **28** or Chromopynone-1 were analyzed by the reactome analysis (appendix Table 9 and Table 11). Chromopynone-1 treatment impairs pathways referring to axon guidance, SREBP-mediated gene expression and gene and protein expression of JAK-STAT signaling after Interleukin-12 stimulation. All suggested pathways were calculated with high p-values and therefore low significance. No link to glucose inhibition can be drawn by these data. In comparison, PROTAC **28**-treated cells showed a highly significant phenotype. The 30 most downregulated proteins showed highly significant values for pathways involved in nonsense mediated decay, the translation of viral mRNA and the formation of a pool of free 40S subunits. The annotated pathways were impaired with low p-value and therefore high significance. PROTAC **28**-treated cells mainly show the downregulation of ribosomal proteins and histones. From the 30 downregulated proteins used for the analysis, only 6 were neither ribosome nor histone-related proteins. Although both compounds were based on the same scaffold and both inhibited glucose uptake, their influence on cellular protein levels and pathways is different. The coupling of an E3 ligase recruiting warhead changed the molecule's properties in a way that secondary effects occur, which were unrelated to glucose uptake inhibition. To elucidate these secondary effects further experiments need to be performed.

However, while PROTAC **28** treatment led to a distinguished phenotype, GLUT-1 was not degraded and GLUT-3 degradation was not detected. In order to monitor protein level changes of GLUT-3 and other glucose transporters different cell lines can be employed in MS analysis. Also, immunoblotting could elucidate cellular protein levels of certain glucose transporters. However, since the binding site of Chromopynone-1 to GLUT-1 and -3 is unknown the PROTACs linker length needs to be varied to investigate its potential to degrade glucose transporters.

Table 4: The reactome analysis of the 30 most upregulated proteins of cells treated with Chomopynone-1 or PROTAC 28.

Compound	Pathway name	p-value
PROTAC	SMAD4 heterotrimer regulates transcription	$3.6*10^{-3}$
	Transcriptional activity of SMAD2/SMAD3	$6.5*10^{-3}$
	Defective SLC34A3 causes Hereditary hypophosphatemic rickets with hypercalciuria (HHRH)	$6.6*10^{-3}$
Chromopynone-1	Striated Muscle Contraction	$4.0*10^{-3}$
	G1/S-Specific Transcription	$4.6*10^{-3}$
	Smooth Muscle Contraction	$7.4*10^{-3}$

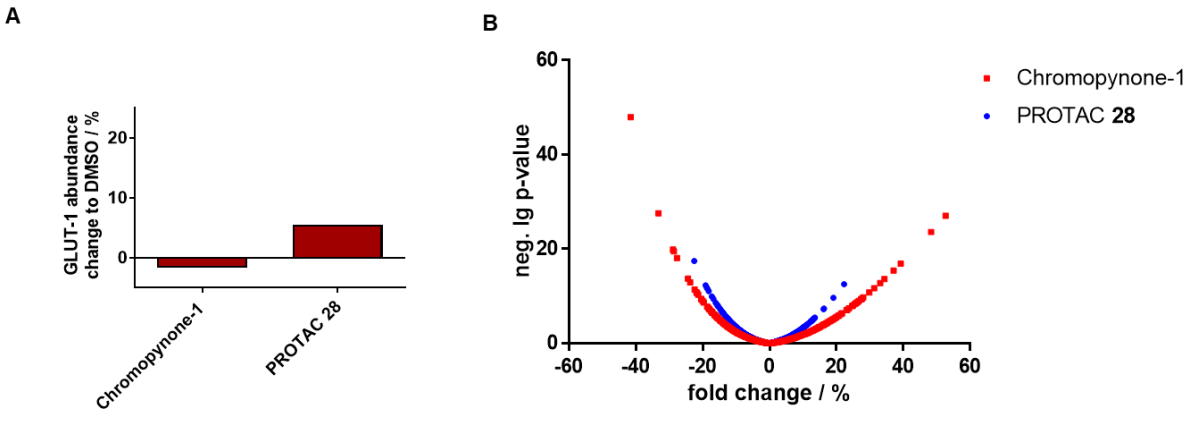

C

Compound	Pathway name	p-value
PROTAC **28**	Nonsense Mediated Decay (NMD) independent of the Exon Junction Complex (EJC)	$1.1*10^{-16}$
	Viral mRNA Translation	$1.1*10^{-16}$
	Formation of a pool of free 40S subunits	$1.1*10^{-16}$
Chromopynone-1	Axon guidance	$9.4*10^{-3}$
	Activation of gene expression by SREBF (SREBP)	$1.1*10^{-2}$
	Gene and protein expression by JAK-STAT signaling after Interleukin-12 stimulation	$1.2*10^{-2}$

Figure 35: The proteome profiling and reactome analysis after treatment with GLUT-1 and -3 targeting agents. (A) Changes in protein levels of GLUT-1 after treatment of HeLa cells with Chromopynone-1 and PROTAC **28** at 1 µM for 24 h. Values are normalized to DMSO-treated cells. (B) Up to 4800 protein were identified and quantified. Each dot represents the mean p-value vs. the change in abundance (n=3). (C) The 30 most downregulated proteins of cells treated with Chomopynone-1 or PROTAC **28** were used for a reactome analysis to explore overrepresented pathways.[45]

In addition, glucose transporters are transmembrane proteins and binding could occur from the outside of the cell such that the pomalidomide warhead is presented on the surface of the cell, where no E3 ligase can be recruited.

In general, transmembrane proteins are subject to proteasomal degradation after they are labelled with ubiquitin and therefore a target class for which the PROTAC technique can be applied.[27] Whether the PROTAC technique is suitable to target glucose transporters needs to be tested by synthesizing more compounds with different linker length and E3 ligase ligands.

3.4 Conclusion

Three PROTACs based on the picomolar PDEδ inhibitor Deltasonamide 1 were synthesized. All PROTACs were able to decrease cellular PDEδ in Jurkat, Panc Tu-I and HeLa cells with the tetraethylene glycol derivative **3** being the most efficient degrader. As a negative control, a methylated pomalidomide derivative was introduced (PROTAC **4**), whose affinity towards cereblon was abolished, and thus did not induce protein degradation. Although the affinity of the active **3** and inactive PROTAC **4** to PDEδ was slightly decreased compared to the parental PDEδ inhibitor Deltasonamide 1, only the active PROTAC **3** reduced cellular PDEδ levels with a DC_{50} of 48 nM and a D_{max} of 83.6% in Panc Tu-I cells. The degradation is dependent on the proteasome, since simultaneous treatment with a proteasome inhibitor restored PDEδ levels. In addition, fusion proteins of PDEδ, i.e. nanoLuc-PDEδ and mCherry-PDEδ, were subject to PROTAC-mediated degradation by employing active PROTAC **3**.

Furthermore, PDEδ PROTAC selectivity was determined by proteome profiling. Out of 4800 proteins, only PDEδ was downregulated, suggesting that PROTAC **3** is highly selective towards its target. Interestingly, PDEδ PROTACs **3**, **4** and Deltasonamide 1 upregulated proteins related to lipid metabolism. Levels of proteins implicated in the mevalonate pathway and regulated by a SRE-dependent promotor were particularly increased. All three compounds increased SRE-mediated transcription. In addition to elevated protein levels, lipid metabolite levels were also affected after Deltasonamide 1 treatment. In this regard, cholesterol biosynthesis intermediates accumulated in the late stages of cholesterol biosynthesis.

Whether this phenotype is chemotype- or PDEδ-mediated could not be clarified. Although Deltazinone 1, a different chemotype targeting PDEδ, showed similar cellular effects as the PROTACs and Deltasonamide 1, the results were inconsistent and further experiments need to be performed such as siRNA knockdown and small molecule pull down experiments to enrich and identify proteins that bind to Deltasonamide 1.

Furthermore, the concept of targeted protein degradation was applied to glucose transporters. PROTACs based on the GLUT-1 and -3 inhibitor Chromopynone-1 were synthesized and tested. Although the 2-DG uptake was successfully inhibited with an IC_{50} of 1 µM, no reduced GLUT-1 levels were detected by proteome profiling.

The PROTAC concept was successfully applied to degrade PDEδ and a new mechanistic feature of PDEδ inhibition was revealed.

This finding demonstrates that new tool compounds are necessary to investigate PDEδs function within the cell. The discovery of a productive PROTAC for glucose transporters failed. In order to establish an efficient PROTAC, new derivatives based on the design principles of PROTACs need to be synthesized and tested.

Part B

Identification of Spindly´s Interaction Partner by Photo-crosslinking

4 Part B

4.1 Introduction

4.1.1 Mitosis

In multicellular organisms, cell division is a major process to ensure growth and regeneration of tissue.[61] The process by which cells duplicate into two identical daughter cells is called cell cycle. This cycle can be divided into four phases: a gap phase G_1, a synthesis phase S, a second gap phase G_2 and a mitotic phase or M phase (Figure 36A). Together, the phases G_1, S and G_2 are also known as interphase. While in the G_1 phase the cell prepares for DNA synthesis and division, the DNA is replicated in the S phase.[62] The cell leaves the S phase with duplicated chromosomes, and enters the G_2 phase. In this phase, the cell grows and increases its protein and organelle masses to ensure accurate cell division. The M phase can be divided into two phases, which are mitosis and cytokinesis.[63] In mitosis, the cell packs DNA in its dense form and properly separates sister chromatids. Once this is accomplished, the cell undergoes cytokinesis, i.e. it splits into two new daughter cells.

Mitosis can be divided into five steps: prophase, prometaphase, metaphase, anaphase and telophase (Figure 36B).[61] In prophase, chromosomes condense into a compact form to prevent the DNA of becoming an unmanageable macro-structure during mitosis. In this form, DNA is no longer available for transcription. Simultaneously, the centrosomes, which are the center of the mitotic spindle, mature and move across from each other in the cell to form the two poles of the spindle apparatus. The mitotic spindle consists mainly of microtubules, which accomplish chromosome segregation in later phases. In prometaphase, microtubules polymerize from both centrosomes and reach out for the chromosomes thereby forming overlapping ends. Microtubules assemble and disassemble until they are bound by kinetochores. These are multi-protein layered structures located at the centromeres, which stabilize microtubule ends and mediate chromosomes binding to microtubules. This is carried out by a “search-and-capture” mechanism, which means that plus-ends of microtubules grow and shorten until they are connected to kinetochores.[64] All these mechanisms ensure rapid kinetochore-microtubule attachment with a minimal number of errors.

Once microtubules from both centrosomes are bound to the kinetochore, chromosomes are aligned to the central spindle by a push-and-pull mechanism.

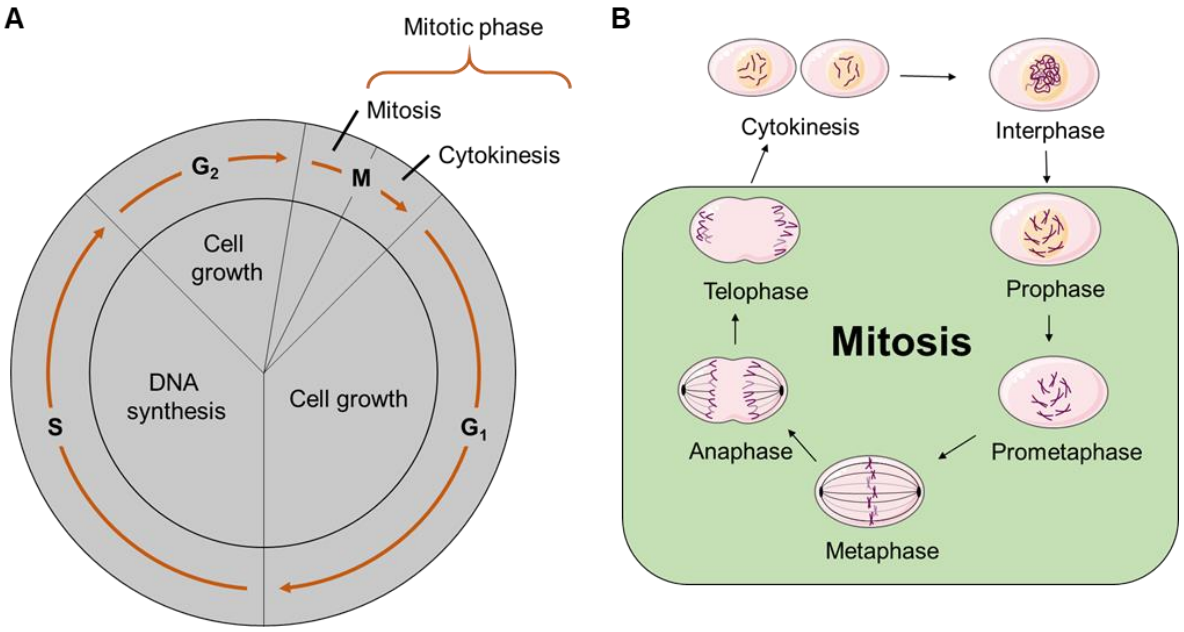

Figure 36: Overview of the cell cycle and the phases during mitosis. (A) The cell cycle consists of four phases. The M phase can be divided into Mitosis and Cytokinesis. (B) Mitosis can be divided into five phases, in which the chromosomes are separated and, after cytokinesis, located into new daughter cells.[63]

This phase is called metaphase and represents a crucial checkpoint of mitosis. Only if all kinetochores are correctly attached to the spindle and congressed at the midzone, with each sister chromatid connected to microtubules emanating from opposite poles, chromatids start to separate. In anaphase, sister chromatids are separated and translocated to the opposite spindle poles. In telophase, the kinetochore-bound microtubules depolymerize, and the nuclear membrane starts to form around the separated chromatids at the poles of the cell. This is followed by cytokinesis and both cell membranes fuse into two new daughter cells.[61]

Proper chromosome segregation is a key event in the cell cycle and is therefore highly controlled. Inaccurate chromosome segregation could lead to aneuploidy and chromosomal instability, which is a common occurrence in cancer.[65] Understanding these mechanisms in detail can lead to new therapies to treat cancerous cells.

4.1.2 Kinetochores

During mitosis, the two sister chromatids are connected by the centromere, at which the kinetochore is located. The kinetochore consists of hundreds of proteins organized in multiple layers.[66] In comparison to the simplest kinetochore, which can be found in budding yeast and is capable of binding one microtubule, kinetochores of higher eukaryotes can bind multiple microtubules.

With only a few exceptions, yeast and vertebrate kinetochore components share the same composition of proteins, suggesting that the composition and organization of kinetochores are conserved throughout the evolution.[67,68] Nowadays, it is not clear if kinetochores of higher eukaryotes are assembled through repetition of microtubule-binding modules already occurring in budding yeast.[69]

Transmission electron microscopy studies have shown that vertebrate kinetochores consist of three layers with different densities: the more dense inner and outer plate and the less dense middle layer.[66,70] The inner layer forms the interface with chromatin, whereas the outer layer is responsible for the interaction with microtubules. This ultrastructure is a step-wise assembly from the chromatin to the microtubules and has a non-linear hierarchy, i.e. layer borders blur. Its composition is regulated by the attachment of microtubules and local signaling pathways.[68]

To ensure attachment of microtubules to each chromatid, kinetochores must act as structural binding motif for microtubules and monitor whether microtubules are bound to both chromatids.

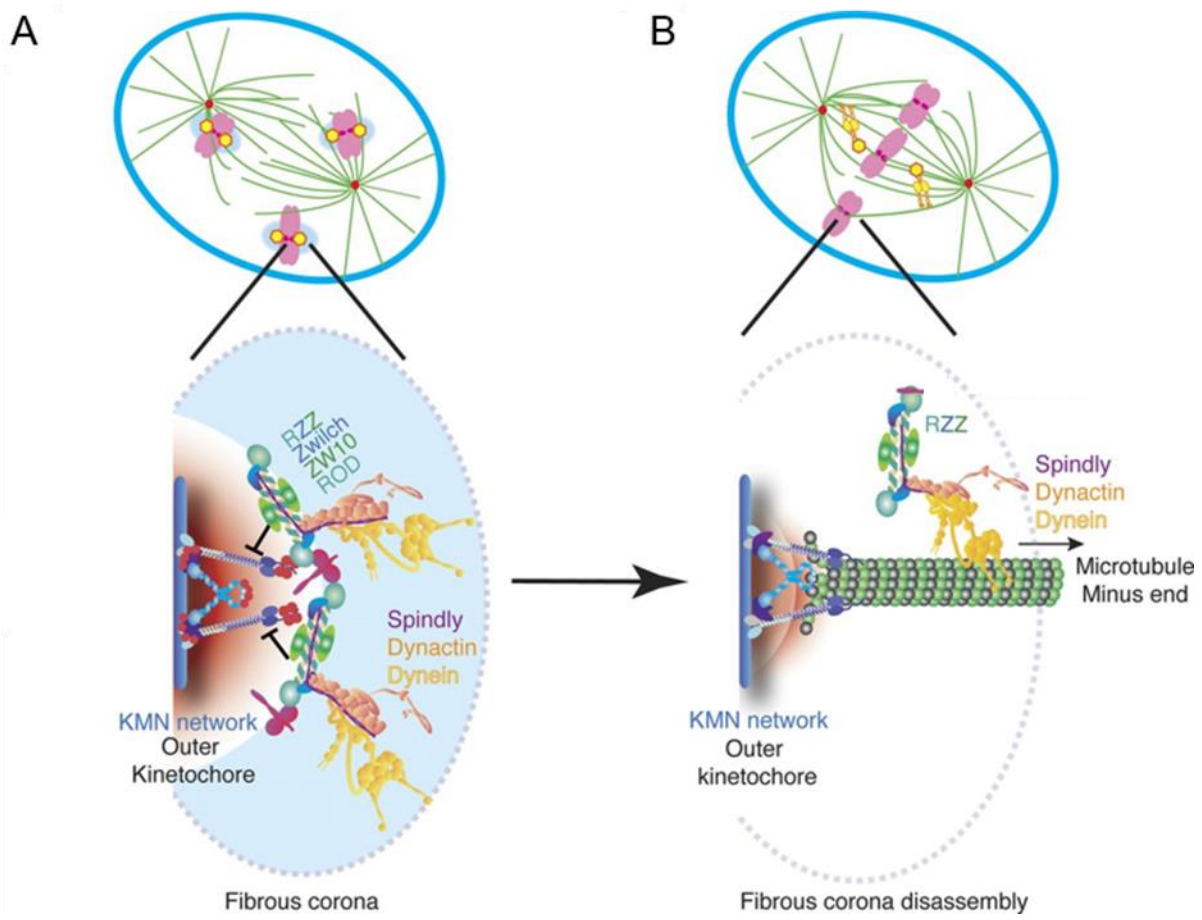

Figure 37: Assembly and disassembly of the fibrous corona. (A) Fibrous corona in its onset state. RZZ and Spindly are recruited to the outer kinetochore and reach out to interact with microtubules. (B) Once the microtubule is attached to the kinetochore, dynein moves the whole complex towards the minus end of the microtubule and stabilizes the microtubule attachment. Adapted from T. McHugh *et al.*.[2]

Therefore, kinetochores are involved in the "sensing" of attachment to opposite spindle poles to ensure bi-orientation, i.e. chromosomes need to be bound to microtubules of both spindle poles. In the absence of microtubules, kinetochores consist of an additional layer, called fibrous corona, which facilitates the capture of microtubules by kinetochores and contributes to the regulation of the checkpoint.

Among other proteins, the Rod-Zw10-Zwilch (RZZ) complex in the fibrous corona plays an essential role in coordinating checkpoint silencing, activation and stabilization of kinetochore-microtubule attachment.[71] The RZZ complex recruits at the kinetochore the protein Spindly in a farnesylation-dependent manner. Spindly is an adaptor protein that brings to the kinetochores dynein and dynactin, a microtubule minus-end-directed motor protein complex. The RZZ-Spindly-Dynein-Dynactin complex transports kinetochore-localized checkpoint proteins along the microtubule towards the centrosomes, thereby silencing the checkpoint.[72]

Because our understanding of the structural organization of the fibrous corona is limited, gaining insight into this structure can help to further elucidate the complex mechanisms that occur during mitosis.

4.1.3 Protein prenylation

Many protein-protein interactions are mediated by posttranslational modifications (PTMs). Investigating these interactions can be challenging, since they are predominantly non-covalent and mostly transient or weak. The most common PTMs are phosphorylation, ubiquitination, acetylation and glycosylation (Figure 38A). In a cellular environment, PTMs modulate protein functions, thus orchestrating the proteome.

Another example of PTMs is prenylations, which cover the modification of cysteines by farnesyl or geranylgeranyl moieties (Figure 38B). Isoprenoid groups in proteins are responsible for increased affinity of proteins for membranes, signal transduction and convey cellular homeostasis.[73,74] Based on computational calculations it is known that up to 2% of the human genome is prenylated, e.g. Ras GTPases or Spindly.[16]

Prenylation is conducted in three steps: prenylation, proteolysis and methylation. The cells source of isoprenoids is the mevalonate pathway, which produces isoprenoids for prenylation and cholesterol from acetyl-CoA. In the first step of the process, proteins are modified by protein prenyltransferases.

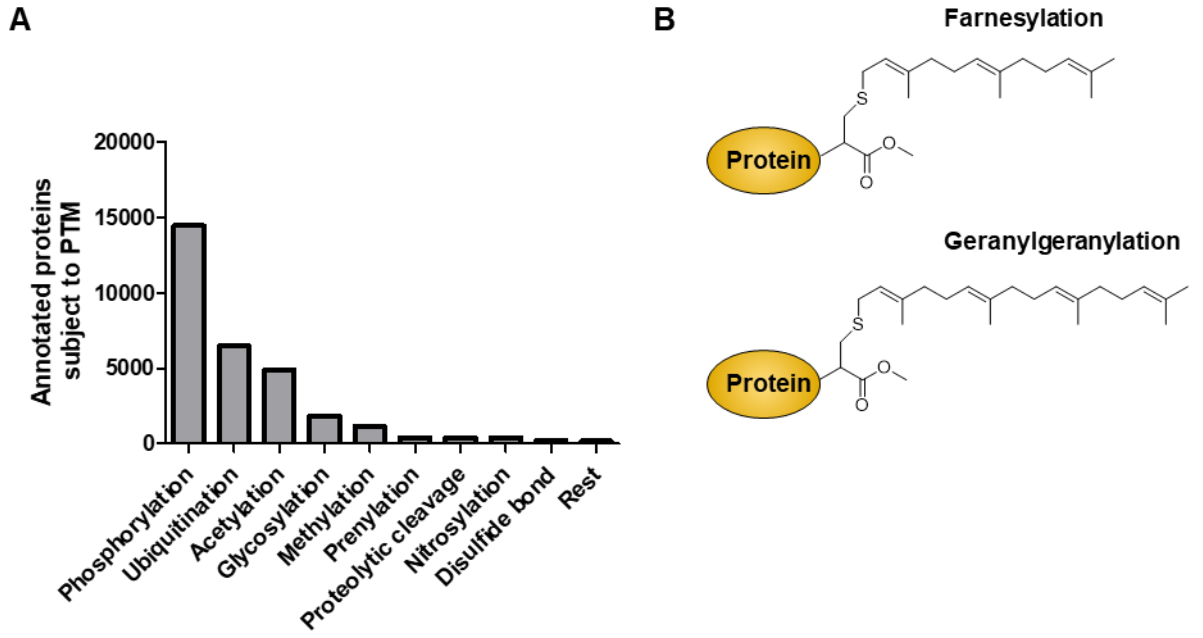

Figure 38: Common PTMs of the human proteome. (A) Number of annotated proteins for the respective PTM within the human proteome.[75] (B) Structure of the two forms of prenylation found in the proteome.

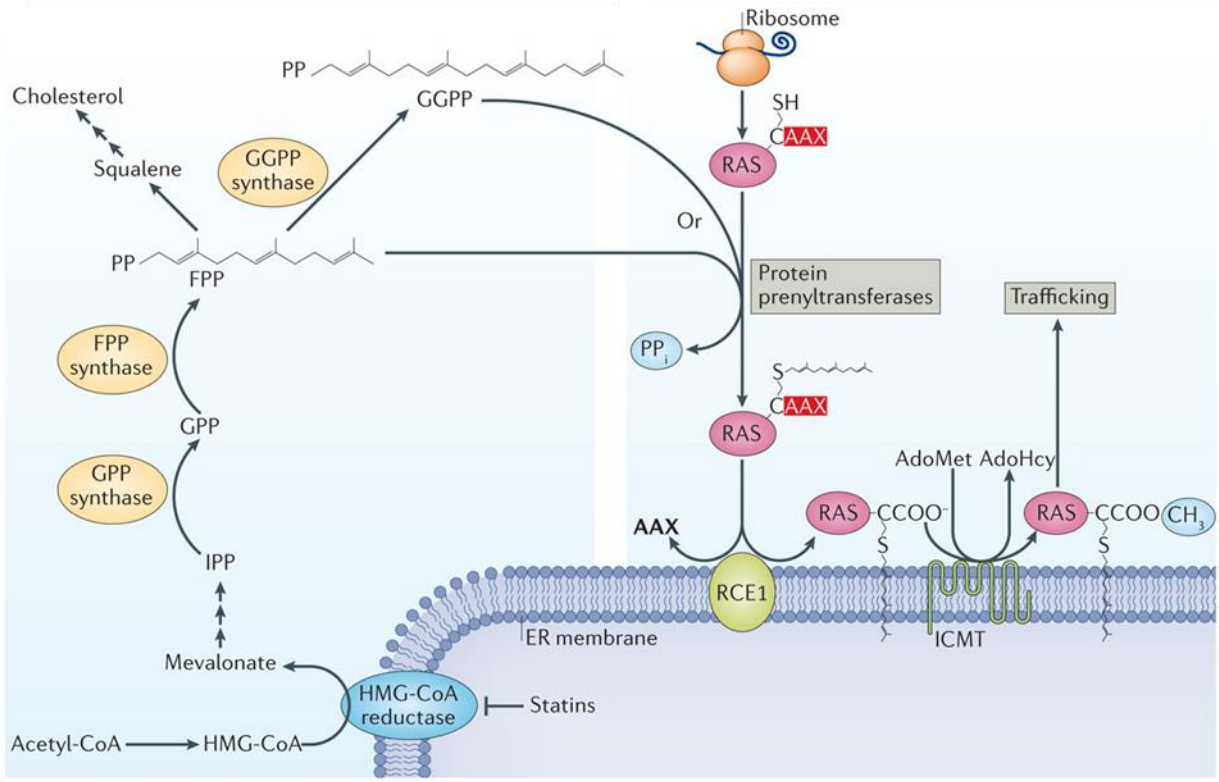

Figure 39: Prenylation of proteins. Isoprenoids are synthesized from acetyl-CoA in the early steps of cholesterol synthesis pathway. The isoprenoids are transferred to a cysteine in proteins containing a CAAX box by a protein prenyltransferase. Then, the last three amino acids are cleaved off by RCE1 followed by methylation of the C-terminus. Illustration from M. Wang and P.J. Casey.[76] RCE1: RAS-converting CAAX endopeptidase 1, FPP: Farnesyl pyrophosphate, GPP: Geranyl pyrophosphate, GGPP: Geranylgeranyl pyrophosphate, AdoMet: methylated S-adenosyl methionine, ICMT: Isoprenylcysteine carboxylmethyltransferase.

They recognize CAAX boxes at the carboxyl termini of proteins, where "C" is the cysteine residue, where the prenyl-group is attached, "A" indicates any aliphatic amino acid and "X" stands for different amino acids. The farnesyl pyrophosphate unit is transferred to the cysteine residue. Then, proteins are further treated by removing the last three amino acids, a step conducted by RAS-converting CAAX endopeptidases (RCE1). The resulting C-terminal cysteine is carboxymethylated by isoprenylcysteine carboxymethyltransferase (ICMT).[74,77]

The attachment of prenyl moieties to proteins increases their membrane affinity and mediates protein-protein interactions (PPI).[76] To investigate such PPIs, photoactive groups can be introduced into farnesyl groups in order to irreversible connect interacting proteins after irradiation with light.

4.1.4 Photoaffinity labelling

Photoaffinity labelling (PAL) finds broad application in many research areas. PAL is a technique that aims to attach a chemical label on a biomolecule of interest. This label can be activated by light to form covalent bonds to binding partners in proximity. It is often used to elucidate drug targets, off-target interactions, assist in studying protein structure and discover novel or alternate binding sites.[78]

The activity of a given protein relies on multiple factors, such as binding partners and ligands. These interactions are mostly non-covalent and only feasible in the environment of a cell. In extracellular interaction studies, local concentrations and cooperative binding effects (e.g. different ions, detergents, missing other proteins) are artificial, leading to false positive and negative results. To mimic the natural environment, interaction studies should be carried out in intact cells, close to natural conditions. Furthermore, interactions do not only rely on the spatial but also on the temporal organization of a cell. Therefore, a space and time dependent technique needs to be applied.

PAL probes offer these required properties. They consist of an affinity ligand, which binds to the protein of interest, and a light reactive warhead, which covalently reacts with the appropriate residues in proximity upon irradiation. The photoreactive group leads only to minor changes in the final molecule and therefore mimics the natural ligand. The probe behaves as the natural ligand until the time point of activation by light.[79]

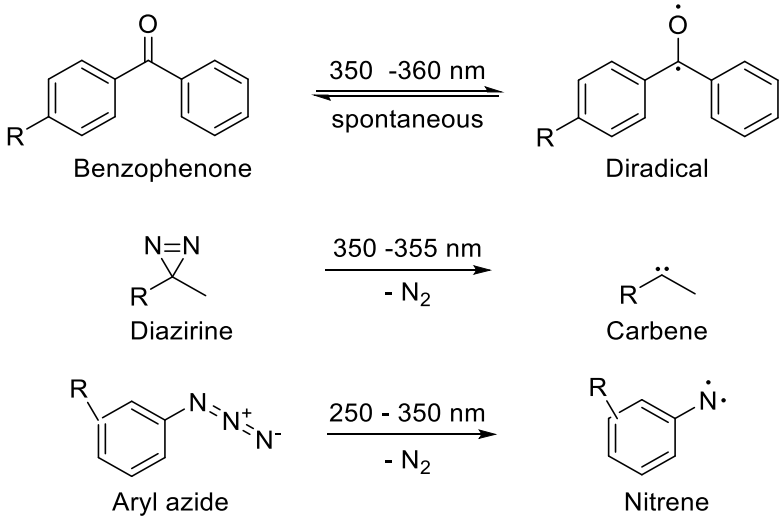

Figure 40: Photoreactive groups used for photolabeling experiments.

This makes PAL a powerful tool to investigate protein-protein or protein-ligand interactions within an intact cellular environment.

Commonly used photoreactive groups are benzophenone, diazirine or aryl azides, which have different properties and advantages based on their activation mechanism and reactive intermediates upon photolysis. Benzophenones form a diradical intermediate under UV light. This can undergo reactions with proteins or ligands in close proximity. In case there is no interaction partner in the surroundings, this active intermediate can revert into its unreactive form, which can be activated again. In contrast, aryl azides and diazirines cannot revert its reactive state, since the expulsion of nitrogen upon photoactivation leaves a carbene or nitrene (Figure 40). These reactive intermediates react then with either binding partners or solvent, which inactivates them for another activation round. The use of benzophenone could lead to higher labelling efficiency, since it only reacts if interaction partners are in proximity. However, longer irradiation times are required, which could harm the sample. In some cases, shorter irradiation time is more important than labelling efficiency. The selection of the photoreactive group relies not only on its reactivity but also on its biological compatibility. Before the photoreactive group forms a covalent bond, reversible binding to the interaction partner should occur. If the affinity for the target is low, labelling is inefficient and the cross-linking product yield is decreased.

Apart from the PAL group-specific disadvantages, there are overall properties, which all photoreactive functional groups should have. They need to be stable in the dark at the pH of the environment, their activation should not interfere with the interactome of the selected target and the novel covalent bond needs to be stable during the detection method. If one of these properties is not available, a different cross-linking technique should be considered.

PAL finds broad applicability in various areas of chemical biology which includes target identification and validation for bioactive small molecules. Ben B. Cravatt and colleagues used this method to identify protein targets of commonly used scaffolds in drug discovery (Figure 41A and B) by employing a trifunctionalized molecule bearing an alkyne, a diazirine and the small-molecule scaffold.

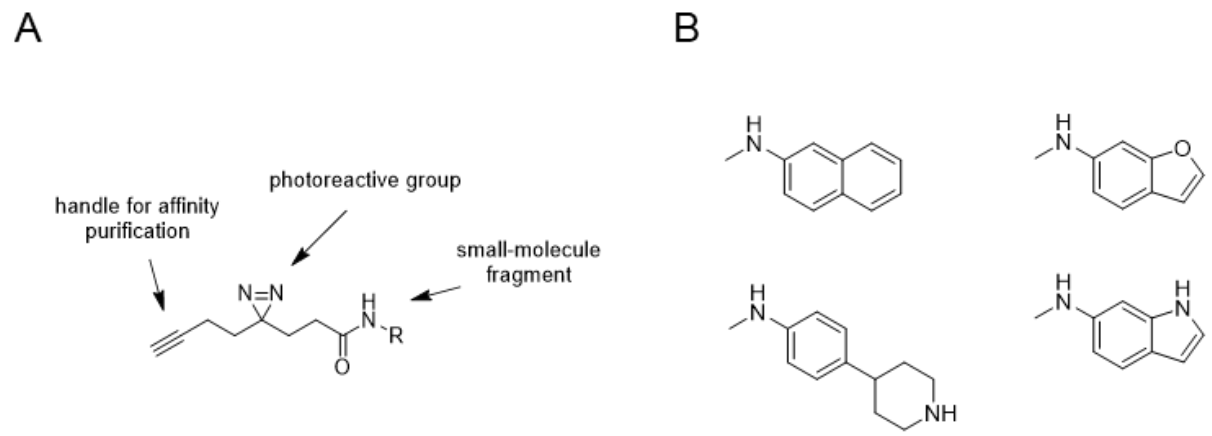

Figure 41: Photoaffinity labelling probes for mapping fragment-protein interactions in cell. (A) Structure of affinity ligand functionalized with photoreactive groups to identify target proteins by chemical proteomics or immunoblotting. (B) Examples of commonly used scaffold in drug design, which were used to identify target proteins.

The alkyne is installed to couple the ligand-protein complexes to solid phase and thus enrich and purify it from complex protein mixtures. Then, the different small-molecule scaffolds lead to different enriched targets. They were able to identify up to 2000 unknown target proteins from 15 different small-molecule scaffold, showing the broad and still large ligandability of the human proteome.[80] PAL offers an unbiased way to covalently attach chemical entities to proteins and therefore the enrichment and subsequent identification of labeled proteins.

4.1.5 Prenyl-PAL-probes

Photoactive groups can be introduced into prenyl-moieties to investigate ligand-mediated protein-protein or ligand-protein interactions. These prenyl-PAL-probes are used to investigate prenyltransferases, carboxymethylates and prenyl-binding proteins.

Farnesyl transferases (FTase) were studied by Distefano and colleagues by introducing a benzophenone into a farnesyl unit (Figure 42A). By farnesylation of a peptide containing a CAAX-box, they were able to investigate FTase tolerance towards different farnesyl analogues. Long incubations times lead to incorporation of the photoactive farnesyl analogues into the peptide. In addition, FTase was covalently labelled by the probes, which gave insights into the binding site of farnesyl to transferases.[81]

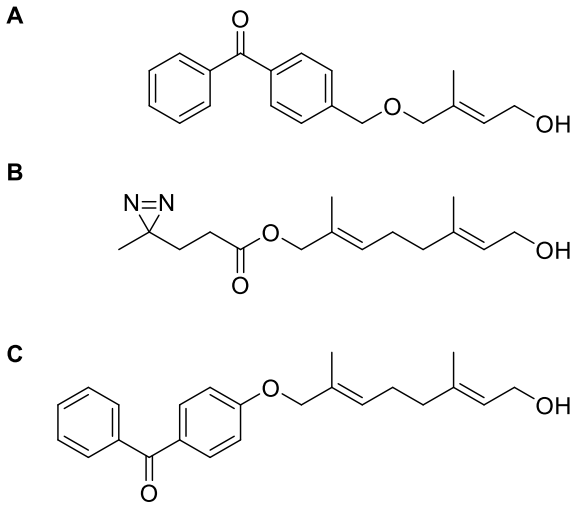

Figure 42: Different prenyl-PAL-probes. (A) Photoactive probe to investigate FTases. (B) Probe to investigate carboxymethylating proteins. (C) Probe to investigate prenyl-binding proteins.

Furthermore, a diazirine was introduced into a farnesyl unit to gain insights into the tolerance spectrum of Ste14p, an ICMT responsible for carboxymethylation of C-terminus during the processing of farnesylated proteins (Figure 42B). A peptide linked to this probe was able to photo-cross link with St14p and enabled the analysis of active-site residues.[82]

To elucidate the processing and transport of farnesylated proteins, the isoprenoid moiety can be modified with a photoreactive group. By introducing such functional group into this anchor, covalent bonds can be formed between interacting proteins, while sustaining natural binding sites (Figure 42C). This technique was used to covalently label PDEδ, which is a prenyl-binding protein. A farnesyl was modified with a benzophenone, which forms a proximity-driven covalent bond after photoactivation. Although this group is sterically demanding, it binds into the pocket of PDEδ with high affinity and led to the covalent modification of PDEδ.[83]

The introduction of functional groups such as benzophenones or diazirines, offer the possibility to investigate the processing and cellular functions of prenylated proteins. Their broad significance for cellular function can be studied with these new tools and could lead to new discoveries relevant for the treatment of diseases.

4.2 Aims

The investigation of structure and function of proteins involved in kinetochore organization is important since this protein complex is crucial for chromosomal separation during mitosis and therefore crucial for accurate DNA segregation into daughter cells. The Rod-Zw10-Zwilch (RZZ) complex is part of the outer layer of the kinetochore and responsible for chromosome attachment to microtubules. The complex interacts with the dynein-binding protein Spindly in a farnesyl-dependent manner, but its actual binding partner and site is unknown. Since unfarnesylated Spindly does not form a complex with RZZ the farnesyl moiety is crucial for complex formation. This suggests that the farnesyl-moiety interacts with the complex and binding partner(s) are novel farnesyl acceptors.

To identify the direct interaction partner(s) of Spindly, the concept of proximity-driven photolabeling was applied. Therefore, different farnesyl analogues containing a photoactivatable group should be synthesized and introduced into Spindly. Upon complex formation of Spindly and RZZ, irradiation with light activates the photoactive prenyl-PAL-probe and a proximity-driven covalent bond should be formed between Spindly and the direct interaction partner(s) within RZZ. Then the peptides should be analyzed by mass spectrometry to discover a mass shift in one Spindly peptide corresponding to a peptide of RZZ, which reveals its interaction partner(s) and site(s). Identification of Spindlys farnesyl acceptor can lead to a new hypothesis of Spindly's function in kinetochore organization during mitosis.

4.3 Results and Discussion

4.3.1 Design and synthesis of photoactivatable farnesyl analogues

To investigate Spindly's binding to the RZZ complex, photo-activatable probes, which should substitute the natural farnesyl moiety in Spindly, were designed and synthesized. Farnesyl pyrophosphate consists of three isoprenoid-units and is very hydrophobic. To keep its hydrophobicity and steric demand, the synthesis was designed starting from geraniol, which lacks one isoprenoid unit. The missing isoprenoid unit was substituted by a photoactivatable group such as diazirine or benzophenone.

First, geraniol was protected using a silyl protection-group. The protected geraniol **29** was oxidized non-selectively, which led to a mixture of three allylic alcohols, which were separated using flash chromatography. Only the *trans* and terminally oxidized product **30** was used for the next reaction step to couple either a 4-hydroxybenzophenone or a diazirine to **30**. The benzophenone was introduced using a Mitsunobu reaction (**31**), while for the diazirine **33** and the second benzophenone **32** a nucleophilic substitution was used. After a deprotection step using fluoride, the resulting alcohol was substituted by a bromide in an Apple reaction. This very unstable allylic halogens were directly converted into their corresponding pyrophosphates by using $(n\text{-}Bu_4N)_3HP_2O_5$. Through ion exchange the farnesyl-analogues were converted into their water-soluble form. Three different photoactivatable probes **37**, **38** and **39** were successfully synthesized and further used in *in vitro* farnesylation assays.

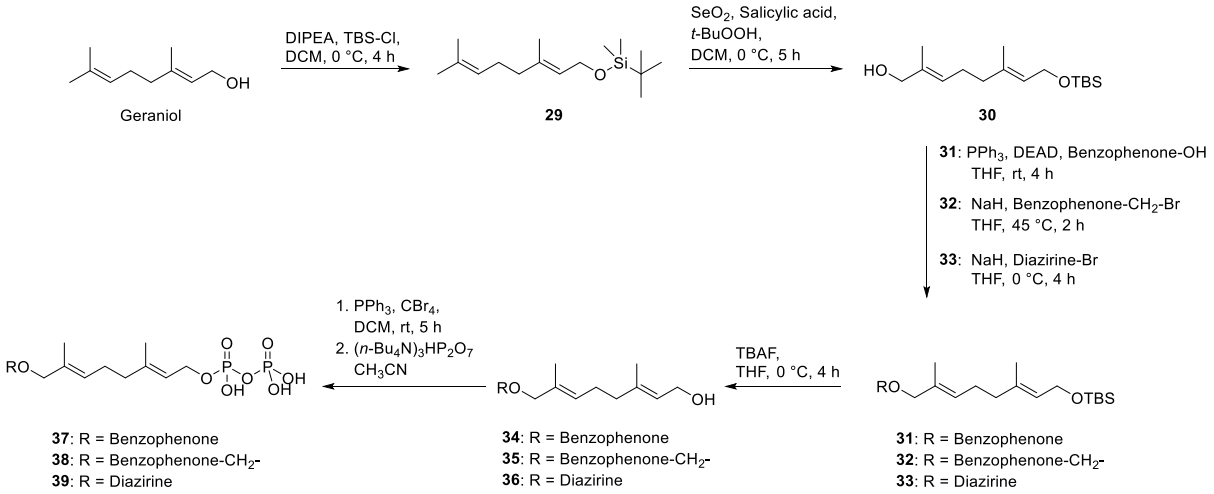

Figure 43: Synthesis route for photoactivatable farnesyl analogues.

4.3.2 Farnesylation of Spindly and interaction to the RZZ-complex

This experiment was performed by Dr. Anika Altenfeld and Sabine Wohlgemuth.

Spindly binds in a farnesyl-dependent manner to RZZ and leads to the recruitment of dynein to kinetochores. To investigate how prenylation contributes to the interaction of Spindly with the RZZ complex, I planned to use UV-crosslinking experiments to establish a covalent bond between the farnesyl moiety of Spindly and Rod-Zw10-Zwilch (RZZ). Therefore, Spindly should be modified using farnesyl derivatives carrying UV-activatable crosslinking group such as benzophenone or diazirine. After the chemical synthesis, these farnesyl analogues were introduced into Spindly by *in vitro* farnesylation (Figure 44A).

Previous studies showed insufficient labelling when using wild-type FTase and sterically demanding farnesyl analogues. Therefore, an engineered FTase$_{W102T_Y154T}$ was used, which showed broad substrate tolerance towards artificial farnesyl analogues.[84] Then, recombinant Spindly was incubated with the FTase, which employs farnesyl pyrophosphates to farnesylate proteins (Figure 44A). To test whether the three artificial farnesyl derivatives interfere with the binding of Spindly to RZZ, size-exclusion chromatography (SEC) was performed. Farnesylated Spindly was incubated with RZZ and transferred onto the column. If Spindly interacts with RZZ, the whole complex should elute earlier from the column, because the effective stokes radius increases upon interaction of RZZ and Spindly and therefore diffusion of this complex into the particles of the column is prevented.

Spindly farnesylated with either benzophenone **37**, **38** or diazirine **39** interacted with RZZ (Figure 44B and C, see black arrows). Thus, the three PAL-farnesyl derivatives have only a minor influence on the prenyl-dependent interaction. As a control, Spindly with its endogenous farnesylation was used in SEC and it showed similar retention time as Spindly carrying the artificial farnesylation. All three farnesyl derivatives have similar affinity to RZZ when attached to Spindly. These data suggest that Spindly bearing the UV-activatable crosslinking group can interact with RZZ and this modification does not influence its farnesyl-dependent interaction.

After elucidating, that Spindly's binding is only slightly influenced by artificial farnesyl moieties, the following experiments focused on the identification of the binding site and partner(s) of Spindly within the RZZ complex.

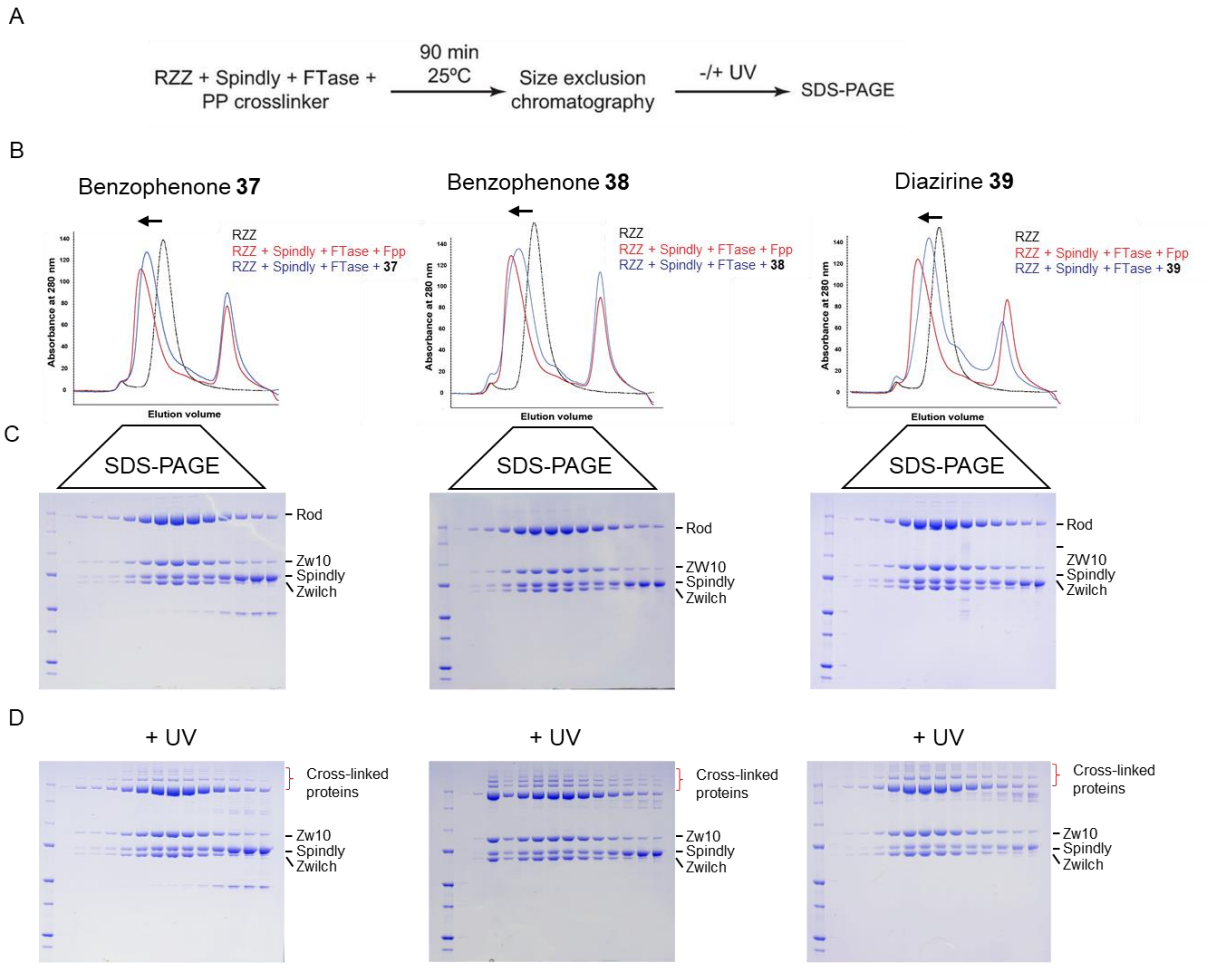

Figure 44: Size exclusion chromatography of RZZ in complex of Spindly farnesylated with different photoactivatable farnesyl analogues. (A) Workflow to investigate the cross-linking product between RZZ and farnesylated Spindly. (B) Chromatogram of SEC of samples of different composition. RZZ complex alone and in complex with Spindly, which was farnesylated with different farnesyl analogues. As controls, each chromatogram shows RZZ alone and in complex with Spindly farnesylated with its natural ligand Fpp. (C) SDS-PAGE of fractions from the earlier eluting peak. (D) SDS-PAGE samples of SEC irradiated with light to induce photocrosslinking. Fpp: Farnesyl pyrophosphate, PP crosslinker: prenyl-PAL-probes pyrophosphate.

4.3.3 Photocrosslinking of Spindly and RZZ

This experiment was performed by Dr. Anika Altenfeld, Dr. Tanja Bange and Dr. Jenny Keller.

To discover the binding site of Spindly to RZZ, photocrosslinking experiments followed by mass spectrometry-based analysis were performed. This technique allows to introduce a covalent bond between Spindly and RZZ followed by tandem mass spectrometry to identify the exact peptide at which the UV-active group reacted.

Spindly bearing one of the UV-activatable crosslinking farnesyl derivatives was incubated with RZZ and irradiated at 365 nm. After 60 min for the benzophenone-bearing compound **10** and **11** and 15 min for the diazirine-bearing compound **12**, the protein suspension was analyzed by SDS-PAGE.

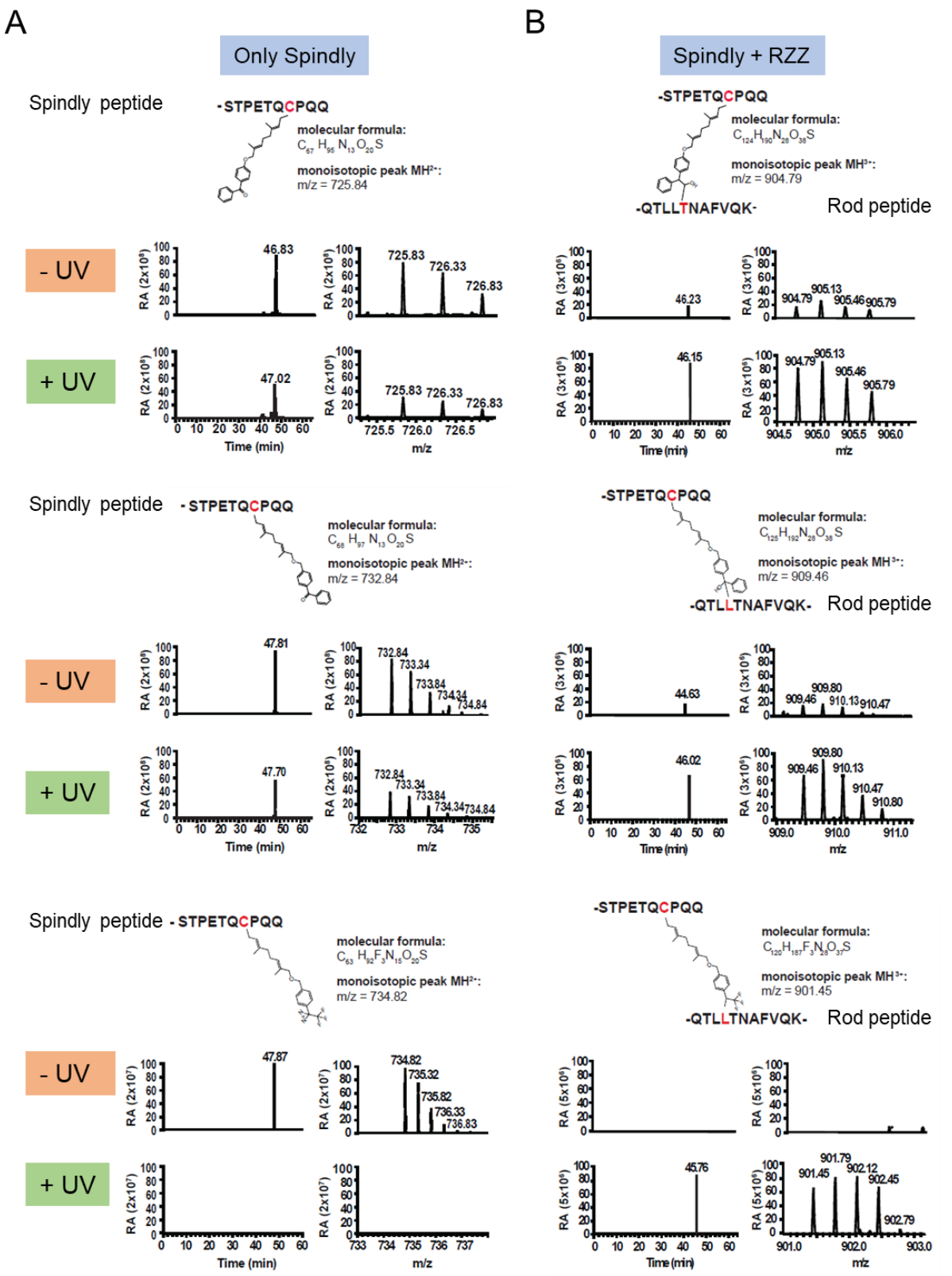

Figure 45: MS spectra of crosslinked products. (A) Mass traces of the peptide of Spindly bound to the corresponding photoactive farnesyl analogue before and after UV irradiation. (B) Mass traces of the aforementioned peptides bound to a peptide of Rod after photocrosslinking.

Compared to the negative control without the use of a photocrosslinking group, new bands appear in samples in which Spindly bears a photoactivatable group (Figure 44D) with molecular mass higher than 250 kDa. Considering the molecular masses of Spindly and the proteins in the RZZ complex, this new bands could result from a covalent bond between Spindly (~70 kDa) and Rod (~250 kDa). To confirm Rod as binding partner for Spindly's farnesyl-moiety tandem mass spectrometry was performed.

First, Spindly's peptide containing the photoactivatable farnesyl analogue was identified before and after UV irradiation. In the case of the benzophenones, mass traces of the peptide were identified suggesting unreacted Spindly was still present. The diazirine bearing peptide could not be detected after UV irradiation. The reason for these two different results lies in the reactivity of the different photoactive groups. Once the benzophenone is activated by light, its intermediate state can be reverted from the diradical state back to its stable form. If there is no amino acid in close proximity, it relaxes and undergoes a second activation cycle. In contrast, the diazirine moiety forms a carbene, which cannot revert its active form and has to react either with amino acids or the solvent.

Thereafter, obtained MS peptide spectra were searched for amino acid modifications according to the masses of the expected reacted photoactive groups bound to Spindly's peptide. Mass spectrometry could show that one peptide corresponding to Spindly is crosslinked to Leu120 or Thr119 in the β-propeller region of Rod. I could identify mass traces of Rod peptides bound to Spindly only in the UV-irradiated samples. Therefore, I concluded that Rod is the acceptor of Spindly's farnesyl-moiety.

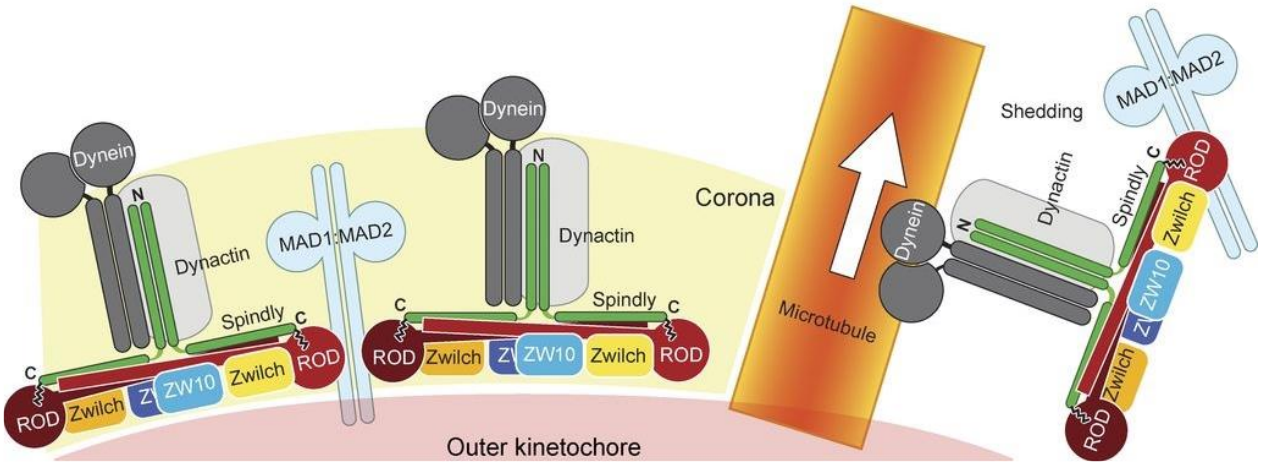

Figure 46: Hypothesis of the function of RZZ and Spindly within the fibrous corona. The RZZ complex (Rod-ZW10-Zwilch) recruit farnesylated Spindly to the fibrous corona. Spindly binds to dynactin and dynein, which is a motor protein for

microtubules. Once microtubules are bound to the kinetochore, dynein translocates the whole complex to the centromeres, which stabilizes the microtubule-bound kinetochore. Image from Mosalaganti *et. al.*.[85]

Previous work showed that other proteins in the fibrous corona like farnesylated CENP-F also bind to RZZ, which raises the question if Rod is a more general acceptor for farnesylated proteins.[86] Rod could be a new example of isoprenoid binding protein from which each is binding a group of different prenylated proteins. Other examples from this group are PDEδ[6] and RhoGDI[5][87].

Furthermore, RZZ recruits Spindly to the kinetochore which itself binds to dynein. An active dynein motor protein translocates the RZZ complex to the centrosomes, which leads to a stabilization of the interaction between kinetochores and microtubules. Spindly alone does not activates dynein, which raises the question whether RZZ increases the ability of Spindly to turn dynein into a progressive motor.[88]

4.4 Conclusion

By using a chemical biology approach, Spindly´s binding partner and site could be identified when in complex with Rod-Zwilch-Zw10 (RZZ). Three different photoactivatable groups were introduced into farnesyl, which were supposed to mimic its natural binding occurrence. To test whether Spindly´s binding affinity remains, Spindly was farnesylated with the farnesyl analogies by using a mutated FTase and analyzed by SEC. These artificial Spindly proteins in complex with RZZ have the same retention times as the natural Spindly, thus, binding affinity remains.

The complex of RZZ and Spindly was irradiated with light, which activates the artificial farnesyl analogues and leads to a proximity-driven covalent bond formation between Spindly and proteins of RZZ. A SDS-PAGE elucidates new band formation at higher molecular weights (>250 kDa) indicating Rod as direct binding partner. Furthermore, the gels were analyzed by mass spectrometry to identify the peptide at which covalent bond formation occurred. This analysis revealed Spindly´s binding site within the β-propeller region of Rod, which is the biggest protein of RZZ. Rod is the acceptor for the farnesyl-moiety of Spindly, whose affinity relies on a combination of farnesyl group and surface interactions.

These findings lead to a new hypothesis of the function of Spindly and Rod, which might be a more general farnesyl acceptor. Further studies will focus on elucidating the mechanistic and function of the farnesyl-dependent interaction between RZZ and Spindly.

5 Experimental part

5.1 Chemistry

5.1.1 General

All reactions were carried out in glassware dried with a heat gun under argon atmosphere. All commercially available compounds were used as provided without further purification. They were purchased from Acros Organics, Alfa Aesar, Sigma Aldrich, TCI Europe, or Fisher. Dry solvents were purchased as laboratory grade and used without further purification (e.g. dichloromethane, acetonitrile, DMF and THF). Analytical thin-layer chromatography (TLC) was performed on Merck silica gel aluminum plates with F-254 indicator. Compounds were visualized by irradiation with UV light or potassium permanganate staining. Column chromatography was performed using silica gel Acros 60 A. Column chromatography was performed using silica gel Merck 60 (particle size 0.040-0.063 mm).

NMR were either measured on DRX400 (400 MHz), Bruker DRX500 (500 MHz), INOVA500 (500 MHz) and DRX600 (600 MHz) at 300 K using $CDCl_3$ or CH_3OD as solvent and internal standard. Multiplicities are indicated as: s (singlet), d (doublet), t (triplet), q (quartet), quin (quintet), m (multiplet) and dd (doublet of a doublet); and coupling constants (*J*) are given in Hertz (Hz).

High resolution mass spectrometry was recorded on a LTQ Orbitrap (Thermo Fisher) coupled to a HPLC-system of Accela (HPLC column: Hypersyl GOLD, 50 mM x 1 mM, particle size 1.9 µm) via electron spray ionization. When annotated molecules were purified with a mass-directed HPLC system from Agilent (Agilent Series 1100/LC/MSD VL) with reversed-phase C4 or C18 column and a flow rate of 20 ml/min.

5.1.2 Synthesis of protein degradation-inducing compounds

5.1.2.1 N-(4-Chlorobenzyl)cyclopentylamine (5)

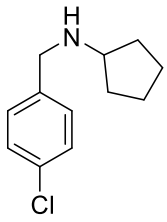

The compound **5** was synthesized according to literature.[14] 4-Chlorobenzaldehyde (10 g, 70 mmol, 1 eq.) and $MgSO_4$ (25.7 g, 210 mmol, 3 eq.) were dissolved in 70 ml dry MeOH. Cyclopentylamine (7.0 ml, 70 mmol, 1 eq.) was slowly added at zero degrees and the reaction stirred for 30 min. Afterwards $NaBH_4$ (1.3 g, 40 mmol, 0.5 eq.) was added portion wise to the ice-cold solution. The solution was allowed to warm up to room temperature and was

stirred for 30 min. The reaction was quenched with water and MeOH removed under reduced pressure. The product was extracted with CH_2Cl_2 and washed with brine. The combined organic phases were dried over $MgSO_4$. The product (12.2 g, 60 mmol, 81%) could be obtained as yellow powder and could be used without a purification step.

^{1}H NMR (400 MHz, $CDCl_3$): δ = 7.29 – 7.23 (m, 4H), 3.73 (s, 2H), 3.13 – 3.03 (m, 1H), 1.89 – 1.79 (m, 2H), 1.74 – 1.64 (m, 2H), 1.58 – 1.48 (m, 2H), 1.41 – 1.30 (m, 2H). Resulting ^{1}H-NMR matched reported literature data.[14]

5.1.2.2 4-Bromo-N-(4-chlorobenzyl)-N-cyclopentylbenzenesulfonamide (6)

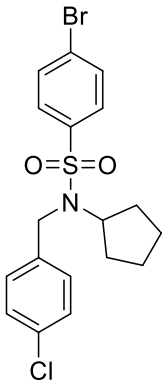

The compound **6** was synthesized according to literature.[14] N-(4-chlorobenzyl)cyclopentanamine **5** (12.2 g, 60 mmol, 1 eq.) and 4-bromobenzenesulfonyl chloride (14.9 g, 60 mmol, 1 eq.) were dissolved in 200 ml CH_2Cl_2 and treated with triethylamine (7.8 ml, 60 mmol, 1 eq.) for 5 h. The reaction was quenched with water, extracted with CH_2Cl_2, washed with brine and dried over $MgSO_4$. The product (20.0 g, 50 mmol, 80%) was obtained without further purification step.

^{1}H NMR (400 MHz, $CDCl_3$): δ = 7.67 – 7.57 (m, 4H), 7.30 – 7.22 (m, 4H), 4.28 (s, 2H), 4.26 – 4.18 (m, 1H), 1.65 – 1.52 (m, 2H), 1.52 – 1.43 (m, 2H), 1.43 – 1.33 (m, 2H), 1.28 – 1.16 (m, 2H). Resulting ^{1}H-NMR matched reported literature data.[14]

5.1.2.3 4-(Benzylthio)-N-(4-chlorobenzyl)-N-cyclopentylbenzenesulfoneamide (7)

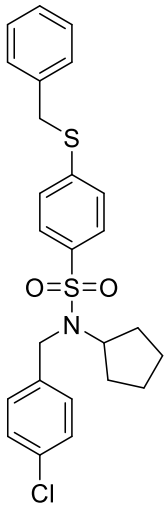

The compound **7** was synthesized according to literature.[14] The compound **6** (19.9 g, 46.5 mmol, 1 eq.) was dissolved in dry 200 ml dioxane and treated with DIPEA (15.8 ml, 90 mmol, 2 eq.). The flask was three times evacuated and flushed with argon. Then, catalyst $Pd_2(dba)_3$ (1 g, 1.2 mmol, 0.03 eq.), Xantphos (1.3 g, 2.33 mmol, 0.05 eq.) and benzylthiol (5.5 ml, 47 mmol, 1 eq.) were added and the reaction heated to reflux overnight. The reaction mixture was then allowed to reach room temperature, filtered and concentrated. The crude was purified by column chromatography (silica, 20% ethyl acetate in cyclohexane) to afford the pure product (22 g, 40 mmol, 78%) as yellow powder.

^{1}H NMR (400 MHz, $CDCl_3$): δ = 7.68 – 7.63 (m, 2H), 7.38 – 7.24 (m, 11H), 4.29 (s, 2H), 4.27 – 4.22 (m, 1H), 4.21 (s, 2H), 1.55 (s, 2H), 1.52 – 1.44 (m, 2H), 1.44 – 1.37 (m, 2H), 1.28 – 1.18 (m, 2H). Resulting ^{1}H-NMR matched reported literature data.[14]

5.1.2.4 4-(N-(4-Chlorobenzyl)-N-cyclopentylsulfamoyl)benzenesulfonyl chloride (8)

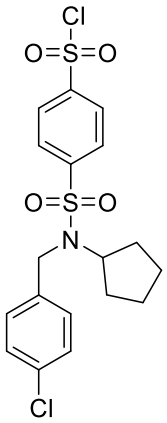

The compound **8** was synthesized according to literature.[14] Compound **7** (6.1 g, 13 mmol, 1 eq.) was dissolved in a mixture of acetonitrile/acetic acid/H_2O (40:1.5:1) and cooled to 0 °C. 1,3-Dichloro-5,5-dimethylhydantoin (5.1 g, 30 mmol, 2 eq.) was added portion wise and stirred for 2 h on ice. The reaction was concentrated under vacuum and dissolved in acetonitrile. The ice-cold solution was treated with $NaHCO_3$ and stirred for 30 min. The organic phase was washed with cold brine, dried over $MgSO_4$ and concentrated under reduced pressure. The product (5.7 g, 10 mmol, 98%) was obtained as yellow solid and could be used without further purification.

^{1}H NMR (400 MHz, $CDCl_3$): δ = 8.17 – 8.11 (m, 2H), 8.05 – 7.96 (m, 2H), 7.42 – 7.25 (m, 4H), 4.37 (s, 2H), 4.36 – 4.27 (m, 1H), 1.74 – 1.64 (m, 2H), 1.62 – 1.54 (m, 2H), 1.53 – 1.44 (m, 2H), 1.38 – 1.27 (m, 2H). Resulting ^{1}H-NMR matched reported literature data.

5.1.2.5 *t*-Butyl 4-(((4-(N-(4-chlorobenzyl)-N-cyclopentylsulfamoyl)phenyl)sulfonamido)-methyl)piperidine-1-carboxylate (9)

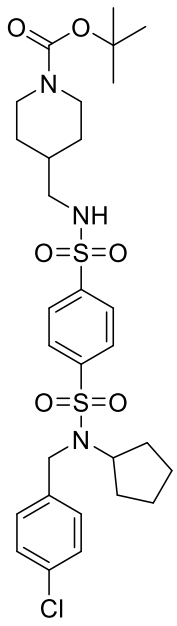

The compound **9** was synthesized according to literature.[14] 4-(N-(4-Chlorobenzyl)-N-cyclopentylsulfamoyl)benzenesulfonyl chloride **8** (6 g, 13.4 mmol, 1 eq.) and *t*-butyl-4-(aminomethyl)piperidine-1-carboxylate (2.9 g, 13.4 mmol, 1 eq.) were dissolved in 300 ml CH_2Cl_2 and treated with triethylamine (2 g, 20 mmol, 1.5 eq.). After stirring for 30 min at 0 °C, water was added, and the product extracted into CH_2Cl_2. The combined extracts were dried over $MgSO_4$ and the solvent removed under reduced pressure. The crude was purified by column chromatography (silica, 30% ethyl acetate in cyclohexane) to afford the pure product (7.9 g, 12.65 mmol, 95%) as yellow powder.

^{1}H NMR (400 MHz, $CDCl_3$): δ = 8.06 – 7.81 (m, 4H), 7.41 – 7.23 (m, 4H), 4.35 (s, 2H), 4.33 – 4.20 (m, 1H), 4.10 (d, *J* = 13.2 Hz, 2H), 3.20 – 3.11 (m, 1H), 1.70

– 1.47 (m, 10H), 1.44 (s, 9H), 1.34 – 1.18 (m, 4H), 1.15 – 1.00 (m, 2H). Resulting ^{1}H-NMR matched reported literature data.[14]

5.1.2.6 4-(((4-(N-(4-Chlorobenzyl)-N-cyclopentylsulfamoyl)-N-((1-pivaloylpiperidine-4-yl)methyl)phenyl)sulfonamido)methyl)benzoic acid (10)

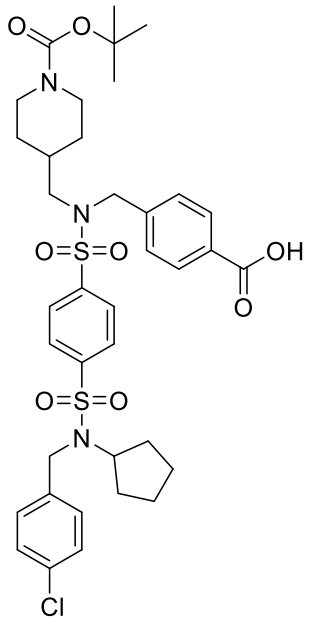

The amine **9** (2.1 g, 3.35 mmol, 1 eq.) and $CsCO_3$ (4.4 g, 13.41 mmol, 4 eq.) were dissolved in 40 ml DMF and after 30 min at room temperature methyl-4-(bromomethyl)benzoate (768 mg, 3.35 mmol, 1 eq.) was added. The reaction was quenched with sat. NaCl solution and the crude product was extracted with ethyl acetate. After combining the organic phases, the solvent was removed under reduced pressure.

The ester (2.6 g, 3.35 mmol, 1 eq.) was used in the next reaction without any purification step in between. The compound was dissolved in 40 ml of a mixture of THF/H2O (2:1) and LiOH (802 mg, 30 mmol, 10 eq.) was slowly added. After 16 h at room temperature the solvent was removed, and the residuals dissolved in cold acetonitrile. The suspension was filtered to afford the pure product (2.1 g, 2.88 mmol, 86%) as white solid.

^{1}H NMR (600 MHz, $CDCl_3$): δ = 8.05 (d, *J* = 8.3 Hz, 2H), 7.96 – 7.89 (m, 4H), 7.38 (d, *J* = 8.2 Hz, 2H), 7.33 – 7.28 (m, 5H), 4.38 (s, 2H, benzylic CH_2), 4.35 (s, 2H, benzylic CH_2), 4.34 – 4.28 (m, 1H, *c*-pen 1-H), 4.01 (d, *J* = 12.8 Hz, 2H, piperidine 2/6-H_B), 3.03 (d, *J* = 7.0 Hz, 2H, N*H*$_2$CH), 2.43 (t, *J* = 11.7 Hz, 2H, piperidine 2/6-H_A), 1.69 – 1.61 (m, 2H, *c*-pen 2/5-H_A), 1.58 – 1.49 (m, 4H, *c*-pen 3/4-H_B and piperidine 3/5-H_B), 1.49 – 1.44 (m, 3H, piperidine 4-H and *c*-pen 3/4-H_A), 1.42 (s, 9H, Boc), 1.34 – 1.23 (m, 2H, *c*-pen 2/5-H_B), 0.96 (qd, *J* = 12.6, 4.2 Hz, 2H, piperidine 3/5-H_A). **^{13}C NMR** (151 MHz, $CDCl_3$): δ = 169.34 (COOH), 154.83 (CO), 145.01 (Ar-C_q), 143.22 (Ar-C_q), 142.06 (Ar-C_q), 136.87 (Ar-C_q), 133.43 (Ar-C_q), 130.74 (CH-Ar), 129.17 (Ar-C_q), 128.85 (CH-Ar), 128.68 (CH-Ar), 128.47 (CH-Ar), 128.16 (CH-Ar), 128.03 (CH-Ar), 79.72 (C_q-Boc), 59.93 (*c*-Pen 1-C), 55.31 (N*C*H$_2$CH), 53.41 (benzylic CH_2), 47.16 (benzylic CH_2), 43.46 (piperidine 2/6-C), 35.27 (piperidine 4-C), 29.83 (piperidine 3/5-C), 29.59 (c-pen 2/5-C), 28.56 (3 x CH_3), 23.41 (*c*-pen 3/4-C). **HRMS** (ESI): $C_{37}H_{47}O_8N_3ClS_2$ $[M+H]^+$: calculated: 760.2488, found: 760.2490.

5.1.2.7 2-(2,6-Dioxopiperidine-3-yl)-4-fluoroisoindoline-1,3-dione (11)

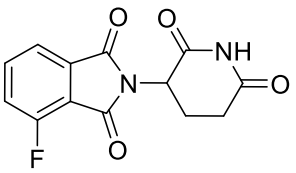

The compound **11** was synthesized according to literature.[89] 3-fluoropthalic anhydride (1 g, 6.1 mmol, 1 eq.) and 3-aminopiperidine-2,6-dione hydrochloride (1 g, 6.1 mmol, 1 eq.) were dissolved in 20 ml acetic acid. The reaction mixture was heated to reflux and stirred overnight. After cooling it down to room temperature, acetic acid was evaporated. The crude was purified by column chromatography (silica, 5% methanol in dichloromethane) to afford the pure product (1.3 g, 4.6 mmol, 75%) as white powder.

^{1}H NMR (400 MHz, DMSO-d_6): δ = 11.12 (s, 1H), 7.98 – 7.92 (m, 1H), 7.80 (s, 1H), 7.73 (t, *J* = 8.9 Hz, 1H), 5.15 (dd, *J* = 12.9, 5.4 Hz, 1H), 2.95 – 2.84 (m, 1H), 2.67 – 2.52 (m, 2H), 2.11 – 2.03 (m, 1H). Resulting ^{1}H-NMR matched reported literature data.

5.1.2.8 4-Fluoro-2-(1-methyl-2,6-dioxopiperidine-3-yl)isoindoline-1,3-dione (18)

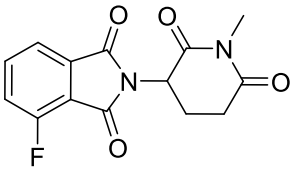

The compound **11** (200 mg, 0.72 mmol, 1 eq.), methyl iodide (123 mg, 0.87 mmol, 1.2 eq.) and K_2CO_3 (86 mg, 0.87 mmol, 1.2 eq.) were dissolved in 2 ml dry DMF. After 2 h at reflux the solvent was removed under reduced pressure and the residuals dissolved in water. The crude product was extracted with CH_2Cl_2 and the combined organic phases dried over $MgSO_4$. The solvent was removed under reduced pressure and the product (134 mg, 0.46 mmol, 63%) was obtained as white solid.

^{1}H NMR (600 MHz, CD_3OD): δ = 7.91 – 7.86 (m, 1H), 7.75 (d, *J* = 7.3 Hz, 1H), 7.57 (t, *J* = 8.8 Hz, 1H), 5.17 (dd, *J* = 13.1, 5.5 Hz, 1H), 3.16 (s, 3H), 2.92 – 2.84 (m, 2H), 2.75 – 2.67 (m, 1H), 2.17 – 2.10 (m, 1H). **^{13}C NMR** (151 MHz, CD_3OD) δ = 173.52, 171.05, 167.72, 165.53, 159.94, 158.19, 138.72, 135.42, 123.87, 120.84, 51.36, 32.42, 27.34, 22.74. **HRMS** (ESI): $C_{14}H_{12}O_4N_2F_1$ $[M+H]^+$; calculated: 291.0776, found: 291.0778.

5.1.2.9 4-((14-Azido-3,6,9,12-tetraoxatetradecyl)amino)-2-(1-methyl-2,6-dioxopiperidine-3-yl)isoindoline-1,3-dione (19)

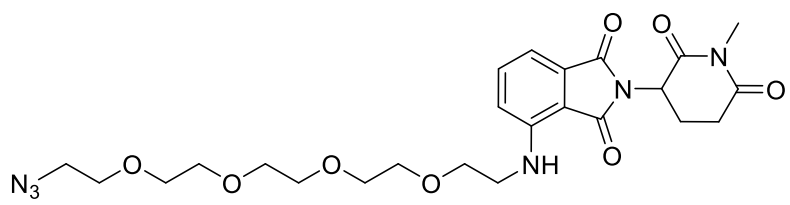

Compound **18** (871 mg, 3 mmol, 1 eq.), N_3-PEG_3-NH_2 (787 mg, 1 mmol, 1 eq.) and DIPEA (1.0 ml, 6 mmol, 2 eq.) were dissolved in 5 ml dry DMF and heated to 90 °C. After 12 h the solvent removed under

reduced pressure and the crude was purified by column chromatography (silica, 30% ethyl acetate in cyclohexane) to afford the pure product (492.0 mg, 0.92 mmol, 31%) as yellow oil.

^{1}H NMR (500 MHz, $CDCl_3$): δ = 7.48 (dd, *J* = 8.5, 7.1 Hz, 1H), 7.09 (d, *J* = 7.0 Hz, 1H), 6.92 (d, *J* = 8.5 Hz, 1H), 6.47 (t, *J* = 5.7 Hz, 1H), 4.93 – 4.87 (m, 1H), 3.71 (t, *J* = 5.5 Hz, 2H), 3.68 – 3.62 (m, 14H), 3.47 (q, *J* = 5.6 Hz, 2H), 3.41 – 3.35 (m, 2H), 3.20 (s, 3H), 3.01 – 2.91 (m, 1H), 2.82 – 2.70 (m, 2H), 2.12 – 2.06 (m, 1H).

5.1.2.10 4-((2-(2-(2-(2-Aminoethoxy)ethoxy)ethoxy)ethyl)amino)-2-(1-methyl-2,6-dioxopiperidine-3-yl)isoindoline-1,3-dione (20)

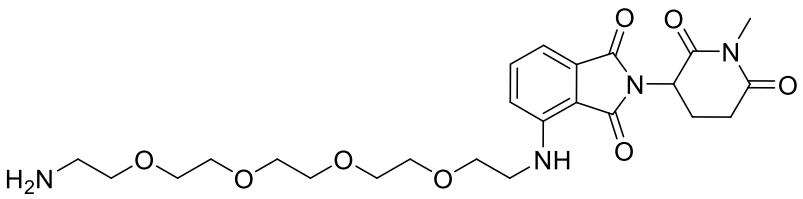

Compound **19** (492 mg, 0.92 mmol, 1 eq.) was dissolved in 6 ml dry THF and polymer-bound PPh_3 (613 mg, 3 mmol/g, 2 eq.) was added. After 3 h at 70 °C the beads were filtered off and the solvent was removed under reduced pressure. The crude was purified by column chromatography (silica, cyclohexane/ethyl acetate/NH_3H_2O = 100/5/1) to afford the pure product (212 mg, 0.42 mmol, 45%) as yellow oil.

^{1}H NMR (600 MHz, CD_3OD): δ = 7.58 (dd, *J* = 8.6, 7.1 Hz, 1H), 7.12 (d, *J* = 8.5 Hz, 1H), 7.08 (d, *J* = 7.0 Hz, 1H), 5.09 (dd, *J* = 12.9, 5.5 Hz, 1H), 3.74 (t, *J* = 5.2 Hz, 2H, OCH_2), 3.70 – 3.60 (m, 14H, 7 x OCH_2), 3.52 (t, *J* = 5.2 Hz, 2H, NH_2CH_2), 3.15 (s, 3H, CH_3), 3.09 (t, *J* = 5.0 Hz, 2H, $NHCH_2$), 2.91 – 2.87 (m, 2H, dioxopiperidine 5-H), 2.72 – 2.65 (m, 1H, dioxopiperidine 4-H_B), 2.13 – 2.07 (m, 1H, dioxopiperidine 4-H_A). **^{13}C NMR** (150 MHz, CD_3OD): δ = 173.66 (CO), 171.46 (CO), 170.81 (CO), 169.23 (CO), 148.24 (Ar-C_q), 137.30 (Ar-CH), 133.91 (Ar-C_q), 118.29 (Ar-CH), 112.15 (Ar-CH), 111.37 (Ar-C_q), 71.59 (OCH_2), 71.47 (OCH_2), 71.43 (2 x OCH_2), 71.39 (OCH_2), 71.11 (OCH_2), 70.64 (OCH_2), 67.82 (OCH_2), 50.85 (CH), 43.22 ($NHCH_2$ [linker]), 40.62 ($NHCH_2$ [linker]), 32.48 (CH_2), 27.35 (CH_3), 23.06 (CH_2). **HRMS** (ESI): $C_{24}H_{35}O_8N_4$ $[M+H]^+$; calculated: 507.2449, found: 507.2443.

5.1.2.11 4-((2-(2-(2-Azidoethoxy)ethoxy)ethyl)amino)-2-(2,6-dioxopiperidine-3-yl)isoindoline-1,3-dione (12)

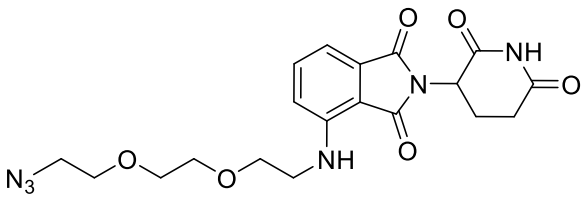

The compound was synthesized according to the procedure used for **19** by using following starting material: compound **11** (200.0 mg, 0.72 mmol, 1 eq.), H_2N-PEG_2-N_3 (250.8 mg, 0.71 mmol, 1 eq.) and DIPEA (246 µl, 1.45 mmol, 2 eq.). The product (174.5 mg, 0.41 mmol, 56%) was obtained as yellow solid and used without further purification.

^{1}H NMR (500 MHz, $CDCl_3$): δ = 8.40 (d, *J* = 33.2 Hz, 1H), 7.51 – 7.44 (m, 1H), 7.09 (dd, *J* = 7.1, 1.6 Hz, 1H), 6.91 (d, *J* = 8.5 Hz, 1H), 6.49 (t, *J* = 5.7 Hz, 1H), 4.91 (dd, *J* = 12.3, 5.3 Hz, 1H), 3.73 (t, *J* = 5.4 Hz, 2H), 3.67 (d, *J* = 1.4 Hz, 6H), 3.47 (q, *J* = 5.5 Hz, 2H), 3.37 (t, *J* = 5.0 Hz, 2H), 2.87 (d, *J* = 15.2 Hz, 1H), 2.72 (d, *J* = 31.6 Hz, 2H), 2.14 – 2.08 (m, 1H).

5.1.2.12 4-((2-(2-(2-Aminoethoxy)ethoxy)ethyl)amino)-2-(2,6-dioxopiperidine-3-yl)-isoindoline-1,3-dione (15)

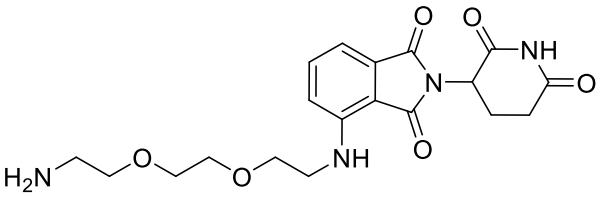

The compound was synthesized according to the procedure used for **20** by using following starting material: compound **12** (143.0 mg, 0.33 mmol, 1 eq.) and polymer-supported PPh_3 (250.8 mg, 0.71 mmol, 1 eq.). The product (63 mg, 0.16 mmol, 46%) was obtained as yellow solid.

^{1}H NMR (600 MHz, $CDCl_3$): δ = 7.51 – 7.45 (m, 1H), 7.11 – 7.08 (m, 1H), 6.92 – 6.89 (m, 1H), 6.51 (t, *J* = 5.7 Hz, 1H), 4.92 – 4.88 (m, 1H), 3.76 – 3.69 (m, 2H), 3.70 – 3.63 (m, 6H), 3.54 – 3.50 (m, 2H), 3.49 – 3.44 (m, 2H), 2.90 – 2.83 (m, 1H), 2.81 – 2.70 (m, 2H), 2.15 – 2.07 (m, 1H). **HRMS** (ESI): $C_{19}H_{25}O_6N_4$ $[M+H]^+$; calculated: 405.1769, found: 405.1768.

5.1.2.13 4-((2-(2-(2-(2-Azidoethoxy)ethoxy)ethoxy)ethyl)amino)-2-(2,6-dioxopiperidine-3-yl)isoindoline-1,3-dione (13)

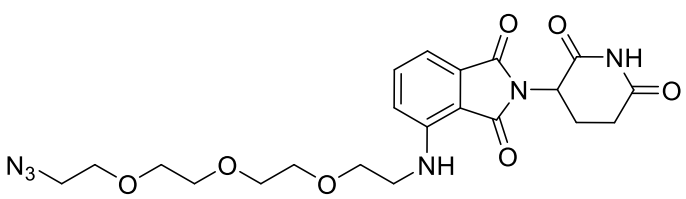

The compound was synthesized according to the procedure used for **19** by using following starting material: compound **11** (276 mg, 1.0 mmol, 1 eq.), H_2N-PEG_2-N_3 (218.3 mg, 1.0 mmol, 1 eq.) and DIPEA (248.4 µl, 2 mmol, 2 eq.). The

product (252.9 mg, 0.56 mmol, 71%) was obtained as yellow solid and used without further purification.

^{1}H NMR (400 MHz, $CDCl_3$): δ = 8.36 (s, 1H), 7.47 (dd, *J* = 8.1, 7.2 Hz, 1H), 7.09 (d, *J* = 7.1 Hz, 0.6, 1H), 6.91 (d, *J* = 8.5 Hz, 1H), 6.47 (t, *J* = 5.7 Hz, 1H), 4.97 – 4.89 (m, 1H), 3.71 (t, *J* = 5.4 Hz, 2H), 3.69 – 3.61 (m, 10H), 3.46 (q, *J* = 5.6 Hz, 2H), 3.36 (d, *J* = 5.1 Hz, 2H), 2.90 – 2.67 (m, 2H), 2.14 – 2.07 (m, 1H).

5.1.2.14 4-((2-(2-(2-(2-Aminoethoxy)ethoxy)ethoxy)ethyl)amino)-2-(2,6-dioxopiperidine-3-yl)isoindoline-1,3-dione (16)

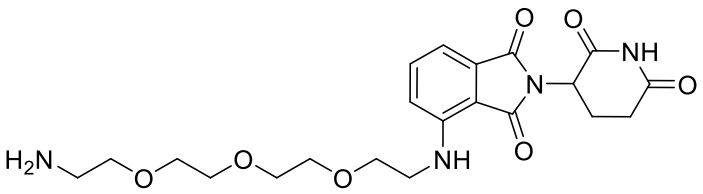

The compound was synthesized according to the procedure used for **20** by using following starting material: compound **13** (374.0 mg, 0.56 mmol, 1 eq.) and polymer-supported PPh_3 (526 mg, 3 mmol/g, 2 eq.). The product (252.9 mg, 0.56 mmol, 72%) was obtained as yellow solid.

^{1}H NMR (500 MHz, $CDCl_3$) δ = 7.49 – 7.41 (m, 1H), 7.09 – 7.01 (m, 1H), 6.90 – 6.84 (m, 1H), 6.54 – 6.44 (m, 1H), 4.90 – 4.85 (m, 1H), 3.73 – 3.67 (m, 2H), 3.67 – 3.55 (m, 10H), 3.53 – 3.48 (m, 2H), 3.46 – 3.39 (m, 2H), 2.90 – 2.84 (m, 1H), 2.75 – 2.66 (m, 1H), 2.53 – 2.40 (m, 1H).
HRMS (ESI): $C_{21}H_{29}O_7N_4$ $[M+H]^+$; calculated: 449.2031, found: 449.2027.

5.1.2.15 4-((14-Azido-3,6,9,12-tetraoxatetradecyl)amino)-2-(2,6-dioxopiperidine-3-yl)isoindoline-1,3-dione (14)

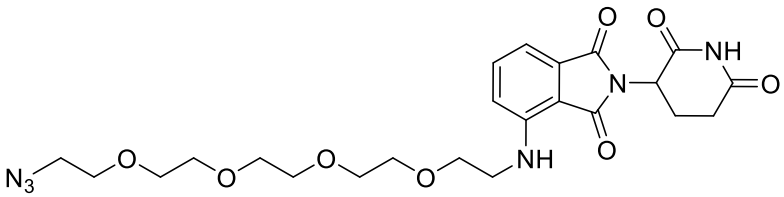

The compound was synthesized according to the procedure used for **19** by using following starting material: compound **11** (1.1 g, 4.0 mmol, 1 eq.), H_2N-PEG_2-N_3 (1.0 g, 4.0 mmol, 1 eq.) and DIPEA (1.49 ml, 2 mmol, 2 eq.). The product (1.0 g, 1.97 mmol, 49%) was obtained and used without further purification.

^{1}H NMR (400 MHz, $CDCl_3$): δ = 8.24 – 8.12 (m, 1H), 7.49 (dd, *J* = 8.5 Hz, 7.2, 1H), 7.10 (d, *J* = 7.1 Hz, 1H), 6.92 (d, *J* = 8.5 Hz, 1H), 6.49 (t, *J* = 5.7 Hz, 1H), 4.91 (dd, *J* = 12.1, 5.4 Hz, 1H), 3.72 (t, *J* = 5.4 Hz, 2H), 3.69 – 3.65 (m, 14H), 3.47 (q, *J* = 5.4 Hz, 2H), 3.38 (t, *J* = 5.1 Hz, 2H), 2.84 – 2.65 (m, 2H), 2.16 – 2.09 (m, 1H).

5.1.2.16 4-((14-Amino-3,6,9,12-tetraoxatetradecyl)amino)-2-(2,6-dioxopiperidine-3-yl)isoindoline-1,3-dione (17)

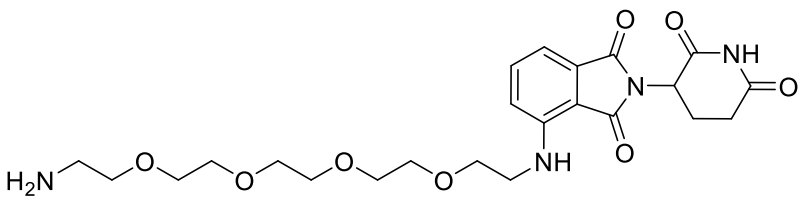

The compound was synthesized according to the procedure used for **20** by using following starting material: compound **14** (1.0 g, 1.97 mmol, 1 eq.) and polymer-supported PPh_3 (1.3 mg, 3 mmol/g, 2 eq.). The product (485 mg, 0.98 mmol, 50%) was obtained as yellow solid.

^{1}H NMR (600 MHz, $CDCl_3$) δ = 7.46 (t, *J* = 7.8 Hz, 1H), 7.07 (d, *J* = 7.1 Hz, 1H), 6.89 (d, *J* = 8.6 Hz, 1H), 6.48 (t, *J* = 5.7 Hz, 1H), 4.88 (dd, *J* = 12.3, 5.3 Hz, 1H), 3.70 (t, *J* = 5.4 Hz, 2H), 3.68 – 3.59 (m, 14H), 3.50 (t, *J* = 5.0 Hz, 2H), 3.44 (q, *J* = 5.3 Hz, 2H), 2.81 – 2.64 (m, 2H), 2.10 – 2.05 (m, 1H). **HRMS** (ESI): $C_{23}H_{33}O_8N_4$ $[M+H]^+$; calculated: 493.2293, found: 493.2291.

5.1.2.17 4-(((4-(N-(4-Chlorobenzyl)-N-cyclopentylsulfamoyl)-N-(piperidine-4-ylmethyl)-phenyl)sulfonamido)methyl)-N-(14-((2-(1-methyl-2,6-dioxopiperidine-3-yl)-1,3-dioxoisoindoline-4-yl)amino)-3,6,9,12-tetraoxatetradecyl)benzamide (4)

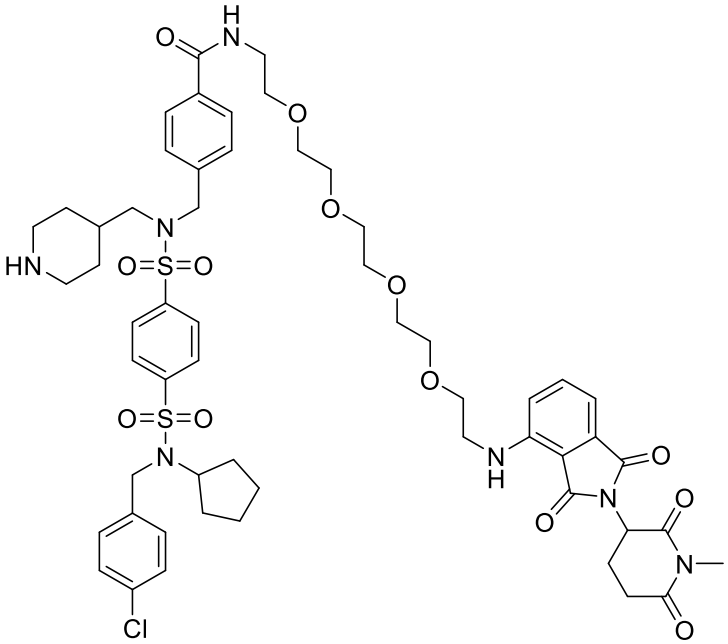

The carboxylic acid **10** (82.6 mg, 0.11 mmol, 1.1 eq.), DIPEA (14.0 mg, 0.1 mmol, 1 eq.) and PyBOP (56.5 mg, 0.11 mmol, 1.1 eq.) were dissolved in 2 ml DMF and stirred for 5 min at room temperature. Then the amine **20** (50 mg, 0.1 mmol, 1 eq.) was added under stirring and left at room temperature for 2 h. Afterwards the reaction was quenched with brine and the product extracted with ethyl acetate. The organic phases were combined and dried over $MgSO_4$. After removing the solvent under reduced pressure, the product could be obtained by flash chromatography (silica, 5% methanol in dichloromethane) as a yellow oil.

The product was dissolved in 10 ml of 50% TFA in CH_2Cl_2 and left stirring for 30 min. The solvent was removed under a continuous air flow and purified using reversed-phase HPLC (C_{18}, H_2O in acetonitrile 10 to 80% over 30 min). The product (20.2 mg, 0.02 mmol, 17%) could be obtained as yellow solid.

^{1}H NMR (700 MHz, CD_3OD): δ = 8.04 – 7.97 (m, 4H), 7.77 (d, *J* = 7.2 Hz, 2H), 7.53 (t, *J* = 7.7 Hz, 1H, , isoindoline 6-C), 7.37 (t, *J* = 7.0 Hz, 4H), 7.32 (d, *J* = 7.6 Hz, 2H), 7.06 (d, *J* = 8.5 Hz, 1H, isoindoline 5-H), 7.04 (d, *J* = 6.8 Hz, 1H, isoindoline 7-H), 5.07 (dd, *J* = 12.9 Hz, 5.2, 1H, dioxopiperidine 3-H), 4.42 (s, 2H, benzylic CH_2), 4.40 (s, 2H, benzylic CH_2), 4.36 – 4.32 (m, 1H, *c*-Pen 1-H), 3.69 (t, *J* = 5.1 Hz, 2H, OCH_2), 3.65 – 3.59 (m, 14H, 7 × OCH_2), 3.55 (t, *J* = 5.1 Hz, 2H, NHC*H*$_2$), 3.47 (t, *J* = 5.2 Hz, 2H, NHC*H*$_2$), 3.30 – 3.28 (m, 2H, piperidine 2-H_A/6-H_A), 3.15 (d, *J* = 8.0 Hz, 2H, NC*H*$_2$CH), 3.11 (s, 3H, NCH_3), 2.89 – 2.85 (m, 1H, dioxopiperidine 4-H_A), 2.77 – 2.64 (m, 4H, piperidine 2-H_B/6-H_B and dioxopiperidine 5-H), 2.10 – 2.06 (m, 1H, dioxopiperidine 4-H_B), 1.80 (d, *J* = 13.0 Hz, 2H, piperidine 3-H_A/5-H_A), 1.71 – 1.66 (m, 1H, piperidine 4-H), 1.63 – 1.58 (m, 2H, *c*-pen 2-H/5-H), 1.57 – 1.52 (m, 2H, *c*-pen 3-H/4-H), 1.51 – 1.38 (2H, *c*-pen 3-H/4-H), 1.37 – 1.21 (m, 4H, *c*-pen 2-H/5-H and piperidine 3-H_B/5-H_B). **^{13}C NMR** (175 MHz, CD_3OD): δ = 173.66 (CO), 171.42 (CO), 170.71 (CO), 169.54 (CO), 169.30 (CO), 148.23 (Ar-C_q), 146.12 (Ar-C_q), 144.35 (Ar-C_q), 141.44 (Ar-C_q), 139.22 (Ar-C_q), 137.27 (isoindoline 6-C), 135.42 (Ar-C_q), 134.03 (Ar-C_q), 133.85 (Ar-C_q), 130.02 (Ar-CH), 129.82 (Ar-CH), 129.48 (Ar-CH), 129.38 (Ar-CH), 129.30 (Ar-CH), 128.74(Ar-CH), 118.34 (isoindoline 5-C), 112.07 (isoindoline 7-C), 111.25 (Ar-C_q), 71.61 (OCH_2), 71.57 (OCH_2), 71.56 (2 × OCH_2), 71.54 (OCH_2), 71.27 (OCH_2), 70.63 (OCH_2), 70.49 (OCH_2), 61.19 (*c*-Pen 1-C), 61.01 (CH), 55.31 (N*C*H_2CH), 53.85 (benzylic CH_2), 50.86 (dioxopiperidine 3-C), 47.97 (benzylic CH_2), 44.71 (piperidine 2-C), 43.25 ($NHCH_2$ [linker]), 41.05 ($NHCH_2$ [linker]), 33.86 (piperidine 4-C), 32.51(dioxopiperidine 5-C), 30.36 (*c*-pen 2-C/5-C), 27.54 (piperidine 3-C/5-C), 27.40 (NCH_3), 24.34 (*c*-pen 3-C/4-C), 23.05 (dioxopiperidine 4-C). **HRMS** (ESI): $C_{55}H_{68}O_{13}N_7ClNaS_2$ $[M+Na]^+$; calculated: 1156.3897, found: 1156.3905.

5.1.2.18 4-(((4-(N-(4-Chlorobenzyl)-N-cyclopentylsulfamoyl)-N-(piperidin-4-ylmethyl)phenyl)sulfonamido)methyl)-N-(14-((2-(2,6-dioxopiperidin-3-yl)-1,3-dioxoisoindolin-4-yl)amino)-3,6,9,12-tetraoxatetradecyl)benzamide (3)

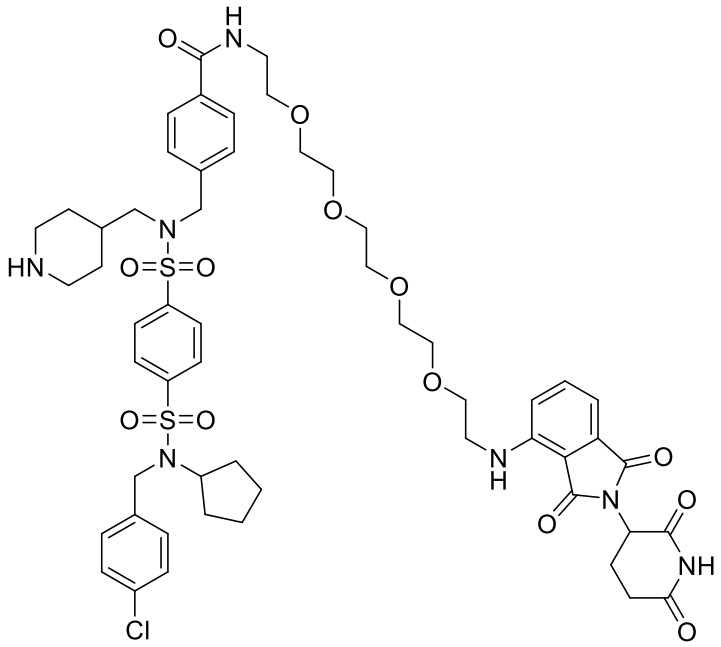

The carboxylic acid **10** (100 mg, 0.13 mmol, 1 eq.), DIPEA (24.6 µl, 143 µl, 1.1 eq.) and PyBOP (75.3 mg, 0.14 mmol, 1.1 eq.) were dissolved in 2 ml DMF and stirred for 5 min at room temperature. Then the amine **17** (122 mg, 0.25 mmol, 1.88 eq.) was added under stirring and left at room temperature for 2 h. Afterwards the reaction was quenched with brine and the product extracted with ethyl acetate. The organic phases were combined and dried over $MgSO_4$. After removing the solvent under reduced pressure, the product could be obtained by flash chromatography (silica, 5% methanol in dichloromethane) as a yellow oil.

The product was dissolved in 10 ml of 50% TFA in CH_2Cl_2 and left stirring for 30 min. The solvent was removed under a continuous air flow and purified using reversed-phase HPLC (C_{18}, H_2O in acetonitrile 10 to 80% over 30 min). The product (52 mg, 50 µmol, 35%) could be obtained as yellow solid.

^{1}H NMR (700 MHz, CD_3OD): δ = 8.07 – 8.00 (m, 4H), 7.80 (d, *J* = 7.2 Hz, 2H), 7.56 (app. t, *J* = 7.6 Hz, 1H, isoindoline 6-C), 7.44 – 7.38 (m, 4H), 7.35 (d, *J* = 7.3 Hz, 2H), 7.09 (d, *J* = 8.5 Hz, 1H, isoindoline 5-H), 7.07 (d, *J* = 7.0 Hz, 1H, isoindoline 7-H), 5.07 (dd, *J* = 13.3, 5.6 Hz, 1H, dioxopiperidine 3-H), 4.45 (s, 2H, benzylic CH_2), 4.43 (s, 2H, benzylic CH_2), 4.40 – 4.34 (m, 1H, *c*-pen 1-H), 3.72 (t, *J* = 5.0 Hz, 2H, OCH_2), 3.68 – 3.62 (m, 14H, 7 × OCH_2), 3.58 (t, *J* = 5.1 Hz, 2H, $NHCH_2$), 3.50 (t, *J* = 5.0 Hz, 2H, $NHCH_2$), 3.32 – 3.30 (m, 2H, piperidine 2-H_A/6-H_A), 3.18 (d, *J* = 7.3 Hz, 2H, NC*H*$_2$CH), 2.91 – 2.83 (m, 1H, dioxopiperidine 4-H_A), 2.80 – 2.68 (m, 4H, piperidine 2-H_B/6-H_B and dioxopiperidine 5-H), 2.15 – 2.10 (m, 1H, dioxopiperidine 4-H_B), 1.83 (d, *J* = 13.7 Hz, 2H, piperidine 3-H_A/5-H_A), 1.74 – 1.67 (m, 1H,

piperidine 4-H), 1.67 – 1.61 (m, 2H, *c*-pen 3-H/4-H), 1.61 – 1.54 (m, 2H, *c*-pen 2-H/5-H), 1.50 – 1.45 (m, 2H, *c*-pen 3-H/4-H), 1.35 – 1.22 (m, 4H, *c*-pen 2-H/5-H and piperidine 3-H_B/5-H_B). **^{13}C NMR** (175 MHz, CD_3OD): δ = 174.63 (CO), 171.61 (CO), 170.69 (CO), 169.56 (CO), 169.28 (CO), 148.21 (Ar-C_q), 146.13 (Ar-C_q), 144.35 (Ar-C_q), 141.44 (Ar-C_q), 139.21 (Ar-C_q), 137.26 (isoindoline 6-C), 135.42 (Ar-C_q), 134.03 (Ar-C_q), 133.87 (Ar-C_q), 130.03 (Ar-CH), 129.83 (Ar-CH), 129.48 (Ar-CH), 129.37 (Ar-CH), 129.30 (Ar-CH), 128.75 (Ar-CH), 118.33 (isoindoline 5-C), 112.06 (isoindoline 7-C), 111.28 (Ar-C_q), 71.63 (OCH_2), 71.58 (OCH_2), 71.56 (2 × OCH_2), 71.53 (OCH_2), 71.27 (OCH_2), 70.60 (OCH_2), 70.49 (OCH_2), 61.20 (dioxopiperidine 3-C), 55.31 (N*C*H_2CH), 53.86 (benzylic CH_2), 50.21 (N*C*H(*c*-pen)), 47.98 (benzylic CH_2), 44.72 (piperidine 2-C), 43.25 ($NHCH_2$ [linker]), 41.04 ($NHCH_2$ [linker]), 33.85 (piperidine 4-C), 32.21 (CH_2), 30.36 (CH_2), 27.54 (CH_2), 24.34 (CH_2), 23.81 (CH_2). **HRMS** (ESI): $C_{55}H_{68}O_{13}N_7ClNaS_2$ $[M+Na]^+$; calculated: 1156.3897, found: 1156.3905.

5.1.2.19 4-(((4-(N-(4-Chlorobenzyl)-N-cyclopentylsulfamoyl)-N-(piperidine-4-ylmethyl)phenyl)sulfonamido)methyl)-N-(2-(2-(2-(2-((2-(2,6-dioxopiperidine-3-yl)-1,3-dioxoisoindoline-4-yl)amino)ethoxy)ethoxy)ethoxy)ethyl)benzamide (2)

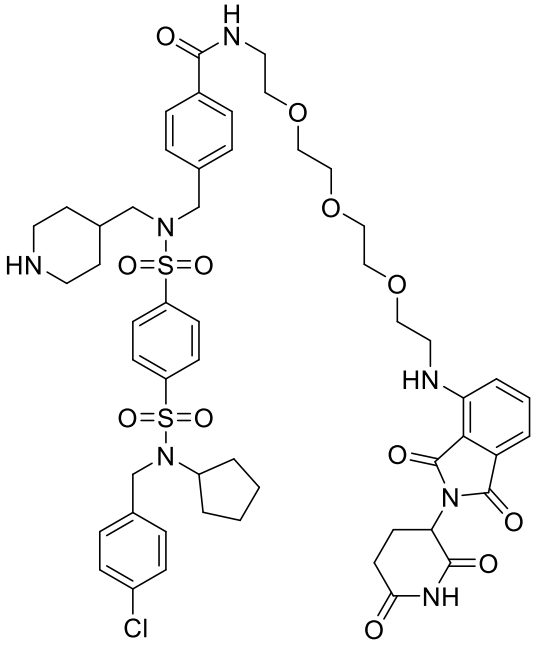

The carboxylic acid **10** (100 mg, 0.13 mmol, 1 eq.), PyBOP (75 mg, 0.14 mmol, 1.1 eq.) and DIPEA (24.6 µl, 0.14 mmol, 1.1 eq.) were dissolved in 2 ml DMF and stirred for 5 min at room temperature. Then the amine **16** (111 mg, 0.25 mmol, 1.88 eq.) was added under stirring and left at room temperature for 2 h. Afterwards the reaction was quenched with brine and the product extracted with ethyl acetate. The organic phases were combined and dried over $MgSO_4$. After removing the solvent under reduced pressure, the product could be obtained by flash chromatography (silica, 5% methanol in dichloromethane) as a yellow oil.

The product was dissolved in 10 ml of 50% TFA in CH_2Cl_2 and left stirring for 30 min. The solvent was removed under a continuous air flow and purified using reversed-phase HPLC (C_{18},

H_2O in acetonitrile 10 to 80% over 30 min). The product (42 mg, 0.04 mmol, 29%) could be obtained as yellow solid.

^{1}H NMR (700 MHz, CD_3OD): δ = 8.04 – 7.97 (m, 4H), 7.75 (d, *J* = 8.4 Hz, 2H), 7.53 (dd, *J* = 8.5, 7.1 Hz, 1H), 7.38 (d, *J* = 8.6 Hz, 2H), 7.35 (d, *J* = 8.3 Hz, 2H), 7.32 (d, *J* = 8.5 Hz, 2H), 7.05 (d, *J* = 8.5 Hz, 1H), 7.04 (d, *J* = 7.0 Hz, 1H), 5.04 (dd, *J* = 12.8, 5.5 Hz, 1H, dioxopiperidine), 4.43 (s, 2H), 4.38 (s, 2H), 4.34 (m, 1H, *c*-pen 1-H), 3.68 (t, *J* = 5.3 Hz, 2H), 3.67 – 3.62 (m, 10H), 3.55 (t, *J* = 5.4 Hz, 2H), 3.45 (t, *J* = 5.3 Hz, 2H), 3.29 – 3.27 (m, 2H, piperidine 2-H_A/6-H_A), 3.15 (d, *J* = 7.4 Hz, 2H, N*H*$_2$CH), 2.88 – 2.82 (m, 1H, dioxopiperidine 4-H_B), 2.77 – 2.66 (m, 3H, piperidine 2-H_A/6-H_A and dioxopiperidine 4-H_A), 2.14 – 2.07 (m, 1H, dioxopiperidine 5-H_A), 1.81 (d, *J* = 12.0 Hz, 2H, piperidine 3-H_A/5-H_A), 1.70 – 1.65 (m, 1H, piperidine 4-H), 1.64 – 1.59 (m, 2H, *c*-pen), 1.58 – 1.53 (m, 2H, *c*-pen), 1.48 – 1.43 (m, 2H, *c*-pen), 1.36 – 1.28 (m, 3H, *c*-pen and dioxopiperidine 5-H_B), 1.24 (d, *J* = 11.2 Hz, 2H, piperidine 3-H_B/5-H_B). **^{13}C NMR** (175 MHz, CD_3OD): δ = 174.63 (CO), 171.64 (CO), 170.68 (CO), 169.56 (CO), 169.28 (CO), 148.19 (Ar-C_q), 146.17 (Ar-C_q), 144.37 (Ar-C_q), 141.41 (Ar-C_q), 139.21 (Ar-C_q), 137.25 (isoindoline 6-C), 135.44 (Ar-C_q), 134.05 (Ar-C_q), 133.88 (Ar-C_q), 130.03 (Ar-CH), 129.81 (Ar-CH), 129.48 (Ar-CH), 129.37 (Ar-CH), 129.29 (Ar-CH), 128.73 (Ar-CH), 118.30 (isoindoline 5-C), 112.04 (isoindoline 7-C), 111.29, 111.28 (Ar-C_q), 71.66 (OCH_2), 71.57 (2 × OCH_2), 71.32 (OCH_2), 70.59 (OCH_2), 70.48 (OCH_2), 61.21 (N*C*H(*c*-pen)), 55.27 (N*C*H_2CH), 53.81 (benzylic CH_2), 50.21 (dioxopiperidine 3-C), 47.98 (benzylic CH_2), 44.73 (piperidine 2-C), 43.23 ($NHCH_2$ [linker]), 41.05 ($NHCH_2$ [linker]), 33.84 (piperidine 4-C), 32.21 (CH_2), 30.36 (CH_2), 27.55 (CH_2), 26.91 (CH_2), 24.34 (CH_2), 23.82 (CH_2), 23.73 (CH_2). **HRMS** (ESI): $C_{53}H_{65}O_{12}N_7ClS_2$ $[M+H]^+$; calculated: 1090.3816, found: 1090.3825.

5.1.2.20 4-(((4-(N-(4-Chlorobenzyl)-N-cyclopentylsulfamoyl)-N-(piperidine-4-ylmethyl)-phenyl)sulfonamido)methyl)-N-(2-(2-(2-((2-(2,6-dioxopiperidine-3-yl)-1,3-dioxoisoindoline-4-yl)amino)ethoxy)ethoxy)ethyl)benzamide (1)

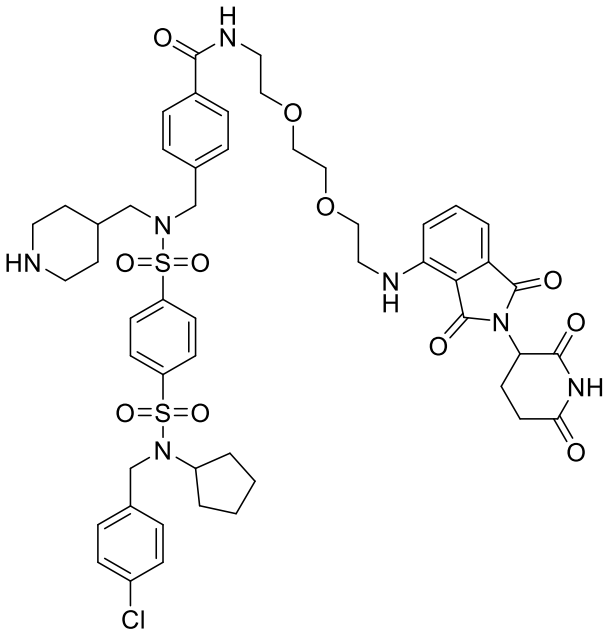

The carboxylic acid **10** (100 mg, 0.13 mmol, 1 eq.), PyBOP (75 mg, 0.14 mmol, 1.1 eq.) and DIPEA (22.4 ml, 0.13 mmol, 1.0 eq.) were dissolved in 2 ml DMF and stirred for 5 min at room temperature. Then, the amine **15** (100 mg, 0.25 mmol, 1.88 eq.) was added under stirring and left at room temperature for 2 h. Afterwards the reaction was quenched with brine and the product extracted with ethyl acetate. The organic phases were combined and dried over $MgSO_4$. After removing the solvent under reduced pressure, the product could be obtained by flash chromatography (silica, 5% methanol in dichloromethane) as a yellow oil.

The product was dissolved in 10 ml of 50% TFA in CH_2Cl_2 and left stirring for 30 min. The solvent was removed under a continuous air flow and purified using reversed-phase HPLC (C_{18}, H_2O in acetonitrile 10 to 80% over 30 min). The product (21 mg, 0.02 mmol, 15%) could be obtained as yellow solid.

HRMS (ESI): $C_{52}H_{61}O_{11}N_7ClS_2$ $[M+H]^+$; calculated: 1046.3554, found: 1046.3563.

5.1.3 Synthesis of PROTAC from Chromopynone-1

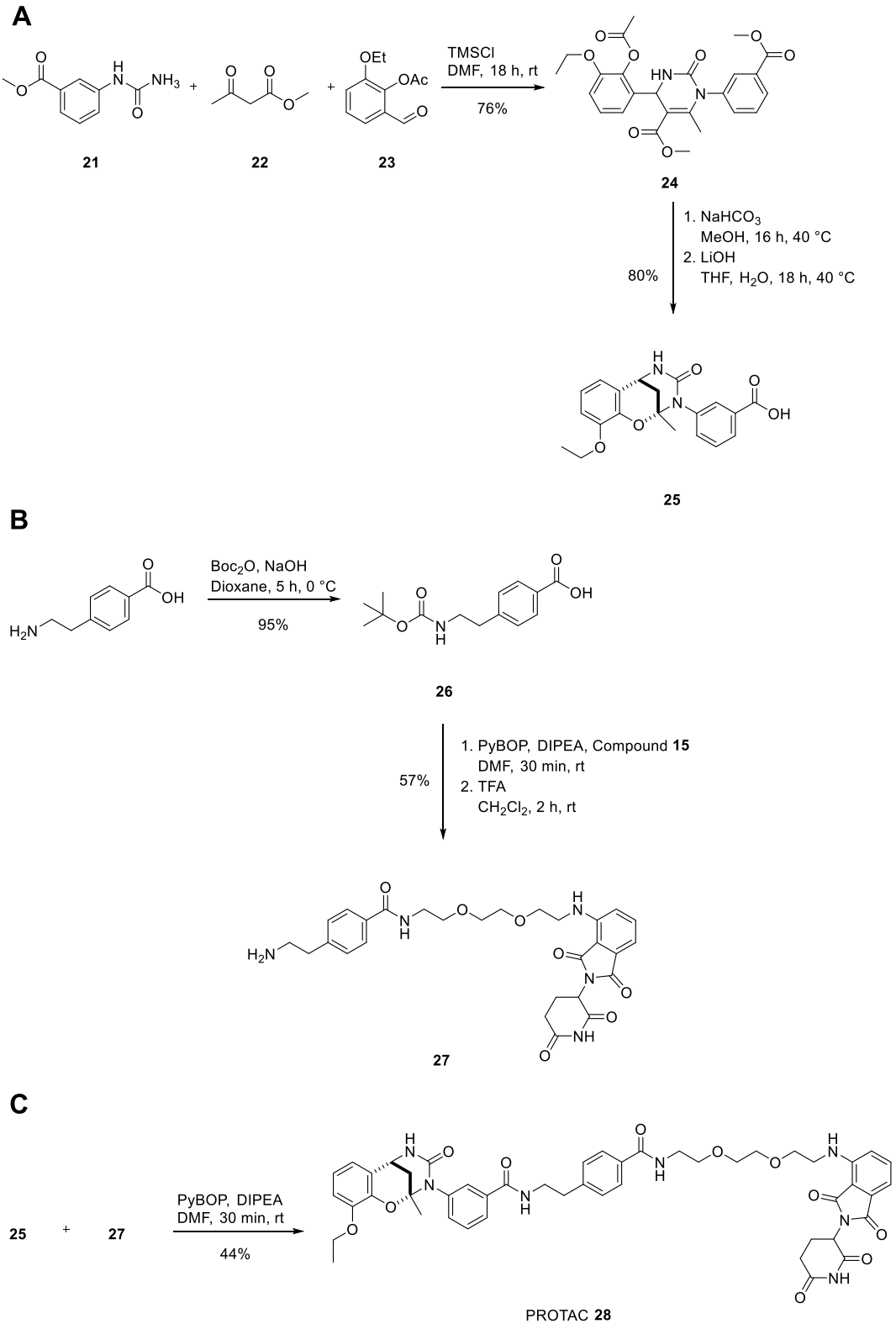

Figure 47: Synthesis of PROTAC. (A) Synthesis of Glut binding part. (B) Synthesis of CRBN binding part. (C) Combination of Part A and B to obtain PROTAC 28.

5.1.3.1 Methyl 3-ureidobenzoate (21)

Synthesis was performed by Dr. George Karageorgis.

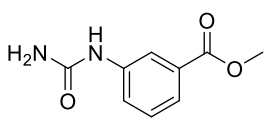

KOCN (50 mmol, 5 eq.) was added to a stirred solution of Methyl 3-amino benzoate (1.51 g, 10 mmol, 0.2 eq.) in H_2O-AcOH (2:1, 100 ml, 0.1 M) and stirred at room temperature. After 18 h a solid was formed and the reaction mixture was cooled to 0 ˚C and filtered *in vacuo*. The amorphous solid was washed with cold H_2O. The colorless (1.66 g, 8.55 mmol, 86%) amorphous solid was collected, dried and used directly.

^{1}H NMR (500 MHz, MeOD): δ = 8.07 (1H, t, *J* = 2.0 Hz, Ph-2H), 7.67-7.63 (2H, m, Ph-4H and Ph-6H), 7.38 (1H, app t, *J* = 7.9 Hz, Ph-5H), 3.91 (3H, s, CO_2CH_3). **^{13}C NMR** (125 MHz, MeOD): δ = 167.1 (CO_2CH_3), 157.8 (NH_2CONH), 140.0 (Ph-C1), 130.5 (Ph-C3), 128.6 (Ph-C5), 123.2 (Ph-C4 or Ph-C6), 123.0 (Ph-C6 or Ph-C4), 119.5 (Ph-C2), 51.2 (CH_3). **HRMS** (ESI): $C_9H_{10}O_3N_2Na$ $[M+Na]^+$; calculated: 217.0584, found: 217.0586.

5.1.3.2 2-Ethoxy-6-formylphenyl acetate (23)

Synthesis was performed by Dr. George Karageorgis.

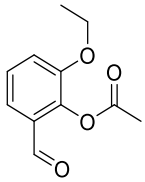

Acetic anhydride (2.0 ml, 21 mmol, 1.05 eq.) was added to a stirred solution of 3-ethoxy salicylaldehyde (3.3 g, 20 mmol, 1 eq.) and DMAP (240 mg, 2 mmol, 0.1 eq.) in toluene (20 ml, 1 M) and the mixture was stirred at rt. After 20 h, the reaction mixture was concentrated *in vacuo* and filtered through a silica column eluting with 50% Ethyl acetate in petroleum ether (500 ml) to give a pale yellow amorphous solid (4.1 g, 19.56 mmol, 97%).

^{1}H NMR (500 MHz, $CDCl_3$): δ = 10.14 (1H, s, Formyl-*H*), 7.44 (1H, dd, *J* = 7.9 and 1.4 Hz, Ph-5H), 7.30 (1H, app t, *J* = 7.9 Hz, Ph-4H), 7.19 (1H, dd, *J* 8.2 and 1.2 Hz, Ph-3H), 4.08 (2H, q, *J* = 6.9, Et-1H_2), 2.39 (3H, s, Ac-2H_3), 1.41 (3H, t, *J* = 6.9 Hz, Et-2H_3). **^{13}C NMR** (125 MHz, $CDCl_3$): δ = 188.7 (Formyl-C), 168.7 (Ac-C1), 151.1 (Ph-C2), 141.9 (Ph-C1), 129.2 (Ph-C6), 126.7 (Ph-C4), 120.9 (Ph-C5), 118.9 (Ph-C3), 64.9 (Et-C1), 20.4 (Ac-C2), 14.6 (Et-C2). **HRMS** (ESI): $C_{11}H_{13}O_4Na$ $[M+Na]^+$; calculated: 231.0628, found: 231.0628.

5.1.3.3 Methyl-4-(2-acetoxy-3-ethoxyphenyl)-1-(3-(methoxycarbonyl)phenyl)-6-methyl-2-oxo-1,2,3,4-tetrahydropyrimidine-5-carboxylate (24)

Synthesis was performed by Dr. George Karageorgis.

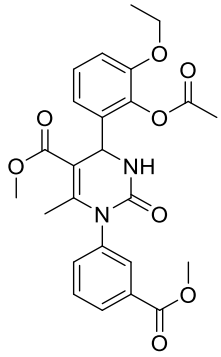

Trimethylchlorosilane (1.5 ml, 12 mmol) was added dropwise to a stirred solution of the appropriate the urea **1** (398 mg, 2 mmol), the aldehyde **2** (416 mg, 2 mmol), and methyl acetoacetate (325 μL, 3 mmol) in DMF (2 ml, 1 M), and the resulting mixture was stirred at room temperature. After 18 h, the reaction was quenched with H_2O (2 ml) and diluted with ethyl acetate (40 ml). The organic layer was extracted sequentially with H_2O (5 × 20 ml), sat. aq. LiCl solution (1 × 20 ml) and sat. aq. NaCl solution (1 × 20 ml), dried over Na_2SO_4, filtered and concentrated *in vacuo* to give a crude product which was purified by flash chromatography eluting with 30-50% ethyl acetate in petrol ether. The product could be obtained as colorless amorphous solid (730 mg, 1.51 mmol, 76%).

^{1}H NMR (500 MHz, $CDCl_3$): δ = 8.01 (1H, d, *J* = 8.1 Hz, 1-Ph-4H), 7.82 (1H, app s, 1-Ph-2H), 7.46 (1H, app t, *J* = 7.7 Hz, 1-Ph-5H), 7.36 (1H, app s, 1-Ph-6H), 7.16 (1H, *J* = 7.9 Hz, 4-Ph-5H), 6.94 (1H, app d, *J* = 7.7 Hz, 4-Ph-4H), 6.84 (1H, app d, *J* = 7.7 Hz, 4-Ph-6H), 5.56 – 5.52 (2H, m, 4-H and N*H*), 3.98 (2H, q, *J* = 7.0 Hz, 4-Ph-3-Et-1H_2), 3.86 (3H, s, 1-Ph-3-CO_2C*H*$_3$), 3.52 (3H, s, 5-CO_2C*H*$_3$), 2.31 (3H, s, 4-Ph-2-Ac-2H_3), 2.10 (3H, s, 6-C*H*$_3$), 1.32 (3H, t, *J* 7.0 Hz, 4-Ph-3-Et-2H_3). **^{13}C NMR** (125 MHz, $CDCl_3$): δ = 169.0 (4-Ph-2-Ac-C1), 168.1 (5-*C*O_2CH_3), 168.0 (1-Ph-3-*C*O_2CH_3), 152.3 (4-Ph-C3), 150.7 (C6), 149.6 (C2), 137.8 (4-Ph-C2 and 1-Ph-C5), 137.5 (1-Ph-C1), 135.5 (1-Ph-C6), 129.7 (1-Ph-C3), 129.4 (4-Ph-C1), 127.1 (4-Ph-C5 and 1-Ph-C4), 118.1 (4-Ph-C6 and 1-Ph-C2), 113.0 (4-Ph-C4), 102.8 (C5), 64.5 (4-Ph-3-Et-C1), 52.4 (5-CO_2*C*H_3), 51.6 (1-Ph-3-CO_2*C*H_3), 49.1 (C4), 20.6 (4-Ph-2-Ac-C2), 18.6 (6-*C*H_3), 14.8 (4-Ph-3-Et-C2). **HRMS** (ESI): $C_{25}H_{27}N_2O_8$ $[M+H]^+$; calculated: 483.1762, found: 483.1767.

5.1.3.4 3-(10-Ethoxy-2-methyl-4-oxo-5,6-dihydro-*2H*-2,6-methanobenzo-[1,3,5]-oxadiazocin-3-(*4H*)-yl)benzoic acid (25)

Synthesis was performed by Dr. George Karageorgis.

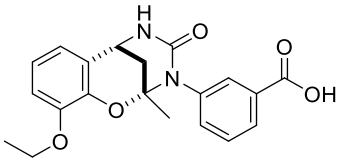

Saturated $NaHCO_3$ aq. solution (15 ml) was added to a stirred solution of the dihydropyrimidinone **24**, (725 mg, 1.5 mmol, 0.1 eq.) in MeOH (15 ml) and the resulting suspension was heated to 40 ˚C. After 16 h the reaction mixture was allowed to cool to room temperature and was concentrated *in vacuo*. The crude was diluted with THF-H_2O (1:1, 15 ml, 0.1 M), LiOH (15 eq. for each methyl ester group) was added and the reaction mixture was heated to 40 ˚C. After 18 h, the reaction mixture was allowed to cool to room temperature and was concentrated *in vacuo* to half volume. The reaction mixture was acidified to pH = 1-2, by slow addition of 1 M aq. HCl solution and was heated to 80 ˚C (probe temperature 82 ˚C). After 6 h, the reaction mixture was allowed to cool to room temperature and extracted with $CHCl_3$-MeOH (8:2, 5 × 20 ml). The combined organic layers were dried over Na_2SO_4, filtered and concentrated *in vacuo* to give a crude product. Enantiomers were separated using a CHIRALPAK-IA column eluting with a gradient of 70-80% (2% EtOH in CH_2Cl_2) in *n*-hexane for 80 min (0.50 ml/min), R_f ent-1: 42.4 min (*S*,*S* configuration); R_f ent-2: 49.7 min (*R*,*R* configuration – collected for further synthesis). Product could be obtained as colorless amorphous solid (442 mg, 1.20 mmol, 80%).

^{1}H NMR (500 MHz, MeOD, NH, OH not observed): δ = 7.97 (1H, d, *J* = 7.5 Hz, Bn-6H), 7.80 (1H, app. s, Bn-2H), 7.53 (1H, app t, *J* = 7.8 Hz, Bn-5H), 7.45 (1H, d, *J* = 7.5 Hz, Bn-4H), 7.00 (1H, dd, *J* = 7.2, 1.6 Hz, 7H), 6.95 (1H, dd, *J* = 7.5, 1.6 Hz, 9H), 6.90 (1H, app. t, *J* = 7.5 Hz, 8H), 4.54 (1H, t, *J* = 2.8, 6H), 4.11 (2H, q, *J* = 7.1 Hz, 10-Et-1H_2), 2.64 (1H, dd, *J* = 13.4, 2.8 Hz, *g*-H_2^1), 2.44 (1H, dd, *J* = 13.4, 2.8 Hz, *g*-H_2^1), 1.47 (3H, s, 2-CH_3), 1.41 (3H, t, *J* = 7.1 Hz, 10-Et-2H_3). **^{13}C NMR** (125 MHz, MeOD): δ = 170.4 (*C*O_2H, not observed directly; verified through HMBC spectrum), 158.5 (C4, not observed directly; verified through HMBC spectrum), 147.9 (C10), 140.5 (C10α and Bn-C3), 137.6 (Bn-C1), 134.0 (Bn-C4), 131.4 (Bn-C2), 127.9 (Bn-C5), 125.8 (Bn-C6 and C6α), 121.4 (C8), 120.7 (C9), 113.3 (C7), 85.4 (C2), 64.5 (10-Et-C1), 44.1 (C6), 34.0 (C*g*), 25.9 (2-*C*H_3), 14.0 (10-Et-C2). **HRMS** (ESI): $C_{20}H_{21}N_2O_5$ $[M+H]^+$; calculated: 369.1445, found: 369.1449.

5.1.3.5 4-(2-((*t*-Butoxycarbonyl)amino)ethyl)benzoic acid (26)

Synthesis was performed by Dr. George Karageorgis.

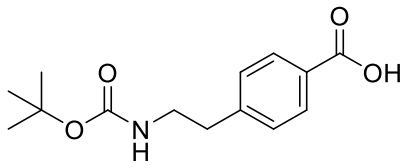

Di-tert-butyl bicarbonate (1.44 g, 1,1 equiv.) was added portion wise to a stirred solution of 4-(2-aminoethyl)benzoic acid hydrochloride (1.21 g, 6 mmol), in dioxane and 2 M aq. NaOH (1:1, 24 ml, 0.25 M), at 0 ˚C. The mixture was allowed to warm to r.t. After 5 h, the crude reaction mixture was conc. *in vacuo* up to half volume and acidified to pH ~1 by slow addition of 10% aq. H_2SO_4. The mixture was extracted with EtOAc (4 × 20 ml) and the combined organic layers were dried over Na_2SO_4, filtered and conc. *in vacuo* to give the carbamate **26**, as a colorless amorphous solid (1.51 g, 5.7 mmols, 95%) which required no further purification.

^{1}H NMR (500 MHz, $CDCl_3$, mixture of rotamers): δ = 7.99 – 7.80 (2H, m, Ph-2H), 7.26 – 7.13 (2H, m, Ph-3H), 3.37 – 3.29 (2H, m, N-Et-1H_2), 2.84 – 2.74 (2H, m, N-Et-2H_2), 1.46 – 1.34 (9H, m, ^{t}Bu-CH_3). **^{13}C NMR** (125 MHz, $CDCl_3$): δ = 170.9 (*C*O_2H), 155.9 (O*C*ONH), 145.5 (Ph-C4), 130.5 (Ph-C2), 129.0 (Ph-C3), 127.6 (Ph-C1), 79.5 (^{t}Bu-C1), 41.5 (*N*-Et-C1), 36.4 (*N*-Et-C2), 28.4 (^{t}Bu-C2). **HRMS** (ESI): $C_{14}H_{20}NO_4$ $[M+H]^+$; calculated: 266.1387, found: 266.1396.

5.1.3.6 4-(2-aminoethyl)-N-(2-(2-(2-((2-(2,6-dioxopiperidin-3-yl)-1,3-dioxoisoindolin-4-yl)amino)ethoxy)ethoxy)ethyl)benzamide (27)

Synthesis was performed by Dr. George Karageorgis.

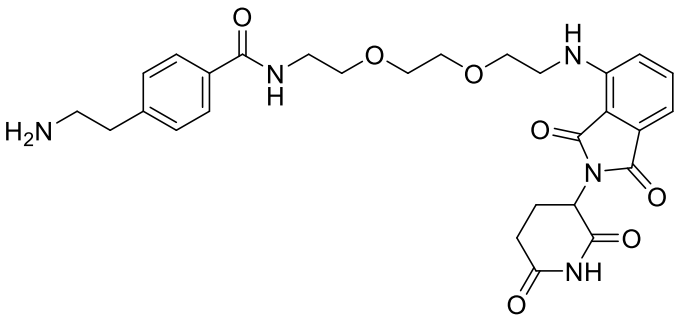

PyBOP (77 mg, 0.15 mmol) was added to a stirred solution of the acid **6** (37 mg, 0.14 mmol) and DIPEA (31 µl, 0.18 mmol) in DMF (1 ml, 0.25 M) and the mixture was stirred at room temperature After 30 min, the amine **15**, (50 mg, 0.12 mmol, 0.8 eq.) was added and the reaction mixture was stirred at room temperature. After 20 h, H_2O (2 ml) was added and the reaction mixture was extracted with CH_2Cl_2-MeOH (8:2, 10 × 5 ml). The combined organic layers were dried over Na_2SO_4, filtered and concentrated *in vacuo* to give a crude product. The crude was diluted in CH_2Cl_2 (1 ml), neat TFA (0.5 ml) was added and the reaction mixture was

stirred at room temperature. After 2 h the reaction mixture was concentrated *in vacuo* to give a crude which was purified by Prep-HPLC (C18 column) eluting with MeCN-H_2O (10-100%, 0.1% TFA), to afford the amine **27** as a colorless amorphous solid (TFA salt, 38 mg, 57% over two steps).

^{1}H NMR (500 MHz, MeOD, mixture of rotamers): δ = 7.67 (1H, d, *J* = 7.2 Hz), 7.43 (1H, app t, *J* = 7.5 Hz), 7.23 – 7.17 (2H, m), 7.01 – 6.91 (2H, m), 3.65 – 3.33 (12H, m), 3.13 – 3.04 (2H, m), 2.98 – 2.82 (2H, m), 2.77 – 2.68 (1H, m), 2.63 – 2.54 (1H, m), 2.03 – 1.93 (1H, m), 1.24 – 1.16 (2H, m). **^{13}C NMR** (125 MHz, $CDCl_3$): δ = 173.2, 170.2, 169.3, 168.3, 167.8, 146.8, 140.2, 137.6, 137.1, 135.8, 133.2, 132.5, 128.8, 128.5, 127.5, 125.7, 116.8, 110.6, 70.1, 69.1, 48.8, 41.8, 40.1, 39.6, 32.9, 30.8, 22.4. **HRMS** (ESI): $C_{28}H_{54}N_5O_7$ $[M+H]^+$; calculated: 552.2453, found: 552.2496.

5.1.3.7 N-(4-((2-(2-(2-((2-(2,6-dioxopiperidin-3-yl)-1,3-dioxoisoindolin-4-yl)amino)ethoxy)ethoxy)ethyl)carbamoyl)phenethyl)-3-(10-ethoxy-2-methyl-4-oxo-5,6-dihydro-2H-2,6-methanobenzo[g][1,3,5]oxadiazocin-3(4H)-yl)benzamide (28)

Synthesis was performed by Dr. George Karageorgis.

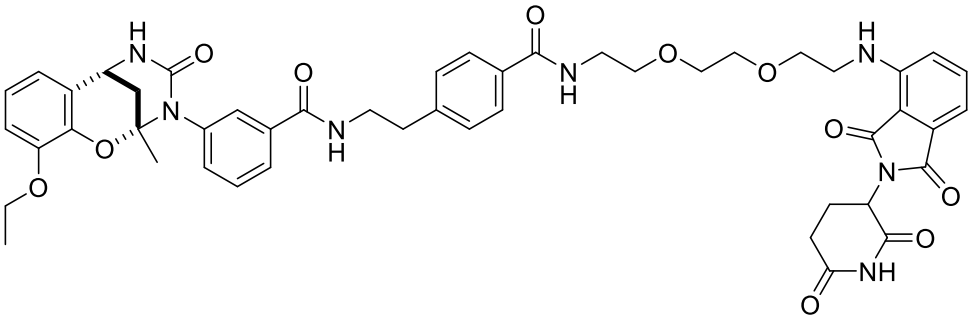

PyBOP (6 mg, 0.01 mmol, 1 eq.) was added to a stirred solution of the acid **25** (4 mg, 0.01 mmol, 1 eq.) and DIPEA (4 µl, 0.02 mmol, 2 eq.) in DMF (100 µl, 0.25 M) and the mixture was stirred at room temperature. After 30 min, the amine **27**, (5 mg, 0.01 mmol) was added and the reaction mixture was stirred at room temperature. After 20 h, H_2O (50 µl) was added and the crude reaction mixture was purified by Prep-HPLC (C18 column) eluting with MeCN-H_2O (10-100%, 0.1% TFA), to afford the amide **28** as a colorless amorphous solid (4 mg, 44%).

^{1}H NMR (500 MHz, $CDCl_3$, mixture of diastereomers): δ = 8.06 (2H, d, *J* = 6.4 Hz), 7.93 (1H, app. s), 7.88 (1H, app. s), 7.50 – 7.43 (3H, m), 7.02-6.92 (5H, m), 6.85 – 6.82 (2H, m), 4.76 – 4.61 (4H, m), 4.51 – 4.44 (2H, m), 4.25 – 4.14 (6H, m), 3.93 (4H, app. s), 3.75 – 3.69 (4H, m),

3.65 (1H, app. s), 3.53 (1H, app s), 2.94 – 2.87 (2H, m), 2.84 – 2.79 (1H, m), 2.64 (1H, d, *J* = 12.8), 2.51 (1H, d, *J* = 12.8), 1.66 (3H, s), 1.51-1.47 (3H, m). **^{13}C NMR** (125 MHz, $CDCl_3$): δ = 168.6, 167.6, 166.3, 161.0, 156.7, 139.9, 137.2, 134.5, 131.1, 129.4, 128.9, 127.4, 124.6, 123.7, 122.7, 122.1, 120.2, 117.2, 113.5, 85.6, 64.5, 52.2, 47.1, 45.0, 42.1, 34.3, 31.6, 26.9, 25.1, 14.8. **HRMS** (ESI): $C_{48}H_{52}N_7O_{11}$ $[M+H]^+$; calculated: 902.3719, found: 902.3671.

5.1.4 Synthesis of photoactivatable farnesyl-analogues

5.1.4.1 Geranyl-*t*-butyldimethylsilylether (29)

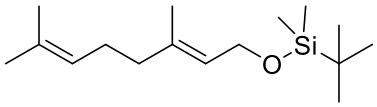

Compound **29** was synthesized according to literature.[83] Geraniol (7.8 g, 50.5 mmol, 1 eq.) and DIPEA (17.2 ml, 101 mmol, 2 eq.) were dissolved in 50 ml dry CH_2Cl_2 and cooled down to 0 °C After the addition of *t*-butyldimethylchlorosilane (11.4 ml, 80 mmol, 1.5 eq.) and 4 h at 0 °C, the solution was washed 5-times with 0.2 M HCl and once with sat. NaCl. The organic phase was dried over $MgSO_4$ and the solvent removed under reduced pressure. The crude was purified by column chromatography (silica, 10% ethyl acetate in cyclohexane) to afford the pure product (13.1 g, 48.5 mol, 96%) as a yellow oil.

^{1}H NMR (500 MHz, $CDCl_3$): δ = 5.31 (t, *J* = 6.2 Hz, 1H), 5.10 (s, 1H), 4.19 (d, *J* = 6.3 Hz, 2H), 2.13 – 2.05 (m, 2H), 2.04 – 1.96 (m, 2H), 1.68 (s, 3H), 1.62 (s, 3H), 1.60 (s, 3H), 0.90 (d, *J* = 1.3 Hz, 9H), 0.07 (d, *J* = 1.3 Hz, 6H). **^{13}C NMR** (125 MHz, $CDCl_3$): δ = 140.86, 137.00, 131.67, 124.59, 124.28, 60.52, 39.70, 26.53, 26.19, 25.84, 18.60, 17.83, 16.50, 3.40, -4.87. Resulting analytical data matched reported literature data.[83]

5.1.4.2 8-Hydroxy-geranyl-*t*-butyldimethylsilylether (30)

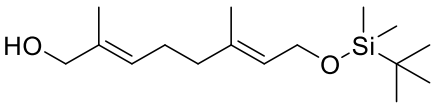

The compound **30** was synthesized according to a literature procedure.[83] SeO_2 (4 mg, 40 µmol, 0.1 eq.), salicylic acid (5 mg, 40 µmol, 0.1 eq.) and di-*t*-butylperoxide (192 mg, 1.5 mmol, 4 eq., 70% in H_2O) were dissolved in 7 ml THF and cooled to 0 °C. After 30 min a solution of **29** (100 mg, 370 µmol, 1 eq.) was added dropwise and the reaction mixture was stirred for 5 h. Afterwards, the solvent was removed under reduced pressure and the aqueous phase was co-evaporated two times with 10 ml toluene (water bath temperature < 36 °C). The residual mixture was dissolved in diethyl ether and washed with sat. $NaHCO_3$ solution. Then, the organic phase was dried over $MgSO_4$, filtered and the solvent removed under reduced pressure. The residual was dissolved in 2 ml MeOH and $NaBH_4$ (7 mg, 0.19 mmol, 0.5 eq.) was added portion wise at room temperature. After 10 min the reaction was quenched with water and the product extracted with diethyl ether. The organic phases were combined and dried with $MgSO_4$. The crude mixture was purified by column chromatography (silica, 20% ethyl acetate in cyclohexane) to afford the pure product (42 mg, 0.15 mmol, 39%) as yellow oil.

^{1}H NMR (500 MHz, $CDCl_3$): δ = 5.31 (t, *J* = 6.2 Hz, 1H), 5.10 (s, 1H), 4.19 (d, *J* = 6.3 Hz, 2H), 2.13 – 2.05 (m, 2H), 2.04 – 1.96 (m, 2H), 1.68 (s, 3H), 1.62 (s, 3H), 1.60 (s, 3H), 0.90 (d, *J* = 1.3 Hz, 9H), 0.07 (d, *J* = 1.3 Hz, 6H). **^{13}C NMR** (125 MHz, $CDCl_3$): δ = 140.86, 137.00, 131.67, 124.59, 124.28, 60.52, 39.70, 26.53, 26.19, 25.84, 18.60, 17.83, 16.50, 3.40, -4.87. **HRMS** (ESI): $C_{16}H_{33}O_2Si$ $[M+H]^+$; calculated: 285.2250, found: 285.2246. Resulting analytical data matched reported literature data.[83]

5.1.4.3 8-(4-Benzoylphenyloxy)-geranyl-*t*-butyldimethylsilylether (31)

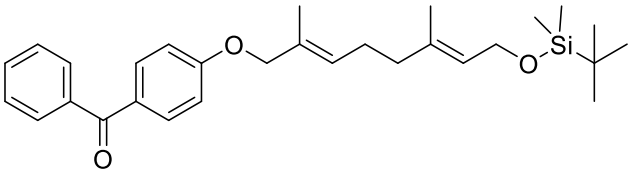

The compound **31** was synthesized according to literature.[83] The silyl ether **30** (250 mg, 0.88 mmol, 1 eq.), Ph_3P (346 mg, 1.32 mmol, 1.5 eq.) and 4-hydroxybenzophenone (209 mg, 1.05 mmol, 1.2 eq.) were dissolved in 2 ml dry THF and cooled to 0 °C. Then, diethyl azodicarboxylate (266 mg, 1.32 mmol, 1.5 eq.) was added dropwise and the reaction stirred for 4 h. Afterward, diethyl ether and water were added, and the crude product extracted. The combined organic phases were washed with brine and dried over $MgSO_4$. The crude was purified by column chromatography (silica, 10% ethyl acetate in cyclohexane) to afford the pure product (151 mg, 0.32 mmol, 37%) as a yellow oil.

^{1}H NMR (500 MHz, $CDCl_3$): δ = 7.81 (d, *J* = 8.8 Hz, 2H), 7.75 (d, *J* = 7.0 Hz, 2H), 7.56 (t, *J* = 7.4 Hz, 1H), 7.47 (t, *J* = 7.5 Hz, 2H), 6.97 (d, *J* = 8.9 Hz, 2H), 5.56 (td, *J* = 6.9, 1.0 Hz, 1H), 5.32 (td, *J* = 6.3, 1.2 Hz, 1H), 4.46 (s, 2H), 4.19 (d, *J* = 6.2 Hz, 2H), 2.22 (dd, *J* = 15.0, 7.3 Hz, 2H), 2.07 (t, *J* = 7.7 Hz, 2H), 1.75 (s, 3H), 1.64 (s, 3H), 0.90 (s, 9H), 0.07 (s, 6H). **^{13}C NMR** (125 MHz, $CDCl_3$): δ = 195.72, 162.83, 138.50, 136.43, 132.64, 131.98, 130.70, 130.19, 129.87, 129.32, 128.31, 125.00, 114.49, 77.36, 74.32, 60.42, 39.03, 26.16, 26.15, 18.58, 16.49, 14.01, -4.90. **HRMS** (ESI): $C_{29}H_{41}O_3Si$ $[M+H]^+$; calculated: 465.2825, found: 465.2820.

5.1.4.4 8-(4-Benzoylphenyloxy)-geraniol (34)

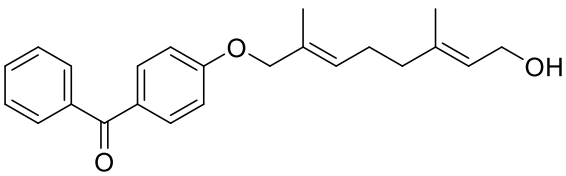

The compound **34** was synthesized according to literature.[83] The silyl ether **31** (220 mg, 0.47 mmol, 1 eq.) was dissolved in 2 ml dry THF and cooled to 0 °C. Afterwards, the reaction was treated with tetrabutylammonium fluoride (569 µl, 0.57 mmol, 1.2 eq., 1 M in THF) and stirred at room temperature for 4 h. The crude product was extracted with diethyl ether and washed

with brine. The combined organic phases were dried over $MgSO_4$ and the solvent removed under reduce pressure. The crude was purified by column chromatography (silica, 50% ethyl acetate in cyclohexane) to afford the pure product (163 mg, 0.45 mmol, 98%) as a yellow oil.

^{1}H NMR (500 MHz, $CDCl_3$): δ = 7.81 (d, *J* = 8.8 Hz, 2H), 7.76 (d, *J* = 8.3 Hz, 2H), 7.56 (t, *J* = 7.4 Hz, 1H), 7.47 (t, *J* = 7.6 Hz, 2H), 6.97 (d, *J* = 8.8 Hz, 2H), 5.55 (t, *J* = 6.5 Hz, 1H), 5.41 (t, *J* = 7.5 Hz, 1H), 4.47 (s, 2H), 4.15 (d, *J* = 6.8 Hz, 2H), 2.26 – 2.20 (m, 2H), 2.13 – 2.07 (m, 2H), 1.75 (s, 3H), 1.69 (s, 3H). **^{13}C NMR** (125 MHz, $CDCl_3$): δ = 132.61, 132.01, 129.89, 129.10, 128.32, 124.08, 114.52, 74.28, 59.53, 53.56, 39.03, 26.10, 16.40, 14.05. **HRMS** (ESI): $C_{23}H_{27}O_3$ $[M+H]^+$; calculated: 351.1960, found: 351.1955. Resulting analytical data matched reported literature data.[83]

5.1.4.5 8-(4-Benzoylphenyloxy)-geranyl-1-diphosphate (37)

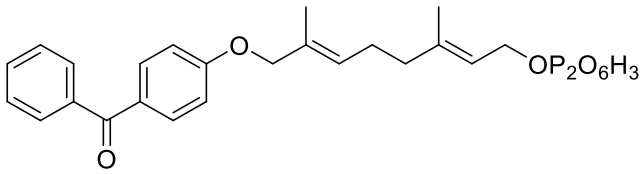

The compound **34** (104 mg, 0.3 mmol, 1 eq.) and PPh_3 (polymer-supported beads, 504 mg, 0.86 mmol) were dissolved in CH_2Cl_2 (5 ml) and stirred for 30 min to allow the beads to swell. Afterwards a solution of tetrabromomethane (170 mg, 0.5 mmol, in 2 ml CH_2Cl_2, 1.2 eq.) was added and the mixture was stirred over night at room temperature. After filtration of the beads, the crude product was extracted with ethyl acetate. The organic phases were combined, and the solvent was removed under reduced pressure. Because of the instability of the allylic bromide it was directly used without any purification step.

The bromide was dissolved in 6 ml Acetonitrile and $(n\text{-}Bu_4N)_3HP_2O_5$ (714 mg, 0.79 mmol, 1.8 eq.) was added slowly. The reaction was allowed to stir for 3 h and then the solvent removed under reduced pressure. An ion-exchange column (Bio-Rad, AG 50W-X8) was used to convert the product to its ammonium form. The resin was packed and washed using three column volumes of 25 vol% NH_3 in water followed by an equilibration step with three column volumes of 2 vol% propanol in aqueous 25 mM NH_4HCO_3-Solution. The dark-red residue was dissolved in a minimal volume of solvent and loaded on the column. Three column volumes of the equilibration solution were applied to the column to convert the product in its ammonium form. Fractions which contained the product were combined and lyophilized to dryness. The resulting white powder (38 mg, 70 µmol, 17%) was purified using preparative HPLC (C_{18}, H_2O in acetonitrile 10 to 80% over 30 min).

^{1}H NMR (600 MHz, 25 mM ND_4OD): δ = 7.85 – 7.82 (m, 2H), 7.78 – 7.75 (m, 2H), 7.67 – 7.62 (m, 2H), 7.13 (m, 2H), 5.69 (t, *J* = 7.0 Hz, 1H), 5.55 (t, *J* = 6.5 Hz, 1H), 4.63 (s, 2H), 4.56 (t, *J* = 6.5 Hz, 2H), 2.30 (t, *J* = 7.3 Hz, 2H), 2.19 (t, *J* = 7.6 Hz, 2H), 1.80 (s, 6H). **^{13}C NMR** (150 MHz, 25 mM ND_4OD): δ = 199.51, 162.81, 142.15, 137.36, 133.16, 133.09, 130.67, 130.01, 129.94, 129.42, 128.58, 120.35, 120.29, 114.98, 114.92, 74.31, 62.44, 62.41, 38.35, 25.57, 22.74, 15.74, 13.15. **^{31}P NMR** (243 MHz, 25 mM ND_4OD): δ = -6.33 (d, *J* = 22.2 Hz), -10.32 (d, *J* = 22.2 Hz). **HRMS** (ESI): $C_{23}H_{29}O_9P_2$ $[M+H]^+$; calculated: 511.1281, found: 511.1288.

5.1.4.6 8-(3-(Methyl)-benzophenone)-geranyl-*t*-butyldimethylsilylether (32)

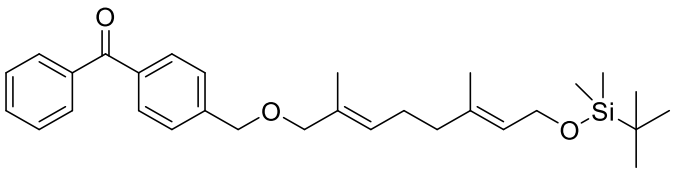

The alcohol **30** (300 mg, 1.1 mmol, 1 eq.) was slowly added to a solution of NaH (84 mg, 2.1 mmol, 2 eq.) in THF (15 ml) at 0 °C. The mixture was stirred for 30 min under ice-cooling before 3-(bromomethyl) benzophenone (580 mg, 2.1 mmol, 2 eq.) was slowly added. After 2 h at 40 °C, the mixture was brought to room temperature and quenched with water (30 ml). The solution was extracted three times with diethyl ether (each 30 ml). Afterwards were the combined organic phases dried over $MgSO_4$. The crude was purified by column chromatography (silica, 20% ethyl acetate in cyclohexane) to afford the pure product (444 mg, 0.93 mmol, 88%) as yellow oil.

^{1}H NMR (400 MHz, $CDCl_3$): δ = 7.82 – 7.76 (m, 4H), 7.63 – 7.55 (m, 1H), 7.53 – 7.43 (m, 4H), 5.50 – 5.40 (m, 1H), 5.36 – 5.26 (m, 1H), 4.53 (d, *J* = 6.6 Hz, 2H), 4.19 (d, *J* = 6.3 Hz, 2H), 3.94 (s, 2H), 2.25 – 2.01 (m, 4H), 1.70 (s, 3H), 1.64 (s, 3H), 0.90 (s, 9H), 0.07 (s, 6H). Resulting analytical data matched reported literature data.[85]

5.1.4.7 8-(3-(Methyl)-benzophenone)-geraniol (35)

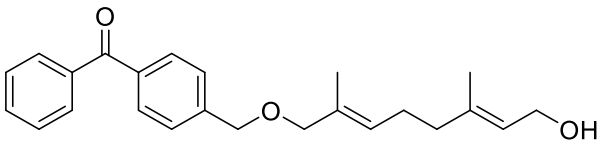

The silyl ether **32** (517 mg, 1.08 mmol, 1 eq.) was dissolved in 5 ml THF. Tetrabutyl-ammoniumfluoride (1.3 ml, 1.3 mmol, 1 M in THF, 1.2 eq.) was added dropwise over 30 min under ice-cooling. After 4 h at room temperature the solution was quenched with brine (20 ml) and the crude product was extracted with diethyl ether (30 ml). The pooled organic phases were dried over $MgSO_4$ and the solvent was removed

under reduced pressure. The crude was purified by column chromatography (silica, 50% ethyl acetate in cyclohexane) to afford the pure product (374 mg, 1 mmol, 95%) as yellow oil.

^{1}H NMR (500 MHz, $CDCl_3$): δ = 7.82 – 7.77 (m, 4H), 7.61 – 7.57 (m, 1H), 7.51 – 7.43 (m, 4H), 5.45 – 5.40 (m, 2H), 4.80 (s, 1H), 4.53 (s, 2H), 4.15 (d, *J* = 6.9 Hz, 2H), 3.94 (s, 2H), 2.24–2.06 (m, 4H), 1.70 (s, 3H), 1.69 (s, 3H). **^{13}C NMR** (125 MHz, $CDCl_3$): δ = 196.61, 143.63, 139.30, 137.85, 136.86, 132.49, 132.37, 130.54, 130.38, 130.15, 128.42, 128.40, 128.28, 127.33, 126.54, 123.90, 76.77, 71.00, 59.51, 39.20, 26.09, 16.39, 14.14. **HRMS** (ESI): $C_{24}H_{29}O_3$ $[M+H]^+$; calculated: 365.2111, found: 365.2119.

5.1.4.8 8-(3-(Methyl)-benzophenone)-geranyl-1-diphosphate (38)

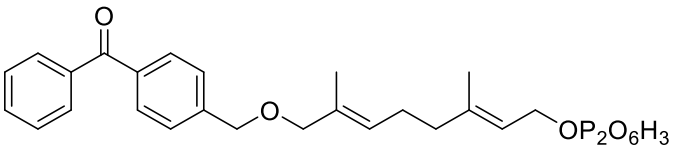

The compound **35** (150 mg, 0.41 mmol, 1 eq.) and PPh_3 (polymer-supported beads, 484 mg, 0.82 mmol, 2 eq.) were dissolved in CH_2Cl_2 (5 ml) and stirred for 30 min to allow the beads to swell. A solution of tetrabromomethane (164 mg, 0.5 mmol, in 2 ml CH_2Cl_2) was added and the mixture was allowed to stir over night at room temperature. After filtration of the beads, the crude product was extracted three times with ethyl acetate (each 20 ml). The organic phases were combined, and the solvent was removed under reduced pressure. Because of the instability of the allylic bromide it was directly used without any purification step.

The bromide was dissolved in 6 ml acetonitrile and then $(n\text{-}Bu_4N)_3HP_2O_5$ (680.73 mg, 0.75 mmol, 1.8 eq.) was added slowly. The reaction was allowed to stir for 3h and afterwards was the solvent removed under reduced pressure. An ion-exchange column (Bio-Rad, AG 50W-X8) was used to convert the product to its ammonium form. The resin was packed and washed using three column volumes of 25 vol% NH_3 followed by an equilibration step with three column volumes of 2 vol% propanol in aqueous 25 mM NH_4HCO_3. The dark-red residue was solved in a minimal volume of solvent and loaded on the column. Three column volumes of equilibration solvent were applied to the column to convert the product in its ammonium form. Fractions which contained the product were pooled and lyophilized to dryness. The resulting white powder (69 mg, 130 µmol, 32%) was purified using preparative HPLC (C_{18}, H_2O in acetonitrile 10 to 80% over 30 min).

^{1}H NMR (600 MHz, 25 mM ND_4OD): δ = 7.93 – 7.88 (m, 4H), 7.85 – 7.80 (m, 1H), 7.71 – 7.62 (m, 4H), 5.62 (t, *J* = 6.7 Hz, 1H), 5.58 (t, *J* = 6.7 Hz, 1H), 4.69 (s, 2H), 4.59 – 4.54 (m,

2H), 4.11 (s, 2H), 2.32 (t, *J* = 7.1 Hz, 2H), 2.22 (t, *J* = 7.4 Hz, 2H), 1.82 (s, 3H), 1.78 (s, 3H). **^{13}C NMR** (150 MHz, 25 mM ND_4OD): δ = 200.67, 143.53, 142.27, 136.92, 136.36, 133.59, 131.72, 130.72, 130.34, 130.27, 128.65, 128.25, 120.34, 120.28, 76.57, 70.37, 62.39, 38.41, 25.55, 15.66, 13.31. **^{31}P NMR** (243 MHz, 25 mM ND_4OD): δ = -6.35 (d, *J* = 22.3 Hz), -10.38 (d, *J* = 22.4 Hz). **HRMS** (ESI): $C_{24}H_{31}O_9P_2$ $[M+H]^+$; calculated: 525.1438, found: 525.1446.

5.1.4.9 8-(3-Trifluoromethyl-3-phenyl-diazirine)-geranyl-*t*-butyldimethylsilylether (32)

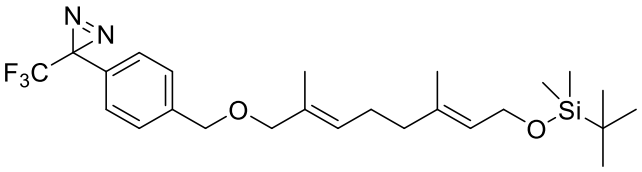

The alcohol **30** (300 mg, 1.05 mmol, 1 eq.) was slowly added under ice-cooling to a solution of NaH (51 mg, 2.1 mmol, 2 eq.) in THF (7.5 ml). The mixture was stirred for 30 min under ice-cooling before the 4-[3-(trifluoromethyl)-3H-diazirin-3-yl]benzyl bromide (589 mg, 2.1 mmol, 2 eq.) was slowly added. After 4 h at room temperature the mixture was brought to room temperature and quenched with water. The solution was three times extracted with diethyl ether (each 20 ml) and the combined organic phases were dried over $MgSO_4$. The solvent was removed under reduced pressure and the crude was purified by column chromatography (silica, 10% ethyl acetate in cyclohexane) to afford the pure product (163 mg, 340 µmol, 32%) as yellow oil.

^{1}H NMR (500 MHz, $CDCl_3$): δ = 7.37 (d, *J* = 8.7 Hz, 2H), 7.17 (d, *J* = 7.9 Hz, 2H), 5.40 (d, *J* = 7.0 Hz, 1H), 5.34 – 5.29 (m, 1H), 4.44 (s, 2H), 4.19 (dd, *J* = 6.3, 0.8 Hz, 2H), 3.88 (s, 2H), 2.22 – 2.14 (m, 2H), 2.08 – 2.02 (m, 2H), 1.67 (s, 3H), 1.63 (s, 3H), 0.90 (s, 9H), 0.06 (s, 6H). **HRMS** (ESI): $C_{25}H_{38}F_3N_2O_2Si$ $[M+H]^+$; calculated: 483.2655, found: 483.2649.

5.1.4.10 8-(3-Trifluoromethyl-3-phenyl-diazirine)-geraniol (36)

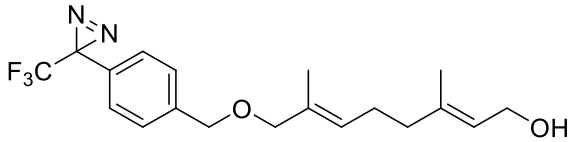

The silyl ether **33** (163 mg, 0.34 mmol, 1 eq.) was dissolved in 6 ml THF. Tetrabutyl-ammoniumfluoride (405 µl, 0.4 mmol, 1 M in THF, 1.2 eq.) was added dropwise over 30 min under ice-cooling. After 4 h at room temperature the solution was quenched with brine (20 ml) and the crude product extracted with diethyl ether (30 ml). The combined organic phases were dried over $MgSO_4$ and the solvent removed under reduce pressure. The crude was purified by column chromatography (silica, 50% ethyl acetate in cyclohexane) to afford the pure product (86 mg, 230 µmol, 69%) as yellow oil.

^{1}H NMR (500 MHz, $CDCl_3$): δ = 7.37 (d, *J* = 8.5 Hz, 2H), 7.17 (d, *J* = 7.8 Hz, 2H), 5.41 (d, *J* = 7.3 Hz, 2H), 4.44 (s, 2H), 4.15 (d, *J* = 6.7 Hz, 2H), 3.88 (s, 2H), 2.24 – 2.15 (m, 2H), 2.11 – 2.04 (m, 2H), 1.68 (d, *J* = 6.9 Hz, 3H), 1.67 (s, 3H). **HRMS** (ESI): $C_{19}H_{22}F_3N_2O_1$ $[(M\text{-}H_2O)+H]^+$; calculated: 351.1679, found: 351.1679.

5.1.4.11 8-(3-Trifluoromethyl-3-phenyl-diazirine)-geranyl-1-diphosphate (39)

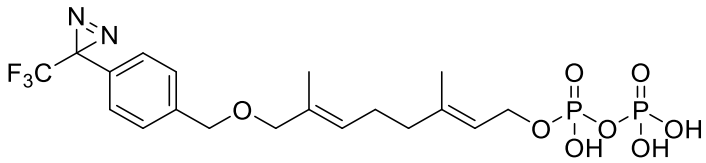

The compound **36** (50 mg, 0.14 mmol, 1 eq.) and PPh_3 (polymer-supported beads, 160 mg, 0.27 mmol, 2 eq.) were dissolved in CH_2Cl_2 (5 ml) and stirred for 30 min to allow the beads to swell. A solution of tetrabromomethane (57 mg, 0.16 mmol, in 2 ml CH_2Cl_2, 1.8 eq.) was added and the mixture was stirred over night at room temperature. After filtration of the beads, the crude product was extracted with ethyl acetate. The organic phases were combined, and the solvent was removed under reduced pressure. Because of the instability of the allylic bromide it was directly used without any purification step.

The bromide was dissolved in 6 ml acetonitrile and $(n\text{-}Bu_4N)_3HP_2O_5$ (332 mg, 0.37 mmol, 1.8 eq.) was added slowly. The reaction was allowed to stir for 3 h and afterwards was the solvent removed under reduced pressure. An ion-exchange column (Bio-Rad, AG 50W-X8) was used to convert the product to its ammonium form. The resin was packed and washed using three column volumes of 25 vol% NH_3 followed by an equilibration step with three column volumes of 2 vol% propanol in aqueous 25 mM NH_4HCO_3-solution. The dark-red residue was solved in a minimal volume of solvent and loaded on the column. Three column volumes of equilibration solvent were applied to the column to convert the product in its ammonium form. Fractions which containing the product were pooled and lyophilized to dryness. The resulting white powder (15 mg, 30 µmol, 14%) was purified using preparative HPLC (C_{18}, H_2O in acetonitrile 10 to 80% over 30 min).

^{1}H NMR (600 MHz, 25 mM ND_4OD): δ = 7.54 (s, 2H), 7.39 (s, 2H), 5.56 (s, 2H), 4.57 (s, 2H), 4.53 (s, 2H), 4.04 (s, 2H), 2.34 – 2.18 (m, 4H), 1.79 (s, 3H), 1.73 (s, 3H). **^{13}C NMR** (150 MHz, 25 mM ND_4OD): δ = 167.02, 165.70, 142.31, 139.57, 131.64, 130.21, 128.94, 128.31, 126.75, 120.25, 76.31, 70.18, 64.25, 62.41, 38.40, 25.52, 23.78, 15.67, 13.28. **^{31}P NMR** (243 MHz, 25 mM ND_4OD): δ = -6.37 (d, *J* = 21.9 Hz), -10.37 (d, *J* = 22.3 Hz). **HRMS** (ESI): $C_{24}H_{31}O_9P_2$ $[M+H]^+$; calculated: 525.1438, found: 525.1446.

5.2 Biology

5.2.1 Material

5.2.1.1 Chemicals and reagents

Name	Supplier	Product number
4-(2-hydroxyethyl)-1-piperazine-ethanesulfonic acid (HEPES), ultrapure	Thermo Fisher Science	11344041
1-Chloro-2,4-dinitrobenzene	Sigma Aldrich	138630
Acetic Acid	Sigma Aldrich	33209
Acetonitrile, HPLC grade	Fisher Chemicals	A998-212
Acrylamide (30%)	AppliChem	A1672
Ammonium bicarbonate (ABC)	Sigma-Aldrich	11213-1KG-R
Ammonium persulfate (APS)	SERVA GmbH	13375
Ampicillin	GERBU Biotechnik GmbH	02738-84
Bovine Serum Albumin (BSA)	SERVA GmbH	11945.03
Bradford Reagent	Bio-Rad	5000001
Bromophenol blue, sodium salt	Carl Roth	A512.1
Chloramphenicol	Sigma-Aldrich	C0378-5G
Chloroacetamide	Sigma-Aldrich	C0267-100G
CM-H_2DCFDA	Thermo Fisher Science	C6827
Column MS peptide (75 µm x 25 cm)	New Objective	FS36PF7508-250H363
cOmplete™, EDTA-free protease inhibitor cocktail	Sigma-Aldrich	11873580001
Coomassie Brilliant Blue G-250	SERVA GmbH	35050
Dimethyl sulfoxide (DMSO)	Sigma-Aldrich	D8418
Dithioerythritol (DTE)	GERBU Biotechnik GmbH	1007.0025
Dithiothreitol (DTT)	GERBU Biotechnik GmbH	1008.0005
Dulbecco’s modified eagle medium (DMEM)	PAN Biotech GmbH	P04-03550
Effectene Transfection Reagent	QIAGEN	301425

Name	Supplier	Product number
Ethanol (EtOH), absolute	Fisher Chemical	E/0650DF/15
Ethanolamine (≥ 98%)	Sigma-Aldrich	E9508
Ethylenediaminetetraacetic acid (EDTA) disodium salt	GERBU Biotechnik GmbH	1034
Fetal bovine serum (FBS)	Gibco	10500-084
Formic acid	J.T. Baker	6037
$FTase_{W102T\_Y154T}$	from Nguyen[84]	
Fugene HD	Promega	E2311
Geneticin (G418) disulfate salt solution	Sigma-Aldrich	G8168
Glucose-6-phosphate dehydrogenase	Sigma-Aldrich	G7877-150UN
Glycerol	Carl Roth	3783.1
Glycine	Carl Roth	3790.2
Hoechst33342	Life Technologies GmbH	H3570
Hydrochloric acid (HCl)	AppliChem	A0658
IncuCyte® Caspase-3/7 Green Apoptosis Assay Reagent	Essen Bioscience	4440
Iodoacetamide	Sigma-Aldrich	I1149-5G
Isopropanol	J.T. Baker	8067
Kanamycin	GERBU Biotechnik GmbH	1091
Lipofectamine® 2000	Thermo Fisher Scientific	11668019
LysC	Wako Pure, Chemical Industries	129-02541
Magnesium chloride ($MgCl_2$), hexahydrate	AppliChem	A3618
MEM Eagle	PAN Biotech GmbH	P04-08500
MEM-non essential amino acids (NEAA) (100x)	PAN Biotech GmbH	P08-32100
Na-EDTA	Carl Roth	8043.2
Nonfat dried milk powder	AppliChem	A0830

Name	Supplier	Product number
NP-40 alternative	Calbiochem	492016
Odyssey blocking buffer (PBS)	Li-COR Bioscience	927-40000
PageRuler™ Plus prestained protein ladder, 10 to 250 kDa	Thermo Fisher Scientific	26620
PBS tablets	Jena Bioscience	AK-102P-L
PhosSTOP phosphatase inhibitors	Sigma-Aldrich	04906837001
Ponceau S solution (0.2 %)	SERVA GmbH	3342.7
Potassium chloride (KCl)	J.T. Baker	0509
RPMI 1640	PAN Biotech GmbH	P04-18047
Sodium chloride (NaCl)	VWR Chemicals	27810.295
Sodium dodecyl sulfate (SDS), pellets	GERBU Biotechnik GmbH	1012
Sodium hydroxide (NaOH)	J.T.Baker	7036
Sodium pyruvate (100 mM)	PAN Biotech GmbH	P04-43100
SuperSignal™ West Femto	Thermo Fisher Scientific	34095
SuperSignal™ West Pico	Thermo Fisher Scientific	34580
Tetracycline	Sigma-Aldrich	T7660-5G
Tetramethylethylenediamine (TEMED)	Carl Roth	2367.3
TMT10plex	Thermo Fisher Scientific	90110
Triethylammonium bicarbonate buffer (TEAB)	Sigma-Aldrich	T7408-100ML
Trifluoroacetic acid (TFA)	Sigma-Aldrich	106232
Tris(2-carboxyethyl)phosphine (TCEP)	Sigma-Aldrich	C4706
Tris-HCl	Carl Roth	9090.3
Triton X-100	SERVA GmbH	39795.02
Trypsin, proteomics grade	Sigma-Aldrich	03708969001
Trypsin/EDTA	PAN Biotech GmbH	P10-023100
Tween-20	Fisher Bioreagents	BB337-100
β-Mercaptoethanol	SERVA GmbH	28625.01

5.2.1.2 Buffers and media

Name	Composition
1x Laemmli buffer	10 mM Tris-HCl, 1 mM EDTA, 1% SDS (w/v), 5% 2-mercaptoethanol (v/v), 10% glycerol (v/v), 0.05% bromophenol blue (w/v), pH 8.0
ABC buffer	20 mM NH_4HCO_3 in mH_2O
Alkylation solution	55 mM iodoacetamide in 25 mM NH_4HCO_3
Coomassie staining solution	40% (v/v) ethanol, 10% (v/v) acetic acid, 0.6% (w/v) Coomassie brilliant blue R250 in H_2O
Cryopreservation Medium	10% (v/v) DMSO in DMEM
Denaturing/reducing buffer	8 M urea, 1 mM DTT in 50 mM Tris-HCl, pH 7.5
Digest solution	0.1 µg/µl Trypsin in 10 mM HCl diluted 1/10 in 25 mM NH_4HCO_3
Farnesylation buffer	50 mM HEPES, 250 mM NaCl, 10 mM $MgCl_2$, 2 mM TCEP, pH 8
Fixation buffer	4% formaldehyde in PBS
KRB	20 mM HEPES, 5 mM KH_2PO_4, 1 mM $MgSO_4$, 1 mM $CaCl_2$, 136 mM NaCl, 0.1% BSA, pH 7.4
LB medium	1% (w/v) tryptone, 0.5% (w/v) yeast extract, 1% (w/v) NaCl
PBS	137 mM NaCl, 2.7 mM KCl, 10 mM phosphate solution, pH 7.4
PBS-C	0.05% (w/v) CHAPS in PBS
PBS-T	0.1% (v/v) Tween-20 in PBS
SDS running buffer	25 mM Tris-HCl, 192 mM Glycine, 0.1% (w/v) SDS
SOB medium	2% (w/v) tryptone, 0.5% (w/v) yeast extract, 8.6 mM NaCl, 2.5 mM KCl, H_2O, 10 mM $MgCl_2$, 10 mM $MgSO_4$
Transfer buffer	25 mM Tris-HCl, pH 8.3, 190 mM glycine, 20% (v/v) methanol

5.2.1.3 Cell lines and bacterial strains

Name	Description	Provider
HeLa	ATCC® CCL-2™	ATCC
HeLa NanoLuc-PDEδ		established by Beate Schölermann
Jurkat	ATCC® TIB-152™	ATCC
Panc Tu-I		gift from H. Kalthoff[13]
HTC116	ATCC® CCL-247™	ATCC
OmniMAX	*E. coli*	
BL21-CodonPlus(DE3)-RIL	*E. coli*	

5.2.1.4 Kits

Name	Supplier	Product number
DC protein assay	Bio-Rad	5000112
Dual-Glo® luciferase assay system	Promega	E2980
MycoAlert™ mycoplasma detection kit	Lonza	LT07-318
QIAGEN Plasmid Midi/Maxi Kit	QIAGEN	12143
Nano-Glo® Luciferase Assay System	Promega	N1110

5.2.1.5 Antibodies

Name	Dilution	Host	Blocking Buffer	Supplier, Catalogue #
Primary antibodies				
anti-actin	1.1,000	rabbit	50% (v/v) Li-COR in PBS-T	abcam, ab8227
anti-ERK1/2	1:500	mouse	50% (v/v) Li-COR in PBS-T	abcam, ab36991
anti-HMGCS	1:500	mouse	5% (w/v) BSA PBS-T	abcam, ab87246
anti-mTOR	1:500	rabbit	50% (v/v) Li-COR in PBS-T	Santa Cruz Biotechnology, sc-517464
anti-PDE6D	1:250	rabbit	50% (v/v) Li-COR in PBS-T	Thermo Fisher Scientific, PA5-22008
anti-pERK1/2	1:500	rabbit	50% (v/v) Li-COR in PBS-T	Cell Signaling Technology, 9101
anti-p-mTOR	1:1,000	rabbit	50% (v/v) Li-COR in PBS-T	Santa Cruz Biotechnology, sc-293133
anti-Vinculin	1:5,000	mouse	50% (v/v) Li-COR in PBS-T	Cell Signaling Technology, 4650
anti-β-tubulin	1:2,500	rabbit	50% (v/v) Li-COR in PBS-T	abcam, ab18251
Secondary antibodies				
anti-rabbit800CW	1:2,500	goat	50% (v/v) Li-COR in PBS-T	Li-COR Bioscience, 926-32213
anti-mouse800CW	1:2,500	donkey	50% (v/v) Li-COR in PBS-T	Li-COR Bioscience, 926-32210
anti-mouse680RD	1:2,500	goat	50% (v/v) Li-COR in PBS-T	Li-COR Bioscience, 925-68070
anti-rabbit680RD	1:2,500	goat	50% (v/v) Li-COR in PBS-T	Li-COR Bioscience, 925-68071

5.2.1.6 Machines and devices

Description	Supplier	Product specification
Automated cell imaging system	Sartorius	IncuCyte® S3
Clean bench for proteome profiling	Thermo Fisher Scientific	MSC-Advantage 1.2
EASY-nLC 1000 Nano LC System	Thermo Fisher Scientific	
Fine scale	Sartorius	Analytical Plus
Hamilton™ syringe, #702	Sigma-Aldrich	
Horizontal rotor	neolab	
IncuCyte® S3 Live Cell Analysis System	EssenBioScience	
Large table-top centrifuge	eppendorf	
Mini Cell Buffer Dam	Bio-Rad	
Mini-PROTEAN® Comb, 10-well, 1.0 mm, 44 µl	Bio-Rad	
Mini-PROTEAN® Comb, 15-well, 1.0 mm, 26 µl	Bio-Rad	
Mini-PROTEAN® Short Plates	Bio-Rad	
Mini-PROTEAN® Spacer Plates with 1.0 mm Integrated Spacers	Bio-Rad	
Mini-PROTEAN® Tetra Cell	Bio-Rad	
Mini-PROTEAN® Tetra Cell Casting Module	Bio-Rad	
Mini-PROTEAN® Tetra Electrode Assembly	Bio-Rad	
Multi-channel pipettes, 10 and 100 µl	eppendorf	Research Plus
Nanospray Flex Ion Source	Thermo Fisher Scientific	
One-channel pipettes 10, 100, 200 and 1000 µl	eppendorf	Research Plus
Plate reader	Tecan	Tecan Infinity M200
Power supply	Bio-Rad	PowerPac™ Basic Power Supply B
Q Exactive	Thermo Fisher Scientific	

Description	Supplier	Product specification
Q ExactiveTM HF Hybrid Quadrupole-Orbitrap equipped with a nano-spray source	Thermo Fisher Scientific	
Spectrophotometer	Thermo Fisher Scientific	Nanodrop 2000c
Thermomixer comfort 1.5 ml	eppendorf	
UltiMate 3000 Nano LC system	Thermo Fisher Scientific	
UltimateTM 3000 RSLC nano-HPLC system	Thermo Fisher Scientific	
Ultrasound device	Bandelin	Sonoplus
Vacuum centrifuge	eppendorf	Concentrator plus

5.2.1.7 Consumables

Name	Supplier	Product number
0.5 ml tubes (standard)	Sarstedt	72.704
1.5 ml tubes (standard)	Sarstedt	72.706
10 µl pipette tips (standard)	Sarstedt	70.1130.100
1000 µl pipette tips (standard)	Diagonal	297800500
15 ml falcon tubes	Sarstedt	62.554.502
2 ml tubes (standard)	Sarstedt	72.695.500
200 µl pipette tips (standard)	Diagonal	32120000
4–20% Mini-PROTEAN® TGX™ precast protein gels, 10-well, 50 µl	Bio-Rad	4561094
5 ml tubes	eppendorf	0030119401
50 ml falcon tubes	Sarstedt	62.547.254
6-well plate (transparent, standard)	Sarstedt	83.3920
96-well plate (transparent, standard)	Sarstedt	83.3924
96-well plate (white, clear bottom)	Greiner	655098
BD Falcon TM cell scraper, 18 cm	BD Biosciences	353085
Cell culture dish 35 x 10 mm, polystyrene	Sarstedt	83.3900
CoolCell® LX	Biocision	BCS-405

Name	Supplier	Product number
Cryo vials	Sarstedt	72.379.992
Immobilon-FL PVDF Membrane	Millipore	IPFL00010
KIMTECH® Science precision tissues	Carl Roth	AA63.2
Microseal® 'B' PCR plate sealing film, adhesive, optical	Bio-Rad	MSB1001
Protein LoBind Tubes 0.5 ml	eppendorf	0030108094
Protein LoBind Tubes 1.5 ml	eppendorf	0030108116
Protein LoBind Tubes 2.0 ml	eppendorf	0030108132
SafeSeal tips premium 10 µl, sterile	Biozym Scientific	693010X
SafeSeal tips premium 100 µl, sterile	Biozym Scientific	692066X
SafeSeal tips premium 1000 µl, sterile	Biozym Scientific	692078X
SafeSeal tips premium 200 µl, sterile	Biozym Scientific	692069X
Superose 6 5/150	GE Healthcare	
T-175 cell culture flask	Sarstedt	83.3912.002
T-25 cell culture flask	Sarstedt	83.3911.002
T-75 cell culture flask	Sarstedt	83.3910.002
Whatman® gel blotting paper, Grade GB005	Sigma-Aldrich	WHA10426994

5.2.1.8 Software and online tools

Name	Developer
ChemDraw Professional 18.0.0.231	PerkinElmer Informatics, Inc.
GraphPad Prism 8	GraphPad Software, Inc.
Image Lab Software 6.0.1	Bio-Rad
MestReNova 20.0.0	Mestrelab Research S.L.
MetaMorph 7.7.8.0	Visitron
Reactome	https://reactome.org/ (18.3.2019)
STRING 11.0	https://string-db.org/cgi/input.pl (18.3.2019)
UniProt	https://www.uniprot.org/ (18.3.2019)

5.2.2 Methods

5.2.2.1 Molecular biology methods

5.2.2.1.1 Transformation of E. coli using heat shock

Competent *E. coli* OmniMAX or BL21-CodonPlus(DE3)-RIL cells were transformed using heat shock. Therefor 50 – 200 ng plasmid DNA were mixed with 100 µl of competent cells and stored for 30 min on ice. After 90 sec heat shock at 42 °C in a water bath, the cell suspension was incubated on for 2 min on ice. Afterwards, 1 ml of preheated SOB medium was added, followed by incubation for 1 h at 37 °C. The cell suspension was plated on LB agar plates containing the corresponding selection marker like ampicillin (100 µg/ml), kanamycin (50 µg/ml), chloramphenicol (25 µg/ml) or tetracycline (10 µg/ml) and incubated overnight at 37 °C.

5.2.2.1.2 Isolation of plasmid DNA

Plasmid DNA was obtained from *E. coli* by using QIAGEN Plasmid Midi and QIAGEN Plasmid Maxi Kits (QIAGEN, Hilden) according to manufacturer's instructions.

5.2.2.1.3 DNA sequencing

Plasmids were sequenced prior to usage by Eurofins Genomics. Therefor plasmids were amplified in *E. coli* and isolated using QIAGEN Plasmid Midi Kit (QIAGEN, Hilden). Isolated and purified plasmids were dried and shipped to Eurofins.

5.2.2.2 Cell biology methods

The experiments were performed using sterile equipment under a laminar flow cabinet. If not stated otherwise, standard consumables were used.

5.2.2.2.1 Cell culture

All cell lines were cultivated in a humidified incubator at 37 °C and 5% CO_2 in the respective medium. HeLa, Panc Tu-I, HEK293T cells were grown in Dulbecco's Modified Eagle's Medium (4.5 g/L glucose, 4 mM glutamine) supplemented with 10% fetal bovine serum, 10 mM sodium pyruvate and non-essential amino acids. Jurkat cells were grown in RPMI 1640 medium supplemented with 10% fetal bovine serum and non-essential amino acids. Adherent cells were passaged every 2-3 days to never reach confluency higher than 80%. Therefore, cells were washed with prewarmed PBS and detached with trypsin/EDTA solution. After 5 mins of

incubation, suspension was diluted with fresh medium to obtain 10 ml of suspension. Then 1 ml of the suspension was added to a fresh flask filled with 9 ml fresh medium. Jurkat cells were maintained in a cell concentration between 1 x 10^5 and 1 x 10^6 viable cells/ml.

5.2.2.2.2 Mycoplasma detection assay

Mycoplasma detection tests were carried out regularly to ensure that cell lines are not contaminated with Mycoplasma pneumoniae. Therefor the MycoAlert™ Mycoplasma Detection Kit was employed according to manufacturer's protocol.

5.2.2.2.3 Thawing of cryopreserved cells

Cells were taken out of the liquid nitrogen tank and the vial was put into the water bath for 5 min at 37 °C. Afterwards, the cell suspension was dissolved in 10 ml prewarmed medium. Then, cells were collected by centrifugation at 300xg for 5 min and the cell pellet was dissolved in 10 ml prewarmed DMEM. The suspension was transferred into a T-75 flask and cultivated overnight. Cells were used after two rounds of passaging.

5.2.2.2.4 Cryopreservation of mammalian cells

For long term storage of cells in liquid nitrogen, cells from a confluent T-75 flask were washed with PBS and detached using trypsin/EDTA. Cells were collected by centrifugation at 300xg and dissolved in 10 ml cryopreservative medium (DMEM containing 10% (v/v) DMSO). The cell suspension was transferred into cryopreservation vials and slowly cooled down to -80 °C (1 °C/min) using CoolCell® Cell Freezing Containers. After 16 h the vials were transferred into a nitrogen tank and stored until further use.

5.2.2.2.5 Live-cell imaging of mCherry-PDEδ

The day prior to treatment, 2,000 HeLa cells were seeded into 96-well plates and incubated overnight. The next day cells were transfected with a mCherry-PDEδ expressing plasmid (gift from Philippe I.H. Bastiaens)[90] by calcium phosphate transfection.

Therefor 2.5 ml 2x HBS was mixed with 2.5 ml of a solution of 40 µg plasmid, 305 µl 2 M $CaCl_2$ and H_2O. After the exchange of the medium 40 µl of this DNA-mix was applied to the cells. One day after the transfection the medium was exchanged with medium containing the compound or DMSO. Fluorescence was detected using the IncuCyte® S3 Live Cell Analysis System and the mean fluorescence per well was normalized to the confluence.

5.2.2.2.6 Establishment of HeLa stably expressing NanoLuc®-PDEδ fusion protein

The cell line was established by Beate Schölermann.

To generate a plasmid for expression of NanoLuc®-PDEδ, cDNA encoding human PDEδ was cloned into the pFN31K vector by using the restriction sites AsiSI and PmeI. HeLa cells were transfected with the generated plasmid using Fugene HD (Promega) using manufacturer's protocol. Transfected cells were exposed to selection growth medium containing 800 µg/ml of G418. After two weeks of incubation, clones were selected and analyzed by immunoblotting to show expression of the fusion protein.

5.2.2.2.7 Detection of NanoLuc® activity

The day prior to treatment, 2,000 HeLa cells, which stably express NanoLuc®-PDEδ, were seeded into a 96-well plate. The next day the medium was exchanged with 100 µl medium containing the compounds. After 24 h NanoLuc activity was measured using the Nano-Glo® Luciferase Assay System (Promega).

5.2.2.2.8 Preparation of cell lysates for immunoblotting

Prior to treatment, 200,000 Panc Tu-I or HeLa stably expressing NanoLuc®-PDEδ cells were seeded into 6-well plates and incubated overnight. If necessary, cells were grown in EGF-free medium, which was added 5 min bevor cell lysis in a concentration of 200 ng/ml. The next day the medium was exchanged with 2 ml medium containing the compounds or DMSO. After the annotated incubation time, cells were washed twice with ice-cold PBS and lysed using 2x Laemmli buffer without reducing agent and bromophenol blue. For the treatment of Jurkat cells, 500.000 cells were dissolved in medium containing the compound or DMSO and incubated for the annotated time. Then, the cells were collected by centrifugation (5 min at 300xg). The cell pellet was dissolved in 2x Laemmli buffer without reducing agent and bromophenol blue. Obtained lysates were sonicated (3 cycles, 10 sec) and protein concentration was determined using DC™ Protein Assay (Bio-Rad) using manufactures protocol. Prior to SDS-PAGE 5% (v/v) DTT and 0.05% (w/v) bromophenol blue was added to each lysate and the samples are heated for 5 min at 95 °C.

5.2.2.2.9 Caspase 3/7 assay

The activity of caspase-3/7 was measured using the IncuCyte® Caspase-3/7 Reagent for Apoptosis (Essen Bioscience). One day prior to treatment, 1,000 HeLa cells were seeded into a

96-well plate and incubated overnight. The next day medium was exchanged for medium containing either DMSO or the compounds and a final concentration of 5 µM of IncuCyte® Caspase-3/7 Reagent. The reagent is a substrate of the caspases and is fluorescent after cleavage. The cleaved product was monitored using the IncuCyte® S3 Live Cell Analysis System. Raw fluorescent intensity values were calculated for each well.

5.2.2.3 Biochemical methods

5.2.2.3.1 In vitro farnesylation and crosslinking of RZZ-Spindly complex

This experiment was performed by Dr. Anika Altenfeld, Dr. Tanja Bange, Dr. Jenny Keller and Sabine Wohlgemuth.

Spindly, RZZ and mutated FTase were incubated together with either farnesyl pyrophosphate or farnesyl derivatives in reaction buffer for 90 min at 25 °C. Next, the reaction solution was loaded onto a Superose 6 5/150 column (GE Healthcare). Eluted fractions were either analyzed by SDS-PAGE or exposed to UV for different time points (benzophenone 60 min, diazirine 30 min). UV-treated samples were then analyzed by MS or SDS-PAGE.

5.2.2.3.2 Determination of protein concertation by Bradford assay

To determine the protein concentration of lysates or purified proteins a Bradford assay was performed. Therefor Bradford reagent was mixed 1:5 with water and 1 ml was transferred into the cuvette. After addition of the protein solution and 5 min incubation at room temperature, the absorption was measured at a wavelength of 595 nm. Protein concentration was determined using a linear regression curve obtained by titrating BSA.

5.2.2.3.3 SDS-polyacrylamide gel electrophoresis (SDS-PAGE)

Protein mixtures were separated by using sodium dodecyl sulphate e (SDS-PAGE). First, the protein mixture was denatured by mixing with 1x Laemmli buffer and incubation for 5 min at 95 °C. Different separation gels from 8 to 15% acrylamide were used according to the size of the analyzed protein. For PDEδ detection 200 µg protein were loaded onto the gel. SDS gels were stored in SDS running buffer and separation occurred for 30 min at 80 V, followed by 60 min at 150 V using Mini-PROTEAN® 3 Cell from Bio-Rad.

Table 5: Composition of separation and stacking gel.

final acrylamide conc.	4%	8%	10%	12%	15%
ddH_2O	6.8	9.3	7.9	6.6	4.6
30% acrylamide	1.7	5.3	6.7	8	10
Tris-HCl (1.5 M, pH 8.8)	-	5	5	5	5
Tris-HCl (1.0 M, pH 6.8)	1.25	-	-	-	-
10% SDS solution	0.1	0.2	0.2	0.2	0.2
10% APS solution	0.1	0.2	0.2	0.2	0.2
TEMED	0.01	0.02	0.02	0.02	0.02

5.2.2.3.4 Immunoblotting

After the separation of protein mixtures by SDS-PAGE proteins were transferred to a polyvinylidene difluoride (PVDF) membrane using a tank blotting system. Therefor the gel was washed once with water and equilibrated in transfer buffer for 20 min. In the meantime, the membrane was activated for 10 sec in methanol and shacked in water for 10 min. After additional 15 min in transfer buffer the blotting chamber was used according to manufacturer's instructions. Therefor the chamber was filled with transfer buffer and proteins were transferred for 60 min at 100 V and 4 °C. To block unspecific binding sites on the membrane, it was incubated with the respective blocking solution according to the conditions needed for primary antibody binding for 60 min (see paragraph 5.2.1.4). The membrane was incubated overnight with the primary antibody at 4 °C under constant shaking. After washing three times with PBS-T the membrane was incubated with the secondary antibody for 60 min at room temperature in the dark. The membrane was washed two times with PBS-T and two times with PBS to remove the secondary antibody. Secondary antibodies were fused to a fluorescent dye (e.g. IR680 or IR800) and fluorescence was detected using a ChemiDoc MP Imaging System.

5.2.2.3.5 SRE reporter gene assay

The SRE reporter gene assay was performed in 96-well plates. Therefor 10,000 HeLa cells were seeded into each well of a 96-well plate and incubated overnight. The next day cells were transfected with two plasmids using Effectene according to manufacturer's protocol. The reporter plasmid contains a firefly luciferase under the transcriptional control of the SRE reporter (gift from Timothy Osborn; Addgene plasmid #60444; http://n2t.net/addgene:60444; RRID: Addgene_60444).[91] The control plasmid encoded *Renilla* luciferase under the control of thymidine kinase (TK) gene promoter, whose luciferase activity is used for internal

normalisation purposes. For compound treatment, medium was exchanged 24 h after the transfection. Compounds and oxysterols were dissolved into the prewarmed medium and added to the cells. After 24 h of treatment, luciferase activities were determined using Dual-Luciferase® Reporter Assay System from Promega. Briefly, medium was exchanged with 1x passive lyses buffer (provided with the kit) and incubated for 30 min at 600 rpm on a multiplate shaker. Then, firefly luciferase activity was measured by dissolving 10 µl lysate into 10 µl substrate for the firefly luciferase in reaction buffer. After detection of the luminescence signal, 10 µl of *Renilla* substrate and firefly luciferase inhibitor were added. The luminescence was again measured in a multiplate reader.

Table 6: Reagents used for transfection.

Substance	Amount
pSynSRE-T-Luc	50 ng
Control plasmid	50 ng
Enhancer	0.8 µl
Effectene	1 µl
DMEM	3 µl
EC Buffer	30 µl

5.2.2.3.6 Fluorescent polarization

Apparent binding constants (K_D) were determined using His_6-PDEδ and a FITC-labelled atorvastatin.[15] First, 100 nM of His_6-PDEδ (gift from Dr. P. Küchler) were incubated with the compound at different concentrations in PBS-C. Then, 10 nM FITC-atorvastatin was added and incubated for another 30 min. The polarization of the emitted light was measured using the Infinite M200 plate reader (Tecan, Austria). Changes in the polarization upon treatment were used to determine the IC_{50} with a three parameter non-liner regression fit (GraphPad Prism 7). Binding constants were obtained by using the following equation:

$$K_D = \frac{IC_{50}}{\frac{1 + [L]_{Atorvastatin}}{K_{D,Atorvastatin}}}$$

5.2.2.3.7 ROS accumulation Assay

Assay was performed by Julian Wilke.

10,000 HeLa cells were seeded into a 96-well plate. The next day, the medium was exchanged with prewarmed medium containing the compounds or DMSO. After 23 h of incubation, CDNB

was added to the cells as reference to induce ROS accumulation and cells incubated for 1 h. Then, the medium was exchanged with the staining medium containing CM-H_2DCFDA and Hoechst-3342 and incubated for 30 min at 37 °C. After 10 min of fixation with a solution of 0.5% PFA, cells were washed three times with PBS. The plate was imaged using Axiovert 200 M and the resulting images are analyzed by MetaMorph®. Briefly, the software identifies the cells with the Hoechst-3342 stain and calculates the fluorescent CM-H_2DCFDA intensity per cell. Therefor it measures the stained area and the integrated intensity.

5.2.2.3.8 2-Deoxy-glucose (2-DG) uptake assay

Assay was performed by Dr. George Karageorgis.

One day prior to the readout, 40.000 HCT116 cells were seeded into a 96-well plate and incubated overnight. Then, cells were incubated in 1 mM 2-DG and compounds or DMSO in glucose-free KRB buffer. After 30 min cell were washed and lysed in 0.06 M HCl and 1% CHAPS for 15 min at 65 °C. The 2-DG uptake is measured in a coupled enzymatic assay. Therefore, 6.4 U/ml glucose-6-phosphate dehydrogenase, 0.2 U/ml diaphorase, 0.1 mM $NADP^+$ and 0.025 mg/ml resazurin were added to the lysates. The fluorescence of resorufin was determined which is proportional to 2-DG uptake with a Tecan Infinite M200 plate reader.

5.2.2.4 Mass spectrometry methodsIdentification of Spindly by nanoLC-MS/MS

This experiment was performed by Dr. Anika Altenfeld, Dr. Tanja Bange, Dr. Jenny Keller and Sabine Wohlgemuth.

Sample preparation

Samples of *in vitro* farnesylated Spindly in complex with RZZ with and without UV irradiation were solved in buffer containing 6 M urea and treated with 10 mM DTT and 55 mM chloroacetamide. Afterwards, urea was lowered to 4 M and LysC (protein/enzyme ratio, 50:1) was added for 3 h. The reaction mixture was diluted to 2 M using 50 mM ammonium bicarbonate and further digested over night with trypsin (protein/enzyme ratio, 50:1). Peptides were desalted using C18 stage tips and dried under vacuum.

NanoHPLC MS/MS analysis

Peptides were separated on an EASY-nLC 1000 Nano LC System (Thermo Fisher Scientific) using a column from New Objective (75-µm inner diameter and 25-cm length). Peptide solution were loaded on the column in buffer A (H_2O with 0.1% formic acid) and separated with a

gradient from 5 to 60% buffer B (100% acetonitrile with 0.1% formic acid) within 50 min at 200 nl/min, while columns temperature was set to 40 °C. The liquid chromatography system was coupled to a quadrupole Orbitrap mass spectrometer (Thermo Fisher Scientific) via a nanospray source. To identify the most abundant precursors for sequencing, a survey scan was performed. The scan range was set to from 300 to 1650 Th, with a resolution of 70,000 at *m/z* 200. Based on this scan, the Q Exactive devices were operated in the data-dependent mode. The target value was set to 3×10^6 and maximum injection time to 20 ms. For sequencing, up to 10 of the most abundant isotope patterns with a charge ≥ 2 were subjected to higher-energy collisional dissociation with a target value of 1×10^5. Normalized collision energy was set to 25, and it was an isolation window of 3 Th used for the Q Exactive. For higher-energy collisional dissociation the resolution of the spectra was set to 17,500 at *m/z* 200 with a maximum ion injection time of 120 ms. The dynamic exclusion of sequenced peptides was set to 20 sec.

Data Analysis

MaxQuant Version 1.5.2.18 was used to process MS raw files. MS/MS spectra were searched using the Andromeda search engine, which is implemented into MaxQuant. The samples were searched against a reduced database containing Spindly and RZZ. Enzyme specificity was set to C-terminal lysine and arginine with up to two miscleavages. Peptides with seven amino acids were considered as hits. As variable modifications we set carbamidomethyl of cysteine, deamidation and oxidation of methionine. Additionally, farnesylation and farnesyl analogues containing the photoactivatable substitution (Benzophenone **37**, **38** Diazirine **39**, **Error! Reference source not found.**) were set as variable modifications. The identification of crosslink products was done by searching for variable modifications of the mass of Spindly peptide containing the farnesyl-moiety. In addition, the y3 ion fragment (PQQ; 372.1878 Th) of Spindly served as diagnostic marker to identify possible cross-links. Every amino acid was searched individually against this modification since the compounds react in a sequence-independent manner. Spectra were carefully inspected, and precursors were required to have a charge state higher than 2.

5.2.2.4.2 Proteome Profiling by nanoLC-MS/MS

The samples were measured and analyzed by Malte Metz, Andreas Brockmeyer, Walburga Hecker and Dr. Petra Janning.

Sample preparation

On day prior to treatment, 400,000 cells were seeded into a 10-mm dish and cultured overnight. The next day the medium was exchanged with DMEM containing 1 µM compound and cultured for 24 h. Then, cells were washed with warm PBS and detached using trypsin/EDTA. Cell suspension was washed twice with ice-cold PBS followed by centrifugation at 300xg. The cell pellet was dissolved in 200 µl PBS containing protease inhibitors (cOmplete™, EDTA-free Protease Inhibitor Cocktail) and subjected to seven freeze-thaw cycles. Therefor cells were snap frozen in liquid nitrogen and placed in a shaker for 2 min at 300 rpm at 25 °C. The lysate was centrifuged for 15 min at 15,000xg at 4 °C. The supernatant was collected, and protein concentration was determined using the Bradford assay.

For mass spectrometry samples (75 µl of 2 g/l protein concentration) were added to 75 µl triethylammonium bicarbonate buffer (TEAB). After addition of 7.5 µl TCEP and incubation at 55 °C for 30 min samples were alkylated with 7.5 µl iodoacetamide (375 mM) for 30 min in the dark. After that proteins were precipitated by treating the solution with 900 µl prechilled acetone and subsequent incubation overnight at -20 °C. On the next day, precipitated proteins were separated by centrifugation for 10 min and 8,000xg at 4 °C. The supernatant was carefully removed, and the protein pellet was left to dry for another 10 min. The pellet was dissolved in TEA-buffer containing trypsin (3.2 ng in 107.5 µL 100mM TEAB) and incubated over night at 37 °C.

TMT label reagents had to be equilibrated at room temperature and 0.8 mg of each label was dissolved in 82 µl anhydrous acetonitrile. After 5 min half of the solution is added to the sample and samples are incubated at room temperature for 2 h. Afterwards, 8 µl of hydroxylamine was added to quench the reaction and the solution was incubated for another 50 min. Then, all samples are pooled to the solvent was evaporated in a speedvac at 30 °C until a dry white pellet remains.

Sample fractionation

Prior to nanoHPLC-MS/MS analysis samples were fractionated into 10 fractions on a C18 column using high pH conditions to reduce the complexity of the samples and thereby increasing

the number of quantified proteins. Therefor samples were dissolved in 120 µl of 20 mM ammonium formate (NH_4COOH) at pH 11, followed by incubation in an ultra-sonicator for 2 min, subsequent vortexing for 1 min and centrifugation at 8,000xg for 3 min at room temperature. Then, 50 µl of the supernatant were injected onto a XBridge C18 column (130 Å, 3.5 µm, 1mm x 150 mm) using a U3000 capHPLCSystem (ThermoFisher scientific, Germany). Separation was performed at a flow rate of 50 µl/min using 20 mM NH_4COO at pH 11 in water as solvent A and 40% 20 mM NH_4COO pH 11 in water premixed with 60% acetonitrile as solvent B. Separation conditions were 95% solvent A/5% solvent B isocratic for the first 10 min, to desalt the samples, followed by a linear gradient up to 25% in 5 min, a second linear gradient up to 65% solvent B in 60 min, and a third linear gradient up to 100% B in 10 min. Detection was carried out at a valve length of 214 nm. The eluate between 15 and 100 min was fractionated into 10 fractions (30 sec per fraction, circular fractionation using 10 vials). Each fraction was dried in a SpeedVac at 30 °C until complete dryness and subsequently subjected to nanoHPLC-MS/MS analysis.

NanoHPLC MS/MS analysis

For nanoHPLC-MS/MS analysis samples were dissolved in 20 µl of 0.1% TFA in water and 3 µl were injected onto an UltiMateTM 3000 RSLCnano system (ThermoFisher scientific, Germany) online coupled to a Q Exactive™ HF Hybrid Quadrupole-Orbitrap Mass Spectrometer equipped with a nanospray source (Nanospray Flex Ion Source, Thermo Scientific). All solvents were LC-MS grade. To desalting the samples, they were injected onto a pre-column cartridge (5 µm, 100 Å, 300 µm ID x 5 mm, Dionex, Germany) using 0.1% TFA in water as eluent with a flow rate of 30 µl/min. Desalting was performed for 5 min with eluent flow to waste followed by back-flushing of the sample during the whole analysis from the pre-column to the PepMap100 RSLC C18 nano-HPLC column (2 µm, 100 Å, 75 µm ID × 50 cm, nanoViper, Dionex, Germany) using a linear gradient starting with 95% solvent A (water containing 0.1% formic acid)/5% solvent B (acetonitrile containing 0.1% formic acid) and increasing to 60% solvent A 0.1% formic acid/40% solvent B in 120 min using a flow rate of 300 nl/min. The nano-HPLC was coupled to the Quadrupole-Orbitrap Mass Spectrometer using a standard coated SilicaTip (ID 20 µm, Tip-ID 10 µM, New Objective, Woburn, MA, USA). Mass range of *m/z* 300 to 1,650 was acquired with a resolution of 60,000 for full scan, followed

by up to 15 high energy collision dissociation (HCD) MS/MS scans of the most intense at least double-charged ions using a resolution of 30,000 and a NCE energy of 35%.

Data analysis

Data evaluation was performed using MaxQuant software (v.1.6.1.0)[92] including the Andromeda search algorithm and searching the human reference proteome of the Uniprot database. The search was performed for full enzymatic trypsin cleavages allowing two miscleavages. For protein modifications carbamidomethylation was chosen as fixed and oxidation of methionine and acetylation of the N-terminus as variable modifications. For relative quantification the type "reporter ion MS2" was chosen and for all lysins and peptide N-termini TMT labels were defined. The mass accuracy for full mass spectra was set to 20 ppm (first search) and 4.5 ppm (second search), respectively and for MS/MS spectra to 20 ppm. The false discovery rates for peptide and protein identification were set to 1%. Only proteins for which at least two peptides were quantified were chosen for further validation. Relative quantification of proteins was carried out using the reporter ion MS2 algorithm implemented in MaxQuant.

The proteinGroups.txt file was used for further analysis. In Excel all proteins which were not identified with at least two razor and unique peptides were filtered off. For further data analysis the "Reporter intensity corrected" corresponding to compound treatment was divided by the "Reporter intensity corrected" of the corresponding vehicle control and the result was written into a new column. This file was stored under a different file name in txt-format. For further data analysis Perseus[93] was used. The calculated ratios of the above-mentioned file were defined as main columns. Proteins resulting from the reverse database search, just identified by site and typical contaminants were filtered off. The ratios of the "Reporter intensities corrected" were logarithmized (log2) and normalized to the median. The mean of the replicates was calculated and the outlier test "Significance A" was performed. The P value was logarithmized (-log10) and the percentage change of the protein expression was calculated using the formula:

$$x = 100 * (2^{normalized\ (log2\left[\frac{\{mean\ of\ reporter\ ion\ intensity\ corrced\ compound\}}{\{mean\ of\ reporter\ ion\ intensity\ correced\ vehicle\}}\right])} - 1).$$

5.2.2.4.3 Quantification of lipid metabolites

The metabolite quantification was performed at TMIC in Canada.

Selected lipid metabolites were quantified by the Metabolomics Innovation Centre in Canada (TMIC). The day prior to treatment, 400,000 HeLa cells were seeded into 10-mm dish and

cultivated overnight. Cells were then treated for 24 h with 1 µM Deltasonamide or DMSO. Then the cells were washed with PBS and detached using trypsin/EDTA solution. Cells were collected by centrifugation for 5 min at 300xg, washed twice with PBS and collected by centrifugation. The liquate was removed and the cell pellet was left behind. The dry cell pellet was snap frozen in liquid nitrogen and shipped on dry ice to TMIC.

Metabolite extraction

Each sample (ca. 20 µl) was added with 100 µl of water containing 0.5 mg/ml of ascorbic acid as antioxidant and two metal beads. Cells were lysed on a MM 4000 mill mixer for 1 min twice at 25 Hz. Then, 600 µl of methanol and 200 µl of chloroform were added. After vortex mixing for 30 sec, the samples were sonicated for 2 min in an ice-water bath. After centrifugation at 15,000xg and for 20 min at 10 °C, the supernatant of each sample was collected and transferred to another tube. The pellet was used to measure protein content of each sample using the standard BCA method. For the supernatant, 300 µl of water and 400 µl of chloroform were added. The tubes were vortexed for 30 sec at 3,000xg, followed by centrifugation to split the whole phase into two phases. The aqueous and organic phases were separated for the following LC-MS runs.

Quantitation of mevalonic acid

Then, 200 µL of aqueous phase was dried down under vacuum and then reconstituted in 25 µl of methanol and mixed with 25 µl of 0.2 µg/ml mevalonate-D_3 as internal standard, 25 µl of 100 mM 3-nitrophenylhydrazine solution and 25 µl of 100 mM EDC HCl-pyridine solution, were added. After vortex mixing, the mixture was allowed to react at 30 ^{o}C for 30 min. After cooling on ice for 1 min, 100 µl of water was added and 20 µl was injected to quantitate MVA by UPLC-MRM/MS.[94] The LC-MS instrument was an Agilent 1290 UHPLC system coupled to a Sciex 4000 QTRAP mass spectrometer, which was equipped with an atmospheric pressure ESI source and was operated in negative-ion multiple-reaction monitoring (MRM) mode. A C18 UPLC column (2.1 x 150 mm, 1.8 µm) was used at 40 ^{o}C; the mobile phase was 0.01% formic acid in water (A) and 0.01% formic acid in acetonitrile (B) for binary-solvent gradient elution. Concentrations were calculated from the linear-regression calibration curve with internal calibration standard, which was prepared in parallel with the sample processing using the standard substance.

Quantitation of sterols

Quantitation of sterols was performed on the same UPLC-MS/MS system by chemical derivatization. Therefor 100 µl of each organic phase was dried down in a speed-vac concentrator. The residue was resuspended in 25 µl of dichloromethane and was mixed with 25 µl of 0.1 µg/ml of cholesterol-$^{13}C_3$ as internal standard. Then, 100 µl of dansyl chloride solution and 50 µl of DMAP solution were added, according to a procedure described in literature.[95] The mixture was allowed to react at 50 ^{o}C for 60 min. After reaction, the solutions were dried in a speed-vac concentrator and the residue was reconstituted in 100 µl of methanol. Then, 10 µl was injected onto a 5-cm long C18 UPLC column for UPLC-MRM/MS on the same LC-MS system, using 0.1% formic acid – isopropanol (1:1) as the mobile phase for binary-solvent gradient elution. To quantitate high-abundance cholesterol, each resultant solution was further diluted 100 times and was reinjected. Concentrations were calculated from the linear-regression calibration curve of each sterol compound, which was prepared in parallel with the sample processing using their standard substances.

Quantitation of phosphate-containing metabolic intermediates in the pathway

For the analysis, 500 µl of aqueous phase was mixed with 100 µl of a solution of HMG-CoA-d_3 as internal standard. After vortex mixing, centrifugation and dried under a nitrogen gas flow at 30 ^{o}C. The residue was dissolved in 100 µl of 50% acetonitrile. 10 µl was injected onto a 15-cm long C18 UPLC column for UPLC-MRM/MS quantitation, using a tributylamine - ammonium acetate in water (A) – acetonitrile (B) as the mobile phase for gradient elution. Concentrations of individual compounds were calculated from their individual linear-regression curves with internal standard calibration, which were prepared in parallel with the sample processing with the use of their standard substances.

Quantitation of isoprenoids

For the analysis, 400 µl of organic phase was added with 30 µl of a ubiquinone 9-d10 (internal standard) solution and was then dried under a nitrogen gas flow. The residue was dissolved in 50 µl methanol-chloroform (1:1). 10 µl was injected to run UPLC-high-resolution MS on a LTQ-Orbitrap Velos Pro mass spectrometer using a custom-developed LC-MS method with positive-ion detection. The ion chromatograms of any detected isoprenoid compounds were extracted with the use of their calculated m/z values within a mass window of 3 ppm. The peak

areas of the ion chromatograms were used for quantitation of any detected isoprenoids with their varying numbers of isoprenyl units from their individual calibration curves.

6 References

[1] H. Zhang, R. Constantine, J. M. Frederick, W. Baehr, *Vision Res.* **2012**, *75*, 19.

[2] E. N. Pugh, T. D. Lamb, *Biochim. Biophys. Acta, Bioenerg.* **1993**, *1141*, 111.

[3] S. K. Florio, R. K. Prusti, J. A. Beavo, *J. Biol. Chem.* **1996**, *271*, 24036.

[4] H. Zhang, R. Constantine, S. Vorobiev, Y. Chen, J. Seetharaman, Y. J. Huang, R. Xiao, G. T. Montelione, C. D. Gerstner, M. W. Davis et al., *Nat. Neurosci.* **2011**, *14*, 874.

[5] G. R. Hoffman, N. Nassar, R. A. Cerione, *Cell* **2000**, *100*, 345.

[6] S. A. Ismail, Y.-X. Chen, A. Rusinova, A. Chandra, M. Bierbaum, L. Gremer, G. Triola, H. Waldmann, Bastiaens, Philippe I H, A. Wittinghofer, *Nat. Chem. Biol.* **2011**, *7*, 942.

[7] V. Nancy, I. Callebaut, A. El Marjou, J. de Gunzburg, *J. Biol. Chem.* **2002**, *277*, 15076.

[8] a) M. C. Humbert, K. Weihbrecht, C. C. Searby, Y. Li, R. M. Pope, V. C. Sheffield, S. Seo **2012**, *109*, 19691; b) N. Dutta, S. Seo, *Biol. Open* **2016**, *5*, 1283; c) E. K. Fansa, S. K. Kösling, E. Zent, A. Wittinghofer, S. Ismail, *Nat. Commun.* **2016**, *7*, 11366.

[9] E. K. Fansa, N. J. O'Reilly, S. Ismail, A. Wittinghofer **2015**, *16*, 1583.

[10] S. Thomas, K. J. Wright, S. Le Corre, A. Micalizzi, M. Romani, A. Abhyankar, J. Saada, I. Perrault, J. Amiel, J. Litzler et al., *Hum. Mutat.* **2013**.

[11] W. Kolch, *Nat. Rev. Mol. Cell Biol.* **2005**, *6*, 827.

[12] M. Schmick, N. Vartak, B. Papke, M. Kovacevic, D. C. Truxius, L. Rossmannek, Bastiaens, Philippe I. H., *Cell* **2014**, *157*, 459.

[13] G. Zimmermann, B. Papke, S. Ismail, N. Vartak, A. Chandra, M. Hoffmann, S. A. Hahn, G. Triola, A. Wittinghofer, Bastiaens, Philippe I H et al., *Nature* **2013**, *497*, 638.

[14] P. Martín-Gago, E. K. Fansa, C. H. Klein, S. Murarka, P. Janning, M. Schürmann, M. Metz, S. Ismail, C. Schultz-Fademrecht, M. Baumann et al., *Angew. Chem., Int. Ed. Engl.* **2017**, *56*, 2423.

[15] B. Papke, S. Murarka, H. A. Vogel, P. Martín-Gago, M. Kovacevic, D. C. Truxius, E. K. Fansa, S. Ismail, G. Zimmermann, K. Heinelt et al., *Nat. Commun.* **2016**, *7*, 11360.

[16] U. T. T. Nguyen, Y. Wu, A. Goodall, K. Alexandrov **2010**, *Chapter 14*, 3.

[17] M. K. Doherty, R. J. Beynon, *Expert Rev. Proteomics* **2006**, *3*, 97.

[18] a) Y. Ohsumi, *IUBMB life* **2006**, *58*, 363; b) M. K. Doherty, D. E. Hammond, M. J. Clague, S. J. Gaskell, R. J. Beynon, *J. Proteome Res.* **2009**, *8*, 104.

[19] A. Hershko, A. Ciechanover, *Annu. Rev. Biochem.* **1998**, *67*, 425.

[20] M. D. Stewart, T. Ritterhoff, R. E. Klevit, P. S. Brzovic, *Cell Res.* **2016**, *26*, 423.

[21] a) A. D. Cox, S. W. Fesik, A. C. Kimmelman, J. Luo, C. J. Der, *Nat. Rev. Drug Discov.* **2014**, *13*, 828; b) A. P. Russ, S. Lampel, *DDT* **2005**, *10*, 1607.

[22] R. A. Copeland, *Nat. Rev. Drug Discov.* **2016**, *15*, 87.

[23] J. Liang, Y. Shang, *Annu. Rev. Physiol.* **2013**, *75*, 225.

[24] a) B. M. Wittmann, A. Sherk, D. P. McDonnell, *Cancer Res.* **2007**, *67*, 9549; b) Y.-L. Wu, X. Yang, Z. Ren, D. P. McDonnell, J. D. Norris, T. M. Willson, G. L. Greene, *Mol. Cell* **2005**, *18*, 413.

[25] K. J. Kieser, D. W. Kim, K. E. Carlson, B. S. Katzenellenbogen, J. A. Katzenellenbogen, *J. Med. Chem.* **2010**, *53*, 3320.

[26] P. Ottis, C. M. Crews, *ACS Chem. Biol.* **2017**, *12*, 892.

[27] G. M. Burslem, B. E. Smith, A. C. Lai, S. Jaime-Figueroa, D. C. McQuaid, D. P. Bondeson, M. Toure, H. Dong, Y. Qian, J. Wang et al., *Cell Chem. Biol.* **2018**, *25*, 67-77.e3.

[28] D. P. Bondeson, C. M. Crews, *Annu. Rev. Pharmacol. Toxicol.* **2017**, *57*, 107.

[29] K. M. Sakamoto, K. B. Kim, A. Kumagai, F. Mercurio, C. M. Crews, R. J. Deshaies **2001**, *98*, 8554.

[30] J. S. Schneekloth, F. N. Fonseca, M. Koldobskiy, A. Mandal, R. Deshaies, K. Sakamoto, C. M. Crews, *J. Am. Chem. Soc.* **2004**, *126*, 3748.

[31] a) A. R. Schneekloth, M. Pucheault, H. S. Tae, C. M. Crews, *Bioorg. Med. Chem. Lett.* **2008**, *18*, 5904; b) Y. Itoh, R. Kitaguchi, M. Ishikawa, M. Naito, Y. Hashimoto, *Bioorg. Med. Chem.* **2011**, *19*, 6768; c) J. Hines, J. D. Gough, T. W. Corson, C. M. Crews **2013**, *110*, 8942.

[32] J. Lu, Y. Qian, M. Altieri, H. Dong, J. Wang, K. Raina, J. Hines, J. D. Winkler, A. P. Crew, K. Coleman et al., *Chem. Biol.* **2015**, *22*, 755.

[33] D. P. Bondeson, A. Mares, I. E. D. Smith, E. Ko, S. Campos, A. H. Miah, K. E. Mulholland, N. Routly, D. L. Buckley, J. L. Gustafson et al., *Nat. Chem. Biol.* **2015**, *11*, 611.

[34] P. M. Cromm, C. M. Crews, *Cell Chem. Biol.* **2017**, *24*, 1181.

[35] M. J. Clague, C. Heride, S. Urbé, *Trends Cell Biol.* **2015**, *25*, 417.

[36] a) S. Fulda, D. Vucic, *Nat. Rev. Drug Discovery* **2012**, *11*, 109; b) E. Varfolomeev, J. W. Blankenship, S. M. Wayson, A. V. Fedorova, N. Kayagaki, P. Garg, K. Zobel, J. N.

Dynek, L. O. Elliott, H. J.A. Wallweber et al., *Cell* **2007**, *131*, 669; c) N. Ohoka, K. Okuhira, M. Ito, K. Nagai, N. Shibata, T. Hattori, O. Ujikawa, K. Shimokawa, O. Sano, R. Koyama et al., *J. Biol. Chem.* **2017**, *292*, 4556.

[37] a) M. E. Matyskiela, S. Couto, X. Zheng, G. Lu, J. Hui, K. Stamp, C. Drew, Y. Ren, M. Wang, A. Carpenter et al. **2018**, *14*, 981; b) M. Ishoey, S. Chorn, N. Singh, M. G. Jaeger, M. Brand, J. Paulk, S. Bauer, M. A. Erb, K. Parapatics, A. C. Müller et al., *ACS Chem. Biol.* **2018**, *13*, 553.

[38] J. Hines, S. Lartigue, H. Dong, Y. Qian, C. M. Crews **2019**, *79*, 251.

[39] a) E. F. Douglass, C. J. Miller, G. Sparer, H. Shapiro, D. A. Spiegel **2013**, *135*, 6092; b) C. Lu, Z.-X. Wang, *Anal. Chem.* **2017**, *89*, 6926.

[40] L. E. M. Miles, *Ricerca in clinica e in laboratorio* **1975**, *5*, 59.

[41] R. D. Roy, C. Rosenmund, M. I. Stefan, *BMC Systems Biology* **2017**, *11*, 74.

[42] M. S. Gadd, A. Testa, X. Lucas, K.-H. Chan, W. Chen, D. J. Lamont, M. Zengerle, A. Ciulli, *Nat. Chem. Biol.* **2017**, *13*, 514.

[43] a) I. Churcher **2018**, *61*, 444; b) J. C. Venter, M. D. Adams, E. W. Myers, P. W. Li, R. J. Mural, G. G. Sutton, H. O. Smith, M. Yandell, C. A. Evans, R. A. Holt et al. **2001**, *291*, 1304.

[44] M. Pettersson, C. M. Crews **2019**.

[45] H. Veisi, *Bull. Korean Chem. Soc.* **2012**, *33*, 383.

[46] M. Hanzal-Bayer, L. Renault, P. Roversi, A. Wittinghofer, R. C. Hillig, *EMBO J.* **2002**, *21*, 2095.

[47] A. Fabregat, K. Sidiropoulos, G. Viteri, O. Forner, P. Marin-Garcia, V. Arnau, P. D'Eustachio, L. Stein, H. Hermjakob, *BMC Bioinf.* **2017**, *18*, 142.

[48] D. Szklarczyk, A. L. Gable, D. Lyon, A. Junge, S. Wyder, J. Huerta-Cepas, M. Simonovic, N. T. Doncheva, J. H. Morris, P. Bork et al., *Nucleic Acids Res.* **2019**, *47*, D607-D613.

[49] L.-P. Sun, J. Seemann, J. L. Goldstein, M. S. Brown **2007**, *104*, 6519.

[50] D. Martinez Molina, P. Nordlund, *Annu. Rev. Pharmacol. Toxicol.* **2016**, *56*, 141.

[51] a) I. Shimomura, Y. Bashmakov, S. Ikemoto, J. D. Horton, M. S. Brown, J. L. Goldstein, *PNAS* **1999**, *96*, 13656; b) M. Fleischmann, P. B. Iynadjian, *Biochem. J.* **2000**, *349*, 13; c) D. Azzout-Marchine, D. Becard, C. Guichard, M. Foretz, P. Ferre, F. Fouelle, *Biochem. J.* **2000**, *350*, 389; d) T. Porstmann, B. Griffiths, Y.-L. Chung, O. Delpuech, J.

R. Griffiths, J. Downward, A. Schulze, *Oncogene* **2005**, *24*, 6465; e) T. Porstmann, C. R. Santos, B. Griffiths, M. Cully, M. Wu, S. Leevers, J. R. Griffiths, Y.-L. Chung, A. Schulze, *Cell Metab.* **2008**, *8*, 224.

[52] T. Sato, A. Umetsu, F. Tamanoi, *Methods Enzymol.* **2008**, *438*, 307.

[53] R. B. Yadav, P. Burgos, A. W. Parker, V. Iadevaia, C. G. Proud, R. A. Allen, J. P. O'Connell, A. Jeshtadi, C. D. Stubbs, S. W. Botchway, *BMC Cell Biol.* **2013**, *14*, 3.

[54] E. L. H. Leung, L. X. Luo, Z. Q. Liu, V. K. W. Wong, L. L. Lu, Y. Xie, N. Zhang, Y. Q. Qu, X. X. Fan, Y. Li et al., *Cell Death Dis.*, *9*, 216.

[55] X. Wang, N. G. Zelenski, J. Yang, J. Sakai, M. S. Brown, J. L. Goldstein **1996**, *15*, 1012.

[56] M. Redza-Dutordoir, D. A. Averill-Bates, *Biochim. Biophys. Acta Mol. Cell Res.* **2016**, *1863*, 2977.

[57] R. Bertolio, F. Napoletano, M. Mano, S. Maurer-Stroh, M. Fantuz, A. Zannini, S. Bicciato, G. Sorrentino, G. Del Sal **2019**, *10*, 1326.

[58] A. Dovas, J. R. Couchman, *Biochem J.* **2005**, *390*, 1.

[59] G. Karageorgis, E. S. Reckzeh, J. Ceballos, M. Schwalfenberg, S. Sievers, C. Ostermann, A. Pahl, S. Ziegler, H. Waldmann, *Nat. Chem.* **2018**, *10*, 1103.

[60] a) M. L. Macheda, S. Rogers, J. D. Best, *J. Cell Physiol.* **2005**, *202*, 654; b) L. Szablewski, *Biochim. Biophys. Acta* **2013**, *1835*, 164.

[61] D. O. Morgan, *The cell cycle : principles of control*, New Science Press Sinauer Associates, London, Sunderland MA, **2007**.

[62] T. Hunt, K. Nasmyth, B. Novák, *Philos. Trans. R. Soc. Lond., B., Biol. Sci.* **2011**, *366*, 3494.

[63] K. E. Barrett, *Gastroenterology* **2013**, *144*, 1569.

[64] R. Heald, A. Khodjakov, *J. Cell Biol.* **2015**, *211*, 1103.

[65] a) A. J. Holland, D. W. Cleveland, *EMBO Rep.* **2012**, *13*, 501; b) L. Hartwell, *Cell* **1992**, *71*, 543.

[66] S. Santaguida, A. Musacchio, *EMBO J.* **2009**, *28*, 2511.

[67] a) K. Kitagawa, P. Hieter **2001**, *2*, 678; b) J. P. I. Welburn, I. M. Cheeseman, *Developmental Cell* **2008**, *15*, 645.

[68] I. M. Cheeseman, A. Desai, *Nat. Rev. Mol. Cell Biol.* **2008**, *9*, 33.

[69] R. P. Zinkowski, *J. Cell Biol.* **1991**, *113*, 1091.

[70] a) D. W. Cleveland, Y. Mao, K. F. Sullivan, *Cell* **2003**, *112*, 407; b) B. F. McEwen, C.-E. Hsieh, A. L. Mattheyses, C. L. Rieder, *Chromosoma* **1998**, *107*, 366.

[71] J. B. Gama, C. Pereira, P. A. Simões, R. Celestino, R. M. Reis, D. J. Barbosa, H. R. Pires, C. Carvalho, J. Amorim, A. X. Carvalho et al., *J. Cell Biol.* **2017**, *216*, 943.

[72] a) R. Karess, *Trends Cell Biol.* **2005**, *15*, 386; b) G. J. P. L. Kops, Y. Kim, B. A. A. Weaver, Y. Mao, I. McLeod, J. R. Yates, M. Tagaya, D. W. Cleveland, *J. Cell Biol.* **2005**, *169*, 49; c) D. A. Starr, R. Saffery, Z. Li, A. E. Simpson, K. H. Choo, T. J. Yen, M. L. Goldberg, *J. Cell Sci.* **2000**, *113 (Pt 11)*, 1939.

[73] a) F. L. Zhang, P. J. Casey, *Annu. Rev. Biochem.* **1996**, *65*, 241; b) S. J. McTaggart, *Cell. Mol. Life Sci.* **2006**, *63*, 255; c) A. M. Griggs, K. Hahne, C. A. Hrycyna, *J. Biol. Chem.* **2010**, *285*, 13380.

[74] M. N. Ashby, *Curr. Opin. Lipidol.* **1998**, *9*, 99.

[75] G. Duan, D. Walther, *PLoS Comput Biol* **2015**, *11*, e1004049.

[76] M. Wang, P. J. Casey, *Nat. Rev. Mol. Cell Biol.* **2016**, *17*, 110.

[77] A. M. Winter-Vann, P. J. Casey, *Nat. Rev. Cancer* **2005**, *5*, 405.

[78] M. Hashimoto, Y. Hatanaka, *Eur. J. Org. Chem.* **2008**, *2008*, 2513.

[79] E. Smith, I. Collins **2015**, *7*, 159.

[80] C. G. Parker, A. Galmozzi, Y. Wang, B. E. Correia, K. Sasaki, C. M. Joslyn, A. S. Kim, C. L. Cavallaro, R. M. Lawrence, S. R. Johnson et al., *Cell* **2017**, *168*, 527-541.e29.

[81] a) I. Gaon, T. C. Turek, M. D. Distefano, *Tetrahedron Lett.* **1996**, *37*, 8833; b) T. C. Turek, I. Gaon, M. D. Distefano, C. L. Strickland, *J. Org. Chem.* **2001**, *66*, 3253.

[82] J. S. Vervacke, A. L. Funk, Y.-C. Wang, M. Strom, C. A. Hrycyna, M. D. Distefano **2014**, *79*, 1971.

[83] M. Alexander, M. Gerauer, M. Pechlivanis, B. Popkirova, R. Dvorsky, L. Brunsveld, H. Waldmann, J. Kuhlmann **2009**, *10*, 98.

[84] U. T. T. Nguyen, Z. Guo, C. Delon, Y. Wu, C. Deraeve, B. Fränzel, R. S. Bon, W. Blankenfeldt, R. S. Goody, H. Waldmann et al., *Nat. Chem. Biol.* **2009**, *5*, 227.

[85] S. Mosalaganti, J. Keller, A. Altenfeld, M. Winzker, P. Rombaut, M. Saur, A. Petrovic, A. Wehenkel, S. Wohlgemuth, F. Müller et al., *J. Cell Biol.* **2017**, *216*, 961.

[86] a) H. R. Ashar, L. James, K. Gray, D. Carr, S. Black, L. Armstrong, W. R. Bishop, P. Kirschmeier, *J. Biol. Chem.* **2000**, *275*, 30451; b) D. Hussein, S. S. Taylor, *J. Cell Sci.* **2002**, *115*, 3403; c) A. J. Holland, R. M. Reis, S. Niessen, C. Pereira, D. A. Andres, H.

P. Spielmann, D. W. Cleveland, A. Desai, R. Gassmann, *Mol. Biol. Cell* **2015**, *26*, 1845; d) D. K. Moudgil, N. Westcott, J. K. Famulski, K. Patel, D. Macdonald, H. Hang, G. K. T. Chan, *J. Cell Biol.* **2015**, *208*, 881.

[87] A. Rak, O. Pylypenko, T. Durek, A. Watzke, S. Kushnir, L. Brunsveld, H. Waldmann, R. S. Goody, K. Alexandrov **2003**, *302*, 646.

[88] R. J. McKenney, W. Huynh, M. E. Tanenbaum, G. Bhabha, R. D. Vale **2014**, *345*, 337.

[89] J. Lohbeck, A. K. Miller, *Bioorg. Med. Chem. Lett.* **2016**, *26*, 5260.

[90] M. Schmick, N. Vartak, B. Papke, M. Kovacevic, D. C. Truxius, L. Rossmannek, P. I. Bastiaens, *Cell* **2014**, *157*, 459.

[91] K. A. Dooley, S. Millinder, T. F. Osborne, *J. Biol. Chem.* **1998**, *273*, 1349.

[92] J. Cox, M. Mann, *Nat. Biotechnol.* **2008**, *26*, 1367.

[93] S. Tyanova, J. Cox, *Methods Mol. Biol. (N. Y.)* **2018**, *1711*, 133.

[94] J. Han, S. Gagnon, T. Eckle, C. H. Borchers, *Electrophoresis* **2013**, *34*, 2891.

[95] H.-F. Schött, S. Krautbauer, M. Höring, G. Liebisch, S. Matysik, *Anal. Chem.* **2018**, *90*, 8487.

7 Appendix

7.1 Supplementary Figures and tables

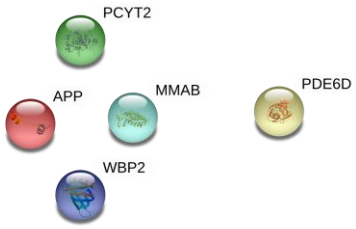

Figure 48: String analysis of upregulated proteins. HeLa cells were treated with 1 µM of PROTAC **3**, **4** or Deltasonamide 1 for 24 h and protein levels were determined by mass spectrometry. Proteins, which are not part of lipid metabolism and upregulated in all three samples are subjected to a string analysis.[48] Edges and nodes would represent known interactions.

Table 7: Upregulated proteins upon treatment with PROTAC 3.

Gene name	Protein name	% change to DMSO
ACSS2	Acetyl-coenzyme A synthetase, cytoplasmic	95.2
HMGCS1	Hydroxymethylglutaryl-CoA synthase, cytoplasmic	86.8
FABP3	Fatty acid-binding protein, heart	83.5
IDI1	Isopentenyl-diphosphate Delta-isomerase 1	64.3
APP	Amyloid beta A4 protein	54.1
NEU1	Sialidase-1	50.1
CYP51A1	Lanosterol 14-alpha demethylase	44.0
PCSK9	Proprotein convertase subtilisin/kexin type 9	38.7
MVD	Diphosphomevalonate decarboxylase	36.7
FDPS	Farnesyl pyrophosphate synthase	36.2
MVK	Mevalonate kinase	34.7
ACAT2	Acetyl-CoA acetyltransferase, cytosolic	33.4
FADS2	Fatty acid desaturase 2	33.0
BANF1	Barrier-to-autointegration, N-terminally processed	31.2
FDFT1	Squalene synthase	29.3
WBP2	WW domain-binding protein 2	27.7
ARHGEF12	Rho guanine nucleotide exchange factor 12	26.5
PDE2A	cGMP-dependent 3,5-cyclic phosphodiesterase	25.6
DHCR24	Delta(24)-sterol reductase	24.8
PCYT2	Ethanolamine-phosphate cytidylyltransferase	23.7
ZSWIM8	Zinc finger SWIM domain-containing protein 8	23.4
FASN	Fatty acid synthase	23.3
LSS	Lanosterol synthase	23.0
SBF2	Myotubularin-related protein 13	22.8
GSK3A	Glycogen synthase kinase-3 alpha	22.3
MMAB	Cob(I)yrinic acid a,c-diamide adenosyltransferase, mitochondrial	22.2
ALCAM	CD166 antigen	21.9
GABARAPL2	Gamma-aminobutyric acid receptor-associated protein-like 2	20.4
RTN1	Reticulon	20.2

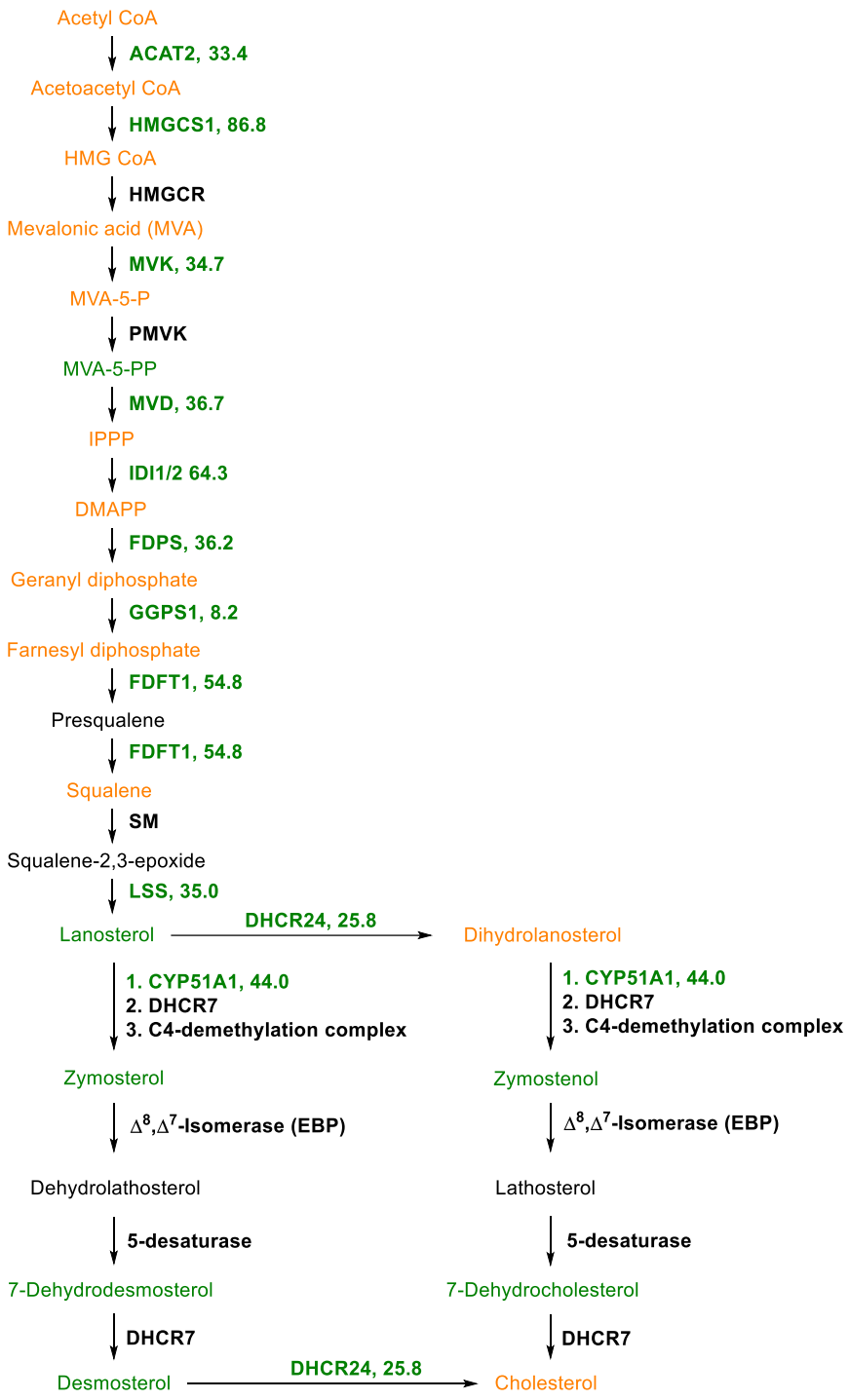

Figure 49: Influence of PDEδ PROTAC treatment on cholesterol biosynthesis and metabolites. HeLa cells were treated with 1 µM of PROTAC **3** or Deltasonamide 1 for 24 h and subject of proteome profiling or metabolomics. Proteins were quantified for cells treated with PROTAC **3** and metabolites were quantified for cells treated with Deltasonamide 1. Green: upregulation compared to DMSO-treated cells; orange: no significant change compared to DMSO-treated cells.; black: not identified; number: fold change to DMSO-treated cells.

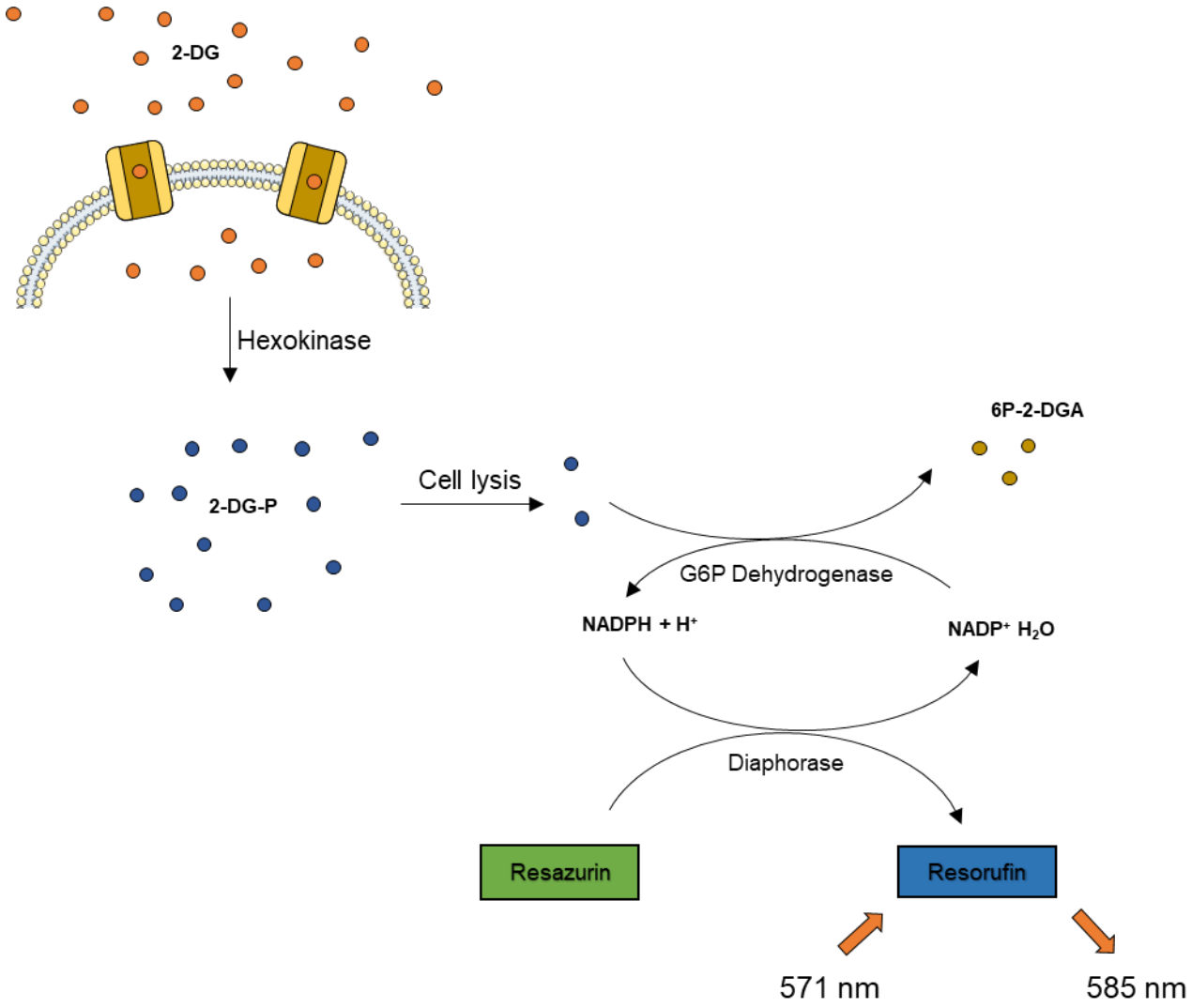

Figure 50: Principle of 2-DG uptake assay. Cells are treated with 2-DG and is taken up by Glucose Transporters. Cellular 2-DG is phosphorylated by a hexokinase. After cell lysis 2-DG-P is dephosphorylated under production of NADPH. This acts as cofactor for a diaphorase which converts resazurin into resorufin, which is fluorescent active.

Table 8: Upregulated proteins in the proteome profiling of HeLa cells treated with PROTAC 28.

Gene name	Protein name	% change to DMSO
SLC25A3	Phosphate carrier protein, mitochondrial	22,3
SLC34A3	Sodium-dependent phosphate transport protein 2C	19,1
RBSN	Rabenosyn-5	16,3
CCDC186	Coiled-coil domain-containing protein 186	16,1
RSF1	Remodeling and spacing factor 1	13,6
CEP76	Centrosomal protein of 76 kDa	13,5
STXBP4	Syntaxin-binding protein 4	13,3
SMCR8	Smith-Magenis syndrome chromosomal region candidate gene 8 protein	13,3
NUDT19	Nucleoside diphosphate-linked moiety X motif 19, mitochondrial	13,2
FAM83G	Protein FAM83G	12,9
CHCHD4	Mitochondrial intermembrane space import and assembly protein 40	12,9
CTU2	Cytoplasmic tRNA 2-thiolation protein 2	12,8
CYP51A1	Lanosterol 14-alpha demethylase	12,8
HSD17B12	Very-long-chain 3-oxoacyl-CoA reductase	12,7
KDM2A	Lysine-specific demethylase 2A	12,6
TBC1D10A	TBC1 domain family member 10A	12,5
INADL	InaD-like protein	12,3
MAPKAPK3	MAP kinase-activated protein kinase 3	12,3
MAPK1IP1L	MAPK-interacting and spindle-stabilizing protein-like	11,8
MRPL42	39S ribosomal protein L42, mitochondrial	11,5
GOLIM4	Golgi integral membrane protein 4	11,2
UNKL	Putative E3 ubiquitin-protein ligase UNKL	11,1
SDHAF3	Succinate dehydrogenase assembly factor 3, mitochondrial	11,0
PRKCDBP	Protein kinase C delta-binding protein	11,0
MTRF1L	Peptide chain release factor 1-like, mitochondrial	10,8
JUNB	Transcription factor jun-B	10,8
MISP	Mitotic interactor and substrate of PLK1	10,7
GSTT1	Glutathione S-transferase theta-1	10,6
CBR4	Carbonyl reductase family member 4	10,4

Table 9: Downregulated proteins in the proteome profiling of HeLa cells treated with PROTAC 28.

Gene name	Protein name	% change to DMSO
HIST2H2AA3	Histone H2A type 2-A	-22,5
HIST2H2BE	Histone H2B type 2-E	-19,1
NPM1	Nucleophosmin	-18,7
HIST1H1C	Histone H1.2	-18,6
HIST1H1D	Histone H1.3	-18,2
RPL10A	60S ribosomal protein L10a	-17,2
HIST1H1A	Histone H1.1	-16,8
RPL27	60S ribosomal protein L27	-16,1
RPL36AL	60S ribosomal protein L36a-like	-16,1
RPL8	60S ribosomal protein L8	-15,7
HIST1H1B	Histone H1.5	-15,5
RBMX	RNA-binding motif proteinchromosome, N-terminally processed	-15,3
RPL36A	60S ribosomal protein L36a	-15,3
SYNM	Synemin	-15,0
RPL34	60S ribosomal protein L34	-15,0
FBL	rRNA 2-O-methyltransferase fibrillarin	-14,9
USF1	Upstream stimulatory factor 1	-14,6
RPL7A	60S ribosomal protein L7a	-14,3
RPL15	60S ribosomal protein L15	-14,2
HIST1H2BN	Histone H2B	-14,0
RRP1	Ribosomal RNA processing protein 1 homolog A	-14,0
HIST1H4A	Histone H4	-13,8
TWSG1	Twisted gastrulation protein homolog 1	-13,7
NAGPA	N-acetylglucosamine-1-phosphodiester alpha-N-acetylglucosaminidase	-13,7
RSL1D1	Ribosomal L1 domain-containing protein 1	-13,3
HIST2H3A	Histone H3.2	-13,3
RPL13	60S ribosomal protein L13	-13,2
RPS4X	40S ribosomal protein S4, X isoform	-13,2
H2AFX	Histone H2AX	-13,1

Table 10: Upregulated proteins in the proteome profiling of HeLa cells treated with Chromopynone-1.

Gene name	Protein name	% change to DMSO
KCTD15	BTB/POZ domain-containing protein KCTD15	52,6
DOCK8	Dedicator of cytokinesis protein 8	48,3
CGREF1	Cell growth regulator with EF hand domain protein 1	39,3
RBX1	E3 ubiquitin-protein ligase RBX1	37,1
AMD1	S-adenosylmethionine decarboxylase proenzyme	34,4
NPRL3	Nitrogen permease regulator 3-like protein	33,1
CDT1	DNA replication factor Cdt1	31,3
SMCR8	Smith-Magenis syndrome chromosomal region candidate gene 8 protein	31,3
PARL	Presenilins-associated rhomboid-like protein, mitochondrial;P-beta	29,8
POTEJ	POTE ankyrin domain family member J	28,0
TPM2		27,7
ZNF512B	Zinc finger protein 512B	27,6
DPH5	Diphthine synthase	27,3
RNASEH1	Ribonuclease H1	26,7
SNRPF	Small nuclear ribonucleoprotein F	26,2
DHRS7B	Dehydrogenase/reductase SDR family member 7B	25,9
TNFSF13B	Tumor necrosis factor ligand superfamily member 13B	25,5
DAAM1	Disheveled-associated activator of morphogenesis 1	25,0
ICE1	Little elongation complex subunit 1	24,7
FRMPD3	FERM and PDZ domain-containing protein 3	23,8
SLC39A14	Zinc transporter ZIP14	23,4
RNASET2	Ribonuclease T2	23,4
POLR2K	DNA-directed RNA polymerases I, II, and III subunit RPABC4	23,2
CENPE	Kinesin-like protein;Centromere-associated protein E	23,1
DAP	Death-associated protein 1	23,1
TRANK1	TPR and ankyrin repeat-containing protein 1	21,7
TMSB4X	Thymosin beta-4	21,4
IGFBP7	Insulin-like growth factor-binding protein 7	21,1
RPS6KB1	Ribosomal protein S6 kinase beta-1	20,8

Table 11: Downregulated proteins in the proteome profiling of HeLa cells treated with Chromopynone-1.

Gene name	Protein name	% change to DMSO
KIAA0355	Uncharacterized protein KIAA0355	-41,5
PPIA	Peptidyl-prolyl cis-trans isomerase A	-33,2
BUB1	Mitotic checkpoint serine/threonine-protein kinase BUB1	-28,8
CALD1	Caldesmon	-28,6
PAPD4	Poly(A) RNA polymerase GLD2	-27,6
YEATS4	YEATS domain-containing protein 4	-24,4
PFN2	Profilin-2;Profilin	-23,7
EVPL	Envoplakin	-22,4
RPS28	40S ribosomal protein S28	-21,9
SNAPC4	snRNA-activating protein complex subunit 4	-21,6
RPAP2	Putative RNA polymerase II subunit B1 CTD phosphatase RPAP2	-21,3
EPB41L3	Band 4.1-like protein 3;Band 4.1-like protein 3, N-terminally processed	-20,4
CD59	CD59 glycoprotein	-20,4
MRPL14	39S ribosomal protein L14, mitochondrial	-20,0
C12orf43	Uncharacterized protein C12orf43	-19,6
MAP2K1	Dual specificity mitogen-activated protein kinase kinase 1	-18,7
ERBB2IP	Protein LAP2	-18,6
FRA10AC1	Protein FRA10AC1	-18,3
RPN2	Dolichyl-diphosphooligosaccharide--protein glycosyltransferase subunit 2	-18,2
CYP51A1	Lanosterol 14-alpha demethylase	-18,0
SLAIN2	SLAIN motif-containing protein 2	-17,9
DCP1B	mRNA-decapping enzyme 1B	-17,9
DDX19B	ATP-dependent RNA helicase DDX19B	-17,5
PIN4	Peptidyl-prolyl cis-trans isomerase NIMA-interacting 4	-17,2
UBQLN4	Ubiquilin-4	-17,2
MAP4	Microtubule-associated protein 4	-17,0
ATG13	Autophagy-related protein 13	-16,8
DNM2	Dynamin-2	-16,5
AMOTL2	Angiomotin-like protein 2	-16,5

7.2 Abbreviations

2-DG	2-Deoxy-D-glucose
ACSS2	Acetyl-coenzyme A synthetase
Ar	aromatic ring
Arl	ADP-ribosylation factor-like protein
ATP	Adenosine triphosphate
BRD4	bromodomain-containing protein 4
BSA	bovine serum albumin
CAN	acetonitrile
CDC42	CDC42 small effector protein 1
CDNB	1-chloro-2,4-dinitrobenzene
cGMP	cyclic guanosine monophosphate
CHAPS	3-[(3-cholamidopropyl)dimethylammonio]-1-propanesulfonate
CRBN	cereblon
DC_{50}	half-maximal degradation concentration
DCM	dichloromethane
DIPEA	*N*,*N*-Diisopropylethylamine
D_{max}	maximal degradation efficacy
DMEM	eagle's minimal essential medium
DMF	Dimethylformamide
DMSO	Dimethyl sulfoxide
DNA	Deoxyribonucleic acid
DTT	Dithiothreitol
E. coli	Escherichia coli
EDTA	ethylenediaminetetraacetic acid
EGF	epidermal growth factor
eq.	equivalents
ERK	extracellular signal-related kinase
ERRα	nuclear hormone receptor estrogen-related receptor α
ERα	estrogen receptor α
FITC	Fluorescein isothiocyanate

FPP	Farnesyl pyrophosphate
FTase	Farnesyl transferase
G_1	first gap phase
G_2	second gap phase
GDP	guanosine pyrophosphate
GLUT	glucose transporter member
GPP	Geranyl pyrophosphate
GRB	Growth factor receptor-bound protein 2
Raf	RAF proto-oncogene serine/threonine-protein kinase
GTP	guanosine triphosphate
HATU	hexafluorophosphate azabenzotriazole tetramethyl uronium
HEPES	4-(2-hydroxyethyl)-1-piperazineethanesulfonic acid
HMG-CoA	3-hydroxy-3-methylglutaryl-CoA
HMGCS	Hydroxymethylglutaryl-CoA synthase
HOBt	*N*-hydroxybenzotriazole
HPLC	high pressure liquid chromatography
IC_{50}	half-maximal inhibitory concentration
ImiD	Immunomodulatory drugs
INPP5E	inositol polyphosphate 5-phosphatase
Insig	Insulin-induced gene 1 protein
K_D	dissociation constant
KRas	GTPase KRas
MAPK	mitogen-activated protein kinase
MS	mass spectrometry
mTOR	mechanistic Target of Rapamycin
MVA	mevalonic acid
NADPH	nicotinamide adenine dinucleotide phosphate
NMR	nuclear magnetic resonance
PAL	photoaffinity labeling
PBS	phosphate buffered saline
PDE	phosphodiesterase

PDEδ	retinal rod rhodopsin-sensitive cGMP 3',5'-cyclic phosphodiesterase subunit delta
PP_i	diphosphate
PROTAC	proteolysis-targeting chimera
PTM	posttranslational modification
PVDF	polyvinylidene difluoride
Ras	rat sarcoma
RCE1	RAS-converting CAAX endopeptidase
Rheb	Ras homolog enriched in brain
RhoGDI	Rho GDP-dissociation inhibitor
RIPK2	receptor interacting serine/threonine protein kinase 2
RNA	Ribonucleic acid
ROS	reactive oxygen species
RPGR	X-linked retinitis pigmentosa GTPase regulator
rpm	rounds per minute
RZZ	Rod-Zw10-Zwilch
SCAP	Sterol regulatory element-binding protein cleavage-activating protein
SD	standard deviation
SDS	sodium dodecyl sulfate
SDS-PAGE	sodium dodecyl sulfate–polyacrylamide gel electrophoresis
SEC	size-exclusion chromatography
SERDs	selective estrogen receptor downregulators
siRNA	Small interfering RNA
SMAD4	mothers against decapentaplegic homolog 4
SOB medium	Super Optimal Broth medium
SOS	Son of sevenless homolog
SRE	sterol regulatory element
SREBP	sterol regulatory element binding protein
TBS	*tert*-butyldimethylsilyl chloride
TCEP	tris(2-carboxyethyl)phosphine
TFA	Trifluoroacetic acid
THF	tetrahydrofuran

TK	thymidine kinase
TLC	thin-layer chromatography
TMT	tandem mass tag
Tris	tris(hydroxymethyl)aminomethane
Ub	ubiquitin
UNC119	protein unc-119 homolog A
UV	Ultraviolet
VHL	von Hippel-Lindau

7.3 Acknowledgments

In den letzten fast 4 Jahren habe ich mit vielen Leuten zusammengearbeitet, die mir dabei sehr geholfen haben, diese Arbeit anzufertigen. Im Folgenden möchte ich einigen dafür besonders danken.

Als erstes möchte ich mich bei Herrn Prof. H. Waldmann bedanken, der mir zunächst die Möglichkeit bot die Promotion unter seiner Betreuung durchzuführen. Auch das ausgezeichnete Arbeitsumfeld, die gewährte Freiheit bezüglich der wissenschaftlichen Herausforderungen und das damit verbundene Wissen, das ich in den letzten Jahren erlangen konnte.

Herrn Prof. M. Engelhard danke ich für die Übernahme des Koreferats.

Ein Dank geht auch an Dr. S. Ziegler, die mir in vielen Gesprächen hilfreiche Denkanstöße gab. Zudem möchte ich ihr Danken für das Korrekturlesen dieser Arbeit.

Auch ganz herzlich möchte ich mich bei Dr. P. Janning für die unzähligen MS-Messungen und Auswertungen bedanken. Ebenso möchte ich mich bei Jens Wamser, Malte Metz, Andreas Brockmeyer, Walburga Hecker und Christiane Heitbrink für die Vorbereitung und Vermessung der Proben ganz herzlich danken.

Ich möchte mich bei Prof. A. Mussacchio, Dr. A. Altenfeld, S. Wohlgemuth, T. Bange und F. Müller für das Initialisieren des Projektes und die sehr gute Zusammenarbeit bedanken.

Meinem Labor- und Bürokollegen, ebenso wie allen Arbeitskollegen am Max-Planck-Insitut, möchte ich für die großartige Untersützung und außerordentliche gute Arbeitsatmosphäre danken. Namentlich möchte ich dabei Dr. L. Robke, Dr. G. Garivet, Dr. P. Martin-Gago, Dr. P. Küchler, Dr. L. Laraia, , Dr. H. Adihou, Dr. P. Cromm, Dr. J. Spiegel Dr. S. Zimmermann, Dr. A. Christoforow, J. Warmers, Dr. S. Patil, Dr. L. Kremer, L. Dötsch, J, Flegel, G. Niggemeyer, M. Schwalfenberg, Dr. N. Martinez, Christine Nowak, Dr. K. Estel, Dr. P. Hagel, Dr. R. Gasper, Dr. J. Jazormbek, Dr. J. Schulte-Zweckel, Dr. S. Kapoor, Dr. M. Rummelt und A. Burhop erwähnen.

Auch für die hervorragende Arbeit im PhDnet möchte ich mich bedanken. Insbesondere möchte ich Dr. L. Kremer, Dr. K. Estel, Dr. P. Hagel, A. Burhop, T. Schneidewind, E. Hennes nennen.

Ein großer Dank gilt auch allen, die diese Arbeit Korrektur gelesen haben. Besonders zu nennen sind dabei Dr. S. Ziegler, Dr. L. Laraia, Dr. G. Garivet, Dr. P. Martin-Gago, Dr. A. Friese und Dr. G. Ciossani.

Nicht zuletzt gebührt ein großer Dank meiner Familie und Freunden, die stehts für mich da waren und mich bei dem Vorhaben der Promotion und des vorangegangenen Studiums sehr unterstützt haben.

7.4 Eidesstattliche Versicherung (Affidavit)

Winzker, Michael
Name, Vorname
(Surname, first name)

141446
Matrikel-Nr.
(Enrolment number)

Belehrung:

Wer vorsätzlich gegen eine die Täuschung über Prüfungsleistungen betreffende Regelung einer Hochschulprüfungsordnung verstößt, handelt ordnungswidrig. Die Ordnungswidrigkeit kann mit einer Geldbuße von bis zu 50.000,00 € geahndet werden. Zuständige Verwaltungsbehörde für die Verfolgung und Ahndung von Ordnungswidrigkeiten ist der Kanzler/die Kanzlerin der Technischen Universität Dortmund. Im Falle eines mehrfachen oder sonstigen schwerwiegenden Täuschungsversuches kann der Prüfling zudem exmatrikuliert werden, § 63 Abs. 5 Hochschulgesetz NRW.

Die Abgabe einer falschen Versicherung an Eides statt ist strafbar.

Wer vorsätzlich eine falsche Versicherung an Eides statt abgibt, kann mit einer Freiheitsstrafe bis zu drei Jahren oder mit Geldstrafe bestraft werden, § 156 StGB. Die fahrlässige Abgabe einer falschen Versicherung an Eides statt kann mit einer Freiheitsstrafe bis zu einem Jahr oder Geldstrafe bestraft werden, § 161 StGB.

Die oben stehende Belehrung habe ich zur Kenntnis genommen:

Official notification:

Any person who intentionally breaches any regulation of university examination regulations relating to deception in examination performance is acting improperly. This offence can be punished with a fine of up to EUR 50,000.00. The competent administrative authority for the pursuit and prosecution of offences of this type is the chancellor of the TU Dortmund University. In the case of multiple or other serious attempts at deception, the candidate can also be unenrolled, Section 63, paragraph 5 of the Universities Act of North Rhine-Westphalia.

The submission of a false affidavit is punishable.

Any person who intentionally submits a false affidavit can be punished with a prison sentence of up to three years or a fine, Section 156 of the Criminal Code. The negligent submission of a false affidavit can be punished with a prison sentence of up to one year or a fine, Section 161 of the Criminal Code.

I have taken note of the above official notification.

Dortmund,
Ort, Datum
(Place, date)

Unterschrift
(Signature)

Titel der Dissertation:
(Title of the thesis):

Biological characterization of farnesyl-mediated protein-protein interactions

Ich versichere hiermit an Eides statt, dass ich die vorliegende Dissertation mit dem Titel selbstständig und ohne unzulässige fremde Hilfe angefertigt habe. Ich habe keine anderen als die angegebenen Quellen und Hilfsmittel benutzt sowie wörtliche und sinngemäße Zitate kenntlich gemacht.
Die Arbeit hat in gegenwärtiger oder in einer anderen Fassung weder der TU Dortmund noch einer anderen Hochschule im Zusammenhang mit einer staatlichen oder akademischen Prüfung vorgelegen.

I hereby swear that I have completed the present dissertation independently and without inadmissible external support. I have not used any sources or tools other than those indicated and have identified literal and analogous quotations.

The thesis in its current version or another version has not been presented to the TU Dortmund University or another university in connection with a state or academic examination.*

*Please be aware that solely the German version of the affidavit ("Eidesstattliche Versicherung") for the PhD thesis is the official and legally binding version.

Ort, Datum
(Place, date)

Unterschrift
(Signature)